DEVELOPMENT OF CHITOSAN/CELLULOSE MULTILAYER PACKAGING FILM INFUSED WITH RESVERATROL TO ENHANCE THE QUALITY AND STORABILITY OF MUSHROOM

Thesis Submitted for the Award of the Degree of

DOCTOR OF PHILOSOPHY

in

Food Science and Technology

By

Adity Bahndral

Registration Number: 12106221

Supervised By

Dr. Rafeeya Shams (28214)

Food Technology and Nutrition

(Assistant Professor)

Lovely Professional University

Punjab, India

Co-Supervised By

Dr. Kshirod Kumar Dash

Food Processing Technology

(Professor)

Ghani Khan Choudhury Institute

of Engineering and Technology

West Bengal, India

LOVELY PROFESSIONAL UNIVERSITY, PUNJAB

2026

DECLARATION

I, hereby declared that the presented work in the thesis entitled "Development of chitosan/cellulose multilayer packaging film infused with resveratrol to enhance the quality and storability of mushroom " in fulfilment of degree of **Doctor of Philosophy (Ph. D.)** is outcome of research work carried out by me under the supervision of Dr. Rafeeya Shams working as Assistant Professor , in the Department of Food Technology and Nutrition/ School of Agriculture of Lovely Professional University, Punjab, India. In keeping with general practice of reporting scientific observations, due acknowledgements have been made whenever work described here has been based on findings of other investigator. This work has not been submitted in part or full to any other University or Institute for the award of any degree.

(Signature of Scholar)

Name of the scholar: Adity Bahndral

Registration No.: 12106221

Department/school: Department of Food Technology and Nutrition/ School of Agriculture

Lovely Professional University,

Punjab, India

CERTIFICATE

This is to certify that the work reported in the Ph.D. thesis entitled " Development of chitosan/cellulose multilayer packaging film infused with resveratrol to enhance the quality and storability of mushroom " submitted in fulfillment of the requirement for the award of degree of **Doctor of Philosophy (Ph.D.)** in the Department of Food Technology and Nutrition / School of Agriculture , is a research work carried out Adity Bahndral , 12106221, is bonafide record of her original work carried out under my supervision and that no part of thesis has been submitted for any other degree, diploma or equivalent course.

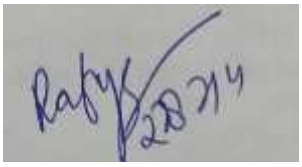

(Signature of Supervisor)

Name of supervisor: Dr. Rafeeya Shams

Designation: Assistant Professor

Department/School: Food Technology and Nutrition, School of Agriculture,

University: Lovely Professional University, Punjab, India

(Signature of Co-supervisor)

Dr. Kshirod Kumar Dash

Designation: Professor

Department: Food Engineering and Technology

University/Institute: Ghani Khan Choudhury Institute of Engineering and Technology,

Malda, West Bengal, India

ACKNOWLEDGEMENT

I deem it a great privilege to express my deepest sense of gratitude originating from the innermost core of my heart to my advisor **Dr. Rafeeya Shams**, **Assistant Professor,** Department of Food Science and Technology, Division of Research and Development, Lovely Professional University, Punjab, for her benevolent guidance, relentless efforts, constructive counselling, critical appreciation, motivation and sense of humor along with the knack of making the difficult task seem simple. I will be very proud to work under her. She is the best supervisor I could ever get.

I extend my sincere thanks to my co-supervisor, **Dr. Kshirod Kumar Dash** for his insightful suggestions, constructive feedback, and time spent reviewing my work. His expertise, patience, and encouragement were instrumental in shaping the direction of my research, and I am incredibly fortunate to have had the opportunity to work under his supervision.

I also owe a big thanks to my committee members, Dr. Prince Chawla, Dr. Sonia Maurya and Dr. Mukul Kumar, for their valuable feedback and insights. Their contributions have been invaluable in refining my research and bringing it to its final form.

Special thanks to my sisterly roommate Dr. Khushbu Sharma (2021-2024 to forever) you have made this experience memorable. Thank you for being a source of emotional support, for the countless laughs, late-night work sessions, and overall sense of community that made this journey so much more enjoyable. You are always being there with a word of encouragement or a much-needed distraction. I've learned so much from you, and I'll always treasure the friendships we've built.

I would like to convey my heartfelt gratefulness to my beloved parents (Mr. Parshant Singh Bandhral and Smt. Rajni Devi), my dearest grandmother (Smt. Shakuntala Devi) and my younger sister (Arushi Bandhral). I am forever grateful for your love, encouragement, and unwavering belief in me. Your sacrifices, both big and small, have made this achievement possible, and I dedicate this work to you.

This thesis would not have been possible without the help of all those mentioned above, and I am truly grateful for their support, both professionally and personally.

Place: LPU, Phagwara 22/11/2025

TABLE OF CONTENT

Particulars	Page No.
Abstract	**xvi-xvii**
CHAPTER-1	
Introduction	**1-5**
CHAPTER-2	
Review of literature	**6-13**
CHAPTER-3	
Hypothesis and objective of the study	**14**
CHAPTER-4	
Materials and methods	**15-51**
CHAPTER-5	
Results and discussion	**52-152**
CONCLUSION	**153-155**
REFERENCES	**156-226**

LIST OF APPENDICES

Particulars	Content	Page No.
Appendix-I	Standard curve	237
Appendix-II	Poster/oral presentation certificate	238-239
Appendix-III	Published research paper	240-242
Appendix -IV	Plagiarism report	243
Appendix -V	Techno-functional properties of different dried MWP	244
Appendix -VI	Techno-functional properties of control films (T1, T2 and T3)	245
Appendix -VII	Antioxidant properties of the treated films (T1, T2, T3 and T4) in comparison with optimized control film (T2)	246
Appendix -VIII	Techno-functional properties of mushroom under storage study	247-249

LIST OF ABBREVIATIONS AND SYMBOLS USED

List of abbreviations	Symbols used
Mushroom waste powder	MWP
Crystalinity index	CI
Vacuum drying	VD
Freeze drying	FD
Hybrid drying	HD
Bulk density	BD
Tapped density	TD
Chitosan	CS
Alkaline insoluble matter	AIM
Low density polyethylene	LDPE
Relative humidity	RH
Polyethylene cups	PE
Nano cellulose	NC
Nanocrystalline cellulose	NCC
Cellulose nanocrystals	CNC
Cellulose nano fiber	CNF
Resveratrol	RES
Malondialdehyde	MDA
Antioxidant activity	AA
Browning degree	BD
Polyphenol oxidase	PPO
1,1-diphenyl-2-picrylhydrazyl	DPPH

Reducing power	**RP**
Reactive oxygen species	**ROS**
Biodegradation test	**BT**
Water vapour transmission rate	**WVTR**
Cost benefit ratio	**CBR**
Water vapor permeability	**WVP**
Oxygen transmission rate	**OTR**
Hydrogen bond intensity	**HBI**
Charge transference	**CT**
Microwave assisted extraction	**MAE**
Zone of inhibition	**ZOI**
2,2'-azino-bis(3-ethylbenzothiazoline-6-sulfonic acid)	**ABTS**
Gallic acid equivalent	**GAE**
Rotation per minute	**rpm**
Analysis of variance	**ANOVA**
Per cent	**%**
Degree celsius	**°C**
Whiteness index	**WI**
Yellow index	**YI**
Chroma	**C***
Hue angle	**h***
Lightness	**L**
Red-green scale	**a**

Yellow-blue scale	**b**
Ultra-violet	**UV**
Treatment	**T**
Elongation at break	**EAB**
Tensile strength	**TS**
Total color difference	**(ΔL*)**
Fourier transform infrared spectroscopy	**FTIR**
Differential scanning calorimetry	**DSC**
Thermogravimetric analysis	**TGA**
Dynamic light scattering	**DLS**
Field emission scanning electron microscopy	**FE-SEM**

LIST OF TABLES

Table No.	Particular	Page No.
1.	Table 4.1. Treatment details for the extraction of chitosan (CS) at various power levels.	24
2.	Table 4.2. Treatment details for the extraction of cellulose at various power levels.	30
3.	Table 4.3. Determination of total cellulose content in mushroom waste powder (MWP).	33
4.	Table 4.4. Different formulations for preparation of films without resveratrol (RES) (Control films).	39
5.	Table 4.5. Different formulations for preparation of films with resveratrol (RES) (Treated films).	40
6.	Table 5.1. Proximate analysis of dried button mushroom waste powder (MWP).	52-53
7.	Table 5.2. Bioactive properties of dried button mushroom waste powder (MWP).	62
8.	Table 5.3. Flow properties and color profile of dried button mushroom waste powder (MWP).	64
9.	Table 5.4. Techno-functional properties of extracted chitosan (CS) powder.	77
10.	Table 5.5. Effect of treatment on Degree of deacetylation (DD), Crystallinity index (CI) and bioactive properties of extracted chitosan (CS) powder.	80

11.	**Table 5.6. Techno-functional properties of extracted cellulose powder.**	**97-98**
12.	**Table 5.7. Determination of total cellulose content in mushroom waste powder (MWP).**	**100**
13.	**Table 5.8. Total color difference (ΔE), lightness (ΔL^*), chroma (C^*), hue (h^*) and whiteness index (WI) of the control films equilibrated at 25 °C.**	**106-107**
14.	**Table 5.9. Mechanical properties, water solubility, swelling index, barrier properties and antioxidant activity of the control films equilibrated at 25 °C.**	**110-111**
15.	**Table 5.10. Total color difference (ΔE), lightness (L*), chroma (C*), hue (h*) and whiteness index (WI) of the treated films equilibrated at 25 °C.**	**123**
16.	**Table 5.11. Mechanical properties and Antioxidant activity of the treated films equilibrated at 25 °C.**	**131-132**
17.	**Table 5.12. Weight loss (%) of different treatments of *Agaricus bisporus* mushroom during storage.**	**139-140**
18.	**Table 5.13. Firmness (N) of *Agaricus bisporus* mushroom during storage under different treatments.**	**141**
19.	**Table 5.14. Respiration rate (mL $kg^{-1}s^{-1}$) of *Agaricus bisporus* mushroom during storage under different treatments.**	**143**

20.	**Table 5.15. Polyphenol oxidase (PPO) activity (U kg^{-1}) of *Agaricus bisporus* mushroom during storage under different treatments.**	**147**
21.	**Table 5.16. Malondialdehyde (MDA) content (mol Kg^{-1}) of *Agaricus bisporus* mushroom during storage under different treatments.**	**148**
22.	**Table 5.17. Browning degree (BD) content (mol Kg^{-1}) of *Agaricus bisporus* mushroom during storage under different treatments.**	**150**
23.	**Table 5.18. Detailed cost estimation for one batch (10 films) of CS-RES-NC based multilayer packaging films.**	**151-152**

LIST OF FIGURES

Figure No.	Particular	Page No.
1.	Figure 2.1. Basic structure of multilayer film	13
1.	Figure 4.1. Pictorial view of (a) Raw white button mushroom (*Agaricus bisporous*) and (b) white button mushroom waste.	16
2.	Figure 4.2. Pictorial representation of preparation of mushroom waste powder (MWP) using different drying methods.	17
3.	Figure 4.3. Microwave assisted extraction method of chitosan from mushroom waste powder (MWP).	25
4.	Figure 4.4. Traditional extraction method of chitosan from mushroom waste powder (MWP).	25
5.	Figure 4.5. Methodology for bleaching of extracted cellulose using sodium hypochlorite (NaClO).	31
5.	Figure 4.6. Determination of total cellulose content in mushroom waste powder (MWP).	34
6.	Figure 4.7. Pictorial view of (a) pure cellulose film and (b) Nanocellulose (NC) film	36
7.	Figure 4.8. Schematic representation of preparation of cellulose derivative as Nanocellulose (NC).	37
8.	Figure 4.9. Schematic representation of preparation of multilayer film (CS-RES-NC)	40

8.	**Figure 5.1. (a) Photographs of mushroom powders obtained by different drying methods and (b) the light microscopic images of mushroom waste powders (MWP) (×25): (a) Vacuum dried MWP; (b) Hybrid dried MWP; (c) Freeze dried MWP.**	**57**
9.	**Figure 5.2. FTIR spectra of mushroom waste powder (MWP) obtained through various treatments such as VD: Vacuum dried MWP, HD: Hybrid dried MWP and FD: Freeze dried MWP.**	**66**
10.	**Figure 5.3. X-ray diffractometry of mushroom waste powder (MWP) obtained through various treatments (FD, VD and HD).**	**68**
11.	**Figure 5.4. Thermogravimetric analysis of mushroom waste powder (MWP) obtained through various treatments such as FD: Freeze dried MWP, HD: Hybrid dried MWP and VD: Vacuum dried MWP.**	**70**
12.	**Figure 5.5. Field Emission Scanning Electron Microscope (FE-SEM) of mushroom waste powder (MWP) obtained through various treatments such as HD: Hybrid dried MWP, FD: Freeze dried MWP and VD: Vacuum dried MWP.**	**72**
13.	**Figure 5.6. Chitosan (CS) powder extracted from mushroom waste powder (MWP) using microwave assisted extraction technique.**	**79**
14.	**Figure 5.7. Fourier transform infrared spectra of chitosan (CS) powder extracted using different treatments.**	**86**
15.	**Figure 5.8. X-ray diffractometry of chitosan (CS) powder extracted using different treatments.**	**88**

16.	**Figure 5.9. Differential scanning calorimetry of chitosan (CS) powder extracted using different treatments showing To, Tm, Tc and ΔH of all the samples.**	**91**
17.	**Figure 5.10. Thermogravimetric analysis of chitosan powder extracted using different treatments.**	**93**
18.	**Figure 5.11. Cellulose powder extracted from mushroom waste powder (MWP) using microwave assisted extraction technique.**	**95**
19.	**Figure 5.12. Observation of cellulose under compound microscope at 10X magnification.**	**100**
20.	**Figure 5.13. Pictorial view of (a) Unbleached cellulose and (b) bleached cellulose.**	**101**
21.	**Figure 5.14. (a) Nano scale dimension and (b) Zeta potential of Nanocellulose (NC) powder.**	**103**
22.	**Figure 5.15. Visual analysis of the control films (T1, T2 and T3).**	**104**
23.	**Figure 5.16. Water solubility (%) of control films (T1, T2 and T3).**	**113**
24.	**Figure 5.17. Fourier transform infrared spectra of optimized control multilayer film (T2).**	**116**
25.	**Figure 5.18. Differential scanning calorimetry of control multilayer films (T1, T2 and T3).**	**118**
26.	**Figure 5.19. Field emission scanning electron microscope images of surface (50x and 500x) and cross sectional (400x and 800x) optimized control multilayer film (T2).**	**119**

27.	**Figure 5.20. Visual analysis of the control film (T0) and Treated films (T1, T2, T3 and T4).**	**120**
28.	**Figure 5.21. Antimicrobial analysis of control (T0) and treated f (T1, T2, T3 and T4) using gram negative bactria and using gram positive bactria.**	**125**
29.	**Figure 5.22. Zone of inhibition of control film (T0) and treated f (T1, T2, T3 and T4) using gram negative bactria and using gram positive bactria.**	**126**
30.	**Figure 5.23. Fourier transform infrared spectra of optimized treated multilayer film (T3).**	**133**
31.	**Figure 5.24. Differential scanning calorimetry of optimized control (T2) and optimized treated multilayer film (T3).**	**134**
32.	**Figure 5.25. Field emission scanning electron microscope images images (50x, 1000x and 5000x) of optimized treated multilayer film (T3).**	**136**
33.	**Figure 5.26. Biodegradation test on optimized treated multilayer film (T3).**	**137**
34.	**Figure 5.27. Shelf life study of mushroom stored at 4°C: Monitoring quality retention and spoilage progression under refrigerated conditions.**	**144**

Abstract

Mushroom waste, primarily derived from post-harvest residues and processing by-products, represents an underutilized biomass rich in bioactive compounds. Lignocellulosic waste from *Agaricus bisporus* contains valuable polysaccharides such as chitin and cellulose, which can be extracted and converted into chitosan and nanocellulose. This study examines the effects of freeze drying (FD), hybrid drying (HD), and vacuum drying (VD) on the physicochemical, functional, and antioxidant characteristics of mushroom waste powder (MWP). The drying technique significantly influenced nutritional composition FD yielded the highest crude protein (23.54%), fat (2.80%), and ash (5.23%) contents, while HD showed the lowest moisture (5.81%) and highest carbohydrate (64.04%) levels. Structural and color analysis revealed that FD and HD powders had floury, homogeneous textures, whereas VD powders were darker and less consistent. FD exhibited superior antioxidant activity, with the highest phenolic (25.07 mg GAE/g), flavonoid (14.48 mg QE/g), and ascorbic acid (14.46 mg/100g) contents, along with enhanced DPPH scavenging and reducing power. Physical properties like bulk density, Carr's index, and Hausner ratio varied significantly with FD showing the best flowability. FTIR, XRD, and TGA confirmed that FD best preserved structure, bound water, hydroxyl groups and thermal stability. SEM revealed porous, sponge-like FD particles that supported higher solubility and rehydration, while HD showed moderate preservation and VD resulted in compact, collapsed particles with reduced functionality. Though energy-intensive, FD effectively preserves structural, nutritional and functional qualities of heat-sensitive materials, making it the preferred drying method. The freeze-dried MWP was used for microwave-assisted extraction of chitosan and cellulose. Chitosan was produced through sequential demineralization (3M HCl, 540 W, 8 min), deproteination (10% NaOH, 180 W, 8 min), and deacetylation (50% NaOH, 360 W, 8 min), yielding a product with pH 7.5, solubility 75%, degree of deacetylation 79.94%, and crystallinity index 1.09. It exhibited 53.97% DPPH scavenging activity and reducing power of 3.58, with FTIR and XRD confirming characteristic OH, C–O, NH_2, and C–N groups and semi-crystalline peaks between 10°–20°. Cellulose was extracted using microwave-assisted alkali delignification and bleaching at 540 W, yielding 10.46%. The resulting powder showed low moisture (4.19%), neutral pH (7.5), moderate solubility (60%), and good flowability (Carr's index 11.36, Hausner ratio 1.13). It was further hydrolyzed with 60% sulfuric acid to obtain nanocellulose (NC) with a particle size of

163.2 ± 2.74 nm and zeta potential of −19.2 ± 0.27 mV. Multilayer films composed of chitosan (CS) and NC (1–2% CS and 2–4% NC) showed significant improvements in mechanical, optical, and barrier properties. Increasing CS–NC content reduced lightness and transparency but enhanced thickness (47.20–126.31 µm), tensile strength (13.77-54.19 MPa), and elongation (45.52-102.72%). Barrier performance improved with decreased WVTR (1.32 g/m² h) and OTR (6.21 cc/m² day), while water solubility decreased (8.16%) and swelling index increased (83.70%). Antioxidant activity increased across formulations (39.77%; RP absorbance 0.68), indicating synergistic effects between CS and NC. Films incorporated with resveratrol (RES; 4 – 16 µg/mL) demonstrated enhanced optical and antioxidant properties. Color difference (ΔE) rose to 90.29, and transparency increased (79.43%). Moderate RES concentrations (12 µg/mL) yielded optimal flexibility (EAB = 74.20%) and antioxidant capacity (DPPH = 74.66%), while excessive RES slightly reduced mechanical strength due to its plasticizing effect. Biodegradability tests revealed 54% weight loss after 30 days of soil burial, confirming eco-friendly degradation. Shelf-life evaluation showed that mushrooms wrapped in CS–NC–RES films, particularly T3 (12 µg/mL RES), retained the most quality with minimal weight loss (10.29%), high firmness (5.11 N) and reduced respiration rate (8.1 mL kg^{-1} s^{-1}). PPO and MDA levels were lowest in T3 (21.1 U kg^{-1}; 2.8 µmol kg^{-1}), and browning degree decreased by 42.9% compared to the control. These results confirm that optimal RES incorporation enhances antioxidant protection, film performance, and the postharvest stability of mushrooms, making CS–NC–RES films a sustainable and effective option for active food packaging.

Key words: Mushroom waste; Cellulose, Microwave-assisted extraction, *Agaricus bisporus*; Browning index; Antioxidant activity; Resveratrol; Chitosan; Shelf life; Crystallinity index; Polyphenol oxidase; Degree of deacetylation; Nanocellulose; Multilayer film; Malondialdehyde; Biodegradation

INTRODUCTION

The consumption of mushrooms has significantly expanded in recent years owing to its enhanced nutritional content and health benefits that are ascribed to being part of proteins, vitamins, minerals, polysaccharides derived from fungi (particularly β-glucans), and antioxidants. Around 20 of the more than 35 edible mushroom species that are commercially grown worldwide are produced on an industrial basis (Pandey et al., 2024; Silva et al., 2024). Among them *A. bisporus* is among the most often eaten mushrooms worldwide (Siwulski et al., 2020). Mushrooms, which belong to the fungi kingdom, offer substantial nutritional benefits, with approximately 2,000 edible species found globally (El Sheikha, 2022). In 2018, the worldwide market worth of farm fresh mushrooms stood at 38 billion USD, with China emerging as the dominant mushroom grower in Asia, making up about 35% of the total global mushroom market share, as reported by (Bhagarathi et al., 2023). Asia countries subsidize maximum mushroom production up to 76%, here after by Europe (17.2 %) and United States (5.9 %) (Yadav et al., 2021). The growth of the mushroom farming in India has experienced tremendous growth in the past few years with the overall output of mushroom reaching about 0.30 million tonnes per year. India exhibits diverse agro-climatic conditions and is primarily an agrarian nation, utilizing roughly 4.37% of its land for cultivation and producing approximately 620 million tons of agricultural waste each year. The global market for *Agaricus bisporus* (white button mushroom) was valued at USD 16.73 billion in 2020 and is projected to reach USD 27.40 billion by 2028 (Zion Market Research, 2021). In India, there is potential to produce up to 3 million tonnes of mushrooms and approximately 15 million tonnes of bio-compost from agricultural waste (Raman et al., 2018). However, industries face losses due to challenges in the safe disposal of mushroom by-products such as stems and deformed mushrooms that do not meet commercial standards, adding to overall production costs (Papoutsis et al., 2020). Implementing value-addition strategies could enhance revenue generation and offset production expenses associated with primary biotechnological outputs (Singh & Thakur, 2023). Unfortunately, the rapid expansion on a commercial scale for use in eatable mushroom notably mushroom stalks along with damaged mushrooms that fail to meet market specifications. These by-products that are usually disposed are highly abundant in useful biopolymers like chitin and chitosan. A high-quality use of such a waste to get a polymer reduces the harmful effects of the environment but also provides value to mushroom processing business by means of sustainable

materials recovery. Current research and industrial efforts are increasingly focused on valorizing mushroom waste to achieve sustainable economic and environmental goals (Pérez-Bassart et al., 2023). This area remains relatively unexplored but holds great promise for the development of recyclable biopolymers in the food packaging sector (Feng et al., 2022). Moreover, proper postharvest handling and drying practices are crucial to maintaining product quality and supporting the growing mushroom industry (Siddiq et al., 2018).

Drying, pickling, and freezing are some of the different preservation procedures that extend the shelf life of mushrooms (Sangeeta et al., 2024). Drying is the most efficient of them to remove all moisture to a safe storing level (Verma et al., 2020). Traditional hot-air drying is also easy and cost-effective but can lead to the loss of color and degradation of nutrients because of prolonged heating (Izham et al., 2022). Lyophilization or FD is said to be the best when it comes to removing moisture without affecting the structure or nutritional value (Nowak et al., 2020; Sajad et al., 2023). It works by means of sublimation and does not remove the texture and bioactive compounds, but it is expensive (Sandhya and Disha, 2020; Mehanna et al., 2022). The development of hybrid drying methods, including microwave-assisted and microwave-vacuum drying, is now an efficient alternative to the traditional drying method by using less energy and time, and enhancing the quality of the product (Acar et al., 2022; Ekezie et al., 2017; Zielinska et al., 2020). The combination of microwave and freeze systems improves drying power by matching temperature and moisture gradients and avoids the overheating of products (Yang et al., 2021; Bhattacharjee et al., 2024). The research indicates that mushroom powder is of high quality with improved color, texture, and rehydration qualities with the use of hybrid systems in contrast to traditional air drying (Das et al., 2020; Kantrong et al., 2014). Therefore, it is essential to choose appropriate drying methods, especially freezing, hybrid and hot-air drying, to obtain high products in mushroom materials (Alp & Bulantekin, 2021; Marcal et al., 2021).

Edible mushrooms, rich in chitin, glucans, and proteins, are an excellent source of dietary fiber that enhances food texture and offers health benefits (González et al., 2020). Chitin, structurally similar to cellulose but containing an acetyl amine group, is a vital biopolymer found in fungi and marine organisms (Cummings, 2024; Rahangdale et al., 2019). Its functionality depends on the degree of acetylation (DA) and deacetylation (DD), which influence its physicochemical properties (Elizalde-Cárdenas et al., 2024). However, chitin's poor solubility and high crystallinity limit its direct industrial use (Korampattu et al., 2024). Therefore, it is commonly

deacetylated to chitosan (CS), a more soluble, biocompatible, and biodegradable polymer with wide applications in food systems (Shoueir et al., 2021; Zhan et al., 2024). Traditional CS extraction is energy-intensive (Da Costa et al., 2023), but microwave-assisted extraction offers a faster (Cheng et al., 2020), more efficient (Hisham et al., 2024), and eco-friendly alternative for both organic and inorganic compounds (Abolhasani & Kumacheva, 2023) improving yield and purity while drastically reducing reaction time (Liaqat et al., 2023; Banik et al., 2021).

Another valuable polysaccharide that can be extracted from mushroom waste powder is cellulose, a linear homopolymer and one of the most abundant, renewable, and biodegradable biopolymers globally produced at a rate of 10^5-10^{10} tons annually (Khan et al., 2022). Owing to its unique properties, cellulose has gained increasing importance in the development of biodegradable and sustainable materials (Banerjee & Arora, 2023). The cellulose extraction process typically involves cleaning, drying, grinding, sieving, defatting, alkaline pretreatment, neutralization, and acid treatment, followed by final drying to obtain purified cellulose fibers. Traditionally, cellulose is derived from plant-based sources such as hardwood, softwood, and bark (Mithun et al., 2023). However, recent trends emphasize cellulose recovery from agricultural residues like rice straw (Lai et al., 2022), wheat straw (Liu et al., 2021), lemon grass straw (Bahndral et al., 2024; et al., 2023), vetiver straw (Seth et al., 2022), little millet straw (Dominic et al., 2022), oat straw (Sjöstedt, 2022), banana pseudostem (Zope et al., 2022), and yellow thatching straw (Ndwandwa et al., 2023). This shift from conventional plant sources to farm waste-based cellulose not only supports economic sustainability but also contributes to efficient waste utilization and environmental conservation. However, mushroom waste is also a source of cellulose that has not been exploited well, due to its abundance of fibrous cell wall polysaccharides. The method has the ability to further enrich the on-farm agro-industrial residues as well as underpin waste valorization and circular bioeconomy efforts.

To achieve the required polymer a number of studies have employed microwave-assisted extraction (MAE) methods. MAE has emerged as a promising green technology for polysachharide recovery from biomass due to its superior energy efficiency, shorter processing duration, and reduced chemical usage compared to conventional extraction methods. As an illustration, Hou et al. (2019) used MAE to extract cellulose in eucalyptus wood whereas Vinhas et al. (2023) used ionic liquids in combination with microwave heating to isolate cellulose in pine wood waste. Nevertheless, these are frequently based on solvents that are not very eco-friendly such as dimethyl

sulfoxide (DMSO), which restricts their sustainability. It has been demonstrated that microwave hydrothermal heating is 2.1-2.8-times more efficient than the traditional hydrothermal systems in terms of biomass processing (Reynosa et al., 2017). However, the heterogeneous material properties may lead to such difficulties as uneven heating and hot spots, the latter can be addressed through the design optimization of reactors and microwave frequency (Haldar and Purkait, 2021; Fia and Amorim, 2023; Fernandes et al., 2023). The alkaline and bleaching treatments performed with the help of microwaves are useful to remove lignin and hemicellulose and increase the crystallinity of cellulose and its thermal stability (Tessera et al., 2024). Cellulose because of its renewability and microstructure has high potential in food packaging, but its hydrogen bonding is difficult to dissolve and manipulate. The recent developments in green solvents systems have facilitated the generation of cellulose-based films that have better barrier and mechanical properties (Liu et al., 2023). The current research is aimed at extracting cellulose in the mushroom waste with the help of chemically mediated microwave treatment and the assessment of its techno-functional and structural features.

Biodegradable packaging materials derived from bio-based substances are gaining prominence due to their ability to reduce crude oil dependence, minimize environmental impact, and lower food waste (Asgher et al., 2020; Reichert et al., 2020; Morinval & Averous, 2022). These materials are particularly suitable for food applications as they limit the migration of harmful substances (Amin et al., 2022). With consumers increasingly preferring natural alternatives over synthetic preservatives, phenolic compounds like resveratrol (RES) have emerged as promising bioactive additives for polymer matrices in food packaging (Batiha et al., 2021; Arruda et al., 2022). The primary mechanisms governing polyphenol–polysaccharide interactions include hydrogen bonding and hydrophobic interactions such as those between the polyphenol's heterocyclic C-ring and the methyl groups of polysaccharides (Xue et al., 2024; Zhang et al., 2023). These interactions can modify key film properties, including solubility, mechanical strength, and barrier performance. Although limited studies have explored these effects in polymeric films, evidence suggests that different polysaccharide–tannin combinations lead to unique structural and functional variations (Eslami et al., 2023). Moreover, factors like the number of hydroxyl groups and molecular flexibility of phenols, along with polysaccharide characteristics, determine binding affinity (Cano et al., 2021; Rocchetti et al., 2022). Overall, understanding these

interactions is vital to enhancing the performance of biopolymer-based films and developing sustainable food packaging solutions.

The novelty of this work depends upon the mean of drying of mushroom waste powder using a combination of vacuum drying (VD), freeze drying (FD) and hybrid drying (HD) method followed by extraction of chitosan and cellulose from the mushroom waste powder using microwave extraction technique and later optimization of the process for fabrication of multilayered packaging film incorporated with bioactive compound. A method for integrating RES into various polysaccharide solutions of cellulose and chitosan is employed to assess whether the varying degrees of bioactive-polysaccharide interactions influence the functionality of the resultant films. The process involves incorporating the bioactive component in dry powder form into the film-forming solution to produce a monolayer film. After semi-drying, a further layer of polysaccharide containing bioactive compounds in dry powder form is introduced to the aqueous solution, forming a second layer on top. RES, irrespective of its source, functioned as a crosslinking agent when integrated into chitosan and cellulose (or its derivatives) films as a result of specific interactions, most notably hydrophobic and the creation of hydrogen bonds. The microstructure, visual, barrier, mechanical, and water solubility, antioxidant capacity, and anti-microbial potential were examined. These polysaccharides based multilayer films are further utilize for reducing post-harvest losses and improves the shelf life of the mushroom.

Chapter 2

REVIEW OF LITERATURE

Kamińska et al. (2025) created thin films using chitosan and konjac glucomannan, incorporating RES. Adding bioactive compounds to biocomposites is common to improve product qualities. The films were analyzed using infrared spectroscopy, SEM and AFM, water absorption tests, and evaluations of structure, radical scavenging, contact angle, and RES release in a skin-like environment. RES altered the film's molecular structure and shape. The films' structural properties deteriorated with additives. The 10% resveratrol sample showed the most swelling. RES-enhanced coatings showed strong antioxidant properties, better wettability, and a reduced contact angle. RES release was initially rapid, reaching about 83.9% maximum, varying by sample. The films exhibited excellent swelling, significant antioxidant effects, and enhanced surface tension, making them suitable for skin applications.

Mohammadi et al. (2023) found that the traditional method of extracting CS from shrimp waste produced a higher molecular weight CS with a yield of 12.7%. Microwave extraction yielded a porous medium molecular mass CS with a yield of 11.8%. The conventional extraction process in a microwave produced medium molecular weight CS with a crystallinity index of 79% and a lower yield of 10.8%. Antimicrobial evaluations showed that CS from the traditional approach was more effective against *Salmonella Typhimurium* (8.57 mm), *Escherichia coli* (8.78 mm), and *Listeria monocytogenes* (9.47 mm). The microwave-assisted CS was most effective against Escherichia coli (8.37 mm) and Staphylococcus aureus (8.05 mm), while showing similar efficacy against *Salmonella Typhimurium* (7.34 mm) and *Listeria monocytogenes* (6.52 mm). Both traditionally and microwave-derived CS showed the strongest antimicrobial effectiveness against the target bacteria.

Shams et al. (2022) studied the structure, bioactive ingredients, color parameters, and characteristics of mushrooms after freeze drying (FD) and cabinet drying (CD). CD mushrooms had higher levels of total protein, fiber, fat, ash, carbohydrates, and energy. FD mushrooms had lower moisture and water activity compared to CD mushrooms. FD samples had lower a* and b*

values and a greater L* value. According to XRD, CD button mushroom powder contained smaller crystals. FD retained compounds better than CD in terms of phenolic content, DPPH scavenging activity, and reducing power assay. FD is excellent for white button mushrooms.

Szadzinska et al. (2021) used a hybrid dryer to dehydrate white mushrooms, studying microwave power (100–200 W) at 30 and 50 ℃ with circulatory convection. This included quality indicators, effective diffusion coefficient, energy consumption, drying time, and drying rate. All hybrid-dried samples showed discoloration and shrinkage. Maximum polyphenol concentration was found at 30℃ with 200W microwave power, retaining 83% of the content. Both drying techniques produced microbiologically stable products with water activity less than 0.5. Drying time decreased significantly (89-93%). Increased microwave power and temperature improved drying rate and moisture diffusivity, enhancing energy efficiency. Energy usage in microwave-convective drying decreased by up to 75% and was unaffected by air temperature.

Cazon et al. (2024) investigated composite multilayer films made of CS and bacterial cellulose (BC), enhanced with glycerol and grape bagasse extract (GE). FT-IR analysis confirmed the structure and connections between BC and CS. The effects of glycerol and GE concentrations were shown by investigating moisture level, swelling capacity, water vapour permeability (WVP) and solubility. GE and glycerol increased moisture content. WVP rose with higher hydrophilic chemical concentrations. Lower swelling ability with increased dissolution followed the inclusion of GE with glycerol. Integration using GE imparted bioactive characteristics within films. The TPC varied between 0 and 1.75 mg GAE/g for dried out film, based upon GE. FTIR revealed improved UV-blocking capabilities. The utilization of natural antioxidant sources in these multilayer films improves their functionality, making them appealing for usage in food packaging.

Bahndral et al. (2024) used lemon grass straw to create cellulose through delignification, removing hemicelluloses and bleaching. They used microwave assisted alkali extraction, followed by characterization. The highest yield of 37.36% was achieved at 540 W microwave power with 8% NaOH for 3 mins and 2 mins of bleaching at 540W. Fourier transform infrared (FTIR) spectroscopy analyzed the physical characteristics of the cellulose, including C–H bonds, C–C bonds, hydroxyl (OH), glycosidic linkage (C–O–C), and carbonyl (C=O). The cellulose showed

high thermal stability. X-ray diffraction (XRD) revealed peaks at 14.8◦, 16.5◦, and 22.5◦, indicating crystalline cellulose. The cellulose had a 70.02% crystallinity index. The microwave-assisted treatment increased cellulose crystallinity. The fibers' thermal conduct suggests they can be used in environments under 200 ℃. FTIR analysis confirmed the removal of wax, lignin, and hemicelluloses.

Wang et al. (2024) reviewed the use of agro-industrial waste, such as maize husks and sugarcane bagasse, for nanocellulose (NC) extraction. Acid hydrolysis and high-pressure homogenization were common methods, along with enzymatic and chemical approaches. The study emphasized NC's biodegradability, biomedical uses, and sustainability. The authors also highlighted the need for more energy-efficient and environmentally friendly extraction processes to aid industrial scaling.

Zhu et al. (2023) studied the process of breaking down lignocellulosic biomass. They proposed a method to purify cellulose using cold caustic extraction and microwave-assisted formic acid hydrolysis. Glucose content was measured using spectrophotometers. The study achieved quick removal of hemicelluloses from hardwood pulp fibers. The highest cellulose content of 91.5% was achieved under optimal conditions, with hemicellulose decreasing to 2.3% and lignin to 6.1%. The decomposition temperature decreased, and the crystallinity index increased. Further research is needed to correlate crystallinity with application performance.

Vinhas et al. (2024) developed a sustainable cellulose extraction method from Eucalyptus and pine waste using microwave-assisted radiation. The process involved basic treatment, hydrogen peroxide bleaching, and alkali reagent bleaching. Results showed improved thermal and mechanical properties compared to initial components. Cellulose was retained, while hemicellulose and lignin were mostly removed. The extraction utilized mild chemical and thermal conditions (120 °C for 3 hrs).

Matharu et al. (2018) studied orange peel waste for NC production using a broad experimental design. They analyzed the Hy-MASS dispensing of citrus-based cellulosic material, varying temperature (120-200 °C), retention time (0-30 min), and concentration (1.4-5.0 wt %).

ANOVA showed improved cellulosic matter yield (25-72%) after microwave processing. Breakdown temperature (345-373°C) and crystallinity index (34-67%) were affected by temperature shifts. SEM and TEM revealed heterogeneous cellulose compounds resembling microfibrillated cellulose (MFC) at lower temperatures.

Sebastian et al. (2019) used statistical methods to determine ideal conditions for chitosan (CS) from *Rhizopus oryzae* NRRL1526. Microwave-assisted extraction (MAE) and autoclave-assisted CS extraction were compared. MAE at 300 W for 22 min yielded the best CS. MAE produced more CS with greater deacetylation (94.6 ± 0.9%) than traditional extraction. Microwave irradiation is a less expensive and more effective method.

Wang et al. (2021) examined the effects of varying high levels of several lemon essential oils (LEO) on quality of mushroom under 4 ℃ after 12 d after incorporation for creating chitosan/zein (C/Z/L films) for strengthening antioxidant as well as antibacterial potential. The progressive increase in LEO concentration boosted EAB as well as regarding the permeability of gases decreasing TS and water vapor permeability. C/Z/L films inhibited mushroom PPO, POD, and microbial growth throughout storage. Mushrooms with 6% LEO film had the lowest rate of respiration while lowest browning score. C/Z/L film used mushrooms had better texture and antioxidant capability. This study found that LEO-loaded C/Z active film might preserve mushroom quality postharvest.

Díaz-Montes et al. (2021) developed films of commercial CS and *Leuconostoc mesenteroides* produced dextran to substitute viable packaging materials. The dextran/chitosan blend films looked into for mushroom bio-packaging, physical, mechanical and permeability properties, rendering to dextran application variations (0.01 - 4.0 % w/v dispersion). The nethermost dextran concentration (0.5% w/v dispersion) resulted in optimal Water vapor permeation (4.09 g mm kPa^{-1} m−2 hr^{-1}), modulus of elastic (~6.54 MPa), bending strength (2.32 MPa), along with prolonged mushroom (*Agaricus bisporum*) spoiling time as much as 28 days under 4 °C. Biofilms can preserve fresh mushrooms, according to the study.

Liu et al. (2019) studied an innovative active packaging material gallic acid grafted chitosan (GA-g-CS) film used to preserve *Agaricus bisporus* mushrooms. They assessed how this film affected the mushrooms' physical and chemical properties and enzyme activity during cold storage. Compared to mushrooms wrapped in chitosan or commercial polyethylene (PE) films, those in GA-g-CS film showed significantly lower respiration rates, aging, malondialdehyde production, electrolyte leakage, superoxide anion generation, and hydrogen peroxide levels. Additionally, mushrooms in GA-g-CS packaging had higher levels of catalase and superoxide dismutase activities, lower polyphenol oxidase activity, and greater total phenolic content, suggesting enhanced antioxidant capacity and better postharvest quality preservation.

Wang et al. (2022) found that a chitosan/zein film with tea polyphenols effectively preserved mushroom quality for 15 days at 4°C. Low-field electromagnetic spectroscopy revealed changes in water molecule arrangement. The film maintained mushroom color, texture, and cell membrane integrity by reducing permeability and malondialdehyde, while also slowing weight loss and respiration. It inhibited polyphenol oxidase and peroxidase, boosted antioxidant enzymes, and demonstrated strong potential for post-harvest preservation.

Pei et al. (2022) created a caffeic acid-grafted-chitosan/polylactic acid (CA-g-CS/PLA) film and evaluated its impact on Agaricus bisporus postharvest quality. The CA-g-CS/PLA film exhibited improved migration characteristics, oxygen transmission rate, and water vapor transmission rate compared to polyethylene (PE) film ($P>0.05$). It also reduced respiration rates and browning, creating a beneficial O2/CO2 environment. Over 15 days, CA-g-CS/PLA significantly decreased hydrogen peroxide, superoxide radicals, and malondialdehyde levels, while increasing catalase and superoxide dismutase activity compared to PE. This suggests CA-g-CS/PLA film's potential for *Agaricus bisporus* postharvest storage and transport.

Chaudhari et al. (2023) demonstrated that cajuput essential oil-loaded chitosan nanoparticles (CjEO-CSNP) extend white button mushroom shelf-life at 4 °C for one week. Characterization via X-ray diffraction, scanning electron microscopy, and dynamic light scattering revealed spherical nanoparticles (43.17–97.03 nm) with nanoencapsulation efficacy (45.86–92.26%) and packing capacity (0.69–8.87%). CjEO-CSNP exhibited biphasic release at varying

pH levels and improved mushroom shelf-life by maintaining visual appearance, firmness, and antioxidant activity, while reducing weight loss and respiration. CjEO-CSNP was deemed safe (LD50= > 1200 mg/Kg) and did not affect taste, suggesting its potential for extending button mushroom shelf life.

Guo et al. (2022) investigated the impact of *Lentinula edodes* (LE) treated with LEP from mushroom stems, stored below 4 °C for 15 days. LEP treatment reduced weight loss, maintained stiffness and elasticity, increased soluble protein, and minimized browning and electrolyte leakage compared to control groups. Ascorbate peroxidase, phenylalanine ammonialyase, catalase, superoxide dismutase, as well as peroxidase activity were all enhanced by LEP, and the storage-induced buildup of hydrogen peroxide was significantly decreased from control material. The study found that 1.5% LEP yielded the best results. LEP enhanced antioxidant activity and inhibited polyphenol oxidase and tyrosinase, extending shelf life by 6 days

Zhang et al. (2019) created chitosan/zein (CS/Z) mix films. Solutions of zein and CS were combined in ratios of 1:0, 1:1, 3:1 and 5:1. Zeta potential assessed film stability, with all solutions stable. SEM, FTIR, XRD and TGA analyzed film properties. Blend films showed better barriers than pure CS. FTIR indicated hydrogen bonds between zein and CS. SEM and XRD confirmed binding. TGA revealed zein enhanced thermal stability. Wrapping films on mushrooms at 4 °C for 12 days was examined. Mushrooms wrapped in a 1:1 zein blend exhibited the highest whiteness index and the lowest respiration, weight loss, and enzyme activity.

Pastor et al. (2013) incorporated antibacterial or antioxidant chemicals into edible films to enhance functionality. Resveratrol (RES), a natural antioxidant, was added to chitosan (CS) and methylcellulose (MC) films. While RES reduced water vapor and oxygen permeability and correlated with antioxidant activity, it altered film structure. This resulted in increased tear resistance and reduced stretchability (26 and 54% reduction of tensile strength at break for MC and CS, correspondingly) and less stretchable upto 65–70% reduction of deformation upon break at maximum RES amount), opacity (significant internal transmittance reduction) and less glossy (60–65% gloss reduction at highest RES level). The films did not inhibit bacterial growth. These films may extend the shelf life of oxidation-sensitive foods.

Samar et al. (2013) extracted chitosan (CS) from shrimp waste chitin using microwave-assisted deacetylation with varying NaOH concentrations and mesh sizes. The rapid synthesis process, compared to conventional methods, showed that deacetylation increased with alkali concentration. Microwave irradiation of 60 mesh chitin with 50% NaOH for 10 min resulted in 95.19% deacetylation. The microwave-synthesized CS exhibited antioxidant activity (47.71–72.31%) and reducing power (2.094–2.367) at 10 mg/ml. Furthermore, CS scavenged DPPH radicals (43.03% to 90.48%) and inhibited the growth of both gram-negative and gram-positive bacteria, with effects varying based on molecular weight and species.

Luo et al. (2010) synthesized quaternized CS in 50 min using microwave irradiation, in contrast to the 6–7 hrs required by conventional heating methods. The quaternized CS produced through microwave irradiation exhibited a slightly reduced degree of substitution (DS) compared to the one synthesized using conventional procedure, despite sustaining a consistent ratio of 6:1 between the intermediate and CS. Degradation reading indicated the one that molecular weight of reduced significantly compared to 4.6×10^5 to 1.1×10^5 within a hr of microwave irradiation, whereas this declined beginning at 4.66×10^5 to 2.10×10^5 in the same interval of time under conventional heating conditions.

Wang et al. (2019) developed a ternary blended film using CS, curdlan and carboxymethyl cellulose, enhancing mechanical and thermal properties. The optimal method for incorporating CD involved maintaining a 60°C temperature and a pH between 12 and 4. This CS/CD/CMC film exhibited superior rigidity, permeation, and mechanical characteristics compared to pure CS. The blending film improved visible light properties. Imaging electron microscopy and FTIR analyses confirmed favorable interactions between CS, CD, and CMC, leading to enhanced properties. This successful technique produced a blending film with advantageous mechanical and thermal characteristics.

Liu et al. (2017) Using the layer-by-layer (LBL) electrostatic deposition technique, created an edible polyelectrolyte multilayer (PEM) coating for fresh-cut apples using CS and carboxymethyl cellulose sodium (CMC). The PEM coating was described as smooth, transparent, showing linear deposition behaviour, and having a clear layered structure. Additionally, the PEM

coating demonstrated the ability to cure itself, with an 87.4% self-healing efficiency. To evaluate the PEM coating's preservation effectiveness, freshly cut apples were coated with it. PEM coating successfully stopped browning, maintained firmness, and controlled weight loss. According to the results, the PEM coating might find use in the preservation industry.

Kateřina Plevová et al. (2025) explored multilayer films using polyethylene (PE), polyamide 6 (PA6) and ethylene vinyl alcohol (EVOH). Raman spectroscopy and DSC characterized LDPE, LLDPE, PA6 and EVOH in single and multi-layer films. Optimized shredding, washing, and polyethylene blend combinations enhanced mechanical properties, particularly strain at break. Recycled film shrinkage resembled commercial shrink films, suggesting potential for sustainable packaging applications.

Akti (2025) created chitosan/alginate/diatomite/cinnamon oil composite films via solution casting and characterized them. SEM showed homogenous diatomite distribution. AFM revealed increased roughness due to diatomite and layer sequence. XRD and FTIR confirmed chitosan-alginate-diatomite interactions. Diatomite enhanced CA film's thermal and mechanical stability. CA@DA-2 film was hydrophilic. Diatomite increased moisture content, solubility, and swelling, but decreased water vapor permeability and opacity (from 23.75 to 3.63 A/mm). The films lacked antibacterial activity against *E. coli*, *Salmonella*, *S. aureus* and *L. monocytogenes*.

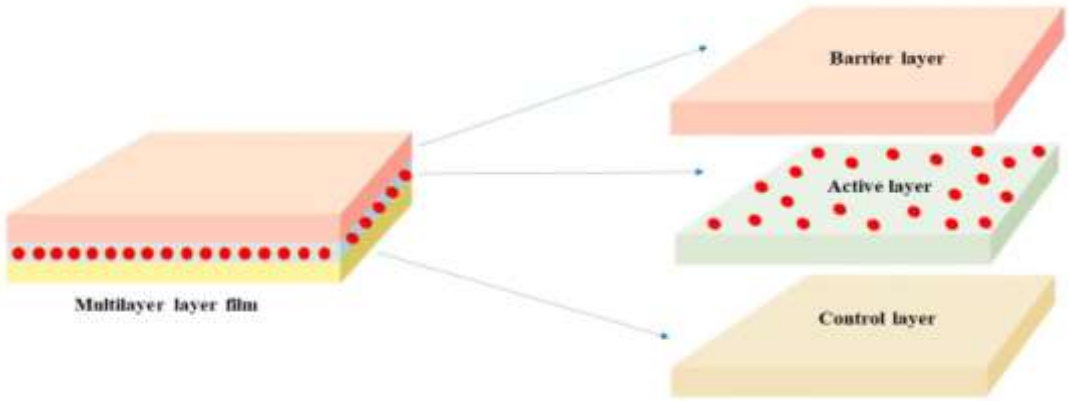

Figure 2.1. Basic structure of multilayer film

Chapter 3

HYPOTHESIS OF THE STUDY

Large production of mushroom waste, which accounts for approximately 20–30% of total mushroom production, leads to environmental pollution; hence, potential utilisation of mushroom waste is required. Mushroom waste powder is rich in chitosan and cellulose hence efficient extraction of these polysaccharides and fabricated into multilayer packaging material helps in reducing the post-harvest losses and prolong the life span of mushroom.

Objectives of the study

The major objectives of the proposal are:

1. To extract and characterize chitosan and cellulose from the mushroom wastes using microwave assisted extraction technique
2. To optimize the process for fabrication of multilayered packaging film incorporated with bioactive compound using extracted chitosan
3. To characterize and evaluate the physiochemical properties of multilayered packaging film
4. To utilize fabricated packaging material for reducing post-harvest losses and shelf life evaluation of mushroom

Expected outcome

Expected outcomes upon completing the thesis include:

1. Efficiently extracted the chitosan and cellulose from the mushroom wastes using microwave assisted extraction technique
2. Fabricated the process of multilayered packaging film incorporated with bioactive compound using extracted chitosan
3. Characterization and evaluation of physiochemical properties of multilayered packaging film
4. Utilization of fabricated packaging material for reducing post-harvest losses and shelf life evaluation of mushroom

Chapter 4

MATERIALS AND METHODS

The work entitled "Development of chitosan/cellulose multilayer packaging film infused with resveratrol to enhance the quality and storability of mushroom" was conducted during the year 2022-2024 in the fields of Lovely Professional University in Jalandhar, Punjab. This section provides an exhaustive overview of the resources along with methods utilized in this study. This chapter briefly describes all materials and methods, including the experiments' location, treatments, and other operations. There is a tabular and graphical description of the statistical analysis of data from SPSS that was obtained from the experimental field.

4.1. Materials

Standard sodium hydroxide pellets (NaOH) ≥98%, hydrochloric acid (HCl) 37%, glacial acetic acid, glycerol, acetone, ethanol was obtained from Sigma-Aldrich (Sigma-Aldrich, St. Louis, MI, USA) and were obtained from Lovely Professional University, Phagwara, Punjab, India. Gallic acid, tannic acid and DPPH (2, 2-diphenyl-1-picrylhydrazyl were from HiMedia. Resveratrol (*trans*-3,4′,5-Trihydroxystilbene) was obtained from TCI Delhi, India. All reagents utilized were of high purity grades, and double distilled water was employed to prepare aqueous solutions.

4.2. Preparation of raw material

White mushroom (*Agaricus bisporus*) by products were obtained from Randhawa mushroom farm, Batala, Punjab, India when the mushrooms are picked. The cap diameter of these medium-sized mushrooms usually fell around between 3 and 4.5 cm. skilled workers gathered the mushrooms first thing in the morning for each batch. The mycelium was removed from the ends of the mushroom stems before collection (Figure 4.1.). Washing, chopping and storing the stalks began the day after harvest at 5°C overnight. The starting moisture level of the chosen samples was 85.74 ± 0.3%. Different drying techniques and their processing conditions are discussed below.

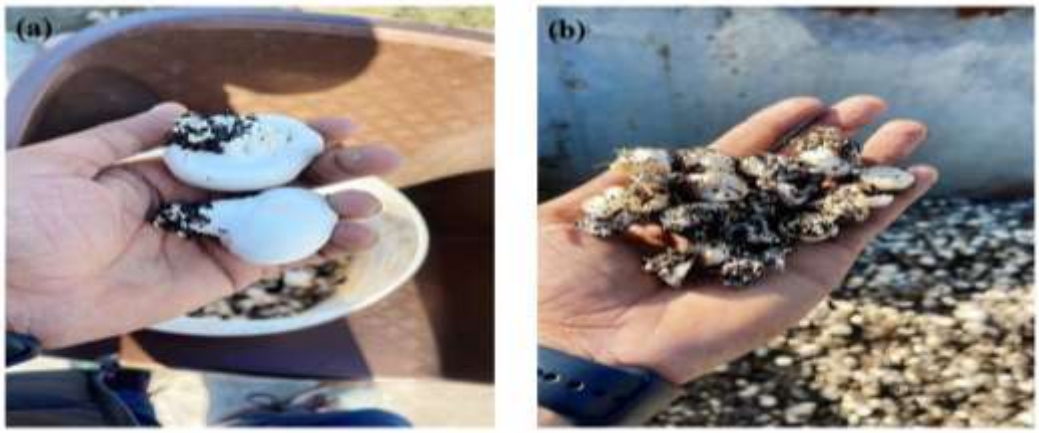

Figure 4.1. Pictorial view of (a) Raw white button mushroom (*Agaricus bisporous*) and (b) white button mushroom waste.

4.3. Drying processes

4.3.1. Freeze drying (FD)

In this study, approximately 500 g of fresh mushroom slices were used for each drying run, which would correspond to an expected yield of 50-60 g powder. The mushroom slices were frozen in a standard freezer (TEFCOLD SE-45, Viborg, Denmark), and subsequently placed in a freeze-drier (Prointech, St. Petersburg, Russia) for 24 hrs at -80 °C, and 5 mTorr pressure (Tarafdar et al., 2017). The mean working pressure within the drying chamber attained 80.0–90.0 Pa, the temperature of the condenser ranged from −49.0 to –50.0 °C, and temperature for the mushrooms throughout drying procedure should not exceed 30 °C. the mean drying duration was 46-48 hrs.

4.3.2. Vacuum drying (VD)

For vacuum drying the, to achieve a constant weight, the samples of mushrooms were washed, cut, followed by drying using vacuum oven dryer on 40 ±2°C at 100 mbar (Ucar et al., 2019). The drying time was 14-16 hrs.

4.3.3. Hybrid drying (HD)

For mushroom waste powder (MWP) mushroom stalks were prefrozen (TEFCOLD SE-45, Viborg, Denmark) and freeze dried (Prointech, St. Petersburg, Russia) at -40 ±5 °C and 80-90 Pa for around 16-18 hrs. The partially dried samples were immediately transferred to a vacuum oven

(30 ±2 °C at 100 mbar) and dried to constant weight over 4-6 hrs. This two stage stage designed to synergistically integrate the structural and quality retention benefits of FD with the energy efficiency and accelerated bound water removal characteristics of VD (Ucar et al., 2019).

4.4. Preparation of dried mushroom waste powder (MWP)

Dehydrated mushrooms, processed through several drying techniques, then pulverized in a powder utilizing a VT-1541 BK grinder (Vitek, Wien, Austria) equipped with outlet designed for the purpose of grinding solids. Grinding duration remained uniform across each and every samples, lasting 60 sec. Samples of the prepared mushroom powder for subsequent investigation were preserved in enclosed moisture free containers in a refrigeration temperature at 4 ℃.

Figure 4.2. Pictorial representation of production of mushroom waste powder (MWP) using different drying methods.

4.5. Proximate analysis of mushroom waste powder (MWP)

4.5.1. Protein

The protein content of the powder was assessed using the Kjeldahl method. This involved determining the total nitrogen content, which was then used to calculate the total protein %. A conversion rate of 6.25 was utilized to transform the nitrogen content into protein % (Ahern et al., 2023). 5 g of the material were measured and transferred into 800 ml Kjeldahl device. Into the flask, 0.5 g copper sulfate, 15 g potassium sulfate, with 40 ml of pure sulfuric acid were added, along with two to three glass beads. The mixture was digested at 420 °C for about 1.5–2 hrs until a clear pale blue (or greenish) solution was obtained. After cooling, 500 ml of water were added, followed by powdered zinc and sodium hydroxide solution to make the mixture alkaline. The flask was linked to a distillation device and 150 ml of settled mixture was taken. It was then titrated using 0.1 N NaOH after adding 5 drops of methyl red indicator. A blank titration was also performed.

4.5.2. Fat

The extraction of crude fats was modified (AOAC International, (2016) with the use of Soxhlet extraction method (SoxtecTM 2055, FossTM, Denmark). Defatted samples (2.5-3 g) were weighed in thimbles and were covered with de-fatted cotton and dried by oven at 103 ℃ for 2 h and cooled 30 min a desiccator. Thimbles and sample cups were inserted in the apparatus with 80 ml of Petroleum ether added to each sample cup. The crude fat was separated at 135 ℃ and a boiling time of 20 min and a rinsing and drying time of 40 min and 10 min respectively. Sample cups were dried in an oven at 103 ℃ at 30 min to evaporate all the solvent and then cups were weighed and the amount of crude fat was determined. Fatty acid identification was done after derivatisation of crude fat stored at -80 ℃ using the formula:

$$\text{Fat (\%)} = \frac{weight\ of\ fat\ residue\ (g)}{weight\ of\ the\ sample\ (g)} \times 100$$

4.5.3. Ash

Approximately 5 g of samples were taken in crucibles and dried in an oven at 105 ± 2 °C until they reached a constant weight. Subsequently, the samples were transferred into a muffle utilized tongs and subjected the material to ashing at 550 ± 5 °C for 4 hrs for a duration of 4 hrs till ash emerged.

The samples were subsequently extracted from the combustion chamber, cooled in a desiccator, then weighed again (AOAC International, 2002). The ash % was computed according to following formula**:**

$$\text{Ash (\%)} = \frac{weight\ of\ ash\ (g)}{weight\ of\ the\ sample\ (g)} \times 100$$

4.5.4. Moisture

The amount of moisture was assessed in accordance with AOAC method no. 945.38. About 5 g of the sample was taken to dry and clean pre-weighed crucibles. The crucibles and their contents were desiccated in a moisture removal oven at 110 °C for four hrs. The samples were subsequently chilled using desiccators and reweighed. The drying procedure was reiterated until a stable weight was attained (AOAC International, 2002).

4.5.5. Carbohydrate

The amount of carbohydrates of the material was ascertained by subtraction when the % of moisture, fat, protein, fiber, and ash were subtracted from 100% (Frances et al., 2023). The formula used was:

$$\text{Carbohydrate (\%)} = 100 - (\text{moisture \%} + \text{fat \%} + \text{protein \%} + \text{fiber \%} + \text{ash \%})$$

4.6. Powder Morphology

Exterior morphology of powdered sample obtained was examined using image analysis (Majid & Nanda, 2017). By applying a specialized AxioCam MRc5 camera and Zen 2 software, an analytical microscope using Axio ZOOM.V16 research class (Carl Zeiss Microscopy, Oberkochen, Germany) was set up to a resolution of ×25 with image fixation. Powder was taken at different parts of the vessel in order to get a good sample. Powders were organized on slides in a way that allowed for the analysis of individual particles.

4.7. Hunter color value

Color profile was obtained with Hunter lab color analyzer (Hunter Lab Colour Flex, Reston, VA, USA) (Shams et al., 2022). The color of the sample was represented by parameters L∗, a∗, and b∗,

where L∗ denotes lightness or whiteness, a∗ indicates redness or greenness, along with b∗ signifies yellowness/blueness. Equipment initially was calibrated using ordinary black with subsequently white tiles. The sample handling plate was then filled of powdered and thereafter placed over the analytical space, where the L∗, a∗, and b∗ values will be recorded.

4.8. Determination of bioactive compounds in mushroom waste powder (MWP)

4.8.1. Total phenolic content (TPC)

The total phenolic content of mushroom powder was determined using the Folin–Ciocalteu method (Singleton and Rossi, 1965; Yılmaz and Ersus Bilek, 2018). About 1 g of sample was extracted with 20 mL of 50% ethanol containing 0.1% HCl using an Ultraturrax at 6,000 rpm for 1 min, followed by incubation at 55 °C for 1 hr and centrifugation at 4,800 × g for 6 min. Then, 0.5 mL of extract was mixed with 2.5 mL of 10% Folin–Ciocalteu reagent, allowed to stand for 5 min, and 2.0 mL of 7.5% Na_2CO_3 was added. The mixture was incubated for 30 min in the dark at room temperature, and absorbance was read at 765 nm using a UV–Vis spectrophotometer. A gallic acid standard curve (0–200 mg L^{-1}) was used, and results were expressed as mg gallic acid equivalent per g dry weight (mg GAE g^{-1} d.b.).

4.8.2. Total Flavonoid content (TFC)

Total flavonoid The contents were evaluated utilizing the colorimetric method proposed by Kim & Lee, (2020), with results presented as mg catechin equivalent per gram of dry weight sample (mg CE g^{-1} d.b.).

4.8.3. Antioxidant activity (AA)

80 percent methanol extracts were evaluated for antioxidant activity (AA) using the reducing power assay technique and 1,1-diphenyl-2-picrylhydrazyl (DPPH) assay (Sigma-Aldrich). (Agunbiade et al., 2022). AA quantified using standard curve established for ascorbic acid in the DPPH assay. The DPPH and RP were quantified as IC50 (mg/ml) and EC50 (mg/ml), accordingly Lower values of IC50 (minimum concentration of sample required to prevent 50% of DPPH activity) and EC50 (concentration showing 50% absorbance) indicate enhanced DPPH scavenging capacity and RP correspondingly. % radical scavenging by DPPH was determined via equation provided below:

$$\text{DPPH Radical scavenging (\%)} = (Ac - A) / Ac \times 100$$

Where, Ac = Absorbance of the control, A = Absorbance of the sample

4.8.4. Ascorbic acid content

Ascorbic acid content was estimated using the 2,6-dichlorophenol-indophenol (DCPIP) titration method following Nielson (2017). The dye was standardized with ascorbic acid standard solution in 3% metaphosphoric acid (HPO_3), yielding a dye factor of 0.5 mg/mL. For analysis, 1 g of sample was extracted with 10 mL of 3% HPO_3, and a 5 mL aliquot was titrated against the dye to a light pink endpoint. Results were expressed as mg ascorbic acid per 100 g sample (mg/100 g) using the standard titration formula.

$$\text{Ascorbic acid (mg/100 g)} = Titre \times Dye\ factor \times Volume\ of\ extract / Aliquot\ of\ extract \times weight\ of\ sample\ taken \times 100$$

4.9. Determination of flow properties of mushroom waste powder (MWP)

4.9.1. Bulk density

In brief, 1 g of mushroom waste powder was put into standard 10 ml measure cylinder without hitting it. Bulk density was thereafter expressed in g/ml (Jindal et al., 2013).

4.9.2. Tapped density

For tapped density, 1 g of CS powder was placed in a 10 ml standard measuring cylinder and the contents of the cylinder were tapped gently for 2 min. The tapped density was also expressed as mg/ml (Jindal et al., 2013).

4.9.3. Hasneur ratio

The Hausner ratio, which assesses flowability, is defined as the proportion of tapped density to bulk density, expressed by the following equation (Jindal et al., 2013):

$$\text{Hasneur ratio} = \frac{Tapped\ density\ (mg/ml)}{Bulk\ density\ (mg/ml)}$$

4.9.4. Carr's index

Carr's index serves as a quantification of compressibility which is determined by the subsequent equation (Jindal et al., 2013):

$$\text{Carr's index (\%)} = \frac{Tapped\ density\ (mg/ml) - bulk\ density\ (mg/ml)}{Tapped\ density\ (mg/ml)} \times 100$$

4.10. Characterization of prepared mushroom waste powder (MWP)

4.10.1. Fourier transform infrared (FTIR) spectroscopy

FTIR (Spectrum 100, PerkinElmer, USA) analysis of prepared MWP powder was carried out in order to examine any changes in the structure of the fibers during the process of drying upon using various methods. The samples were powdered and mixed with KBr to prepare pastilles, and then pressed into thin plates for FTIR analysis. FTIR Spectra were taken from 4,000 to 400 cm^{-1}, at a resolution for 4 cm^{-1} (Li et al., 2014).

4.10.2. X-ray powder diffractometry (XRD)

XRD investigation of the obtained MWP powder was conducted using an EcoX-ray diffractometer (Deutsch D8 Advance ECO-Bruker). Particle size was controlled to be as large as 200 μm, and the pattern of diffraction was analyzed using means of Cu-Kα radiation with a wavelength of 1.54 Å, covering angle ranges from 5° to 50°. The crystallinity index (CI) can be calculated by using the Segal equation shown in equation below (Kallel et al., 2016):

$$\text{CI} = 100 \times \frac{I_{002} - I_{am}}{I_{002}}$$

where I_{002} and I_{am} are the peak intensities at crystalline and amorphous regions respectively.

4.10.3. Thermogravimetric analysis (TGA)

The thermal endurance of each sample was evaluated utilizing a Thermogravimetric Analyser (Q5000 series, TA Instruments, USA). Approximately sample of 10 mg was heated using open alumina pans in a helium environment, starting at 30 °C up to approximately 800 °C with

10 °C/min heating rate. % moisture content was measured from the TGA thermogram using TA Universal Analysis software (Hassainia et al., 2019).

4.10.4. Field Emission Scanning Electron Microscope (FE-SEM)

The surfaces of the powder particle structures were observed using a Field emission scanning electron microscopy (FE-SEM) (MIRA-LMU, Tescan, BrnoKohoutovice, Czech). Thoroughly mixed samples of mushroom waste powders were applied to conductive carbon tape and covered with a thin layer of carbon (10 nm) using a QR 150 spraying system. Images with different magnification were taken for each sample (Piskov et al., 2022).

4.10.5. Statistical analysis

All experiments were conducted in triplicates. The results were presented as mean ± standard deviation. SPSS software (version 16.0, IBM, Chicago, IL, USA) was used to carry out statistical analyses. Mean values were considered significant at 95% confidence level ($p < 0.05$).

4.11. Methodology for isolation of chitosan (CS) from mushroom waste powder (MWP)

The extraction of CS from MWP was accomplished using three sequential steps: Demineralization, deproteinization, and deacetylation, each carried out for a fixed duration of 8 min (El Knidri et al., 2016). Demineralization was conducted in a glass beaker positioned within domestic microwave oven (Model IFB 30BRC2, India). 10 g of powdered sample was treated with a solution of 3M HCl at a ratio of 1:10 (sample to solvent) and heated for 8 min at various power levels (as shown in Table 4.1) Subsequently, the mixture was filtrated and rinse off three times using distilled water prior being dried at 40±2 °C temperature. For deproteinization, the sample was poured in glass beaker within a home held microwave oven (Model IFB 30BRC2, India). Then it was blended with a 10% NaOH solution at 1:10 ratio (sample to solvent) and heated for 8 min at various power levels, as indicated in Table 1 and Figure 4.3. Subsequently, the solution was filter out and wash off three times with distilled water before being dried at 40±2 °C temperature. Deacetylation was conducted in a glass beaker within a domestic microwave oven (Model IFB 30BRC2, India). Sample was merged using 50% NaOH solution at 1:20 ratio (sample to solvent) and heated for 8 min at various power levels as shown in Figure 4.4. For demineralization, 10g of MWP was mixed using 1 M HCl aqueous solution at a 1:15 solid-to-solution ratio. This process took place in a water

bath shaker (Memmert GmbH, Wisconsin, USA) at 30 ±2 °C, with continuous stirring in at 200 rpm for 2 hrs to eliminate calcium carbonate and other calcium salts (Omer et al., 2019). Subsequently, for deproteination, the extract was treated with a 1 M sodium hydroxide solution at a 1:15 w/v ratio. This mixture was then refluxed using magnetic stirrer with hot plate (Model DBK 30MAG12D, India) (at 90±2 °C for 2 hrs to remove proteins and fats (Omer et al., 2019). The extracted chitin was then deacetylated using a 60 wt% NaOH aqueous solution at a 1:15 w/v ratio. This process was conducted in a 100±2 °C water bath with agitation (Model SI- SWB/30LTPID Microprocessor, India) at 200 rpm for 8 hrs as shown in Figure 4.4. Afterwards, the mixture was strained and thoroughly washed with deionized water before being dried at a temperature of 40±2 °C. The extracted CS was packaged within low density polyethylene (LDPE) afterwards retained in a refrigerator at 4±2 °C prior the study was completed.

Table 4.1 Treatment details for extraction of chitosan (CS) at various power levels.

Treatments	Demineralization (8 min; 3M HCl in 1:10)	Deproteination (8 min; 10% NaOH in 1:10)	Deacetylation (8 min; 50% NaOH in 1:20)
T1	360W	180W	360W
T2	360W	180W	540W
T3	360W	360W	360W
T4	360W	360W	540W
T5	540W	180W	360W
T6	540W	180W	540W
T7	540W	360W	360W
T8	540W	360W	540W

W=Watt

Figure 4.3. Microwave assisted extraction method of chitosan from mushroom waste powder (MWP).

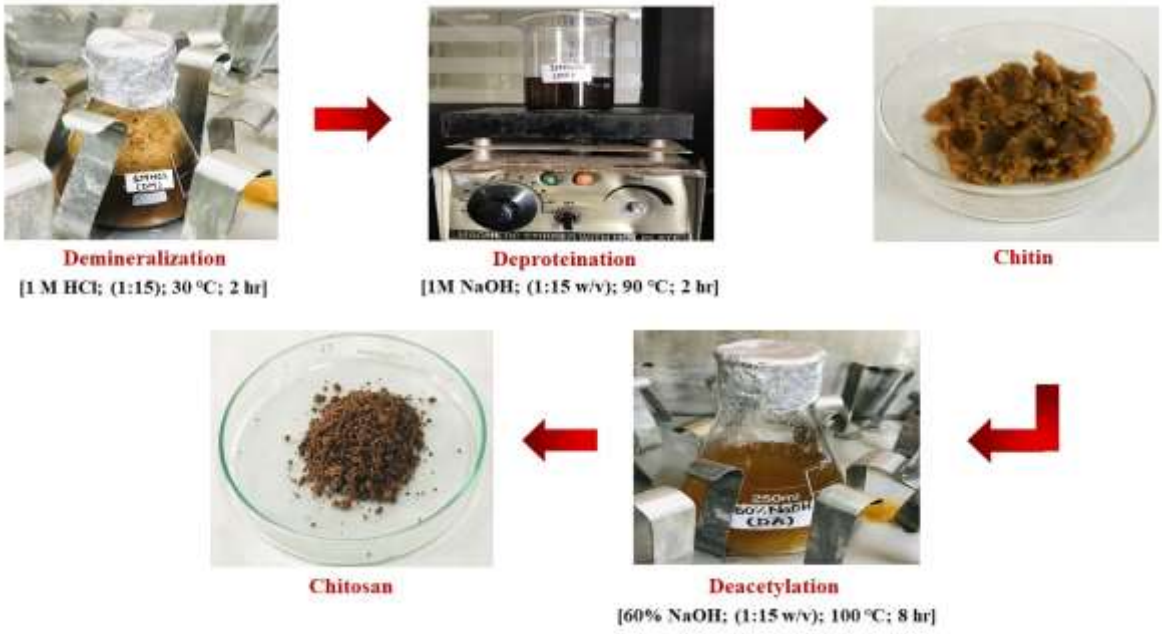

Figure 4.4. Traditional extraction method of chitosan from mushroom waste powder (MWP).

4.12. Techno-functional properties of extracted chitosan powder

4.12.1. Yield

After measuring the amount of CS that was extracted, the yield was measured employing equation below (Agarwal et al., 2018):

$$\text{Yield (\%)} = \frac{Practical\ yield\ (g)}{Theoritical\ yield\ (g)} \times 100$$

4.12.2. pH and Solubility

Using a pH meter, the CS solution's pH was measured (LT-50 microprocessor pH meter, India) by placing a 5g sample into a clean and dry 150 ml beaker holding 40 ml of deionized water, stirring, and centrifuging for 5 min using centrifuge (REMI R-02, mini centrifuge, India), the pH of the supernatant was assessed. CS powder (0.2 g) excerpted was blended in a 20 ml solution of 1% acetic acid in beaker. This mixture was then blent on a magnetic stirrer (REMI 2 MLH magnetic stirrer, India) about 250 rpm for 30 min around 25 °C temperature. Then, solution was strained using a Millipore 20μ nylon membrane filtration assembly. Insoluble portion is known as the retardant, accumulated on membrane filter, was rinsed using water that has been distilled. The subsequent equation was employed to ascertain the solubility for CS:

$$\text{Solubility (\%)} = 100 - \left[\frac{Weight\ of\ insoluble\ fraction}{Initial\ weight\ of\ the\ sample}\right] \times 100$$

4.13. Determination of flow properties of extracted chitosan

4.13.1. Bulk density (BD)

In brief, 1 gram of powdered CS was put into standard 10 ml measure cylinder without hitting it. Bulk density was thereafter expressed in g/ml (Jindal et al., 2013).

4.13.2. Tapped density (TD)

Regarding tapped density, 1 g of powdered CS was dropped in 10 ml standard weighing cylinder, and cylinder was hit repeatedly about 2 min. Tapped density was additionally represented as mg/ml (Jindal et al., 2013).

4.13.3. Hasneur ratio (HR)

Proportion of tapped density compared to bulk density assesses flowability and is referred to as the Hausner ratio, represented by the subsequent equation (Jindal et al., 2013):

$$\text{Hasneur ratio} = \frac{Tapped\ density\ \ (mg/ml)}{Bulk\ density\ (mg/ml)}$$

4.13.4. Carr's index (CI)

Carr's index serves as a quantification of compressibility which is determined by the subsequent equation (Jindal et al., 2013):

$$\text{Carr's index (\%)} = \frac{Tapped\ density\ (mg/ml) - bulk\ density\ \ (mg/ml)}{Tapped\ density\ \ (mg/ml)} \times 100$$

4.13.5. Degree of deacetylation (DD) of extracted chitosan powder

An infrared spectroscopy (IR) approach used to assess how much of deacetylation degree (DD) in CS. The baseline for calculating the DD was established accordingly described by (Zhang et al., 2012) and the computational equation is presented in equation below:

$$DD = 100 - \left[\frac{A1655}{A3450} \times 100\right] / 1.33$$

A1665 and A3450 represent absorbance values on 1655 cm^{-1} for the amide-I band, reflecting the N-acetyl molecule content, while at 3450 cm^{-1} over the hydroxyl group, employed as an internal reference to adjust the film thickness and variations in concentration of CS powder. Factor '1.33' denotes the ratio of A1665/A3450 for completely N-acetylated CS presuming that for complete deacetylated CS the ratio had a value of zero.

4.13.6. Crystallinity

Crystallinity index of CS powder was additionally assessed through FTIR analysis using a Perkin Elmer instrument (Spectrum 100, PerkinElmer, USA). Formula for computing crystallinity is provided in equation below (Agarwal et al., 2018):

$$CI= \frac{A1379}{A2929}$$

Where, A1379 and A2929 are the absorbance at 1379 cm^{-1} and 2929 cm^{-1}

4.14. Determination of bioactive compounds in extracted chitosan powder

4.14.1. Antioxidant Activity (AA)

Scavenging activity of CS on 1,1-diphenyl-2-picrylhydrazyl (DPPH) radicals (D4313-TCI America) was evaluated using a modified method from (Pasanphan et al., 2015). CS samples (from 0.125 to 1.0 mg/ml) in 0.2% solution of acetic acid (A9705-Sigma-Aldrich) were admixed with 1 ml from a methanolic DPPH the solution, yielding ultimate DPPH concentration of 1.0 mM. Mixture was then vigorously agitated then permitted to sit in darkness for 30 min, following that absorbance recorded at 517 nm relative to blank. Ascorbic acid (PHR1008-Sigma-Aldrich) served as the reference standard. Scavenging capacity was then computed using formula below:

$$\text{Antioxidant activity (\%)} = \frac{A517\ of\ control - A517\ of\ sample}{A517\ of\ control} \times 100$$

4.14.2. Reducing Power Assay (RP)

The reducing power (RP) was assessed following the method of (Pasanphan et al., 2015). CS samples (0.125 to 1.0 mg/ml) were combined using 2.5 ml of buffered phosphate (0.2 M, pH 6.6) (76847-Sigma-Aldrich) and 2.5 ml of 1% potassium ferricyanide (P1979- TCI America). The reaction solution underwent incubation within water bath (STXUWB25, India) on 50 °C over 20 min. Following that, 2.5 ml of 10% trichloroacetic acid (T6399- Sigma-Aldrich) was appended, then the centrifugation of the mixture was completed at 3,000 rpm for 10 min using centrifuge

(REMI R-02, mini centrifuge, India). 2.5 ml of the solution from upper layer was combined with 2.5 ml of deionized water and 0.5 ml of 0.1% ferric chloride (157740-Sigma-Aldrich). The absorbance for the resulting solution has been determined at 700 nm, with rise in absorbance indicating higher reducing power.

4.15. Characterization of extracted chitosan powder

4.15.1. Fourier Transform Infrared Spectroscopy (FTIR)

FTIR analysis of prepared CS powder was measured to detect and recognize the appearance of functional groups, components and nature of bonding. Various samples were analyzed using a Perkin Elmer instrument (Spectrum 100, PerkinElmer, USA) having resolution of 4 cm^{-1} within 4000 to 400 cm^{-1} range (Liu et al., 2013).

4.15.2. X-ray powder diffractometry (XRD)

The crystalline characteristics of the extracted CS powder were analyzed using an Eco X-ray diffractometer (Deutsch D8 Advance ECO-Bruker) following the method of Agarwal et al. (2018). The analysis employed Cu–Kα radiation (λ = 1.54 Å) over a 2θ range of 5°–50° with a step size of 0.02°. Powdered samples (<200 μm) were scanned at room temperature, and the resulting diffraction patterns were used to evaluate the crystallinity and structural properties of the CS powder.

4.15.3. Thermogravimetric analysis (TGA)

Thermal endurance of each sample was evaluated utilizing Thermogravimetric Analyser (Q5000 series, TA Instruments, USA). Approximately sample of 10 mg was heated using open alumina pans in a helium environment, starting at 30 °C up to approximately 800 °C with 10 °C/min heating rate. % moisture content was measured from the TGA thermogram using TA Universal Analysis software (Hassainia et al., 2018).

4.15.4. Differential scanning calorimetry (DSC)

Thermal property of CS samples was analyzed through Differential Scanning Calorimeter (DSC), model SDT Q600 from TA Instruments. Samples were weighed and laid in hermetic pans and subjected to heating at 25 °C up to 700 °C at a rate of 5 °C/min (Gichuki et al., 2022).

4.16. Methodology for isolation of cellulose from mushroom waste powder (MWP)

Cellulose fibers have been separated and purified form dried MWP through microwave-assisted chemical procedure (Li et al., 2014). 10 g of MWP was added to 150 mL of different strength of (w/v) NaOH solution was thereafter exposed to microwave irradiation at different power level and time combination (as shown in Table 4.2). Mushroom pulp derived from the combining microwave along with alkali treatment was subsequently filtered and rinsed three times using distilled water until neutralization was achieved. The samples underwent microwave-assisted bleaching to eliminate remaining hemicellulose and lignin potentially present in the neutralized sample. Neutralized sample has been bleached by immersion in 5 % H_2O_2 and subjected to microwave heating at 540 W for 2 min as shown in Figure 4.5. Bleached pulp went through filters and rinsed using distilled water till it achieved a neutral pH followed by drying at 35± 5°C.

Table 4.2. Treatment details for extraction of cellulose at various power levels.

Treatments	Delignification (3min)	Bleaching (2min)
T1	180W (4% NaOH)	540W
T2	180W (8% NaOH)	540W
T3	180W (12% NaOH)	540W
T4	360W (4% NaOH)	540W
T5	360W (8% NaOH)	540W
T6	360W (12% NaOH)	540W
T7	540W (4% NaOH)	540W
T8	540W (8% NaOH)	540W
T9	540W (12% NaOH)	540W
T10	720W (4% NaOH)	540W
T11	720W (8% NaOH)	540W
T12	720W (12% NaOH)	540W

W: Watt

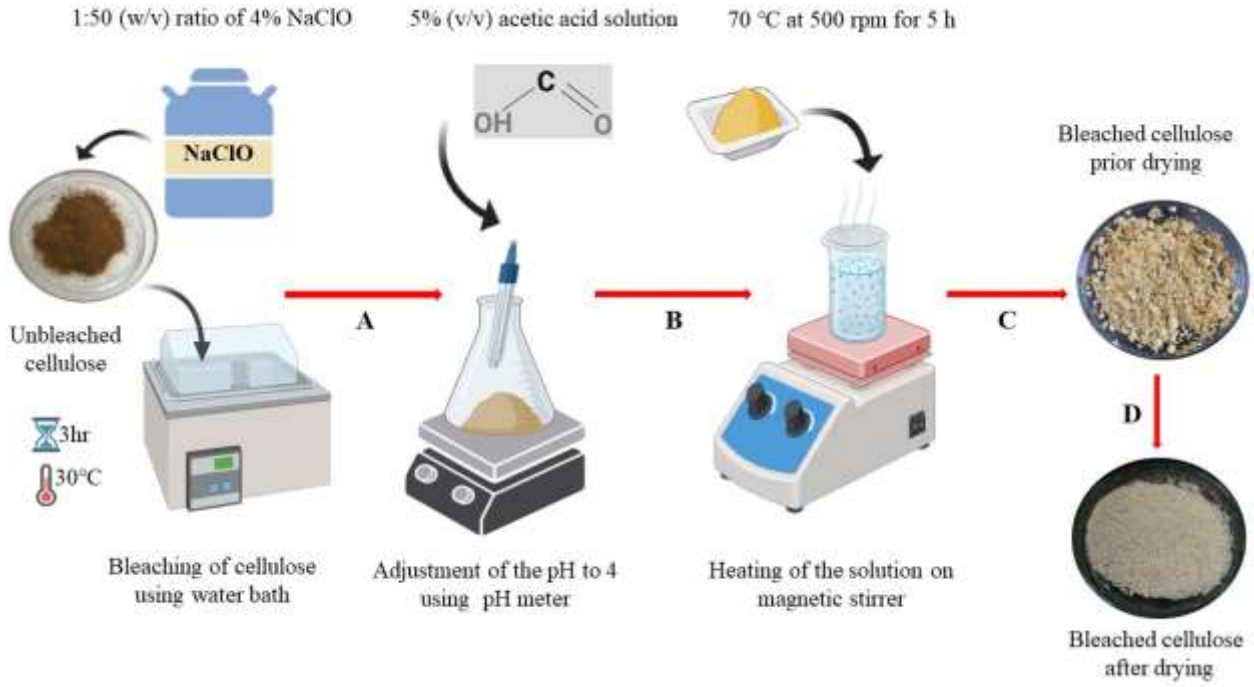

Figure 4.5. Methodology for bleaching of extracted cellulose using sodium hypochlorite (NaClO).

4.17. Techno-functional properties of extracted cellulose powder

4.17.1. Yield

After measuring the amount of CS that was extracted, the yield was measured employing equation below (Agarwal et al., 2018):

$$\text{Yield (\%)} = \frac{Practical\ yield}{Theoritical\ yield} \times 100$$

4.17.2. pH and Solubility

Using a pH meter, the cellulose solution's pH was measured (LT-50 microprocessor pH meter, India) by placing a 5g sample into a clean and dry 150 ml beaker holding 40 ml of deionized water, stirring, and centrifuging for 5 min using centrifuge (REMI R-02, mini centrifuge, India), the pH of the supernatant was assessed. Cellulose powder (0.2 g) excerpted was blended in a 20-milliliter

solution of 1% acetic acid in beaker. This mixture was then blent on a magnetic stirrer (REMI 2 MLH magnetic stirrer, India) about 250 rpm for 30 min around 25 °C temperature. Then, solution was strained using a Millipore 20µ nylon membrane filtration assembly. Insoluble portion is known as the retardant, accumulated on membrane filter, was rinsed using water that has been distilled. The following equation was used to determine the solubility for cellulose:

$$\text{Solubility (\%)} = 100 - \left[\frac{Weight\ of\ insoluble\ fraction}{Initial\ weight\ of\ the\ sample} \right] \times 100$$

4.18. Determination of flow properties of extracted cellulose

4.18.1. Bulk density

In brief, 1 g of cellulose powder was put into a standard 10 ml measure cylinder without hitting it. The bulk density was then written as g/ml (Jindal et al., 2013).

4.18.2. Tapped density

Regarding tapped density, 1 g of powdered cellulose was dropped in a 10 ml standard weighing cylinder, and the cylinder was hit repeatedly for 2 min. The tapped density was additionally represented as mg/ml (Jindal et al., 2013).

4.18.3. Hasneur ratio

The ratio of tapped to bulk density gives the measure of flow ability and is known as Hasneur ratio as given by the following equation (Jindal et al., 2013):

$$\text{Hasneur ratio} = \frac{Tapped\ density\ \ (mg/ml)}{Bulk\ density\ (mg/ml)}$$

4.18.4. Carr's index

Carr's index is the measure of compressibility and is calculated using the following equation (Jindal et al., 2013):

$$\text{Carr's index (\%)} = \frac{Tapped\ density\ (mg/ml) - bulk\ density\ \ (mg/ml)}{Tapped\ density\ \ (mg/ml)} \times 100$$

4.19. Determination of total cellulose content in mushroom waste powder (MWP)

First, put 3 mL of the acetic/nitric solution into a test tube with an estimated quantity of sample (either 0.5 g or 1 g). Then, use a vortex mixer to mix the sample well. After that, put the sample tube within a water bath that is 100°C over 30 min. After that, let the tube cool down, and then spin the inside for 15 to 20 min. Dispose of the supernatant and use distilled water to wash the residues. The residues should be mixed with 10 mL of 67% H_2SO_4 and left alone for 1 hr. As shown in Table 4.3, dilute 1 mL of the solution until it has a final amount of 100 mL. Take 10 mL of the anthrone reagent and add 1 mL of the diluted solution. Make sure the contents are well mixed. Take the tube out of the hot water and let it cool down. Then, use 630 nm to measure the color. Use anthrone reagent and pure water to set a blank. For the standard, put 100 mg of cellulose within a test tube and add 1 mL of the solution to cool it down. Then do the rest of the steps as state above. Use a range of amounts from 0.4 to 2 mL, which is equal to 40 to 200 mg of cellulose, to create the color in the same way that is shown in Figure 4.6. and measure the cellulose in the sample by drawing the usual graph (Updegroff et al., 1969).

Table 4.3. Determination of total cellulose content in mushroom waste powder (MWP).

Concentration of cellulose	Amount of cellulose 1mg/ml cellulose	Sterile water to a final volume of 1ml
0 µg	0 µl	10000 µl
20 µg	20 µl	980 µl
40 µg	40 µl	960 µl
60 µg	60 µl	940 µl
80 µg	80 µl	920 µl
100 µg	100 µl	900 µl

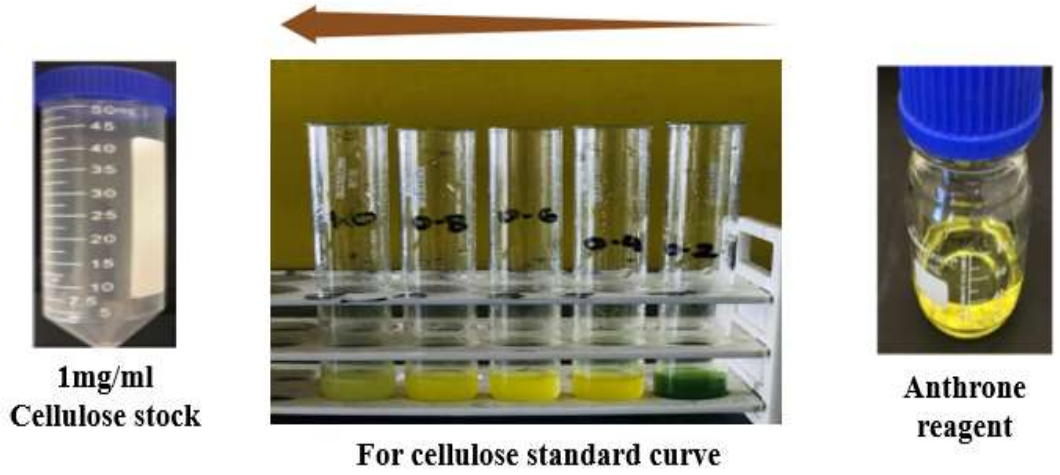

Figure 4.6. Determination of total cellulose content in mushroom waste powder (MWP).

4.20. Characterization of extracted cellulose

4.20.1. Fourier transform infrared (FTIR) spectroscopy

FTIR (Spectrum 100, PerkinElmer, USA) analysis of prepared cellulose powder was conducted to investigate alterations in the fiber structure during the process (Delignification and bleaching). Samples were mixed using KBr to prepare pastilles, further pressed inside the thin plates for FTIR analysis. FTIR Spectra were taken from 4,000 to 400 cm^{-1}, at a resolution for 4 cm^{-1} (Li et al., 2014).

4.20.2. X-ray powder diffractometry (XRD)

XRD investigation of the obtained powdered cellulose was conducted using an EcoX-ray diffractometer (Deutsch D8 Advance ECO-Bruker). Particle size was controlled to be as large as 200 μm, and the pattern of diffraction was analyzed using means of Cu-Kα radiation with a wavelength of 1.54 Å, covering angle ranges from 5° to 50°. The crystallinity index (CI) can be calculated by using the Segal equation shown in equation below (Kallel et al., 2016):

$$CI = 100 \times \frac{I_{002} - I_{am}}{I_{002}}$$

where I_{002} and I_{am} are the peak intensities at crystalline and amorphous regions respectively.

4.20.3. Thermogravimetric analysis (TGA)

Thermal endurance of each sample was evaluated utilizing a Thermogravimetric Analyser (Q5000 series, TA Instruments, USA). Approximately sample of 10 mg was heated using open alumina pans in a helium environment, starting at 30 °C up to approximately 800 °C with 10 °C/min heating rate. % moisture content was measured using TGA thermogram via TA Universal Analysis software (Hassainia et al., 2019).

4.20.4. Differential scanning calorimetry (DSC)

Thermal property of cellulose samples was analyzed through Differential Scanning Calorimeter (DSC), model SDT Q600 from TA Instruments. Samples were weighed and laid in hermetic pans and subjected to heating at 25 °C up to 700 °C at rate of 5 °C per min (Gichuki et al., 2022).

4.20.5. Statistical analysis

All experiments were conducted in triplicates. The results were presented as mean ± standard deviation. SPSS software (version 16.0, IBM, Chicago, IL, USA) was used to carry out statistical analyses. Mean values were considered significant at 95% confidence level ($p < 0.05$).

4.21. Bleaching of optimized cellulose

The produced powder was decolorized with 50 mL of 4% sodium hypochlorite at 30 ℃ over 3 hrs. The solid-to-liquid ratio was established at 1g of powder with 50ml of bleaching reagent solution. This step was done twice. The sample's pH was modified to 4 by employing a 5% (v/v) acetic acid solution, thereafter heated to 70℃ with continuous agitation via an overhead stirrer at 500 rpm for 5 hrs. Following bleaching, pH was neutralized with deionize water, and bleached fibers were maintained at 60 ℃ in hot-air oven till fully dried (Umesh et al., 2022).

4.22. Synthesis of nanocellulose (NC) from cellulose

The stable cellulose based films was not feasible to prepare due to low solubility as shown in Figure 4.7. thus it became necessary to modify cellulose into NC for the preparation of films. Acid hydrolysis was performed on the bleached substance to isolate micro cellulose. During this procedure, 10 g of bleached cellulose has been hydrolyzed using 60% sulfuric acid for 2 hrs at a

fiber-to-acid ratio of 1:30, while being continuously and vigorously stirred with a rapid magnetic stirrer (Figure 4.8). At the conclusion of the reaction period, the reaction of hydrolysis was terminated by the addition of distilled water. Surplus acid has to be eliminated using centrifugation at 10,000 ×g for 10 min till pH attained 7.0. Subsequently material drying occurred in tray drier using 55℃ over 24 hrs, crushed into a fine powdered form, and kept in sealed glass containers for subsequent experimental investigation (Chawla et al., 2023).

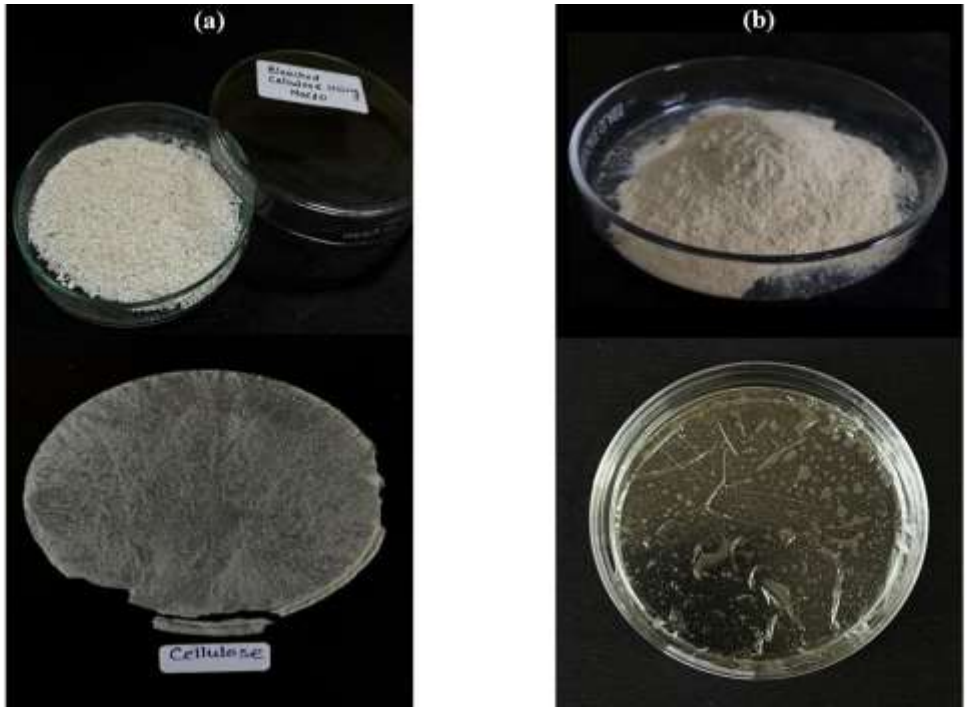

Figure 4.7. Pictorial view of (a) pure cellulose film and (b) Nanocellulose (NC) film.

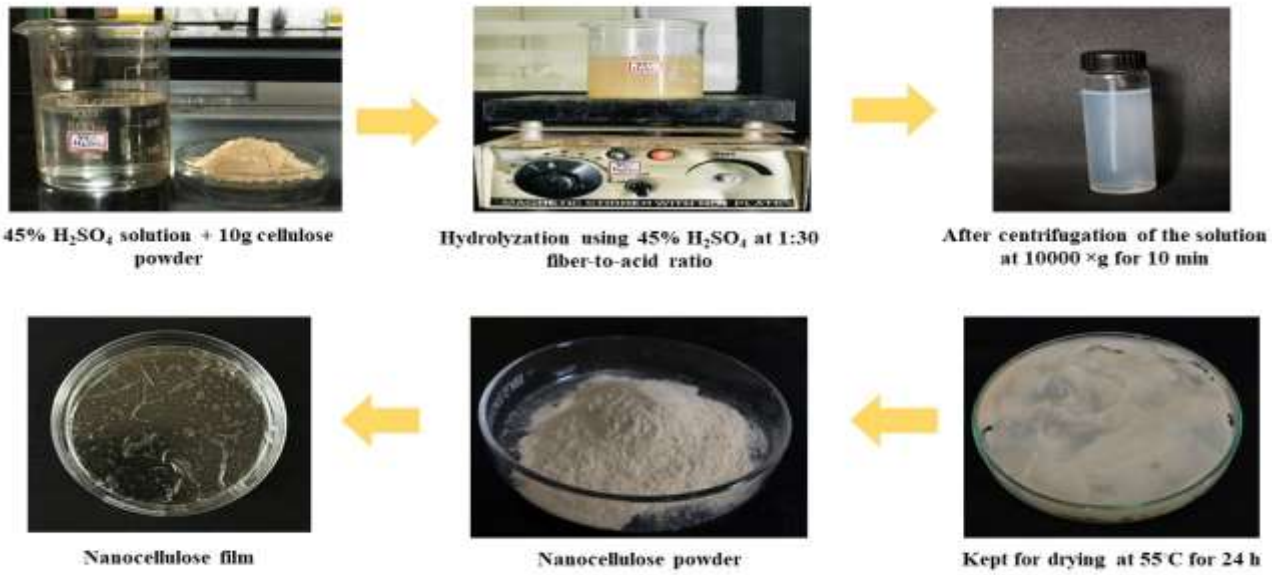

Figure 4.8. Schematic representation of preparation of cellulose derivative as Nanocellulose (NC).

4.23. Characterization of Nanocellulose (NC)

4.23.1. Yield

Weight of the synthesized NC was quantified also the yield was computed using the equation below (Agarwal et al., 2018):

$$\text{Yield (\%)} = \frac{Practical\ yield}{Theoritical\ yield} \times 100$$

4.23.2. The particle size of the Nanocellulose (NC)

Particle size of the NC was noted using zeta potential analyzer (Zetasizer Nano ZS, Malvern Instruments Ltd. Malvern, WR14 1XZ, UK) according to Guo et al. (2020). Briefly, the 100 mg sample of NC was combined with 10 mL of 0.01 mM phosphate buffer inside polystyrene latex cell along with subjected to ultrasonication using a probe sonicator (Sonics and Materials Inc.,

New Town, CT, USA). Measurements were subsequently conducted using the detector positioned perpendicularly, at 25°C along with a wavelength of 633 nm. The overall charge surface distribution and particle dimensions of the cellulose were ascertained.

4.24. Preparation of multilayer films using optimized chitosan and nanocellulose (NC)

4.24.1. Preparation of film forming solutions

Film-forming solution: The specified quantities of NC (2g, 3g and 4g) were evenly distributed in 100 mL of deionized water, to which 30% (w/v) glycerol was incorporated. The mixture was agitated at 1200 rpm on a magnetic stirrer hot plate for 45 min at 70 ℃ until a homogeneous dispersion was obtained (Jannatyha et al., 2020). For CS solution take desired amount of extracted CS (1g, 1.5g and 2 g) powder of extracted CS powder add 30% (w/v) weight of glycerol to it The mixture was agitated at 5000 rpm using a magnetic stirrer hot plate for 7-8 hrs at a temperature of 70-80 ℃ till an even dispersion was achieved. All CS solutions underwent filtration using 0.45 μm pore-size PTFE as filter membranes to eliminate impurities (Qiao et al., 2021). For Resveratrol (RES) solutions, To the previously made NC solution, 100 mg of RES dissolved in 96% ethanol was added. After that, they were mixed for 4 min at 13,500 rpm using a rotor-stator (Ultraturrax DI25). During handling, the RES solution was kept in amber glass flasks to prevent light exposure (Pastor et al., 2013).

4.25. Preparation of multilayer film using layer by layer (LBL) assembly

4.25.1. Preparation of control films

The process began with the casting of 20-25 mL of CS film formation solution at different concentrations onto a long horizontal glass plate with dimensions of 177 cm2 and a diameter of 15 cm^2. The plate was subsequently dried at 35±5 °C until it became solid but still sticky, a condition known as semi-drying. After that, the aforementioned CS semi dried film to form the second layer was doused with 10 mL of a film-forming solution of NC at several concentrations followed by drying at 35±5 °C. The dried films were maintained at normal temperature with 50% relative humidity over a minimum of 48 hrs for subsequent analysis. (Pastor et al., 2013). Pure NC and CS (RES free) were characterized as control (as shown in Table 4.4.).

Table 4.4. Different formulations for preparation of films without RES (Control films).

Polysaccharide	T1	T2	T3
CS (g)	1	1.5	2
NC (g)	2	3	4

4.25.2. Preparation of treated films

In order to preparation of CS-RES-NC films containing RES, In 100 ml of sterile water, 1.5 g of powdered NC was dissolved. To get a homogenous solution, film solution was agitated with a magnetic stirrer for 45 min at 70 °C and 1200 rpm in order to disperse the NC entirely. To make the solution more flexible, 0.3 ml of glycerol (30% v/w depending on NC weight) was added and mixed at 70 °C for 10 min. Afterwards, the resulting solution was brought down to 55°C and a range of RES concentrations (4, 8, 12 and 16 µg/ml) were added to the solution being used to produce the film. Next, the solutions that formed the film were mixed using an ultra-turrax homogenizer (IKA T10 Basic) set to 13,500 rpm for three min while the mixture was left at room temperature. The last step was to pour 25 ml of the CS film-forming solutions onto Teflon plates with a diameter of 10 cm and then to dry them in the oven for approximately 10 h at 30 °C ± 5 (as in Figure 4.9). Once the CS-RES films are semi dried or partially dried/moist, 20 ml of NC suspension was poured on the top of that and kept for drying. The dried films were subsequently removed out of the plates and preserved in a dehydrator at 25 °C and 53% of relative humidity prior to testing. Before testing, the films were subjected to ultraviolet radiation for 2 min under a laminar hood to remove possible pollutants (Dashipour et al., 2015).

The process was repeated in the following pattern: CS-RES (4 µg/ml)-NC, CS-RES (8 µg/ml)-NC, CS-RES (12 µg/ml)-NC and CS-RES (16 µg/ml)-NC were labeled as T1, T2, T3 and T4 respectively with T0 as the control (No RES) (as shown in Table 4.5).

All films were segmented into pieces measuring 7 × 7 cm, 2 × 2 cm and 2.54 × 15 cm. for the measurement of color and optical properties, water vapor transmission rate (WVTR), Oxygen transmission rate (OTR) water solubility (WS) and tensile strength (TS) along with elongation at break (EB), respectively.

Table 4.5. Different formulations for preparation of films with RES (Treated films).

Polysaccharide	T1	T2	T3	T4
CS (g)	1.5	1.5	1.5	1.5
RES (µg/ml)	4	8	12	16
NC (g)	3	3	3	3

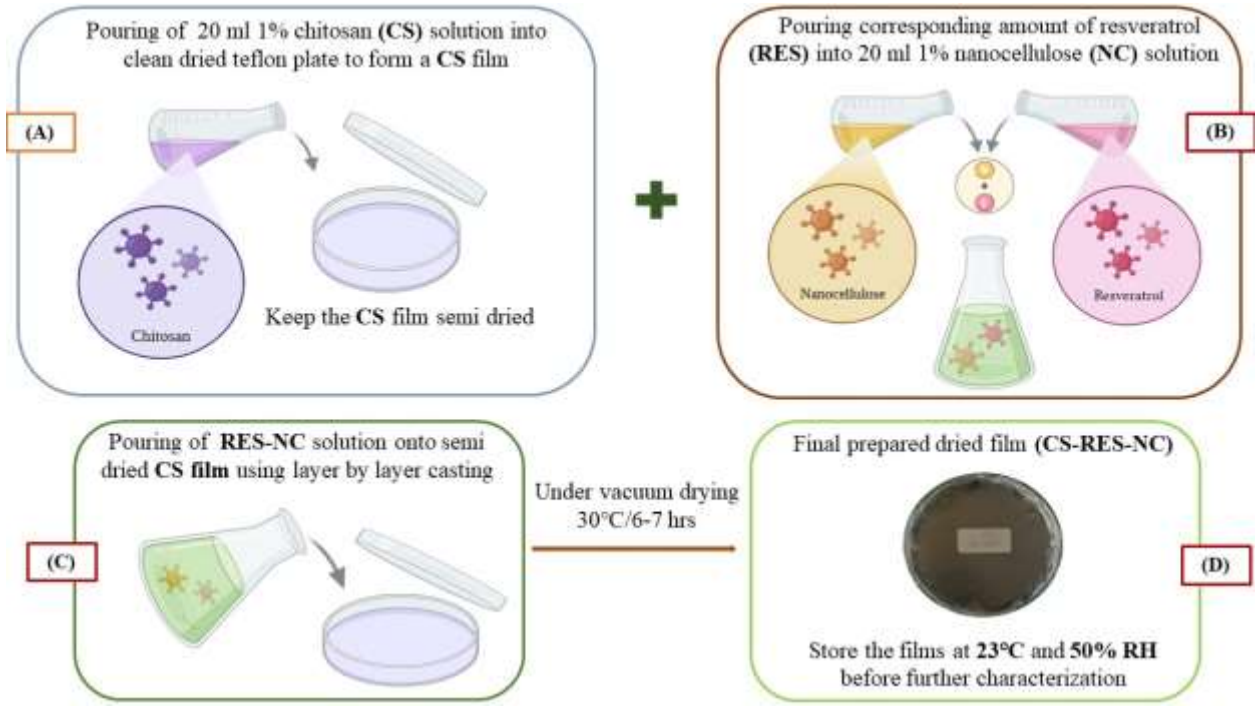

Figure 4.9. Schematic representation of preparation of multilayer film (CS-RES-NC)

4.26. Apparent color and optical properties of the control film

4.26.1. Visual analysis of the control films

Films were subjected to visual analysis by assessing their homogeneity, specifically regarding consistent colors and the existence of insoluble particles (Liu et al., 2015).

4.26.2. Hunter color properties

The color parameters of film samples were analyzed by Dr. Lange Micro Color II LCM6 Colorimeter (Apeldoorn, The Netherlands) by following the method reported by Olewnik-Kruszkowska et al. (2022) with minor changes. The white plate was used as a reference. For the film color characterization, (L*), (a*), and (b*) values were measured L represents lightness, a indicates green-red, and b signifies blue-yellowness. The present study identifies L*, a*, and b* as components of a control sample (NC film). Five measurements were obtained for each film type at various points, followed by the calculation and reporting of the average value and standard deviation. The equations used for calculating overall color difference (ΔE) and yellow index (YI) are as follows:

$$\Delta E = [(L-L^*)^2 + (a-a^*)^2 + (a-a^*)^2]^{1/2}$$

$$YI = \frac{(142.86 \times b)}{L}$$

4.26.3. Light transmission and transparency

Film samples were divided into rectangles measuring 1 cm × 4 cm and subsequently positioned within the spectrophotometer test cell (Akhtar et al., 2023). The ultraviolet–visible (UV) spectrum of the films was obtained in the range of 200 to 800 nm utilizing an UV spectrophotometer (UV-1800, Shimadzu Corporation), with an empty cell serving as the reference. Transparency was assessed through determining its absorbance at 600 nm, calculated using the following equation below:

$$\text{Transparency } \left(\frac{A600}{x}\right) = \frac{-logT600}{x}$$

T600 represents the efficiency of transmission at 600 nm, A denotes the absorbance at 600 nm, and x indicates the film thickness in millimeters.

4.27. Measurement of physical properties of the control films

4.27.1. Thickness measurement

Thickness of NC-RES-CS films was assessed by measuring at eight distinct points through a digital micrometer Sylvac S229 Swiss (Yverdon, Switzerland). Results were presented as average values with standard deviation (SD).

4.27.2. Tensile strength (TS) and elongation at break (EB)

Tensile strength (TS) and elongation at break (EB) of the films were measured using a universal testing equipment (Jiangdu Renheng Machinery Factory, Jiangsu, China). Utilizing a previously described procedure with certain adjustments (Liu et al., 2013), the samples were shaped to a width of 25 mm and a length of 80 mm. The stretching velocity was established at 10 mm/min. Five composite specimens underwent testing. Each mixture was subjected to a minimum of five replicates, while the average values were documented. The TS of films was ascertained in accordance with the equation below:

$$\text{TS} = \frac{F\,max}{L \times W}$$

F_{max} is the maximum tension during the stretching process. L is the width of the films, and W is the thickness. The EAB of films was determined according to equation below:

$$\text{EAB\%} = \frac{L1 - L0}{L0} \times 100\%$$

L0 denotes the starting length of the films, while L1 represents the length at which the membrane ruptures.

4.28. Permeability test on control films

4.28.1. Water vapor transmission rate (WVTR)

Five samples of every film type were evaluated. The WVTR ($g/m^2/24h$) was ascertained gravimetrically via a modification described by Thakur et al. (2017). Plastic cups with a depth of 5.5 cm and an average diameter of 4.25 cm were used to measure the WVTR of the films. For the study, the films samples were sliced into discs with dimensions marginally exceedingly the cup's diameter. 10 g of dried calcium sulfate was added in each cup to keep the relative humidity 97 % RH at zero percent inside the cup. These cups have different composition films discs covering them. Every cup was thereafter positioned in a desiccator containing a saturated K_2SO_4 solution

which was utilized to preserve a 97 % RH at a temperature of 25 °C. The cups were measured each 24 hrs, while the weight increase was recorded as an indicator of time. The slope was determined by a linear regression analysis (weight change vs time). Ultimately, the gradient Δm/Δt (g/h) and transference surface area (m^2) were divided to calculate the water vapor transmission rate (WVTR).

$$\text{WVTR } (g/m^2/day) = \frac{\Delta m}{\Delta t \times A}$$

4.28.2. Oxygen transmission rate (OTR)

Oxygen transmission rate (OTR) of the films was assessed utilizing a Mocon Ox-Tran 2/21 (ST or SH module, Minneapolis, MN, USA) in compliance with ASTM Standard F1927 (ASTM 2007) at 23 °C and regulated relative humidity (RH). Thin samples were secured within the diffusion cell and then purged of remaining oxygen utilizing an oxygen-free gas as the carrier. Subsequently, pure oxygen (99.9%) was supplied into the external container of the diffusion cell (50% RH), and the oxygen molecules penetrating through the film into the internal chamber (90% RH) were transported to the sensor via the carrier gas. The OTR was determined by regulating the airflow speed at a steady state relative to the oxygen saturation gradient and expressed as [cc/m2·day·atm]. All sheets were measured in triplicate.

4.29. Water solubility (WS)

Water solubility studies were conducted using a temperature-controlled shaker (SHZ-B, Shanghai Boxun Industry & Commerce Co., Ltd Medical Equipment Factory). Film samples (2 × 2 cm^2) were desiccated to an even weight (M0) at 150 °C then thereafter immersed in a beaker holding 200 mL of distilled water, which was constantly agitated at a constant rotational speed of 50 rpm at 25 °C. After 12 hrs, the materials were extracted by filtration over a 100-mesh screen, desiccated to a consistent weight and subsequently measured instantly (M1) (Al-Naamani, Dobretsov, & Dutta, 2016). The WS of films was calculated using the following equation:

$$\text{WS} = \frac{\text{M0} - \text{M1}}{\text{M0}} \times 100$$

4.30. Swelling index (SI)

To evaluate the swelling characteristics, film samples were dried at 105°C till a constant weight was achieved, then weighed (W1) and immersed in a 50 mL beaker containing 30 mL of water at 25°C for 24 hrs (Riaz et al., 2018). The wet films have been superficially dried using filter paper and subsequently weighed (W2). Each sample underwent triplicate analysis. The degree of swelling was determined using the equation provided below:

$$\text{Swelling Index (\%)} = \frac{W1-W2}{W1} \times 100$$

4.31. Antioxidant activity (AA) of the control film

4.31.1. 1,1-diphenyl-2-picrylhydrazyl (DPPH) activity

Scavenging activity of films on 1,1-diphenyl-2-picrylhydrazyl (DPPH) radicals (D4313-TCI America) was evaluated using a modified method from (Agunbiade et al., 2022). Film samples (of equal weight) in 1 ml of 1% solution of acetic acid (A9705-Sigma-Aldrich) were admixed with 2 ml from a methanolic DPPH the solution, yielding ultimate DPPH concentration of 1.0 mM. Mixture was then vigorously agitated then permitted to sit in darkness for 30 min, following that absorbance recorded at 517 nm relative to blank (methanol and acetic acid). Scavenging capacity was then computed using formula below:

$$\text{DPPH Radical scavenging (\%)} = (Ac - A)/Ac \times 100$$

Where, Ac = Absorbance of the control, A = Absorbance of the sample

4.31.2. Reducing Power (RP) Assay

The reducing power (RP) has been assessed using the method described by Pasanphan et al. (2015). CS samples ranging from 0.125 to 1.0 mg/ml were mixed with 2.5 ml of buffered phosphate (0.2 M, pH 6.6) (76847-Sigma-Aldrich) along with 2.5 ml of 1% potassium ferricyanide (P1979-TCI America). The reaction mixture was incubated at 50 °C for 20 min within a water bath (STXUWB25, India). After the incubation period 2.5 ml of 10% trichloroacetic acid (T6399-Sigma-Aldrich) was added, followed by centrifugation of the mixture at 3,000 rpm for 10 min using a REMI R-02 mini centrifuge (India). 2.5 ml of the solution from the upper layer was mixed

in 2.5 ml of deionized water along with 0.5 ml of 0.1% ferric chloride (157740-Sigma-Aldrich). The absorbing capacity of the resultant solution was measured at 700 nm, with an increase in absorbance signifying greater reducing power.

4.31.3. Statistical analysis

The data are presented as mean ± standard deviation. The data were initially assessed using SPSS (version 17.0, SPSS Inc, Chicago, IL, USA) and underwent analysis of variance (ANOVA). The dunken test was employed to analyze the differences between pairs of means. The difference was deemed statistically significant when $p < 0.05$. All experiments were conducted in triplicate.

4.32. Apparent color and optical properties of the treated film

4.32.1. Visual analyses of the treated films

The films were subjected to visual analysis by assessing their homogeneity, specifically regarding consistent colors and the existence of insoluble particles (Liu et al., 2015).

4.32.2. Hunter color properties

The color parameters of film samples were analyzed by Dr. Lange Micro Color II LCM6 Colorimeter (Apeldoorn, The Netherlands) by following the method reported by Olewnik-Kruszkowska et al. (2022) with minor changes. The white plate was used as a reference. For the film color characterization, (L*), (a*), and (b*) values were measured L represents lightness, a indicates green-red, and b signifies blue-yellowness. The present study identifies L*, a*, and b* as components of a control sample (NC film). Five measurements were obtained for each film type at various points, followed by the calculation and reporting of the average value and standard deviation. The equations used for calculating overall color difference (ΔE) and yellow index (YI) are as follows:

$$\Delta E = [(L-L^*)^2 + (a-a^*)^2 + (a-a^*)^2]^{1/2}$$

$$YI = \frac{(142.86 \times b)}{L}$$

4.32.3. Light transmission and transparency

The film samples were divided into rectangles measuring 1 cm × 4 cm and subsequently positioned within the spectrophotometer test cell (Akhtar et al., 2023). The UV–visible spectrum of the films was obtained in the range of 200 to 800 nm utilizing an ultraviolet–visible spectrophotometer (UV-1800, Shimadzu Corporation), with an empty cell serving as the reference. Transparency was assessed through determining its absorbance at 600 nm, calculated using the following equation below:

$$\text{Transparency } (\frac{A600}{x}) = \frac{-logT600}{x}$$

T600 represents the efficiency of transmission at 600 nm, A denotes the absorbance at 600 nm, and x indicates the film thickness in millimeters. The formula suggests that higher transparency values correspond to a higher level of opaqueness.

4.33. Measurement of physical properties of the treated films

4.33.1. Thickness measurement

The thickness of NC-RES-CS films was assessed by measuring at eight distinct points through a digital micrometer Sylvac S229 Swiss (Yverdon, Switzerland). Results were presented as average values with standard deviation (SD).

4.33.2. Tensile strength (TS) and elongation at break (EB)

The tensile strength (TS) and elongation at break (EB) of the films were measured using a universal testing machine from Jiangdu Renheng Machinery Factory, Jiangsu, China. Samples were shaped to a width of 25 mm and a length of 80 mm, following a previously described procedure with modifications (Liu et al., 2013). The stretching speed was established at 10 mm/min. Five composite specimens underwent testing. Each set was tested with a minimum of five replicates, and the mean values have been presented. The TS of films was established based onto equation below:

$$\text{TS} = \frac{F\,max}{L \times W}$$

Fmax represents the peak tension observed throughout the stretching method. L represents the width of the films, while W denotes the thickness. The EAB of films was calculated using the following equation:

$$\text{EAB } \% = \frac{L1-L0}{L0} \times 100\%$$

L0 represents the starting length of the films, while L1 denotes the length at which membrane breakage occurs.

4.34. Antioxidant activity (AA) of the treated film

4.34.1. 1,1-diphenyl-2-picrylhydrazyl (DPPH) activity

Scavenging activity of films on 1,1-diphenyl-2-picrylhydrazyl (DPPH) radicals (D4313-TCI America) was evaluated using a modified method from (Agunbiade et al., 2022). Film samples (of equal weight) in 0.2% solution of acetic acid (A9705-Sigma-Aldrich) were admixed with 1 ml from a methanolic DPPH the solution, yielding ultimate DPPH concentration of 1.0 mM. Mixture was then vigorously agitated then permitted to sit in darkness for 30 min, following that absorbance recorded at 517 nm relative to blank. Ascorbic acid (PHR1008-Sigma-Aldrich) served as the reference standard. Scavenging capacity was then computed using formula below:

$$\text{DPPH Radical scavenging (\%)} = (Ac - A)/Ac \times 100$$

Where, Ac = Absorbance of the control, A = Absorbance of the sample

4.34.2. Reducing Power (RP) Assay

Reducing power (RP) was assessed following using a particular procedure (Pasanphan et al., 2015). CS samples (0.125 to 1.0 mg/ml) were combined using 2.5 ml of a buffered phosphate (0.2 M, pH 6.6) (76847-Sigma-Aldrich) with 2.5 ml of 1% potassium ferricyanide (P1979- TCI America). Reaction solution underwent incubation inside a water bath (STXUWB25, India) at 50 °C for 20 min. After incubation, 2.5 ml of 10% trichloroacetic acid (T6399- Sigma-Aldrich) was appended, then the centrifugation of mixture was completed about 3,000 rpm over a duration of 10 min using centrifuge (REMI R-02, mini centrifuge, India). 2.5 ml of the solution from

topmost layer was combined with 2.5 ml of distilled water with 0.5 ml of 0.1% ferric chloride (157740-Sigma-Aldrich). The absorbing capacity of the resulting solution was recorded at 700 nm, with rise in absorbance indicating higher reducing power.

4.35. Biodegradation test (BT)

The biodegradation of the fabricated film samples was performed according to the methodology established by He et al. (2021). The NC-RES-CS film samples, measuring 2 × 2 cm, were buried in a soil pot to a depth of 2 cm for a duration of 45 days. The soil was irrigated bi-daily to preserve moisture levels. At the completion of the study, the soil's water content was 35.8%. At the end of each week, the specimens were taken out, and weight reduction was quantified. Each sample was analyzed in triplicate, and the mean was computed.

4.35.1. Statistical analysis

The data are presented as mean ± standard deviation. The data were initially assessed using SPSS (version 17.0, SPSS Inc, Chicago, IL, USA) and underwent analysis of variance (ANOVA). The dunken test was employed to analyze the differences between pairs of means. The difference was deemed statistically significant when $p < 0.05$. All experiments were conducted in triplicate.

4.36. Mushroom preparation, treatments and storage

Agaricus bisporus fruiting bodies were collected from a nearby farm at the bud stage. The samples were delivered to the laboratory within 30 min and stored in the freezer at 4 °C. After 24 hrs, the undamaged fruit bodies exhibited consistent size and maturity, characterized by a white color and without defects were screened. Mushrooms were randomly divided into five groups of 3-4 mushrooms in each group. Then the mushrooms were packed into 8.1 cm × 7.4 cm low-density polyethylene (PE) cups (0.04 mm thick) five different groups as T0 (with no RES as a control), T1, T2, T3 and T4 (with varied RES concentration as 4, 8, 12, 16 μg/ml respectively):

T0 with CS-NC (no RES), T1 with CS-RES (4 μg/ml)-NC, T2 with CS-RES (8 μg/ml)-NC, T3 with CS-RES (12 μg/ml)-NC and T4 with CS-RES (16 μg/ml)-NC. Every package included 138.50 ± 4.06 g of mushrooms. Every treatment group comprised three replicates, from which three were picked at random. The processed mushrooms were stored in a freezer at 4 °C, and measurements were taken on days 0, 3, 6, 9, 12 and 15.

4.36.1. Weight loss

The reduction in weight of mushrooms was expressed as a proportion of the initial weight and computed using the following equation:

$$\text{Weight loss (\%)} = \frac{W0 - W1}{W0} \times 100$$

Where W0 represents the starting weight of a mushroom, and Wt denotes the actual weight of a mushroom during time t.

4.36.2. Texture Profile Analysis (TPA)

The stiffness of the mushroom head was assessed using a texture analyzer (TA-XT, Stable Micro Systems UK) fitted with a P/75 probe. The testing velocity was 5 mm/s.

4.36.3. Respiration rate

Select three mushrooms of uniform size for every treatment and place them in a plastic/glass container. The already made containers were covered with the control and treated films and then tied with elastics and stored at 4 ℃ for 24 hrs. Thereafter, the CO_2 concentration was quantified utilizing an O_2/CO_2 analyzer after every 24 hrs (Check Point, Hangzhou, China). Gas samples were extracted from the bottles using a 20 mL syringe. The respiration rate was determined using the following equation:

$$\text{Respiration rate (mL kg}^{-1}\text{s}^{-1}) = \frac{\Delta yCO2 \times V}{100 \times W \times \Delta t}$$

Where Δy_{CO2} is the concentration increment (%), V (mL) is free volume, W (kg) is weight of mushroom, Δt (s) is testing time (Zhang et al., 2020).

4.36.4. Polyphenol oxidase (PPO)

3 g of mushroom were mixed using 6 mL of 0.05 M phosphate buffer at pH 6.8, followed by centrifugation at 10,000×g and 4 °C for 20 min. The supernatant was obtained and utilized to assess the activity of PPO. The evaluation of PPO activity was conducted according to the study by Liu et al. (2019). Initially, 0.2 mL of supernatant (with 0.2 mL of phosphate buffer serving as

a control) was combined with 4.8 mL of phosphate buffer and 1 mL of catechol. The absorbance was collected at 420 nm at 30 sec intervals for a duration of 120 sec. A single unit of activity for PPO was defined as the quantity of enzyme that induced a shift of 0.01 in absorbance per min, with results given as U kg^{-1} fresh weight.

4.36.5. Malondialdehyde (MDA) content

The MDA content was assessed using the methodologies outlined by Ni et al., (2021). Mushrooms (1 g) were processed with 4 mL of 10% (w/v) trichloroacetic acid (TCA) and subsequently centrifuged at 10,000g for 15 min at 4℃. 2 mL of thiobarbituric acid (TBA) was incorporated into 2 mL of the residue and subjected to boiling for 20 min. The mixture was then rapidly cooled and centrifuged for 20 min at 10,000g (Zhang et al., 2020). The absorption value of the reaction mixture was measured at 532 nm, 600 nm and 450 nm, as well. The determination of MDA content was conducted using the following equations:

$$c = 6.45 \times (A532 - A600) - 0.56 \times A450$$

$$\text{MDA (mol Kg}^{-1}) = \frac{c \times VR}{VS \times W}$$

Here, c denotes the MDA concentration within the reaction mix; VR indicates the volume of the extracting solution; VS refers to the volume of the extracting solution utilized for the experiment; and W represents the fresh weight of the mushroom sample.

4.36.6. Browning degree (BD)

The mushrooms were measured at 5g and combined with cold distilled water in a ratio of 1:10 (w/w). The mixture was homogenized in a blender for 30 sec and then centrifuged at 8000 r/min for 15 min. Subsequently, the resultant solution was maintained at 25℃ for 5 min, and the absorbance was recorded at 410 nm. The supernatant obtained was analyzed at a wavelength of 410 nm, with the OD410 serving as an indicator of the browning degree (Fattahifar et al., 2018).

4.36.7. Statistical analysis

The data are presented as mean ± standard deviation. The data were initially assessed using SPSS (version 17.0, SPSS Inc, Chicago, IL, USA) and underwent analysis of variance (ANOVA). The

dunken test was employed to analyze the differences between pairs of means. The difference was deemed statistically significant when $p < 0.05$. All experiments were conducted in triplicate.

Chapter 5

RESULTS AND DISCUSSION

5. Proximate analysis of mushroom waste powder (MWP)

5.1. Crude protein content

The total protein content of powdered button mushroom waste is significantly affected by the drying process, as shown in Table 5.1. The value is highest in FD at 23.54% moderate in VD is 22.68% and least in HD as 22.07%. FD eliminates water through sublimination under low temperature and pressure, which reduces thermal degradation, thus maintaining native protein content and amino acid integrity. Recent studies indicate that protein retention rates can exceed 90% when employing cold conditions vacuum/freeze protocols (Zhang et al., 2022). VD circulated high-temperature air at 30° C with high velocity in the dryer's chamber, denaturing protein and reducing the amount of protein compared to FD, which retains protein more effective (Chen et al., 2017) (Tolera and Abera, 2017) (Yang et al., 2020). HD, which integrates FD and VD, generally results in moderate protein rentention.

The initial low temperature safeguards the protein, while the following vacuum stage enhances moisture extraction without significant thermal degradation (Santos et al., 2021). Furthermore, the porous microstructure generated by FD facilitates rehydration along with protein extraction during analysis, while the denser structure resulting from VD hinders extractability (Fernandes et al., 2022). The mechanistic and structural factors elucidate the observed ranking (FD > HD > VD) in crude protein content, consistent with recent research in mushrooms and analogous food matrices.

Table 5.1. Proximate analysis of dried button mushroom waste powder (MWP).

Parameters	Freeze drying (FD)	Vacuum drying (VD)	Hybrid drying (HD)
Moisture (%)	6.16 ± 1.22 [b]	7.31 ±1.46 [a]	5.81 ± 1.18 [c]
Crude protein (%)	23.54 ± 1.13 [a]	22.68 ±0.86 [b]	22.74 ± 1.25 [c]
Crude fat (%)	2.80 ± 2.21 [a]	1.47 ±1.01 [c]	2.51 ± 2.13 [a]

Ash (%)	5.23 ± 1.06 [a]	5.18 ±1.05 [a]	5.05 ± 0.808 [a]
Carbohydrate (%)	63.36± 1.50 [a]	62.52 ± 1.33 [ab]	64.04 ± 0.877 [b]

Means following by the same letter in a row are not significantly different ($p>0.05$) according to the least significant difference (LSD) test.

5.2. Crude fat content

Mushrooms typically have a reduced fat content; however, they include polyunsaturated fatty acids that are vital for human health and lead to the decrease of blood total cholesterol and low-density lipoprotein levels. The elevated linoleic acid level is a primary factor in considering mushrooms a nutritious food (Mustafa et al., 2022; Gupta et al., 2018). Table 5.1 indicates that FD powders exhibited a greater crude fat content of 2.80%, in contrast to VD, which recorded 1.47%, and HD, which recorded 2.51%. The crude fat content in mushrooms typically ranges from 1.1 to 8.3 g/100 g dry weight (Naknaen et al., 2015), and the fat content significantly changes based on the mushroom species and growing techniques. The findings demonstrated that all examined dried mushrooms possessed a low fat %. Mushrooms are generally low-calorie foods due to their minimal fat content. The drying procedure led to a reduction in the fat content of button mushrooms, likely attributable to oxidation reactions, as the fat in mushrooms predominantly comprises polyunsaturated fatty acids which are highly prone to oxidation when exposed to heat/ drying medium (Bashir et al., 2020).

Low-temperature sublimation in FD effectively preserves heat-sensitive lipids and reduces oxidation, resulting in enhanced preservation of fat (Nombona et al., 2021). In contrast, VD can decrease extractable fat by accelerating lipid degradation by thermal oxidation and the volatilization of unsaturated fatty acids through the application of moderate heat under reduced pressure (Zhou et al., 2019). The HD method integrates FD's mild first drying with subsequent VD, resulting in intermediate fat retention. The initial freeze step stabilizes lipids, while the subsequent vacuum step efficiently removes moisture with minimized exposure to higher temperatures (Gamage et al., 2020). Furthermore, FD generates a porous microstructure that facilitates solvent penetration along with lipid extraction during analysis, whereas the denser matrix of VD may impede fat extractability (Silva et al., 2022). These processes contribute to the

explanation of the following order of crude fat content: FD > HD > VD, which is in line with recent findings in food matrices such as mushrooms.

5.3. Total ash content

Ash is characterized as completely non-combustible inorganic salts. Potassium and phosphorus are the primary ash constituents in mushrooms. Research indicates that mushrooms are rich in minerals and may serve as a superior source of minerals compared to vegetables (Haro et al., 2020). The ash concentration in mushroom samples is significantly affected by the drying temperature and duration of exposure. This investigation shown that reduced exposure duration led to diminished ash content, which is significant for the mineral content in samples (Nuramira et al., 2022). Upon assessing the impact of various drying techniques on ash content, the FD powder exhibited an ash level of 5.23%, while the VD powder showed 5.18%, and the HD powder recorded 5.05% (Table 5.1.). No significant difference ($p>0.05$) in ash content was observed between FD and VD mushroom samples; however, the marginal increase in ash content in the FD powder may be attributed to the low temperatures and vacuum conditions utilized during FD, which minimized biochemical and microbial reactions, resulting in enhanced mineral preservation and consequently higher total ash values (Singhal et al., 2022). These findings are consistent with research on mushroom and plant foods, which indicates that variations in ash content resulting from drying methods are minimal (Wu et al., 2024; Arrieta et al., 2014). FD, VD, and HD successfully maintain the inorganic elements of MWP, which is crucial to ensuring its nutritional and functional significance as a sustainable food ingredient.

5.4. Total moisture

The removal of moisture during processing may enhance nutritional retention in the mushroom by prolonging its shelf life. The mass of the mushroom diminished rapidly as the temperature rise (Castellanos-Reyes et al., 2021). The data in (Table 5.1.) show the impact of FD, VD and HD on physico-chemical characteristics of button mushroom waste powder. The moisture % of the FD powder was determined at 6.16%, which was lower than the VD powder at 7.31%, and also lower than the HD at 5.81These values obtained from FD powder were in accordance with the *Pleurotus sajor-caju* powder (Das et al., 2020; Sajad et al., 2023). VD powder is marked by an uneven moisture removal process, exhibiting rapid extraction initially and a gradual decline in rate during

successive drying, resulting in the production of a dense layered structure in food products (Piskov et al., 2018). Moreover, traditional drying methods induce detrimental alterations in plant products, including excessive shrinkage, discolouration, oxidation of functional constituents, and significant deterioration of nutritional and sensory attributes (Orikasa et al., 2018). The HD powder particles exhibited a more homogeneous structure compared to the FD sample (Ando & Nei, 2023). The low-temperature sublimation process of FD under high vacuum effectively eliminates both bound and free water while maintaining microstructure, leaving behind very little moisture a characteristic that has been extensively studied in food applications (Tang et al., 2023). In contrast, VD employs low temperatures under reduced pressure, potentially resulting in residual bound water partly because of the denser matrix created during the drying process (Lee & Chen, 2022). HD, which begins with FD to remove the majority of water and is followed by drying VD to eliminate residual moisture, effectively integrates the advantages of both methods, resulting in thorough dehydration in a reduced timeframe (Gao et al., 2024). The observed moisture trends align with recent research on mushrooms and other hygroscopic food matrices, indicating that FD and HD offer enhanced moisture removal compared to VD alone, which is essential for extending shelf life and ensuring microbial stability.

5.5. Available carbohydrate

Carbohydrates serve a crucial part in nutrition as they supply energy for humans. Polysaccharide is the predominant carbohydrate found in mushrooms and is recognized for its immunomodulatory and anticancer activities (Araújo-Rodrigues et al., 2024). Polysaccharides are commonly coupled with other components, including proteins and uronic acids. A direct correlation was identified between these chemical constituents and the radical scavenging effects of polysaccharides (Yarley et al., 2021). The carbohydrate composition of mushrooms encompasses fibers, including the structural polysaccharides beta-glucans, chitin, hemicelluloses, and pectin substances. The available carbohydrates were determined using the difference approach, which relies on other proximate components (Antunes et al., 2020). The FD product contained 63.36% carbohydrates, the VD product had 62.52%, and the HD powder contained 64.04% carbohydrates (Table 5.1.). The comparable outcome of FD powder against HD powder indicates that microwaving facilitates superior retention of polysaccharides due to its elevated drying rate and reduced temperature, suggesting that hybrid drying is a more effective method for preserving polysaccharides in button

mushroom powder. Consequently, the HD mushroom functions as a beneficial source of dietary fiber with caloric content. The carbohydrate % rises when moisture content diminishes throughout the drying process due to nutrient concentration. Carbohydrates, similar to most heat-sensitive components in food, typically diminish in functionality. The elevation of carbohydrates in HD samples compared to FD can be ascribed to concentration effects resulting from enhanced moisture removal in the vacuum stage, along with potential structural transformations driven by Maillard reactions that augment quantifiable reducing sugar portions during the drying process (Zhang et al., 2023). The increase in carbohydrates in HD samples compared to FD can be attributed to concentration effects resulting from more extensive moisture removal during the second (vacuum) stage, along with potential structural transformations driven by the Maillard reaction that enhance quantifiable decreasing sugar proportions during drying (Zhang et al., 2023). FD is effective in preserving heat-sensitive nutrients; however, it may result in reduced the decomposition of complex carbohydrates, into simpler sugars, which can lead to a slightly decreased measured carbohydrate content (Sagar & Kumar, 2010). VD involves moderate heat applied under reduced pressure, which may lead to thermal breakdown or partial caramelization of sugars, resulting in decreased carbohydrate yields (Ramachandran et al., 2024). Comparable findings have been documented in various mushroom species and plant-based matrices, indicating that multi-stage drying techniques improve carbohydrate content by enhancing extractability and inducing structural modifications (Alvi et al., 2022). The findings indicate that HD provides a balance between the preservation and enhancement of carbohydrate availability, which may enhance the functional properties of MWP in value-added food applications.

5.6. Powder morphology and Microstructural properties

The external and volumetric structures of the mushroom powders were evaluated, and the microstructural characteristics of the surfaces of their constituent particles were investigated, since drying conditions affect the grinding characteristics and food powder morphology affects their final properties (Aparna et al., 2021; Oyinloye & Yoon, 2020). These parameters effects on four different drying procedures were evaluated. The visual properties and optical microscopy results of the powders under analysis are shown in Figure 5.1. The texture of the FD and HD samples was floury. The remarkable consistency and smoothness of the HD powder were its distinguishing features. The VD sample was a little out of the powder range. Rapid moisture loss in the initial

phase and uneven moisture removal over time are characteristics of VD. Kotwaliwale et al. (2007) noted a high density of dried mushrooms (*Bisporous spp.)* when examining the texture of those dehydrated by hot air drying. This was corroborated for mushroom fruiting body fragments in a prior study (Piskov et al., 2018). The dense dry substance was more challenging to pulverize into fine particles; hence the consistency of the VD powder was described as granular.

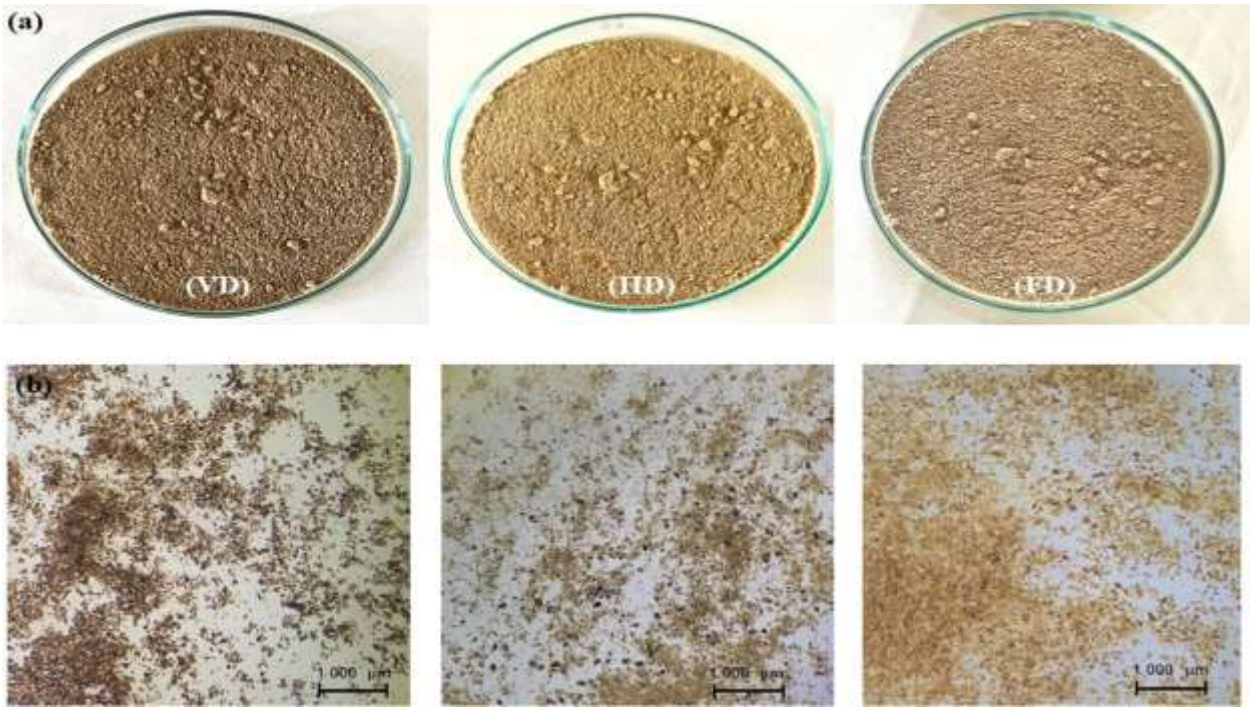

Figure 5.1. (a) Photographs of mushroom powders obtained by different drying methods and (b) the light microscopic images of mushroom waste powders (MWP) (×25): (a) Vacuum dried MWP; (b) Hybrid dried MWP; (c) Freeze dried MWP.

5.7. Hunter color values

One crucial factor affecting a product's consumer appeal is its colour. It provides a sense of comparative change in the case of powders. The colour profile of the mushrooms was greatly impacted by the drying procedures. Because it is correlated with their vulnerability to high

temperatures, a decrease in lightness (L∗ value) or an increase in yellowness (b∗ value) is thought to be a significant indicator of colour degradation in mushrooms. With lower L∗values of 58.73 in VD powder, higher L∗values of 77.28 in HD powders and optimal L∗values of 82.84 in FD powder, it was shown that the mushroom samples dried by VD were darker than the HD samples than FD. The observed values for a∗ (redness) and b∗ (yellowness) were 30.88 and 74.75, respectively (Table 5.3.). This phenomenon can be attributed to the reduced presence of oxygen in a drying chamber at low temperature and pressure, resulting in less enzymatic and non-enzymatic browning reactions (Tsikrika et al., 2022). In contrast, FD produced minimal color alteration due to the sublimation of frozen ice, diminished oxygen availability and the inactivation of the polyphenol oxidase enzyme, as well as, to a lesser degree, phenol peroxidase, owing to the lower temperature that inhibits enzymatic browning reactions, thereby stabilizing color (Harguindeguy et al., 2020). The browning degree and whiteness of samples showed a smooth change tendency during total drying time (Duan et al., 2016). The color obtained during FD occurs between enzyme and substrate in the cell sap of button mushroom occurred due to ice melting, and the products presented darkness, redness and yellowness during latter drying period (Pei et al., 2014). Similarly, this pattern was also found by (Shams et al., 2022a and Yang et al., 2020) in mushroom dried powders. Hence, the principal behind the darker color of VD and HD *A. bisporpus* could be due to the transformation of phenolic compounds into quinones, and this subsequently change into melanin (a brown pigment), leading to the Maillard reaction (a non-enzymatic browning reaction) among proteins or amino acids and reducing sugars, dependent upon heating temperature and duration, potentially responsible for the development of brown compounds (Nath et al., 2022). Furthermore, these drawbacks sometimes result in thermal degradation, producing goods with altered textures (heightened hardness and chewiness, and diminished cohesiveness and elasticity), browning, an undesirable flavor, and a reduction in nutritional content (Kutlu et al., 2022). This results from the transformation of polysaccharides into oligosaccharides and the occurrence of Maillard reactions. The browning process often arises from a disturbance of the cellular membrane integrity in mushrooms, facilitating the interaction between phenolic chemicals and enzymes. Membrane integrity can be compromised by rough handling, low relative humidity, aging and the growth of pathogenic microorganisms (Amaya-Farfan & Rodriguez-Amaya, 2021). The optimal color characteristics, most similar to those of fresh mushroom samples, were achieved for FD. Isik & Izlin (2014) and Cianni et al. (2023) indicated that the color values of dried

mushroom samples are a crucial quality standards influencing consumer approval, with items exhibiting elevated L* values being favored.

5.8. Determination of bioactive compounds in mushroom waste powder (MWP)

5.8.1. Total phenolic content (TPC)

Polyphenols and flavonoids, prevalent in plant-based foods and herbal products, are recognized for their significant bioactive qualities (Zhang et al., 2022). These chemicals demonstrate antioxidant, anti-inflammatory, anticancer, antibacterial and cardioprotective properties, neutralize free radicals, regulate inflammatory pathways, suppress tumor proliferation and address microbial infections (Ullah et al., 2020; Saleem et al., 2022). In this study, Table 5.2. shows the effect of drying methods on total phenols and flavonoid of button mushroom powder. The average polyphenol content for the raw material was 26.59 mg GAE g^{-1} dry matter on average, but in the case of dry mushroom samples the total phenolic content was in the range of highest in FD powder 25.07 mg GAE g^{-1} owing to the low temperature and vacuum condition than the HD followed by VD with value of 20.91 mg GAE g^{-1} and 18.57 mg GAE g^{-1} respectively. The heat treatment resulted in loss of polyphenols with different drying treatments. The lower phenolic content in vacuum dried powders may be attributed to the exposure of samples to elevated temperatures for extended durations and enzymatic processes facilitated by air and light leading to the reduction in total phenolic content (Cao et al., 2021). The antioxidant compounds stored in cytoplasm would be more vulnerable to heat as a result of deteriorations in cellular structure (Ebone et al., 2019). The stored compounds within intracellular structure would also be exposed to encounter polyphenol oxidase enzyme after treatments, which may also cause degradation (Ebrahimi & Lante 2022). Sajad et al. (2023) and Ucar & Karadag (2019) observed a similar pattern, noting that during FD, the creation of ice crystals within the cellular structure of the sample may cause disruption, facilitating solvent access and enhancing the extraction of phenolic compounds, thereby improving the preservation of phenolic content. Likewise, Araya-Farias et al. (2011) reported a mere ~4% reduction in phenolic content of seabuckthorn berries following FD under controlled vacuum conditions highlighting the efficacy of FD in maintaining bioactive compounds. A comprehensive evaluation of HD techniques indicated that FD preserved the highest levels of phenolic antioxidants relative to alternative methods, thereby underscoring its effectiveness for bioactive preservation. The findings corroborate our observations that FD exhibits greater phenolic retention than HD, which in turn surpasses VD.

5.8.2. Total flavonoid content (TFC)

The TFC of mushroom powder were affected by drying operation dependent of process temperature. The drying temperature and time combination mutually affected the degradation rate of bioactive compounds. Moreover, elevated drying temperature would rapidly inactivate polyphenol oxidase (Alara et al., 2018) which may be linked to non-destructive effect of higher temperature levels in this study. Numerous published studies demonstrate the impact of drying temperature on the breakdown rate of bioactive chemicals in plants tissues as increasing temperature causes lower retention (Belwal et al., 2022). The flavonoids, sub group of phenolics, are known to be more susceptible to thermal effects mainly due to the structural differences (Ioannou et al., 2020). Table 5.2. indicates that the FD powder had the maximum flavonoid concentration at 14.48 mg GAE/g, surpassing the HD method. of mg 10.57 mg GAE/g followed least with VD with value of 6.07mg GAE/g. Similar results of FD dried mushroom powder were also reported in fruiting bodies of *P. sajor-caju, P. ostreatus,* and *P. sapidus* (mg/g) (Jeena et al., 2024) indicating that drying at low temperature (FD) maintained higher overall antioxidant activity than drying at high temperature (VD and HD). In bamboo species, FD yielded the highest TFC across various drying techniques (Benjamin, et al., 2022). Additionally, broader assessments of aromatic plant by-products indicate that FD more effectively preserves antioxidant-rich flavonoids compared to vacuum or hot-air drying methods (Kumar et al., 2022). The observations corroborate the ranking of total flavonoid content retention as follows: FD > HD > VD. The difference between the TFC of VD samples could be explained by thermal degradation of glycosylated flavonoids, which are sensitive to heat and can be hydrolyzed and oxidized under long-term conditions with high temperature. In comparison, FD helps to preserve flavonoid structures by reducing enzymatic and oxidative degradation of glycosylated and aglycone forms (Chua et al., 2021; Hiranvarachat et al., 2020).

5.8.3. Antioxidant activity (AA)

Antioxidant activity was assessed by DPPH scavenging activity and reducing power assays, represented as IC50 (mg/ml) and EC50 (mg/ml). According to Gulcin and Alwasel (2023), the DPPH radical is primarily used to test how well antioxidants are capable of getting rid of free

radicals. On the other hand, the reduced power assay is used to test how well natural antioxidants can give up electrons. The active ingredients in *A. bisporous* mushrooms have the most impact on antioxidant capacity of white button mushrooms. The antioxidant activity was observed to rise with elevated temperatures. To put it in order, the DPPH of dehydrated Agaricus mushrooms is VD > HD > FD. A lower IC50 value means that the radical scavenging ability is higher. It was found that FD samples had the quickest scavenging of DPPH (EC50 = 6.62 mg/ml) while the reduced power assay (IC50 = 3.84 mg/ml) in contrast to HD and VD powders, which exhibited EC50 values of 7.75 mg/ml and 13.86 mg/ml, and IC50 values of 4.76 mg/ml and 6.05 mg/ml, respectively (Table 5.2). The measured antioxidant activity correlates with the discovered and quantified phenolic compounds in the samples, as demonstrated by the strong correlation coefficients between the EC50 values of antioxidant activity and the amounts of each phenolic compound. HD, conversely, optimized the antioxidant properties of the dehydrated mushrooms, especially regarding their elevated efficacy in inhibiting lipid oxidation (Kumar et al., 2023). This shows that the mushrooms drying time affects not only their ingredients but also their antioxidant benefits in a big way. Chaaban et al. (2017) discovered that the degradation products formed during phenols degradation influenced antioxidant activity in three ways: 1) antioxidant activity could decline because the degradation products had less antioxidant activity; 2) antioxidant activity could be maintained at a consistent level because the breakdown products had identical antioxidant activity as the native flavonoids; and 3) the antioxidant activity could go up because the breakdown products were more powerful. Similar trend was also observed by Zhang et al. (2009); Peng et al. (2021); Shams et al. (2022a); Das et al. (2023) and Soontharapirakkul & Kotpat (2023) finding that mushroom antioxidant activity is better kept in FD powder than in VD as well HD. FD is better at keeping antioxidants because it uses low temperature and vacuum, which mean that polyphenolic substances are less likely to break down or oxidize (Bhatta et al., 2020).

5.8.4. Ascorbic acid content

Several factors affect how vitamin C breaks down, such as pH, moisture level, air, light, metallic ion catalysis, as well as the temperature (Yin et al., 2022). As shown in Table 5.2. Increasing the heating temperature makes it harder for vitamin C to stay fresh. This is because vitamin C oxidizes quickly and can't handle high temperatures (Bernaś & Jaworska 2016). The oxidation of vitamin C produces dehydroascorbic acid, which can subsequently undergo additional oxidation to yield a

variety of compounds. Furthermore, elevated drying temperatures may accelerate the degradation rate owing to the enhanced water solubility characteristics (Ferrada et al., 2021). The ability to retain of ascorbic acid in button mushroom powder was superior in FD yielding 14.46 mg/100g compared to HD at 11.78 mg/100g and VD at 8.13 mg/100g (Table 5.2) this shows that the ascorbic acid content differed significantly ($p < 0.05$) among drying methods. The minimal ascorbic acid concentration was observed in the VD process. This was anticipated due to the heat sensitivity of ascorbic acid, which may degrade during heat treatment and prolonged exposure (Singhal et al., 2020; Horuz et al., 2017). The FD method exhibited greatest efficacy due to the freezing effect inside the chamber and the low temperature. Powders may be able to retain more ascorbic acid if they are freeze dried. The amount of vitamin C of HD fruits was unaffected by their interaction. In studies on *Ipomoea aquatica*, FD demonstrated considerably greater vitamin C levels than oven and sun drying, which result in rapid degradation due to heat alongside oxidation (Joshi et al., 2021). In Volvariella volvacea mushrooms, FD samples demonstrated greater retention of vitamin C compared to oven-dried and sun-dried samples, highlighting the effectiveness of FD in safeguarding heat-sensitive substances (Koffi et al., 2024). In apricot slices, vacuum freeze-drying maintained the highest ascorbic acid content compared to other drying methods, such as pulsed vacuum drying and infrared drying, thereby supporting the trend of FD > HD > VD (Yang et al., 2024). Together, these results confirm that FD is the best technique for retaining ascorbic acid in powdered mushroom waste, followed by HD and VD after that. Positive correlations between TPC of fractions of *A. bisporous* and their antioxidant activities have been identified.

Table. 5.2. Bioactive properties of dried button mushroom waste powder (MWP).

Parameters	Total phenolic content (mg GAE g^{-1})	Total flavonoid content (mg CE g^{-1})	DPPH scavenging activity (EC50; mg/ml)	Reducing power assay (IC50; mg/ml)	Ascorbic acid (mg/100g)
Vacuum drying (VD)	18.57± 0.01[c]	6.07 ± 0.05[c]	13.86± 0.04[a]	6.05± 0.01[a]	8.130 ± 0.02[a]
Hybrid drying (HD)	20.91± 0.01[b]	10.57± 0.06[b]	7.75± 0.05[b]	4.76± 0.02[b]	11.785 ± 0.02[b]
Freeze	25.07 ± 0.02[a]	14.48± 0.06[a]	6.62± 0.07[c]	3.84± 0.04[c]	14.461 ± 0.03[c]

drying (FD)					

CAE stands for catechin, while GAE stands for gallic acid.

Statistically, the mean values in the columns containing distinct letters differ ($p < 0.05$) as per the results of the least significant difference (LSD) test.

5.9. Determination of flow properties of mushroom waste powder (MWP)

There was a correlation between the powders' bulk and tap densities, as well as their water content and particle shape, for VD, FD and HD. Both bulk and tapped densities were significantly affected by the drying processes. Table 5.3 revealed lower bulk (0.405 g/ml) and tap densities (0.478 g/ml) of FD powders than of VD (0.492 and 0.625 g/ml) and HD (0.503 and 0.612 g/ml). Powders that have a high water-binding capacity (>10% w.b.) are prone to agglomerating, which raises the interparticle voids and, thus, density. Therefore, when the moisture content is reduced, bulk and tap densities are reduced. Poovai et al. (2023), Piskov et al. (2022) and Meghwal et al. (2024) noted the same in fig fruit, button mushroom, and wild banana seed powders. FD was effective in reducing the powder volume and density because the frozen water was directly sublimated to vapor, which facilitated the preservation of a better shape, reduced shrinkage, and porous structure (Ando and Nei, 2023). Carr Index (15.063) and Hausner Ratio (1.177) values were also lower in the FD samples (compared to VD, 21.283 and 1.271, respectively) indicating a higher level of flowability and reduced cohesiveness. Carr (1965) and Hausner (1967) reported that the FD powder had a very good flowability (less than 15 in the case of CI, less than 1.2 in the case of HD), whereas VD and HD exhibited fair-to-good flow properties. Li et al. (2021) also found similar results in FD cantaloupe powders. The low volumetric density of FD samples was due to the fact that the sublimation process did not affect the structural integrity (Sarkar et al., 2021). VD and HD powders, in turn, were dense (VD less than HD), which was also in agreement with the reports of Michalska et al. (2023) and Poovai et al. (2023), who explained the higher density by lower porosity and particle agglomeration. The rate of evaporation is improved with higher drying temperature resulting in porous fragmented constructions and limiting the fluidity of the powder by creating a glassy matrix (Koc et al., 2021; Izli et al., 2022). Possible factors that contribute to the development of partial agglomeration in FD samples include the microstructural alterations of freezing and inter-particle electrostatic interactions of ultrafine particles as recently observed by Ouaabou et al. (2021) and Zhao et al. (2020). The volumetric density was the highest with HD

powders, probably because small and uniform particles have less pore space and are more densely packed (Mehrabi et al., 2023; Talebi et al., 2024; Izli et al., 2022). In general, FD yielded superior flowable powders with better structural porosity whereas HD and VD gave denser powders with a marginally low handling property.

Table. 5.3. Flow properties and color profile of dried button mushroom waste powder (MWP).

Parameters	Bulk density (g/ml)	Tapped density (g/ml)	Carr's index	Hausner ratio	l*	a*	b*	Whiteness index (WI)
Freeze drying (FD)	0.405± 0.048 [b]	0.478± 0.022 [b]	15.063± 0.005 [c]	1.177± 0.041 [a]	82.84± 2.26 [a]	0.79± 1.62 [c]	28.29± 1.76 [c]	84.77± 1.01 [a]
vacuum drying (VD)	0.492± 0.042 [a]	0.625± 0.019 [a]	21.283± 0.009 [a]	1.271± 0.036 [a]	58.73± 1.147 [c]	30.88± 1.656 [a]	74.75± 0.756 [a]	32.81± 0.557 [c]
Hybrid drying (HD)	0.503± 0.015[a]	0.612± 0.061 [a]	16.445± 0.033 [b]	1.211± 0.005 [a]	77.28± 1.41 [b]	7.14± 2.16 [b]	60.27± 1.244 [b]	54.88± 0.45 [b]

A* indicates a reddish-green hue, b* a yellowish-blue hue, and WI is the total whiteness index; l* denotes brightness. Mean values of triplicates ±SD are used to express the data. Based on the least significant difference (LSD) test, there is a statistically significant difference ($p < 0.05$) in the mean values of the same column that displays distinct letters.

5.10. Characterization of prepared button mushroom waste powder (MWP)

5.10.1. Fourier Transform Infrared (FTIR) Spectroscopy

Comparing FTIR spectra of mushroom powder subjected to vacuum drying (VD), hybrid drying (as HD), freeze drying (as FD) provided insights into the chemical structure changes especially in proteins, polysaccharides, phenolics, and moisture content. The Broad O–H Stretching observed in the wavenumber range 3200–3600 cm^{-1} corresponds to moisture and hydroxyl groups in polysaccharides and phenolics. In FD broad and intense peak was observed indicating that it retains more bound water and intact hydroxyl groups. In HD slightly narrower peak indicates some

moisture loss. In case of only FD narrower and weaker peaks indicted significant moisture loss and possible degradation of hydroxyl-rich compounds. The wave number corresponding to 2800–3000 cm^{-1} indicated C–H Stretching corresponds to aliphatic chains in fatty acids and other organic compounds. The results indicated minimal variation among drying methods in this region (2800–3000 cm^{-1}) (as shown in Figure 5.2.). There was slight reduction in intensity observed in VD method due to heat-induced degradation. The wave number corresponding to 1600–1700 cm^{-1} and 1500–1600 cm^{-1} indicates Amide I and II Bands that corresponds to protein secondary structure (Amide I: C=O stretch; Amide II: N–H bending + C–N stretching).

FD and HD showed strong and well-defined peaks showing better protein structure preservation. In case of VD there is moderate intensity indicating partial denaturation. In case of VD weakened or slightly shifted peaks indicates protein denaturation or maillard reaction products. The wave number corresponding to 1700–1750 cm^{-1} indicates C=O Stretching that corresponds to carbonyl groups from esters, acids, and aldehydes. FD and HD showed clear peak showing retention of bioactive compounds whereas VD showed reduced intensity showing breakdown of some compounds. The wave number corresponding to 1000–1200 cm^{-1} indicates C–O–C and C–O Stretching that corresponds to polysaccharides and sugars. In HD and FD strong, sharp peaks are observed showing good preservation of polysaccharide structure. In VD slight reduction in intensity showing partial degradation of sugars. The wave number corresponding to 600–1500 cm^{-1} is the fingerprint region indicates complex region with overlapping bands related to carbohydrates, amino acids, and other minor compounds. In FD rich and distinct features are observed whereas HD and VD slight flattening is observed. Boruah et al. (2025) found substantial retaining of phenolic and polysaccharide groups in FD *Garcinia lanceifolia*, with significant O–H (3441 cm^{-1}) and C=O (1722 cm^{-1}) stretching, compared to VD's broader, weak. Shams et al. (2022) and Lin et al. (2014) found sharper polysaccharide with protein related bands in FD mushrooms, while HD and VD showed spectrum shifts and lower intensities. In *Boletus edulis*, FD maintained strong O–H (3503 cm^{-1}) and amide I/II (1626, 1554 cm^{-1}) bands, but thermal drying reduced them (Rasika & Amarasinghe, 2023. In *Ganoderma lucidum*, FD preserved unique polysaccharide peaks (1151-1035 cm^{-1}) while VD samples destroyed or expanded them (Zhou et al., 2017), demonstrating its greater structural and bioactive integrity.

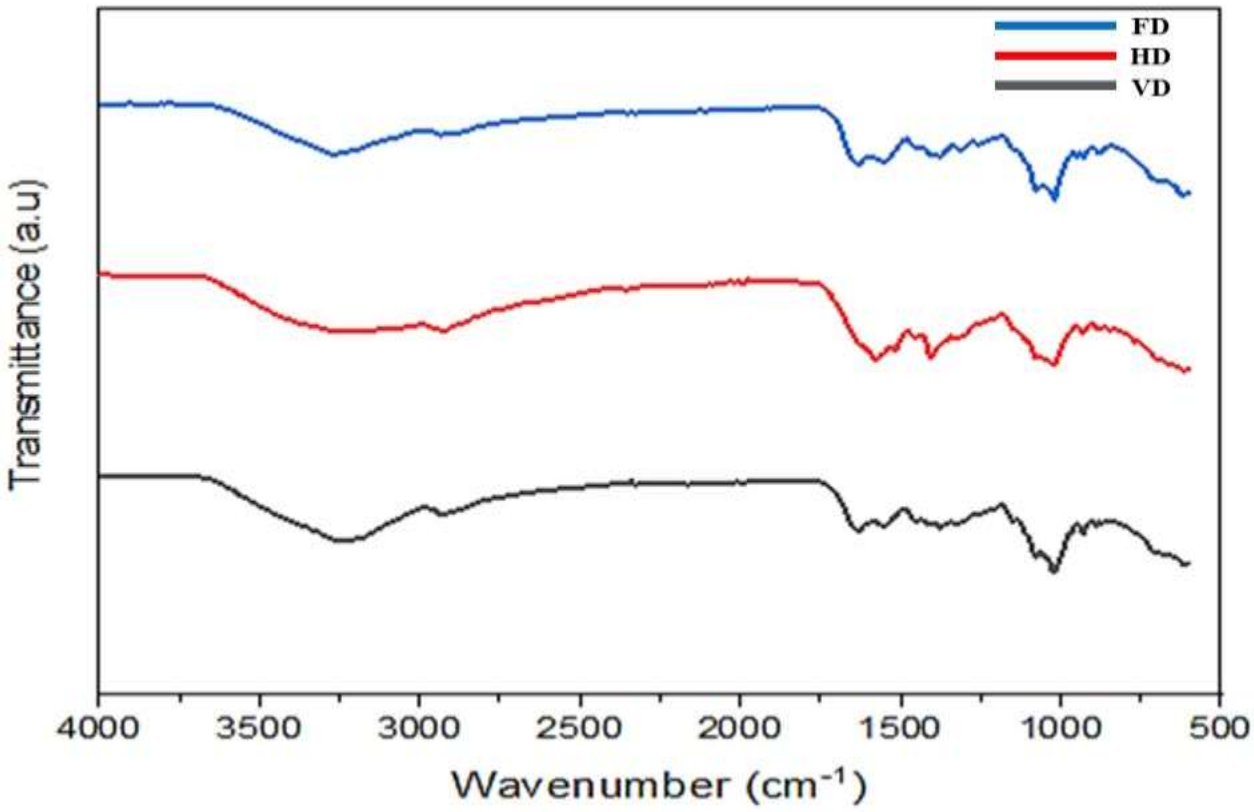

Figure 5.2. FTIR spectra of mushroom waste powder (MWP) obtained through various treatments such as VD: Vacuum dried MWP, HD: Hybrid dried MWP and FD: Freeze dried MWP.

5.10.2. X-ray powder diffractometry (XRD)

XRD Comparison of hybrid drying (as HD), freeze drying (as FD) and vacuum drying (as VD) of mushroom waste powder (MWP) showed waste powder is largely amorphous due to the high content of polysaccharides, proteins, and phenolic compounds. However, some crystalline peaks are observed that may have been originated from minerals (e.g., calcium, potassium salts) or ordered polysaccharide chains (like chitin or β-glucans). FD and HD showed lowest crystallinity with broad humps and no sharp peaks which indicated that the powder retains amorphous structure and minimal molecular rearrangement. VD mushroom powder showed moderate crystallinity with slightly sharper features than FD and some partial ordering due to mild heating and pressure changes. In XRD the amorphous hump was typically observed around 2θ value of 18°–25° in

mushroom polysaccharides. Sharp Peaks were observed at 2θ value of 20° (Figure 5.3.). Using relative peak intensity or area under the curve it was found that FD had 10–20% crystallinity, HD had 20–30% crystallinity and VD had 30–40% crystallinity. The XRD indicated that solubility, bioavailability, and nutrient retention of FD and HD was very higher in comparison to VD. The powder flowability was poor in FD and HD due to amorphousness. The FD and HD maintains an amorphous structure, ideal for preserving bioactive compounds whereas VD leads to mild crystallization, balancing stability and bioavailability. XRD studies consistently show that FD enhances the crystallinity and structural integrity of powdered biomaterials compared to VD and HD powder. According to Ma et al. (2020), FD mushroom powders exhibited more defined and intense XRD peaks, indicating a higher degree of crystallinity, which is attributed to the minimal thermal damage and preservation of the native structure during sublimation. Similarly, Zhou et al. (2017) demonstrated that polysaccharide powders obtained from *Ganoderma lucidum* via FD retained a more ordered microstructure than those obtained through HD, which showed broader and less intense peaks due to partial amorphization. In a comparative analysis, Chin et al. (2021) confirmed that FD maintained the molecular arrangement of starch and cellulose components better than HD, resulting in greater XRD peak sharpness and stability. These findings underline the role of FD in producing powders with enhanced structural order and potential functional performance, critical for food and pharmaceutical applications.

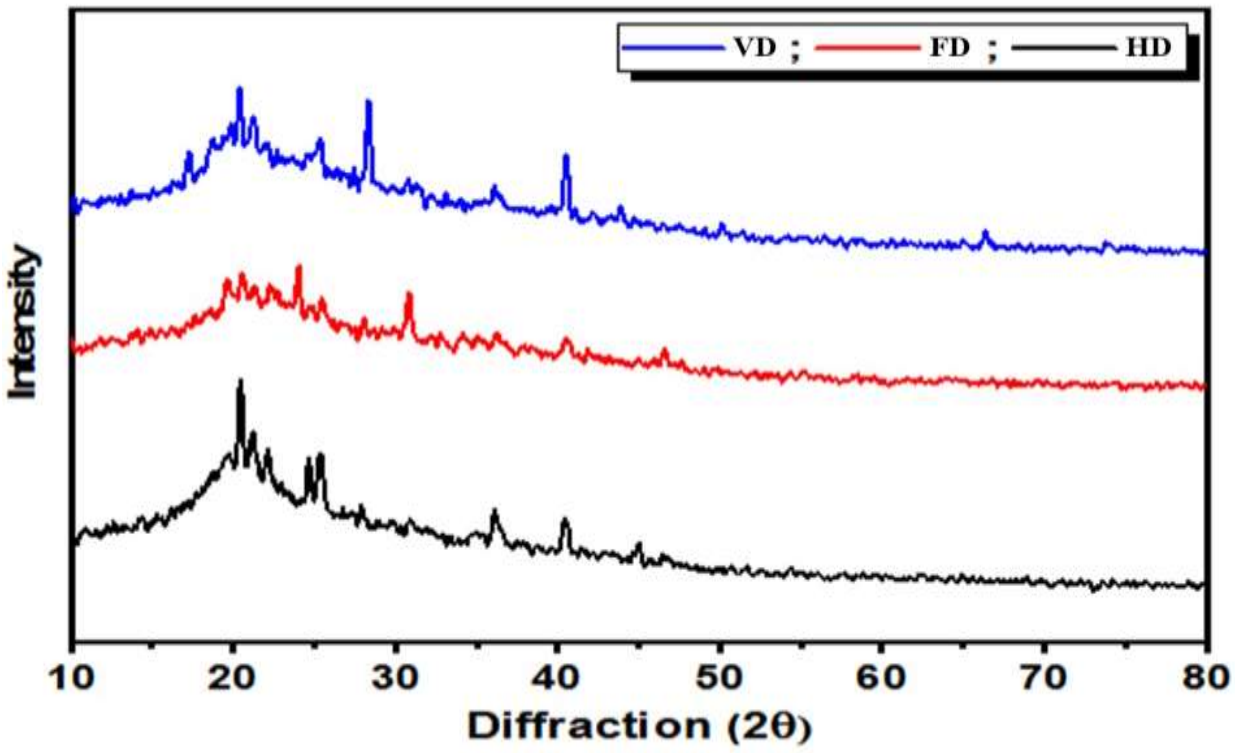

Figure 5.3. X-ray diffractometry of mushroom waste powder (MWP) obtained through various treatments (FD, VD and HD).

5.10.3. Thermogravimetric analysis (TGA)

The thermal degradation behavior of (MWP) subjected to freeze drying (as FD), hybrid drying (as HD), and vacuum drying (as VD) was investigated using TGA. TGA study showed that FD is the most thermally stable of the three drying processes. The FD sample showed the least initial weight loss (~2–5%), main weight loss (~20–30%), and maximum residual weight (~60–70%), demonstrating an improved retention of thermally stable substances and less thermal degradation. In contrast, HD showed moderate stability, characterized by greater initial (2–5%) and major (30–40%) reductions in weight and lesser residue (~50–60%), indicating biomolecule breakdown. VD had the lowest stability, with significant initial (>10-15%) and main (50-60%) weight losses including the lowest residue (~40-50%) due to intensive temperature exposure (Figure. 5.4). Numerous studies indicate that FD plant and fungal resources exhibit greater thermal stability than

their thermally dried equivalents, aligning with the current findings. Singh et al. (2023) shown that FD *Lentinula edodes* powders kept greater residual mass and exhibited a delayed onset of significant weight loss, indicating a retention of thermally resistant polysaccharides and proteins. Rasika and Amarasinghe (2023) noted that FD *Boletus edulis* exhibited higher char yield in TGA, attributed to reduced structural collapse, while hot-air-dried samples experienced rapid degradation. Zhou et al. (2017) attributed the increased final residue in FD samples of *Ganoderma lucidum* to diminished the thermal degradation of polysaccharide-protein complexes. The findings are consistent with the study by Shams et al. (2022) on FD *Agaricus bisporus*, which indicated that fewer initial mass loss and greater residual weight corresponded to improved preservation of bound water alongside bioactive macromolecules. The literature collectively indicates that FD reduces molecular deterioration during drying, resulting in enhanced thermal resistance, as demonstrated in the present study.

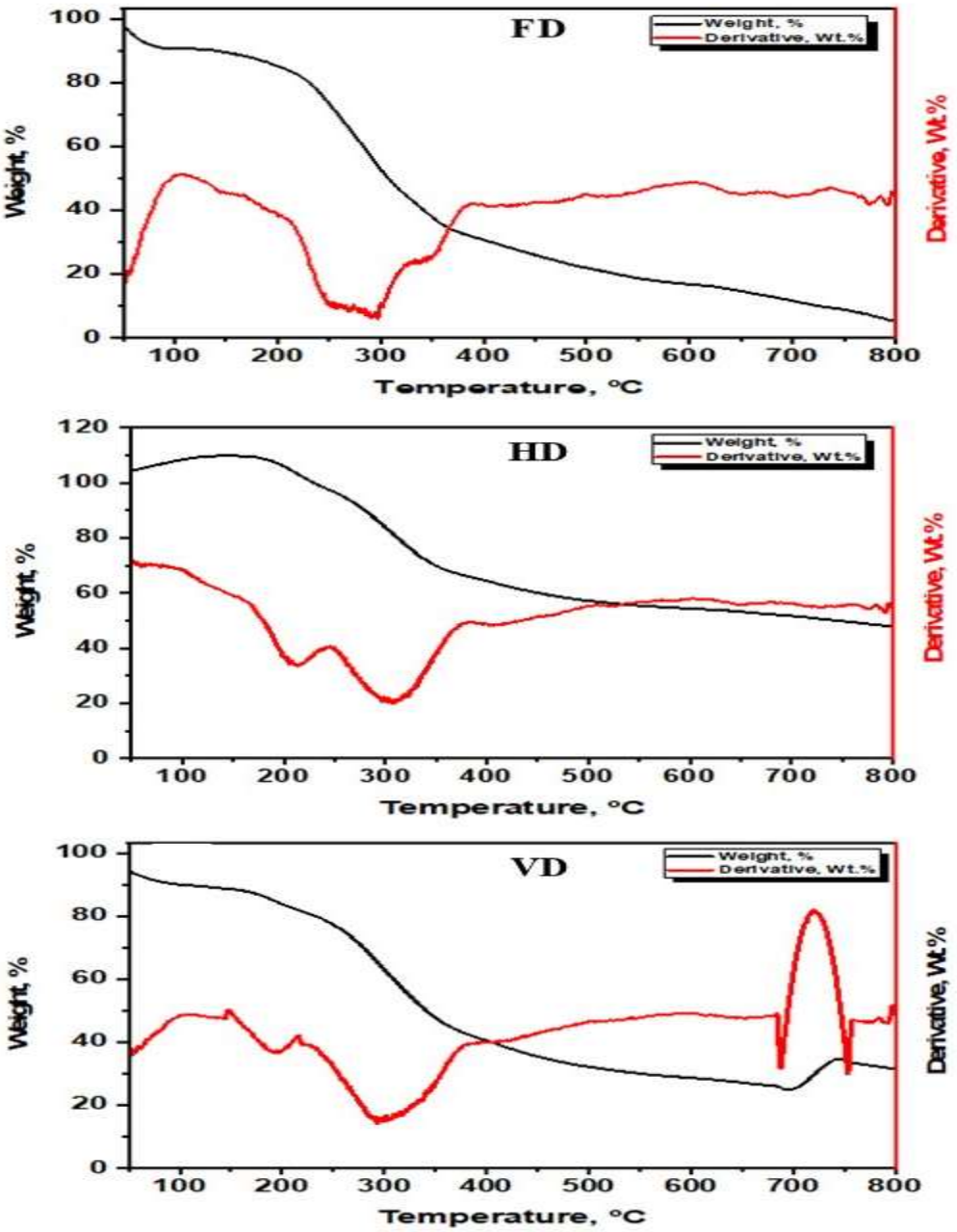

Figure 5.4. Thermogravimetric analysis of mushroom waste powder (MWP) obtained through various treatments such as FD: Freeze dried MWP, HD: Hybrid dried MWP and VD: Vacuum dried MWP.

5.10.4. Field Emission Scanning Electron Microscope (FE-SEM)

The microstructure of mushroom waste powder (MWP) generated by hybrid drying (as HD), freeze drying (as FD) and vacuum drying (as VD) was examined using FE-SEM at magnifications of 330x, 2000x, and 4000x (as shown in Figure 5.5.). The morphology indicated that the VD powder is Irregular, shriveled, compact particles compared to FD particles were porous, flaky, and sponge-like structure. The FE-SEM structure indicated that VD powder has less porous structure while HD and FD powder has more porous structures indicating that VD mushroom powder has low porosity and FD powder has high porosity. The surface texture was found to be smooth and collapsed however in case of FD powder the surface texture was rough with more open pores. The particle size of VD powder was lower due to collapsed surface roughness whereas the particle size of FD powder was greater due to sublimation driven structural retention. Due to all these features the VD powder has lower rehydration and solubility, HD powder has medium rehydration and solubility and FD powder has better rehydration as well as faster solubility. Therefore, VD powder has cell wall collapse and shrinkage, limiting porosity. The FD process preserved the original structure due to sublimation, retaining pore networks. This indicated that FD resulted in superior microstructural integrity, which improves functional properties and hence has better for applications requiring quick solubility such as beverages. On the other hand, VD powder is more compact and hence have longer shelf stability in the formulation. These findings are supported by Tontul and Topuz (2017) reported that FD tomato pulp powder exhibited sponge-like porous structures with minimal shrinkage, while HD samples showed compact and fused particle networks, negatively impacting solubility and rehydration. Similarly, Goyal et al. (2018) analyzed aloe vera powders and noted that FD maintained distinct surface microstructures with well-defined cell boundaries even at 2000x magnification, while vacuum drying led to rupture and coalescence of cell walls. Likewise, Kumar et al. (2018) observed comparable results in jackfruit seed flour, where FE-SEM at 2000x showed that FD powders exhibited distinct, well-separated starch granules, unlike the agglomerated structure found in HD samples. These findings reinforce that FD is more effective in preserving microstructural integrity, which is critical for achieving better powder functionality and quality.

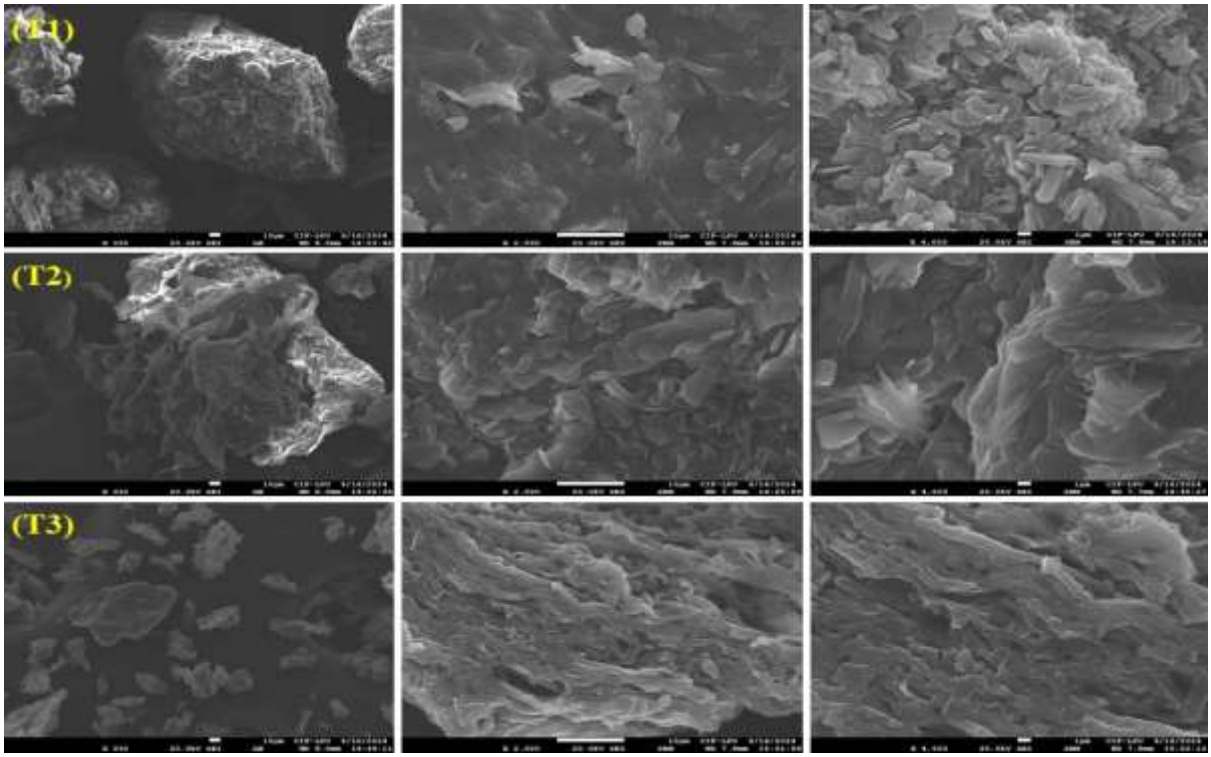

Figure 5.5. Field Emission Scanning Electron Microscope (FE-SEM) of mushroom waste powder (MWP) obtained through various treatments such as HD: Hybrid dried MWP, FD: Freeze dried MWP and VD: Vacuum dried MWP.

5.11. Techno-functional properties of extracted chitosan (CS) powder

5.11.1. Yield

The techno functional nature of CS powder obtained from different treatments at varied power levels were shown in following Table 5.4. all the corresponding values are summarized. CS was effectively obtained by the deacetylation process of mushroom chitin. The quality and techno-functional characteristics of prepared CS can significantly alter relying on quality of mushroom CS and the methods employed in its preparation. The fraction yield of CS obtained ranged from 6.18% to 6.98%. This variance can be attributed during the deproteination process where reduction in the acetyl group from chitin was seen when undiluted alkali (NaOH) solution was used, as explained by (Agarwal et al., 2018). (Boureghda et al., 2021) reported similar results when extracting chitin from various segments of *A. bisporous* (Stipe and gills), yielding 7.4% and 5.9%,

respectively, using acetic acid. In a parallel study investigating the amount of chitin of the pileus and stipes of mushroom at various growth stages of *A. bisporus*, *Lentinula edodes*, and *Pleurotus ostreatus*, the influence of the growing stage was examined, (Vetter, 2007) found that *A. bisporus* exhibited the highest chitin levels ie., 6.94 to 7.84% using acid like HCl for extraction, Moreover, the entire fruit body yielded even higher, reaching up to 8.68%. The moisture % after extraction of CS under various conditions was assessed, and the corresponding values are presented in Table 5.4. The moisture % was obtained in T5 i.e., 6.01% and the yield obtained to the respective treatment is 6.98%, whereas the yield and moisture content for T0 (using traditional extraction technique) was obtained to be 6.09% and 5.75% respectively. Moisture content has a significant impact on the power of strong NaOH needed during the deacetylation process. Thus, this might weaken the effectiveness of removing acetyl groups from chitin, accordingly affecting overall DD of end product shown by (Novikov et al., 2023). (Malm, 2021) and (Ibitoye et al., 2018) extracted CS from grasshoppers and house crickets, achieving maximum yields of 5.7% and 5.8%, respectively, using traditional extraction methods throughout the extraction process. The reason for reduced mass loss primarily attributed to the removal of proteins and minerals during deproteinization and demineralization processes (Da Silva Lucas et al., 2021). As reported, inadequate HCl concentration in traditional methods may result in reduced yields of ultrapure chitin. Conversely, excess acid may accelerate the degradation of polymeric chains, affecting the original polymer's molecular weight (Pillai et al., 2009; Roy et al., 2017). (Mohammadi et al., 2023) found contrasting results when comparing shrimp CS obtained via traditional and microwave-powered extracting methods. The research highlighted that the physico-chemical properties were notably affected by variations in heating process parameters. The traditional method produced heavy molecular weight CS with 12.7% yield, whereas microwave extraction produced medium molecular weight CS with a porous structure, yielding 11.8%. When microwave conditions were applied to conventional extraction, lesser molecular weight CS was obtained with the minimal yield of 10.8% and a reduced crystallinity index. Research conducted by (Naznin, 2005) reported a moisture % ranging from 6.62 to 8.01% when employing various concentrations of the alkaline solution utilized in the deacetylation process. The research conducted out by (Alishahi et al., 2011) indicated a moisture content of 2.5% in CS. The variance in these values may be attributed to the drying method employed in the current study, which involved sun drying for 6 hrs before oven drying. Implementing this approach could further decrease moisture % in

both CS and chitin, resulting in a reduced moisture content. CS extracted from fly pupae displayed a moisture content of 2.46%, which contributes to increased thermal stability. The lower moisture content inside polymeric chains attributed to the water molecules being adsorbed, resulting in a plasticizing impact on both thermal constancy as well as structure (Dehghannya & Ngadi, 2024). In contrast, CS sourced from shrimp (*Litopenaeus vannamei)* shells had a higher moisture content of 8.95% (Zapata-Luna et al., 2023). CS exhibits significant hygroscopic properties because it can create hydrogen chains with water using both its amino and hydroxyl groups. Commercial powdered CS typically exhibits a moisture range of 5.89% to 7.86% (w/w), a factor found to be unaffected by the DD or molecular weight, as highlighted by (Ssekatawa et al., 2021). In (Ssekatawa et al., 2021) study, CS extracted from Ugandan edible mushrooms using traditional methods exhibited moisture content fluctuations of up to 6.4%. This variation may stem from the earliest moisture % of the fresh sample materials and the ecological factors during storage (Wang & Zhuang, 2022). Also, the powder compressibility is most significantly influenced by moisture content, as noted by (Badwan et al., 2015). Elevated moisture content tends to reduce granule porosity and the likelihood of fragmentation, thereby enhancing granule strength, as explained by (Tofiq et al., 2022). Findings from the research by (Szymańska & Winnicka, 2015) intended that maintaining a low dewiness in CS, typically ranging from 6-10%, is crucial for enhancing its ability to form hydrogen bonding. Additionally, it was highlighted that a higher water content within the CS structure accelerates the polymer's degradation through hydrolysis reactions (Viljoen et al., 2014).

5.11.2. Solubility and pH

Solubility of CS performs a crucial function in evaluating the quality of CS obtained from either plant or animal sources. Greater solubility is indicative of higher purity and quality in the obtained CS (Bonilla et al., 2019). CS solubility can be impacted by various factors during the deacetylation of chitin, such as temperature, duration and alkali strength (El Knidri et al., 2018). For example, varying the heating duration and temperatures deacetylating chitin from same shrimp species using a consistent concentration of concentrated NaOH led to varying solubilities of consequent CS (de Queiroz Antonino et al., 2017). From this Table 5.4. CS obtained from T5 treatment showed the best solubility (%) i.e. 75.98, however the solubility and pH content for T0 was obtained to be 59.04 and 6.6 respectively. The observed variations in CS solubility in extraction could be

attributed to a high DD and the optimal pH are the fundamental parameters intimidating solubility. In a separate study by (Ssekatawa et al., 2021), CS derived from mushrooms showed moderate solubility ranging from 69% to 86% when extracted using traditional methods. This variation in solubility could be caused by the existence of inorganic minerals that were not entirely eliminated within demineralization, which significantly influenced solubility (Pellis et al., 2022). The solubility of CS, as documented in reviewed research papers ranges between 26.13% - 99.86% (Islam et al., 2019); (Chen et al., 2022; Cheng et al., 2020; Zapata-Luna et al., 2023). When CS is disintegrated in acetic acid, it gains a positive charge through the protonation of inherent amino groups, forming NH^{+3}. With increasing pH, the amine groups lose their protonation, causing CS to lose its positive charge and become indissoluble starting from pH 6.5. Insolvability is evident in the visual appearance of CS solution, which turns cloudy (Zapata-Luna et al., 2023). Marine source CS such as crab, fish, and shrimp, crab and fish exhibited solubilities of 70%, 60% and 78% respectively. Moreover, solubility is dependent on the operational temperature during the deacetylation process, with increased temperatures thereby resukting in solubility (Kumari et al., 2016). (Hossain & Iqbal, 2014) highlighted several key factors that affect solubility of CS, viewing temperature, duration of deacetylating, strength of alkali, ratio of chitin to basic solution and particle size. As per (Zhao et al., 2023), lesser solubleness of CS suggests insufficient process of deacetylation. The complete dissolvable property of CS relies on the reduction in the acetyl groups during deacetylating and a DD may potentially impact the results, as emphasized by (Weißpflog et al., 2021).

Considering the influence of pH, as per (Aranaz et al., 2021) CS oligomers demonstrate solubleness throughout a wide pH spectrum, ranging between acidic to basic circumstances together with pH 7.4. pH of the mushroom debris derived CS in T5 treatment is 7.5±0.1 closely aligning with the acceptable pH range for standard CS. CS solutions tend to undergo phase separation when the pH exceeds 6.5, whereas solubility is observed at pH levels below 6.5. When in a soluble state, CS becomes positively charged because of having protonated amino groups (Elsabee et al., 2009). In solutions with a pH ranging from 6.0 to 6.5 the unbound amino groups in CS structure experience reduced protonation, leading to increased hydrophobicity along the CS chain. At pH levels below 6, CS chains have the capability to interact electrostatically with molecules or polymers that carry a negative charge such as anionic glycosamino glycans and proteoglycans. When the pH is elevated, exceeding approximately 6.5, the amino groups present

in CS undergo deprotonation. This deprotonation can result in hydrophobic interactions between CS and various substrates, such as fatty acids and cholesterol, as exhibited in the research done by Dash et al. (2011). CS is a substance characterized by its restricted solubility in water, alkaline solutions, and many commonly employed organic solutions. Nonetheless, it can partially solvable in diluted aqueous acid solutions, like diluted acetic acid (Inamdar & Mourya, 2014; S. Kumari et al., 2016). In an aqueous acid solution, CS undergoes protonation because of the amino groups within its molecular framework which enhances its solubility (Inamdar & Mourya, 2014; Pillai et al., 2009; Roy et al., 2017) From the mentioned treatments, three treatments T2, T5 and T8 are selected on the basis of techno-functional properties like yield, moisture content, pH, solubility and flow properties. The T2, T5 and T8 treatments resulted more yield. Considering the flow properties, these treatments also offered insights good powder properties and good flowability indicating porous nature.

5.12. Determination of flow properties of extracted chitosan (CS)

This research investigated the bulk density (BD) and tapped density (TD) along with carr's index, and Hausner ratio, to comprehend the rheological attributes of isolated CS powders. Bulk and tapped density measurements offer insights into powder flowability. By utilizing both these values, the carr's index was determined, where a lower carr's index indicates improved powder flowability. Carr's values categorize flow properties into different ranges: 5 to 10 as excellent, 12 to 16 as good, 18 to 21 as fair, and 23 to 28 as poor (Azubuike et al., 2012). Conversely, for the Hausner ratio, a value below 1.20 shows beneficial flowability, while a value of 1.50 or above indicate deficient flow qualities. In this investigation, the CS extracted under T5 conditions (540W:180W:360W) demonstrated Carr's index of 10.46 suggesting excellent or free-flowing features. The Hausner ratio for this sample was 1.11 which is underneath the threshold of 1.25 (demonstrating excellent flowability), additional verifying its favorable flow traits. For T0 lesser bulk and tapped density values are obtained ie., 0.67 and 0.83, however with respect to carr's index and hausner ratio the values are 19.27 and 1.24 respectively (Table 5.4.). The process of synthesis significantly influences the bulk, tapped, and packing characteristics of CS powders obtained from mushroom waste. Elevated bulk and tapped density may arise from minimal particulate irregularities, indicating a porous nature in the CS structure, as suggested by (Yarangsee et al., 2021). This could also imply that the CS has undergone a deproteinization treatment with a lower

alkali concentration, as described by (Iber et al., 2022). Furthermore, the physico-chemical properties of CS T5 (540W:180W:360W), derived through deacetylation from chitin in mushroom waste, closely resemble those of commercially sourced CS from shrimp shells or crab, as indicated in the literature. The obtained values for the Hausner ratio line up consistently with Carr's index. These results are consistent with the outcomes anticipated by Sreeharsha et al. (2024). In Olorunsola et al. (2017) CS extracted from shells of *Callinectes gladiator* using a traditional method exhibited a 62.7% DD along with 2.88 viscosity. The bulk density was measured at 0.60, with a tapped density of 0.74. Additionally, the % Carr's index was 18.90 and Hausner's ratio was 1.23. According to these measures, the CS exhibited acceptable flow characteristics and exhibited the maximum true density. True/Tapped density, which excludes all void spaces, indicates the extent to which a powder can be compacted. Bulk density reflects a powder's compressibility a lower bulk density suggests a greater tendency for densification, often due to particle irregularities and a porous structure (Taylor, 2021). The findings of our research aligned with those of (Iber et al., 2022) & (Iber et al., 2023), where bulk density mean value ranged among 0.19 to 0.28 g/mL, and tapped density dropped between 0.26 to 0.35 g/mL. An Improved bulk and tapped density of CS indicates greater porosity of the material (Iber et al., 2022). While CS from certain sequences in the current study may seem to have varying levels of porosity, the variation observed was not deemed significant. Another study involving the extraction of CS from giant freshwater prawns reported bulk and tapped densities of 0.25 g/mL and 0.32 g/mL, respectively, which aligns with the results of the present study (Iber et al., 2023).

Table 5.4. Techno-functional properties of extracted chitosan (CS) powder.

S. No.	Chitosan sample	% Moisture	% Yield	pH	% Solubility	Bulk density (g/ml)	Tapped density (g/ml)	Carr's index	Hasneur ratio
1.	T0	5.75±0.03^{d}	6.09±0.01^{c}	6.6±0.01^{a}	59.04±0.03^{a}	0.67±0.04^{b}	0.83±0.02^{d}	19.27±0.04^{c}	1.24±0.03^{a}
2.	T1	7.21±0.13^{a}	6.65±0.11^{a}	6.7±0.1^{a}	60.45±0.11^{a}	0.74±0.01^{a}	0.89±0.01^{a}	16.85±0.15^{a}	1.20±0.01^{a}

3.	T2	7.12±0.11^{a}	6.56±0.09^{a}	6.5±0.2^{a}	60.39±0.12^{a}	0.73±0.01^{a}	0.85±0.007^{b}	14.11±0.81^{b}	1.16±0.01^{b}
4.	T3	7.86±0.04^{b}	6.26±0.03^{b}	7.0±0.2^{b}	70.19±0.29^{b}	0.71±0.01^{b}	0.86±0.002^{c}	17.44±0.14^{c}	1.21±0.02^{a}
5.	T4	7.67±0.08^{c}	6.18±0.02^{c}	6.8±0.2^{b}	70.83±0.81^{b}	0.72±0.01^{a}	0.85±0.009^{b}	16.47±0.01^{a}	1.19±0.02^{a}
6.	T5	6.01±0.08^{d}	6.98±0.10^{d}	7.5±0.1^{c}	75.98±1.23^{c}	0.77±0.01^{c}	0.86±0.002^{c}	10.46±0.08d	1.11±0.01^{c}
7.	T6	5.89±0.07^{d}	6.61±0.07^{e}	7.4±0.2^{c}	75.21±0.82^{c}	0.70±0.01^{b}	0.84±0.01^{d}	16.66±0.08^{a}	1.20±0.01^{a}
8.	T7	6.82±0.08^{e}	6.39±0.1^{f}	7.2±0.1^{b}	70.62±0.89^{b}	0.75±0.02^{a}	0.86±0.008^{e}	12.79±0.23^{b}	1.14±0.01^{d}
9.	T8	6.31±0.04^{f}	6.28±0.07^{f}	7.0±0.2^{b}	70.51±1.09^{b}	0.74±0.01^{a}	0.86±0.004^{e}	13.45±0.74^{b}	1.13±0.02^{d}

Each column's values denoted by a different superscript letter are statistically distinct from each other ($p<0.05$).

Figure 5.6. Chitosan powder extracted from mushroom waste powder (MWP) using microwave assisted extraction technique.

5.13. Degree of deacetylation (DD) of extracted chitosan (CS) powder

DA significantly impacts the quality of CS, with higher purity associated with an increased DD. Agarwal et al. (2018) observed that DD in CS varies relying on the variety and preparation technique, varying from 56% to 99%, with average around 80%. (Foster et al., 2015) defined CS as chitin having a DD more or equal to 75%. (Aldila et al., 2020) indicated that DD is persuaded by the strength of NaOH, highlighting the difficulty in removing acetyl groups bound in chitin. Thus, a considerable concentration of NaOH/KOH and elevated temperatures are required, as noted by (S. Kumari et al., 2017). This necessity stems from the significant influence of steric hindrance on the deacetylation process of chitin stemming from inherent chitin structure (Vicente et al., 2021). The hindrance caused by the dense structure of chitin inhibits the accessibility of OH- ions to attack the amino group. Moreover, the rate of diffusion OH- ions to both the outward and the interior of the chitin molecule is heavily reliant on the concentration of alkali (Aldila et al., 2020). Furthermore, the extent of deacetylation observed in commercial CS varies among 70% to 85%, as indicated by (Rasweefali et al., 2022). In our investigations, the DD of CS ranged among

75.09% to 79.94%, with the optimal outcome observed at a power level of 180W in T5 (Table 5.5.). The DD in the process of its production from mushroom waste is liable on various conditions. Studies have indicated that the DD tends to decrease with a rise in deproteinization temperature, a trend we also observed in our own research. In addition, using a traditional method, another mushroom species yielded CS having 78.1% DD. This DD value affects various properties of CS, including biological, physicochemical, and mechanical traits, as discussed by (Ssekatawa et al., 2021). The lower energy input into the system may have led to partial deacetylation of chitin, preventing it from fully solubilizing in an acidic medium (Pillai et al., 2009; Roy et al., 2017). Elevated-temperature processing adversely affects the DD of CS, as given by (Abdou et al., 2008), (Aldila et al., 2020) and (Cheng et al., 2020). In a separate investigation, (Yarnpakdee et al., 2022) documented DD values ranging among 73.56% to 75.56% for CS derived from aquatic mantis shrimp, which was constructed employing different deacetylation times (Zapata-Luna et al., 2023). Increasing the DD results in more amino groups being present in the C2 location of CS, leading to a greater plus charge and enhanced antimicrobial action (Thambiliyagodage et al., 2023). Nevertheless, deacetylation through acidic conditions and high temperatures is not the preferred method due to its detrimental impact on glycosidic bonds, polymer chain breakage, and the production of darker-colored CS. In contrast, gentler treatments result in CS with a lighter color, as observed in the findings of (Huq et al., 2022).

Table 5.5. Effect of treatment on Degree of deacetylation (DD), Crystallinity index (CI) and bioactive properties of extracted chitosan (CS) powder.

S. No.	Chitosan sample	DD	CI	% DPPH	% RP
1.	T2	75.71 ± 0.80^{ab}	1.06 ± 0.12^{ab}	42.06 ± 0.01^{a}	2.41 ± 0.02^{a}
2.	T5	79.94 ± 0.13^{c}	1.09 ± 0.1^{a}	53.97 ± 0.01^{c}	3.58 ± 0.02^{c}
3.	T8	75.09 ± 0.34^{b}	1.02 ± 0.1^{c}	51.33 ± 0.01^{b}	2.94 ± 0.01^{b}

Each column's values denoted by a different superscript letter are statistically distinct from each other ($p<0.05$).

5.13.1. Crystallinity

The crystallinity of CS obtained using microwave methods is outlined in Table 5.5**.** The crystallinity of CS produced in treatments T2, T5 and T8 are 1.06, 1.09 and 1.02 respectively. However, A notable correlation exist within DD and crystallinity of CS. The molecular chain of non-deacetylated chitin is comparatively consistent and demonstrates a high degree of chronicity, resulting in elevated crystallinity. Deacetylation induces diversity in the molecular chain, resulting in decreased crystallinity due to increased intermolecular hydrogen bonding and networking of polymer chains. CS displays two primary peaks on the XRD diffractogram, typically occurring around 10° and 20° 2θ angle values. The initial peak corresponds to the 020 plane (amine I - acetylated amine group in CS), while the second peak is associated with the 110 plane (amine II - free amine group in CS). The 020 reflections are attributed to acetamide groups capable of forming hydrogen bonds with water, leading to the formation of hydrated crystals (Dziedzic & Kertmen, 2023). As a part of studies carried out by Agarwal et al. (2018), CS samples prepared using a traditional method exhibited a crystallinity index of 0.95. This was achieved by employing a 30% NaOH in a ratio of 1:50 (w/v) for extraction, followed by deacetylation under working pressure of 15 psi at 121 °C for 30 min following an autoclave. This time around, the NaOH solution penetrating the amidst of α-chitin sequence may have been impeded by intermolecular network, resulting in a reduced DD in the sample. This method also exposes the sample to potential thermal and shear degradation common in conventional approaches. Microwave-assisted heating, however, could enhance our findings by promoting improved solvent mixing, which aids the penetration of solvents within the polysaccharide arrangement and facilitates the reaction (De Oliveira Silva et al., 2024). Nevertheless, with improved DD, the molecular chain has a tendency to homogenize, resulting in a corresponding rise in crystallinity (Lopes et al., 2021). During the reaction process, CS produced via microwave exhibited relatively high crystallinity, suggesting a more ordered arrangement of molecular chains. This indicates that microwave radiation could enhance the uniformity and completeness of the deacetylation reaction. Indeed, with a high DD, CS possesses fewer acetyl groups in its structure. Consequently, there is a reduction in intermolecular hydrogen bonding between hydroxyl and acetyl groups within its parallel arrangement, resulting in a lower degree of crystallinity (Nguyen et al., 2022).

5.14. Determination of bioactive compounds in extracted chitosan (CS) powder

5.14.1. Antioxidant Activity (AA) and reducing power (RP) assay

Taking action against hydrogen radicals is a crucial part of antioxidation. The purple color of the solution is caused by the absorption of light at 517 nm by the hydrogen-free radical in DPPH (2,2-diphenyl-1-picrylhydrazyl). The interaction between DPPH and proton radical scavengers causes this color to fade rapidly. (Aradmehr & Javanbakht, 2020). The AA of CS produced in treatments T2, T5 and T8 are 42.06%, 53.97% and 51.33% (as shown in Table 5.5.) respectively with the optimal outcome observed at a power level of 180W in T5 having highest DD i.e., 79.94%. Ascorbic acid showed moderate to high scavenging abilities of 55.14%. The RP of respective CS samples shown in Table 5.5. at concentration of 1mg/ml showed moderate values of 2.41%, 3.58% and 2.94% for CS produced in treatments T2, T5 and T8. Thus, AA of CS was determined to be moderately effective at scavenging DPPH radicals. It appears that the scavenging abilities of CS improve as the DD increases. These judgements align with the outcomes stated by (Samar et al., 2013) and where the CS from shrimp waste having DD range of 67.58–78.83%, 76.89–83.05% and 88.39–95.19% showed AA in the range of 16.14–20.54%, 21.27–25.18% and 21.03–32.76% at 1mg/ml, respectively. The scavenging capabilities of CS appear to enhance with higher DD due to the increased presence of C2 amino groups, which obstruct the oxidation of ascorbic acid, consequently boosting their AA. Current findings corroborate this hypothesis, indicating that the appearance of free amino groups plays a significant contribution in achieving effective antioxidant performance. Specifically, higher (DD) led to CS with improved antioxidant properties. Reducing power (RP) sample concentration of of CS of 1mg/ml exhibited modest range (ranging from 1.87 to 2.28, 1.98 to 2.10, and 0.62 to 1.89) across the same CS samples. Another study highlighted the significance of extended deacetylation and its influence on scavenging action by generating highly deacetylated products (Avelelas et al., 2019). This study compared chitooligosaccharides (DD: 86−93%) with aqueous dissolved CS (DD: 55−62%) and demonstrated the amino acid chain could be a significant role in neutralizing free radicals.

According to (Kusnadi et al., 2022), after extracting white shrimp (*Penaeus indicus*) CS, AA of the Manufactured CS and CS extract for DPPH radical scavenging varied between 18.80% to 42.27% with a DD of 78.60%, and 13.45% to 33.86% having DD of 73.46%, respectively. CS having improved DD has the potential for increased AA because of the higher concentration of

amino compounds in its arrangement. Here AA can be correlated with maximum inhibitory concentration value (IC50). According to (Chlif et al., 2021), a lower IC50 value indicates higher AA of the sample. The analysis results showed that the scavenging abilities of extracted CS, market based DPPH radicals and CS/ascorbic acid yielded IC50 values of 4.25 mg/mL, 5.2 mg/mL, and 1.45 mg/mL, separately. Similar positive correlation is is based on the findings from (Hafsa et al., 2016) upon extracting CS from *P. longirostris* shrimp shell CS indicated DD at 73.68% and 83.55% exhibited antioxidant values of 21.25% and 44.17%, respectively. Thus, it can be inferred that higher DD in CS leads to higher antioxidant values.

Earlier research has demonstrated that the AA of CS is substantially influenced by its DD (Doval et al., 2023). This is attributed to the appearance of active hydroxyl and amino groups in CS chains, which can interact with unbound radicals (Wu et al., 2024) CS capability to scavenge radicals may arise from the interaction coupling protonated amino groups and unattached radicals, as suggested by (Wang et al., 2024), Numerous researchers have proposed the scavenging action of CS which involves the a powerful macromolecule radical is formed through a reaction of CS active hydrogen atoms with radicals of hydroxyl along with superoxide anion within CS molecule, at C−2 (NH_2), C−3 (OH), and C−6 (OH) positions are the main hydrogen origins as described by (Parameswaran et al., 2024).

5.15. Characterization of extracted chitosan (CS) powder

5.15.1. Fourier transform infrared (FTIR) spectroscopy

The FTIR spectra of CS samples through various treatments is shown in Figure 5.7. FTIR analysis of mushroom CS revealed distinct peaks that match the functional groups found in CS extracted from mushrooms. CS exhibits distinct peaks at particular wave numbers that indicate its structural constituents. The FTIR spectra of CS display peaks, including O-H stretching peak typically ascertained in the range between 3200-3600 cm^{-1}. Peaks detected within the limits between 2850-3000 cm^{-1} signify the C-H expansion. Similarly, the existence of C=O stretching in Amide I is indicated by the appearance of peaks around 1650-1655 cm^{-1}, while the presence of N-H deflection in Amide II is indicated by peaks around 1595-1605 cm^{-1}. The existence of C-O-C expansion was displayed by the occurrence of vertices between 1060-1150. The peaks and intensities observed in mushroom CS deviated a little based against the treatment exerted, likely due to differences in molecular forms and derivation methods used. The analysis of the FTIR spectrum facilitated the

identification of these distinctive functional groups and the verification of the molecular structure of CS.

The FTIR analysis exhibited the representative absorption peaks of T2 sample at the wavenumbers of 614 cm^{-1}, 1024, 1374 cm^{-1}, 1554 cm^{-1}, 1628 cm^{-1}, 2921 cm^{-1} and 3261 cm^{-1}. The absorption vertices of T5 sample were observed at 595 cm^{-1}, 1063 cm^{-1}, 1376 cm^{-1}, 1559 cm^{-1}, 1653 cm^{-1}, 2360 cm^{-1}, 2919 cm^{-1} and 3261 cm^{-1} wavenumbers. T8 sample displayed the characteristic absorption vertices at the wavenumbers of 843 cm^{-1}, 1024 cm^{-1}, 1448 cm^{-1}, 1649 cm^{-1} and 3262 cm^{-1}. An additional characteristic absorption peak was detected at wavenumber of ~ 2360 cm-1 in the case of the T5 sample while the characteristic peak observed at the wavenumber (2919 – 2921) cm^{-1} in the case of T2 and T5 samples was not detected in the T8 sample. Almost all the characteristic peaks observed in all the samples were similar except the aforementioned peaks. The shifting of the peaks in the higher wavenumbers with higher peak intensities was noted in T5 sample compared to the T2 and T8 samples which signifies better intra and intermolecular bonding of the T5 sample. Lowest characteristic absorption peak intensities detected in the case of the T8 samples could be ascribed to the weaker intra and intermolecular bonding frameworks. Thus, the FTIR analysis demonstrated the T5 sample as the better molecular bonding structure or the least affected one during the microwave-assisted extraction of mushroom CS.

The depiction of CS using FTIR derived results alike to those received in earlier analyses. Specifically, the stretching0+ of the amide I band, attributed to the C=O group in CS retrieved from crayfish and shrimp, was found to be at 1660.41 cm^{-1} and 1658.48 cm^{-1} correspondingly (Ossamulu et al., 2023). Whereas the peaks at the wavenumber 2918 cm^{-1} and 2921 cm^{-1} of the obtained *Agaricus bisporus* CS symbolizes the stretch vibration of CH3 group as shown by (Shahadha et al., 2023). (Shahadha et al., 2023) also showed the Peaks at 1554 and 1559 cm^{-1}. The appearance of the vertice at around 1 in the relevant spectra indicates the N-H group in the second II amide bond. These findings regarding functional groups align with those reported by (Hadidi et al., 2020) where two peaks emerged at 1065 cm^{-1} approves the existence of C-O-C stretching. However similar results ratify the existence of C-N stretching at 1350-1450 cm-1 by (Hadidi et al., 2020) where when diagnosing CS produced by FTIR device. Similar bands with comparable intensities are also noted nearly at 1550 and 1650 cm^{-1} in the CS spectrum, corresponding to the expansion vibrations of N-H and C=O (in the $NHCOCH_3$ group) accordingly shown in the literature by (Da Silva Lucas et al., 2021). Similar FT-IR band with equivalent strength was also

observed in the CS isolates from C. echinulate, the carbonyl stretching displayed frequency range of about 1643 and 1588 cm^{-1}. Peaks observed at 1315–1320 cm^{-1} was denoted to the amide III bands. Two absorption bands at roughly 1655 as well as 1625 cm^{-1} are distinctive of amide groups that are hydrogen-bonded (Azeez et al., 2023). The findings corroborate previous reports regarding the production of CS from house cricket flour. Key functional groups like -NH and -OH bands, located near 3400 and 3300 cm^{-1} singly, were identified. Moreover, the spectrum showed the lengthening of the C=O bond at 1645 cm^{-1}, the deflection of the N-H bond of the principal amine at 1555 cm^{-1} and the C-O bond expansion that corresponds with1qtfrsd1 five-carbon cyclic ether at approximately 1009 cm^{-1} (Espinosa-Solís et al., 2024). As mentioned in previous literature, unique bands in certain regions of 1020-1065 cm-1 confirm the C-O expansion. Additionally, the band located near 890 cm^{-1} is attributed to the out-of-plane vibration of the C-H β-glycosidic bond (Martín-López et al., 2020) (Wiercigroch et al., 2017). The lack of the band near 1540 cm^{-1} in the FTIR spectrum showed successful removal of proteins after deproteinization step. This particular band, which is attribute of N-acetyl groups and conforms the N-H twisting of amide-II, was hardly seen in our FTIR data, consistent with previous findings (Da Silva Lucas et al., 2021). Inside the fingerprint zone (600–1500 cm^{-1}), range 1147 and 1160 cm^{-1} exhibited sufficient absorbance intensity across all samples, demonstrating the lengthening of an asymmetric C–O bond and suggesting the existence of a glycosidic bonds among samples. depending on the wavenumbers observed, it could be inferred that all the extracted samples consist of CS (Lam et al., 2023). The peaks and intensities observed in mushroom CS showed slight variations relying on the treatment used. These differences possibly attributed to the distinct molecular framework and derivation techniques operated. The analysis of the FTIR spectrum enabled the recognition of these distinct functional band and the confirmation of the molecular structure of CS.

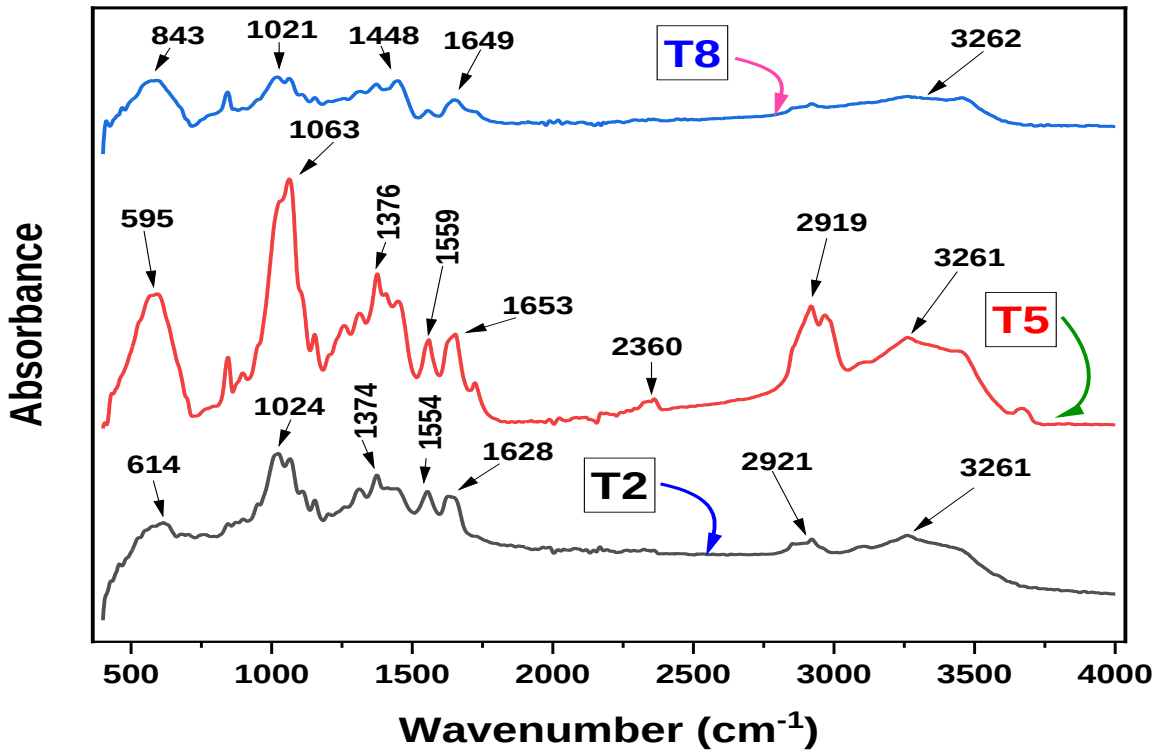

Figure 5.7. Fourier transform infrared spectra of chitosan samples extracted using different treatments.

5.15.2. X-ray powder diffractometry (XRD)

The CS diffractogram obtained using three different treatments T8, T5 and T2 is shown in Figure 5.8. The crystalline framework of mushroom-derived CS was assayed through X-ray diffraction (XRD), revealing the influence of extraction process. The X-ray diffraction (XRD) arrangement of mushroom CS exhibited distinct characteristics attributed to structural differences when equated to CS obtained from alternative sources. The XRD pattern can be swayed by factors like molecular weight, crystallinity and CS purity derived from mushrooms. The impact of the extraction technique on the crystalline structure in these diffractograms was observed. CS commonly displayed clear peaks in XRD as a result of its semi-crystalline characteristics. The primary peak attributed to CS was observed at 2θ values ranging from 10 to 20 degrees. The magnitude and location of this peak exhibited variations relying on the level of DD of CS, as well as its molecular mass. Examining the XRD graph entitles for the finding of the crystalline properties, level of crystallinity, and crystallographic structure of the CS obtained from mushrooms. The XRD curve

showed a broad amorphous peak at 2θ value of 19.2° in all the samples. The crystalline peak of T2 was found to be at a 2θ value of 26.4 while at 26.0° for the T5 sample. Distinctive peaks of the T8 samples were obtained the 2θ values of 26.3°, 29.4°, 32.3°, 33.5° and 37.8°. The peaks with improved crystallinity and larger peak intensities at the 2θ values of 29.4°, 32.3°, 33.5° and 37.8° of the T8 sample signified the more crystalline character compared to the remaining two (T2 and T5) samples. These peaks represent typical crystal patterns of α-chitin, which is the most prevalent type found in CS. The presence of these peaks is associated with ordered regions that involve the acetamide groups and hydrogen bonds (Lopes et al., 2021). The magnitude and location of this peak exhibited variations depends on DD of the CS and its molecular weight.

Rahayu et al. (2022) stated that these peaks are indicative of pure CS. However, the crystallinity index (CrI) of the CS got from these mushroom waste samples are lesser than the values documented in the literature. Ghassemi et al. (2021) observed that low values of the crystalline index indicate an abundance of amorphous glucan within the chitin structure further indicating that the purity of mushroom CS extracted from *A. bisporous* waste is lower. Comparable diffraction peaks were detected for the exoskeleton of White shrimp (*Litopenneaus vannamei*) by (Martín-López et al., 2020). where crystalline planes at 2θ ≈ 19.7° can be attributed to origin of chitin (Da Silva Lucas et al., 2021). According to the literature, certain chitosan XRD formats show two distinct vertices, typically near 2θ ≈ 10° and 20°, as observed for CS obtained from *Agaricus bisporus* (Hassainia et al., 2018). The emergence has also been noted as DD rises as more steps are added during microwave extraction, indicating the presence of hydrated crystalline allomorphic CS (Martín-López et al., 2020). Comparable outcomes were also documented by (Triunfo et al., 2022) and (Tolesa et al., 2019), where chitin displayed prominent sharp peaks at 9° and 19°, along with 3 to 4 weaker peaks near 13°, 21°, 23° and 26°, depicting the α-form of the polymer. Equivalent representative vertices at 10.0 and 20.0 were disclosed in CS samples obtained from tiger shrimp supporting their CS nature with large difference in the strength of the XRD pattern throughout the orders. The level of deacetylation in CS determines its crystallinity. CS is classified as fully crystalline when it reaches 100% DD, whereas any form with partial acetylation is categorized as semi-crystalline (Iber et al., 2023). The presence of crystallites within the amorphous zone of CS possible because of residual chitin that remains unreacted within the molecules (Kozma et al., 2022). Current investigation led by (Espinosa-Solís et al., 2024). a comparable XRD pattern was observed, exhibiting a similar form and location to those identified

in the sample gained in this study. This confirms the distinctiveness of the compounds. Furthermore, the crystalline heights observed at around 9.6, 19.6, 21.1, and 23.7 degrees in 2θ affirm that the chitin obtained is in the α-chitin form. Analyzing the XRD pattern enables the determination of the crystalline properties, level of crystallinity and crystallographic structure of the CS obtained from mushrooms.

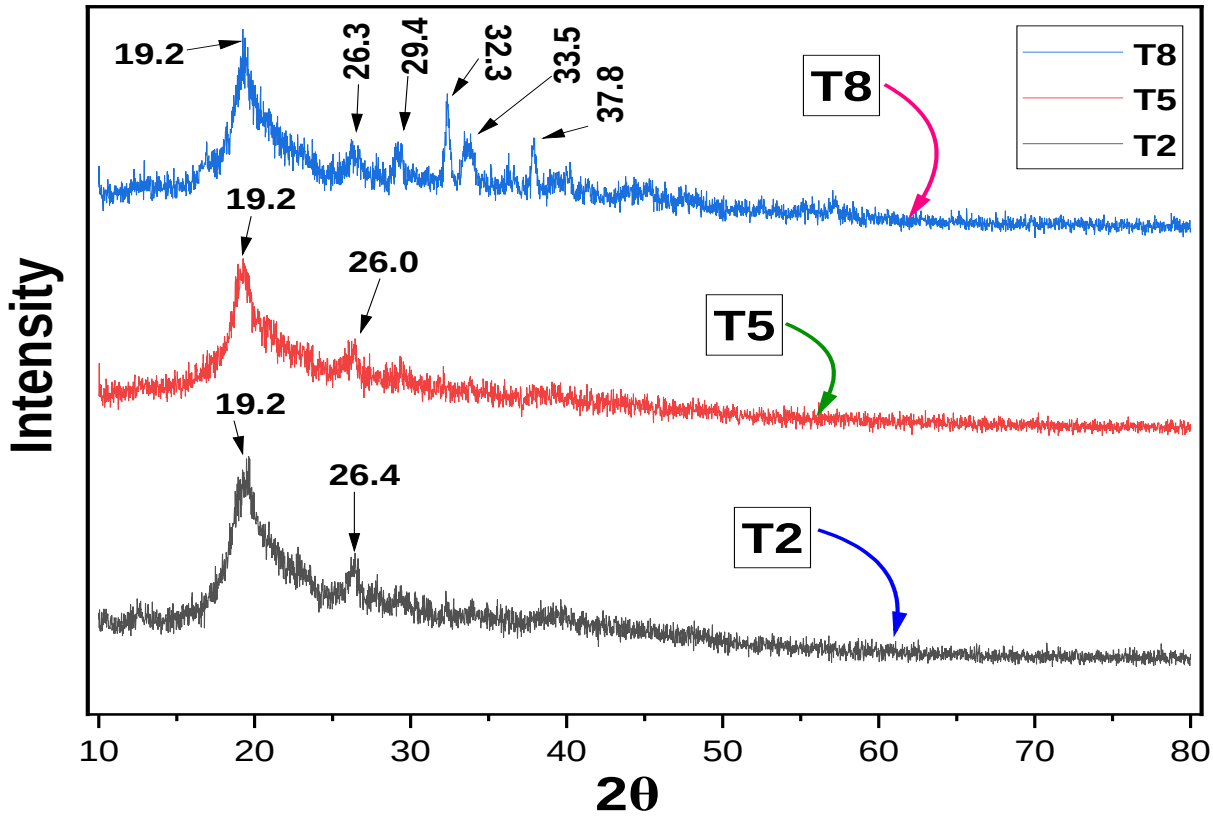

Figure 5.8. X-ray diffractometry of chitosan powder extracted using different treatments.

5.15.3. Differential scanning calorimetry (DSC)

DSC quantifies the transfer of heat (either into or out of) a sample in comparison to a reference material, with respect to temperature variations. CS frequently undergoes a glass transition, transitioning from a amorphous form to a rubbery or viscous one. The transition temperature offered worthy insights concerning flexibility and mobility of the CS polymer chains. CS can exhibit melting or crystallization peaks, which indicate changes between different solid states, depending on its purity and molecular structure. This knowledge is essential for comprehending its stability and prospective applications in controlled-release formulations or scaffold creation. DSC detected endothermic peaks associated with the liberation or uptake of moisture within the CS specimen. Differences in the DSC curve relative to pure CS may suggest modifications resulting from chemical changes or the use of additives during the extraction or processing of CS from mushrooms. The utilization of DSC for thermal study of low molecular weight CS, derived from mushrooms, revealed a broad endothermic peak in the temperature reach around 80-120 °C because of dehydration process of water.

Moreover, the observed rise in exothermic enthalpies of CS resulting from various treatments suggests variations in the molecules' intramolecular bonding strength, likely due to chain shortening. The To, Tm, Tc and ΔH of all the analyzed samples are shown in the Figure 5.9. The To values were 59.8 °C, 65.0 °C and 91.0 for T2, T5 and T8 samples accordingly. Tm and Tc values were 82.4 °C, 87.5 °C and 99.1 °C; and 97.5 °C, 98.2 °C and 114.1 °C respectively for T2, T5 and T8 samples. ΔH values of all the samples were 0.046 J/g, 0.011 J/g and 0.791 respectively for T2, T5 and T8 samples. Higher values To, Tm, Tc and ΔH of the T8 samples indicated better thermal characteristics contrasted to the T5 and T2 samples. However, how much sodium hydroxide was used to deacetylate and deproteinize phases impacts thermal stability of the samples. A gain in the strength of the NaOH results in a slender improvement in heat resistance. This observation is further supported by comparing the temperatures and heat change at the point of disintegration with those of market based CS (Soon et al., 2018). The application of DSC for thermal study of low molecular weight CS, derived from mushrooms, revealed a wide endothermic peak in the temperature reach of 87-100 °C, this process can be imputed to the dehydration process of water.

According to (Da Silva Lucas et al., 2021) market-based CS showed an exothermic having Tmax of 110.18 °C, akin to that discovered in CS extracted from mealworm's cuticles (111.96 °C).

Above temperature drift is typical of the transition in the agglomeration phase, suggesting the removal of remained vapour within the sample, along with the initiation of material combustion as also noted in other studies (Hadidi et al., 2020; Molina-Ramírez et al., 2021; Ijaz et al., 2022). Likewise, thermogram derived from DSC analysis of CS extracted from cricket flour exhibits an exothermic rise at 185 °C, indicating the temperature at which crystals form (Tc). This suggests that the thermic aspects of CS align with its crystalline nature (Espinosa-Solís et al., 2024). In a different DSC thermogram of CS, two peaks are observed. The initial peak (endothermic, below 100 °C) is linked to the removal of the vapour. Second signal (exothermic, around 300 °C) is connected to the breakdown of the CS pyranose ring. The melting temperature of CS determined through DSC analysis is approximately 110 °C (Dziedzic et al., 2023). Thermal breakdown necessitates heat gain to disrupt hydrogen binding, a reaction recognized as an endothermic height, with the energy required for the reaction to happen. It is crucial to emphasize that for polysacharides melting situation (highest temperature) represents general melting point of crystallites. This is not a actual value for sample but quite rely on the molecular weight (Molina-Ramírez et al., 2021). Moreover, the observed rise in exothermic enthalpies of CS resulting from various treatments suggests variations in the molecules' intramolecular bonding strength, likely due to chain shortening.

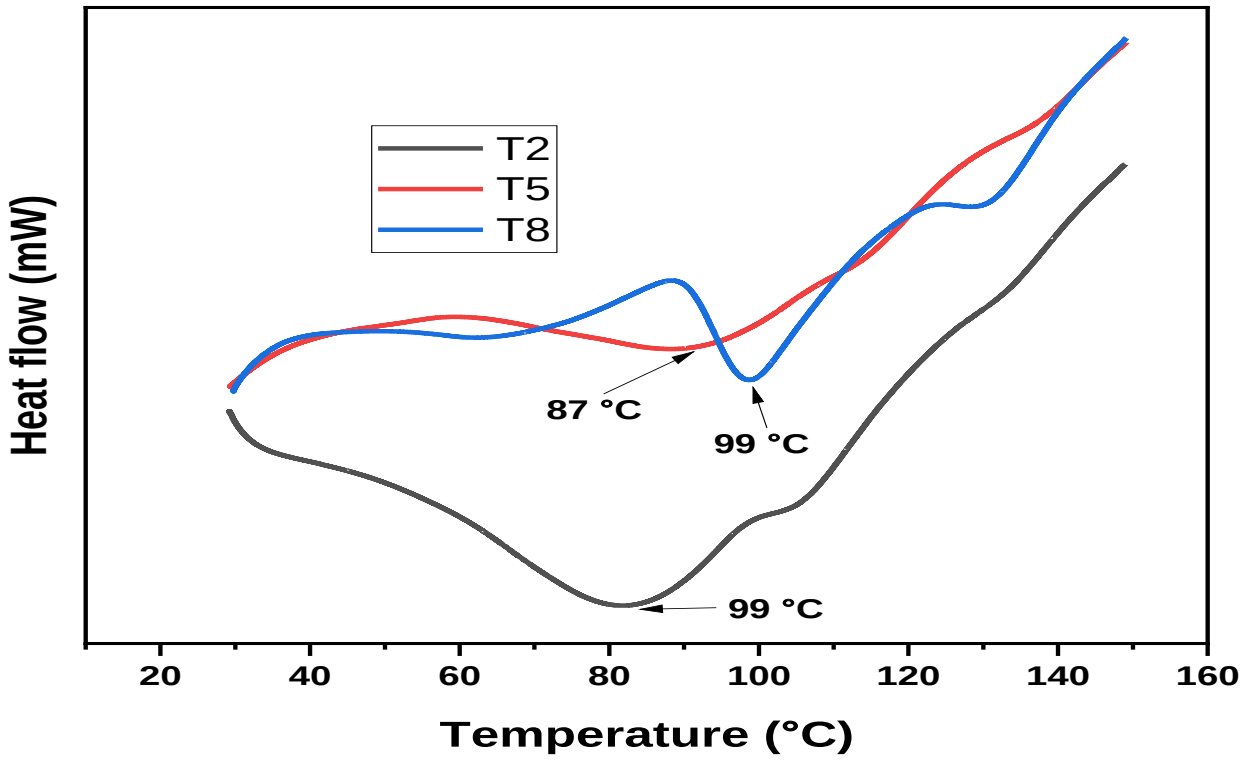

Figure 5.9. Differential scanning calorimetry of chitosan powder extracted using different treatments showing To, Tm, Tc and ΔH of all the samples.

5.15.4. Thermogravimetric analysis (TGA)

Outcome of TGA conducted on CS extracted from mushroom is demonstrated in Figure 5.10. TGA results of CS derived from mushrooms demonstrated the variation in weight of the CS sample in relation to temperature. The curve exhibits indications of weight reduction occurring in three distinct phases. The initial phase of weight reduction, amounting to 13.61% of the total weight, takes place between 10 to 150 °C. At first, there was a little decrease in weight caused by the evaporation of moisture or volatile components in the CS sample. This phenomenon took place at lower temperatures. Next stage begins at around 150 °C and extends up to 350 °C with weight reduction of 48.08%. Hence, the primary deterioration transpired at elevated temperatures. Within the temperature ranging from 350-450 °C, a notable reduction in weight of 38.03% occurred during the third stage. The disintegration of saccharides in organic molecules and the eventual decomposition of organic materials are the primary causes of this weight loss. The TGA curve

exhibited a substantial reduction in weight, indicating the heat decomposition of the CS polymeric structure. Following the breakdown process, a residue bulk remained. The residue is composed of ash or non-volatile components that remain unaffected by the heating process. The contention is further supported by a residual % of 0.1372%, which confirms the absence of organic materials at temperatures above 500 °C suggests that the biopolymer does not contain any metal or inorganic components. The TGA curve yielded insights into the temperature stability and degradation behavior of the CS derived from mushrooms. TGA thermogram exhibited the three thermal decomposition phases of all the samples. The first stage occurred at ≤170 °C whereas the second and the third stages occurred at 201-500 °C and 500-800 °C separately.

Mass losses during the first stage were 12.9 %, 11.4 % and 24.1 % respectively for T2, T5 and T8 samples, which could be attributed to the moisture/water loss. The mass losses in the second stage were 55.4 %, 54.9 % and 57.3 % respectively for T2, T5 and T8 samples which can have assigned due to the CS degradation. The residual masses during the last stage of the thermal degeneration which was mainly inorganic material were 17.9 %, 19.8 % and 9.4 % for T2, T5 and T8 samples respectively. The relatively greater thermal stability Showing the T5 sample during the extraction of CS from mushrooms using microwaves was confirmed by the TGA curves of all samples. (Liyanage et al., 2022) obtained CS from white leg shrimp (*Litopenaeus vannamei*) with a thermal stability of 360 °C. The initial stage of degradation for both chitin and CS occurred between 30-100 °C, primarily because of the water disappearance from the samples. After the saccharide structure of the molecules was reduced, the next stage of degradation occurred between 250 and 500 °C through evaporation or deamination processes. Another TGA curve displayed a comparable two-stage degradation pattern for CS, with an initial weight loss of 6.58% occurring at approximately 100 °C due to water removal. A significant weight reduction of 51.47% observed between 297–450 °C is attributed to the partitioning of CS and the breakdown of its amine group (Dalhatu et al., 2023). Similarly, (Tolesa et al., 2019), depicted that the mass loss of shrimp shell CS occurred in three steps. In the first stage, a 3-5% mass loss was noted at temperatures around as a result of water vaporization, 120 °C. Above 170 °C, the heat retention of ingrained chitin step by step drops, and its deterioration is completed at 441 °C. Moreover, the thermal profile of commercial α-chitin begins to decline at 267 °C and attain its decomposition at 406 °C. These results are steady with the results given by (Ijaz et al., 2022) (Huang et al., 2022) and (Da Silva Lucas et al., 2021). Despite that this is linked to enhanced heat resistance for chitin. Following the

deacetylation of chitin's branch chain, the order of crystalline level diminishes. Hence, the thermal resistance of the resulting CS is inferior to the original chitin. TGA spectra of CS extracted from mealworm cuticles exhibited similar thermograms, as presented in our study. It was noted that the thermogram of the polymer exhibits two primary stages of decomposition. The first decomposition occurs at 60-70 °C, leading to decrease chitin and CS accounted for 11.1% of their initial weight, followed by 70.9% at 210-270 °C, and was completely decomposed at nearly 400 °C. The TGA curve provided insights into the temperature stability and degradation behavior of the CS derived from mushrooms.

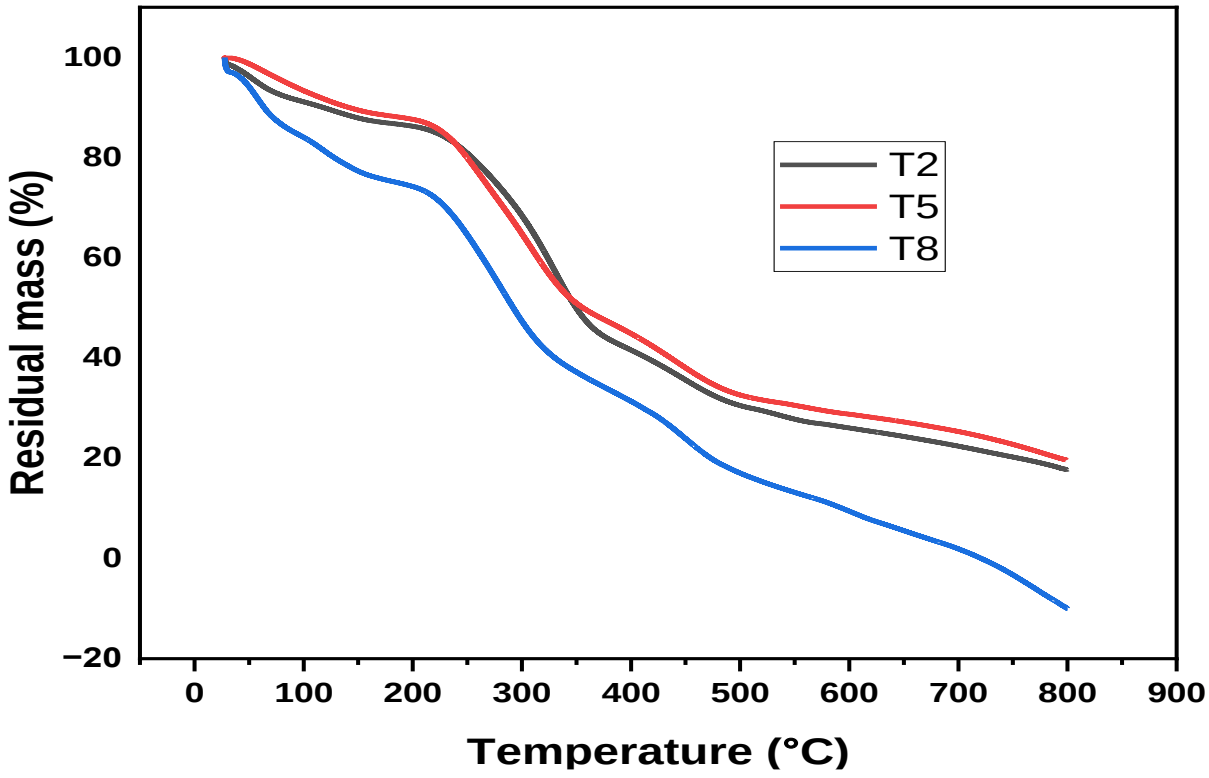

Figure 5.10. Thermogravimetric analysis of chitosan powder extracted using different treatments.

5.16. Techno-functional properties of extracted cellulose powder

5.16.1. Yield and moisture content

The techno-functional characteristics of cellulose powder subjected to various treatments at different power levels were evaluated, and the findings are presented in Table 5.6. The degree of cellulose extraction, delignification, and hemicellulose hydrolysis are significantly influenced by the treatment parameters such as alkali concentration, extraction duration, and microwave power. While considering the moisture content, the final product exhibited a moisture range of 4.02% to 5.30%. As illustrated in Table 5.6. MWP yield, following different treatments, ranged from 6.0% to 10.46%. The ultimate dry weight of the powder along with maximum yield was most substantial for treatment T8, employing a power level of 540W with 8% NaOH, and lowest yield for treatment T3, utilizing a power level of 180W with 12% NaOH. Ningsi et al. (2020) and Lestari et al. (2021) noted a comparable pattern when examining the influence of NaOH concentration on cellulose yield. Elevated quantities NaOH might markedly affect the final product of cellulose undergoing extraction operations. A study conducted using Kepok banana hump indicated that elevating NaOH content from 5% to 15% led to a reduction in cellulose output from 64.9% to 41.9%, with the peak yield occurring at 10% NaOH (Ningsi et al., 2020). Study using powdered water hyacinth revealed that a 10% proportion of NaOH resulted in a cellulose yielding 32.66%, demonstrating a decrease in yield with increased levels of NaOH (Lestari et al., 2021). A concentrated sodium hydroxide solution (12%) facilitates cellulose extraction by efficiently eliminating lignin and hemicellulose, hence increasing yield. Nonetheless, it may also result in partial degradation of cellulose, diminishing its molecular mass and perhaps impacting its quality. The alkali treatment enhances cellulose production; nevertheless, careful regulation is essential to maintain a balance between extraction efficiency and the integrity and purity of the fiber (Wang et al., 2021). However, this may influence the structural characteristics of cellulose knowns as Over alkalization, leading to partial depolymerization and breakdown of cellulose chains, therby giving lesser yield, weak crystalline structure and lower mechanical durability (Hassan et al., 2021). The findings indicate that whereas NaOH effectively removes lignin and hemicellulose, high doses may deteriorate cellulose, thereby diminishing the overall yield. Consequently, regulating NaOH concentration is essential to enhance cellulose extraction efficiency. Mohamad et al. (2022) also reported a similar influence on cellulose yield. However, high-power microwaves and NaOH dose can degrade cellulose fibers excessively. According to Zhang et al. (2017), high

heat can impair cellulose production by reducing its molecular weight. Further reducing cellulose production, excessive microwave power can thermally degrade and generate waste products that are undesirable (Lopez et al., 2020).

Figure 5.11. Cellulose powder extracted from mushroom waste powder (MWP) using microwave assisted extraction technique.

5.16.2. pH and solubility

Rheological properties can serve as indicators with a profound influence on the final dry product. While there has been limited focus on the solution state and rheological properties before precipitation, these properties are crucial in identifying specific factors that could contribute to

mechanical properties (Li et al., 2021). As per the United States Pharmacopoeia (2004) and the British Pharmacopoeia (2004), cellulose is expected to have a pH within the range of 5-7. The pH of the microcrystalline cellulose samples prepared in this study is 7.2, which falls within the acceptable range for standard cellulose. It is noteworthy that the commercial-grade cellulose sample, commonly claimed as an excipient in the pharmaceutical industry, exhibits a pH similar to that of the prepared cellulose samples, as indicated in the table (Table 5.5.) (Ndika et al., 2019). Cellulose is notably amphiphilic, and its limited solubility in water is primarily attributed to hydrophobic interactions. Additionally, the solubility of cellulose in water becomes more pronounced at extreme pH values, as highlighted by Lindman et al. (2010). Various cellulose derivatives, like methyl cellulose or hydroxyethyl cellulose, can exhibit high water solubility despite possessing a considerable capacity for intermolecular hydrogen bonding, often comparable to that of cellulose itself, as indicated by Medronho et al. (2012). Fresh mushrooms' pH fluctuates between 5.8 to 6.8, based on species and climate. Most edible mushrooms, like *A. bisporus* possess a pH of 6.0 to 6.5. Thus, extracting mushroom cellulose NaOH considerably changes its pH. Due to the high alkaline nature of NaOH, cellulose isolated from mushroom biomass at 4%, 8%, and 12% increases in Ph as shown in Table 5.5 also. Mushroom natural cellulose, found in relatively acidic to near-neutral pH conditions (usually pH 5.8–6.5), initially maintains an equilibrium of charge and structure. Hemicellulose and lignin break down when NaOH concentration increases because alkalinity disturbs hydrogen bonding in the cellulose matrix. This chemically modifies the cellulose surface, increasing its alkalinity and their pH (Hassan et al., 2021). Alkaline hydrolysis is more vigorous at 12% NaOH, which may partially degrade cellulose and raise pH due to leftover alkali. Despite the longer washing procedures needed to eliminate this excess alkali, the cellulose may keep a little higher pH than that treated with 4 and 8% (Zhang et al., 2017). Thus, alkali treatment removes contaminants and raises cellulose pH in accordance to NaOH concentration.

Concerning the solubleness of cellulose, it is commonly acknowledged that cellulose is challenging to go into solution, with only a less range of solvents present. A significant period of exploration occurred in 1930s, during which four major types of solvents were found and are still under study today: ammonia, phosphoric acid, ionic liquids, amine oxides, and sodium hydroxide in water as outlined by Budtova & Navard, (2016). According to the data in the Table 5.5. treatment T8, conducted at 540W using 8% NaOH, exhibited the highest solubility up to 60%. This result may be attributed to the fact that solubility tends to increase as the chain length of

cellulose decreases. Acidic or neutral conditions makes the celluloe insoluble due to the strong hydrogen bonding among cellulose chains and second due to its crystalline makeup. This prevents its dissolution. However, when ph is lowered during hydrolysis it turns the cellulose into its subunits or glucose theeby affecting the anhydroglucose polymer's N-glycosidic linkages, under high temperature further converting into cellulose nanocrystals (Medronho et al., 2012).

Table 5.6. Techno-functional properties of extracted cellulose powder.

S. No.	Cellulose sample	% Moisture	% Yield	pH	% Solubility	Bulk density	Tapped density	Carr's index	Hasneur ratio
1.	T1 (180W,4 %)	4.51± 0.07^{cd}	6.11± 0.25^{e}	6.1± 0.17^{h}	50± 0.60^{c}	0.37± 0.04^{a}	0.43± 0.07^{a}	13.95± 0.56^{bcd}	1.16± 0.05^{b}
2.	T2 (180W,8 %)	4.37± 0.04^{de}	8.54± 0.31^{c}	6.3± 0.15^{gh}	50± 0.75^{c}	0.36± 0.02^{a}	0.42± 0.04^{a}	14.29± 0.71^{bcd}	1.17± 0.08^{b}
3.	T3 (180W,12%)	4.11± 0.03^{gf}	6.0± 0.45^{e}	6.6± 0.17^{ef}	50± 0.52^{c}	0.36± 0.02^{a}	0.41± 0.03^{ab}	12.20± 0.15^{cd}	1.14± 0.08^{b}
4.	T4 (360W,4 %)	4.23± 0.08^{ef}	7.65± 0.21^{d}	6.7± 0.17^{ef}	50± 0.05^{c}	0.25± 0.03^{b}	0.30± 0.07^{b}	16.67± 0.13^{bc}	1.20± 0.07^{b}
5.	T5 (360W,8 %)	4.14± 0.03^{gf}	9.19± 0.11^{b}	7.0± 0.15^{cd}	50± 0.19^{c}	0.35± 0.04^{a}	0.42± 0.05^{a}	16.67± 0.11^{bc}	1.20± 0.07^{b}
6.	T6 (360W,12%)	4.02± 0.04^{g}	7.78± 0.06^{d}	7.2± 0.1^{bc}	55± 0.26^{b}	0.35± 0.04^{a}	0.43± 0.06^{a}	18.60± 0.21^{b}	1.23± 0.08^{b}
7.	T7 (540W,4 %)	5.30± 0.03^{a}	8.60± 0.24^{c}	7.3± 0.1^{b}	55± 0.16^{b}	0.40± 0.02^{a}	0.48± 0.06^{a}	16.67± 0.59 ^{bc}	1.20± 0.10^{b}
8.	T8	4.19±	10.46±	7.5±	60±	0.39±	0.44±	11.36±	1.13±

	(540W,8 %)	0.02^{gf}	0.09^{a}	0.1	0.46^{a}	0.03	0.07^{a}	0.43^{d}	0.05^{a}
9.	T9 (540W,12%)	4.05± 0.10^{gf}	8.95± 0.144^{b}	7.7± 0.1^{a}	60± 0.22^{a}	0.33± 0.04^{a}	0.40± 0.07^{ab}	17.50± 0.94^{b}	1.21± 0.07^{b}
10	T10 (720W,4 %)	5.26± 0.24^{ab}	8.08± 1.15^{cd}	6.5± 0.1^{fg}	45± 0.76^{d}	0.35± 0.06 ^{a}	0.43± 0.07^{a}	18.60± 0.69^{b}	1.23± 0.12^{b}
11	T11 (720W,8 %)	5.1± 0.15^{b}	8.04± 0.23^{cd}	6.8± 0.1^{de}	45± 0.29^{d}	0.33± 0.05^{a}	0.47± 0.07^{a}	29.70± 0.32^{a}	1.42± 0.13^{a}
12	T12 (720W,12%)	4.57± 0.12^{c}	7.96± 0.06^{cd}	7.0± 0.14^{cd}	50± 0.43^{c}	0.33± 0.04^{a}	0.39± 0.05^{ab}	15.38± 0.21^{bcd}	1.18± 0.06^{b}

Each column's values denoted by a different superscript letter are statistically distinct from each other ($p<0.05$).

5.16.3. Determination of flow properties of extracted cellulose

Bulk density offers a prediction of a material's flowability, whereas tap density assesses the efficiency with which a powder can be densely packed into a compact area through persistent tapping. In broad terms, elevated bulk and tapped densities suggest enhanced possibility for material flow and reorganization under compaction (Duruaku et al., 2023). Carr's compressibility and Hausner indices were computed as ratios indicating the disparity among tapped and bulk densities. Carr's compressibility index confers a conception of a powder's compressibility, indicating its compressibility level, whereas the Hausner index evaluates the cohesion among particles. Regarding Carr's index, values falling within the ranges of 5-10, 11-15, 16-20, and 21-25 signify excellent, good, fair, and poor flow nature of the material, correspondingly (Bahndral et al., 2024). Conversely, in case of Hausner ratio, value below 1.20 indicate favorable flowability, while a value of 1.50 or above reveals poor flow properties for the sample. According to the findings of this research, the cellulose extracted at 540W using 8% NaOH exhibited a Carr's index of 11.90, indicating good or free-flowing properties (Table 5.5). However, the Hausner ratio was

for the same was 1.13, falling below 1.25 (indicating good flowability), further confirming its favorable flow characteristics in comparison to the commercial cellulose displayed a Carr's index of 21.05% and a Hausner ratio of 1.25. The favorable flow characteristics observed in cellulose are likely attributed to differences in particle shape, size, and surface area among the powders. Hence, the values recorded for the Hausner ratio align with those of the Carr's index. Comparable outcomes can be correlated with the finding reported by Liu et al. (2023). Likewise, Rao et al. (2024) found that lemongrass cellulose extracted using 8% NaOH and 540 W microwave radiation had a Carr's Index of 11.90, indicating outstanding flowability and structural integrity. Similarly, Tasnim et al. (2023) extracted the micro crystalline cellulose which showed that improved flow characteristics. The one treated with 20% NaOH resulted in a Carrs index of 14.43 where as the hausner ratio of 1.17, indicatibg good flowability. Whereas the unmodified one showed poor flowability.

5.17. Determination of total cellulose content in mushroom waste powder (MWP)

Cellulose, a principal basic polysaccharide in plants, is the most prevalent organic substance in nature, consisting of glucose units linked as repeating disaccharide cellobiose units with extensive cross-linkages. It additionally serves as a significant constituent of certain agricultural byproducts. Cellulose performs acetolysis with an acetic/nitric reagent, resulting in the formation of acetylated cellodextrins, which dissolve and hydrolyze into glucose molecules upon exposure with 67% H_2SO_4. The glucose molecule undergoes dehydration to provide hydroxymethyl furfural, which reacts with anthrone to produce a green-colored product, with color intensity evaluated at 630 nm. The data demonstrate a substantial quantitative recovery of pure cellulose, reaching 61.37%, as illustrated in Table 5.7. A thermochemical technique is outlined for quantifying cellulose in mushrooms MWP. Lignin, hemicellulose, as well as xylosans are taken out using an acetic acid/nitric acid reagent, while the residual cellulose is solubilized in 67% H_2SO_4. and quantified via the anthrone reagent. Consequently, the approach provides a quantifiable recovery of pure cellulose from MWP. Before that a basic demonstration was performed using Iodine reagent to confirm the presence of starch in the extracted cellulose and later was observed under microscope at 10X magnification as shown in Figure 5.12. However, the color change of cellulose fibers from yellow brown to blue black shows the positive test thereby the presence of starch in the extracted cellulose. Iodine testing works on the premise that when starch and Amylose react, a blue-black

complex is formed with iodine. A charge transference complex (CT) is formed between iodine and the helical structure of amylose and the charge transfer complex of polyiodide (Formation of cluster of ions when potassium-iodide dissociates into iodide ions) and because amylose electrons are stimulated by elevated energy levels when they absorb light, the resulting complementary hue is seen by humans as a blue-black.

Table 5.7. Determination of total cellulose content in mushroom waste powder (MWP).

Concentration (%)	Cellulose (%)
20	24.79
40	21.33
60	34.04
80	48.44
100	61.37

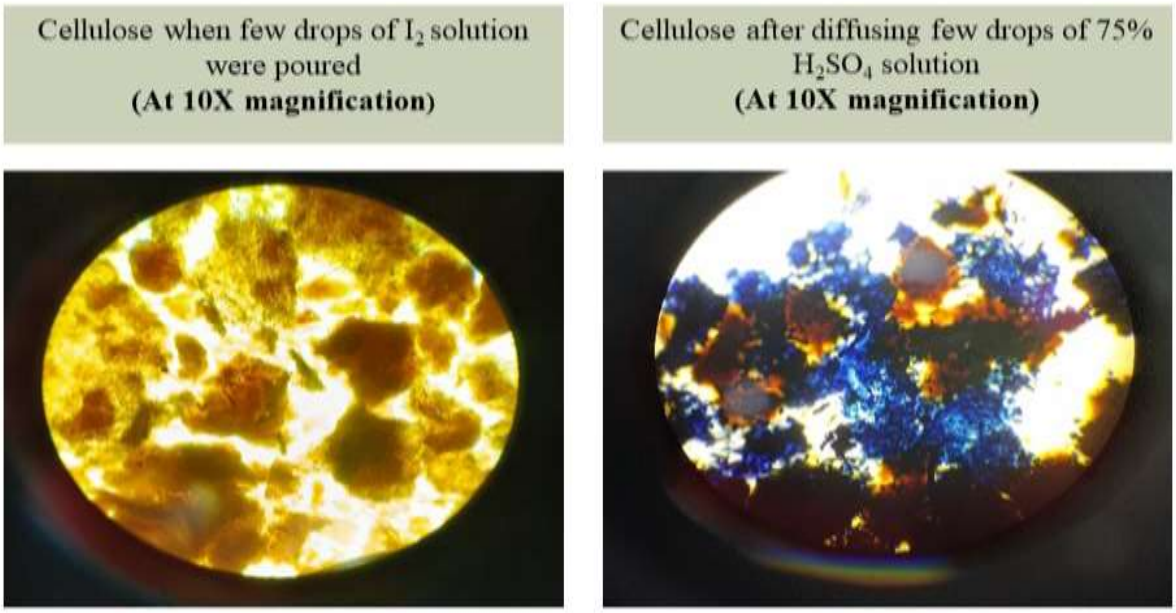

Figure 5.12. Observation of cellulose under compound microscope at 10X magnification.

5.18. Bleaching of optimized cellulose

The photos in Figure 5.13. show the raw biomass product, bleached cellulose, along with non-bleached cellulose in terms of their microstructural conformation and appearance with sodium hypochlorite (NaClO). Prior to grinding, the fibers showed an elongated vertical structure, suggesting the presence of a lignin component that remained complexed with the cellulose fiber. The cellulose waste from mushrooms had a light brown initial hue. When the bleached samples were heated to 30°C for three hrs, the light brown hue of the cellulose waste from mushrooms was decolored in a 4% NaClO solution. A white cellulosic biomass was produced when the aryl ether linkages or β-O-4 bonds in lignin were oxidized. The action of sodium chloride, the main ingredient in chlorine bleach, is well-known as a powerful bleaching agent because of its capacity to kill vegetative bacteria, fungus, lipid and nonlipid viruses, and other types of liquid samples (Block & Rowan, 2020). The production of a white, homogeneous powder structure confirmed that the acid hydrolysis synthesis process was successful.

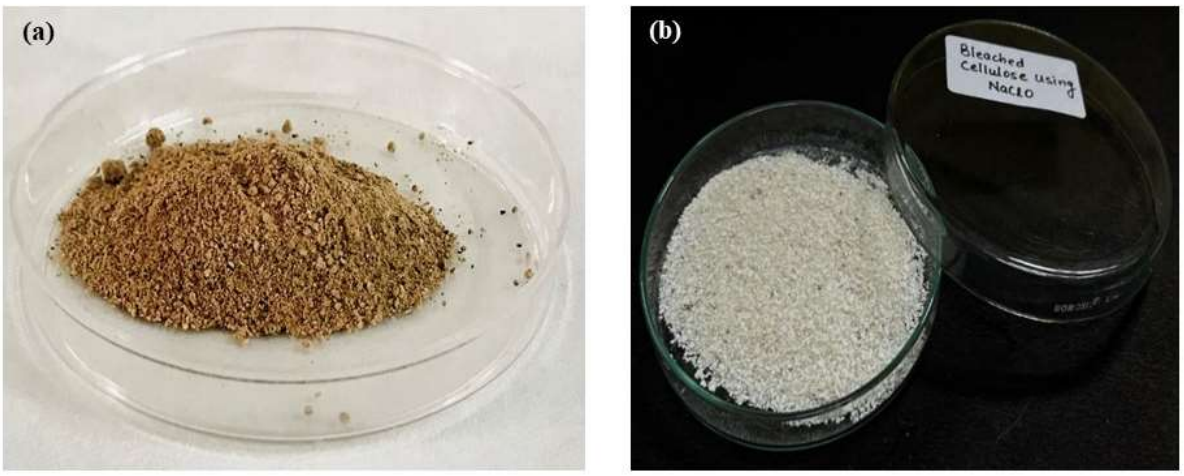

Figure 5.13. Pictorial view of (a) Unbleached cellulose and (b) bleached cellulose.

5.19. Characterization of Nanocellulose (NC)

5.19.1. Yield

NC was effectively derived from MWP employing acid hydrolysis a final yield of 28.06% efficiency. This illustrates the capability of agricultural fungal byproducts being an ecologically friendly and value-enhancing resource for NC manufacturing. Recent studies have shown the feasibility of diverse farm waste as renewable sources for NC manufacturing, providing both high yields and advantageous material properties. Banana peel waste has been utilized for the extraction of nanocrystalline cellulose (NCC), yielding around 29.9% by hydrolysis with acids (Sulaiman et al., 2022). Cocoa pod shell and conocarpus fibre produced 25% along with 19% NCC, accordingly, using comparable processing procedures (Sulaiman et al., 2022). same from banana pseudostem through a process involving TEMPO oxidation, the ultrasonic radiation, alongside acid hydrolysis, resulting in cellulose at a purity of 91.33%, appropriate for its further transformation as tiny fibers of cellulose (CNF) and cellulose nanocrystals (CNC) (Jonoobi et al., 2019). The treatment of rice husk using hydrolysis in acids and high-pressure homogenization yielded NC exhibiting a crystallinity index of 62% to 72%, demonstrating the effective elimination of amorphous cellulose and the successful isolation of NC (Islam et al., 2023). These findings confirm the viability of food industry by-products as an economical, environmentally sustainable resource for high-yield NC manufacturing, consistent with the objectives of environmentally sound material as well as waste valorization.

5.19.2. Particle size of Nanocellulose (NC)

Particle size evaluation, together with zeta potential data, has confirmed the nanoscale characteristics of cellulose given in Figure 5.14. The NC sample exhibited an average particle size of 163.2 nm in length and a total surface charge of −19.2 mV. Acid hydrolysis was conducted with sulfuric acid, resulting in the micro cellulose surface acquiring half ester sulfate groups, which led to a significant dispersion of negatively charge. The significant NC's negatively charged dispersion makes it a promising polymeric material for creating bio-friendly films as well as nanocarriers. The results of this work are in agreement with those of Yang et al. (2017), who used dynamic light dispersion along with diffraction to determine the zeta potential and particle size of three different types of cellulose demonstrated a comparable trend in both measures. In a comparable manner, Chawla et al. (2023) used an alkaline method to extract cellulose from corn

husk by means of the use of an acid treatment aimed at delignification and the purification of cellulose. Subsequently, acid hydrolysis was conducted to isolate NC utilizing a 60% sulfuric acid solution for a duration of 2 hrs, keeping the fiber-to-acid ratio at 1:30, all while ensuring constant and constant stirring throughout the process. A particle size of 149.67 nm was found to be the average for corn husk cellulose with a total charge on the surface measured at -20.2 Mv.

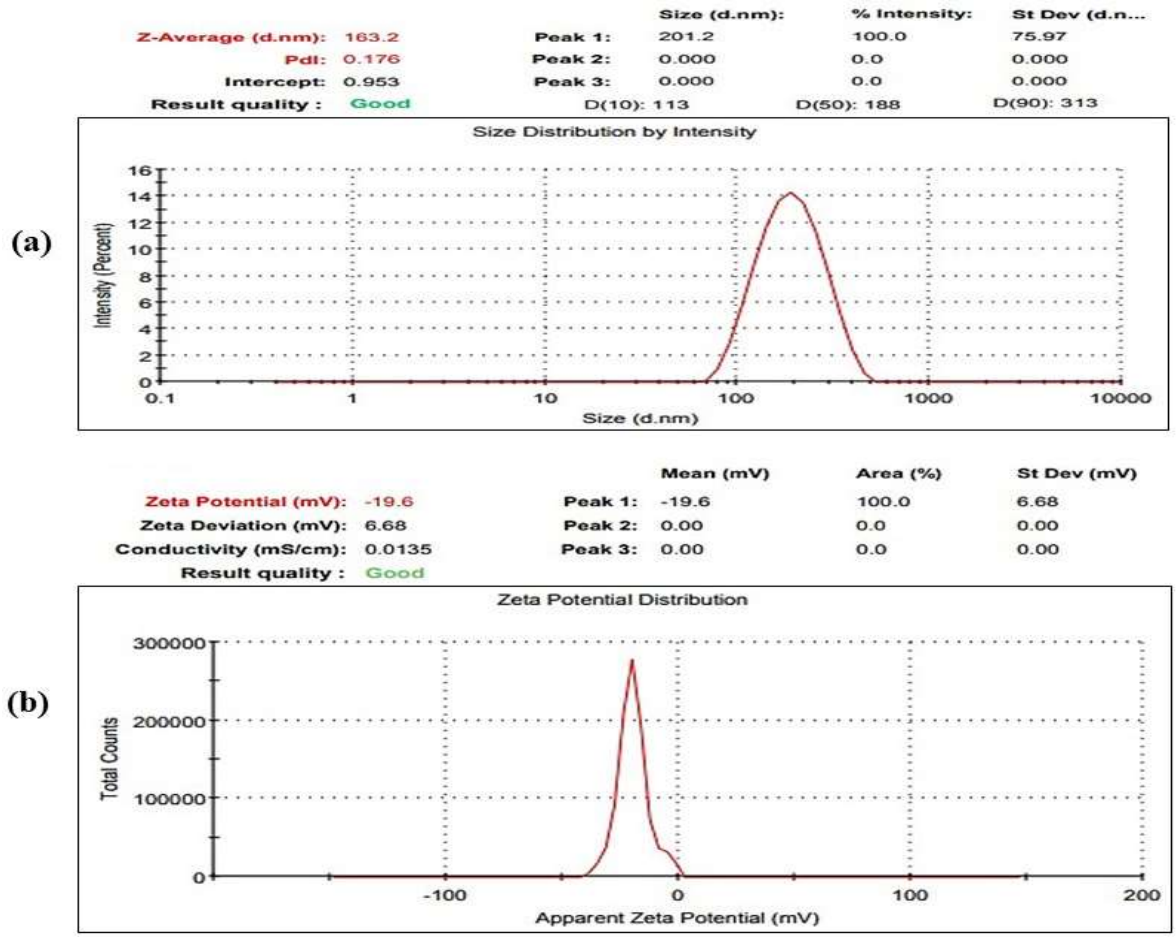

Figure 5.14. (a) Nano scale dimension and (b) Zeta potential of prepared Nanocellulose (NC) powder.

5.20. Apparent color and optical properties of control film

5.20.1. Visual analysis of the control films

The surface color and opacity of manufactured films are crucial in food applications, as they directly influence customer perception and the durability of packaged food products. The interaction between CS and NC within films resulted in the films color properties noticeably changed. From an aesthetic perspective, the films exhibited transparency with a slight yellow tint (Figure 5.15). The influence of CS incorporation on film opacity was examined, as transparency is a crucial attribute of food packaging.

Figure 5.15. Visual analysis of the control films (T1, T2 and T3).

5.20.2. Hunter color properties

The optical properties of multilayer films are essential for applications in food packaging, biomedical materials, and coatings. The levels of CS and NC markedly affect film transparency, color, and brightness, thereby influencing consumer perception and functional attributes, including UV resistance and bioactivity. This study examines the variations in Hunter color parameters like L (lightness), a (red-green scale), b* (yellow-blue scale), ΔE (total color difference), WI (whiteness index), C* (chroma), and H* (hue angle) in relation to the increasing content of CS and NC in multilayer films T1, T2, T3, and T4, as presented in Table 5.8. The Lightness (L*) values diminished as the concentrations of CS and NC increased, decreasing from 84.107 in T1 to 59.7

in T3. This suggests that elevated levels of CS and NC result in darker films, likely attributable to enhanced polymer density and reduced light transmittance. Supporting research by Siracusa et al. (2018) demonstrated that the integration of biopolymers into films lowers L* due to light scattering and increased film thickness. The studies conducted by Pereda et al. (2011) and Rhim et al. (2006) also demonstrated a comparable effect of elevated biopolymer concentration, resulting in increased opacity and diminished brightness in films. Furthermore, the color parameters a* and b* exhibited notable alterations; a* transitioned from negative (-0.66 in T1) to positive (29.86 in T3), signifying an enhancement in red hues, while b* values grew from 26.73 to 77.1675, leaving the films more yellowish. The observed changes correspond with earlier research on biopolymer-based films conducted by Siripatrawan and Harte (2010), indicating a shift from a subtle greenish hue (T1) to a pronounced red tint (T3), probably resulting from the elevated concentration of NC affecting light scattering and absorption characteristics. Wang et al. (2020) observed comparable trends, indicating that bio-based films displayed heightened red-yellow tones as a result of polyphenol interactions. The ΔE increased from 28.281 in T1 to 89.589 in T3, indicating significant color deviations. Increased levels of CS and NC resulted in enhanced visual distinctiveness of the films, consistent with the findings of Jonaidi Jafari et al. (2021), who reported increases in ΔE for NC-based films. The WI decreased from 73.029 in T1 to 18.048 in T3, indicating a reduction in whiteness attributed to the opacity induced by NC and interactions between CS and polyphenols. Tanpichai et al. (2019) observed comparable water intake reductions in NC composite films, which correlated with the formation of a polymer network. C* and H* exhibited an increase with the elevation of CS and NC content. C* increased from 25.754 in T1 to 80.493 in T3, reflecting more intense colors, while H* changed from -0.392 to 21.98, indicating a shift towards yellow-red hues. Cheng et al. (2021) observed that increased biopolymer content improves color vibrancy through structural modifications in films. The findings demonstrate that increasing the content of CS and NC significantly modifies the optical properties of films, thereby affecting their practical applications.

5.20.3. Light transmission and transparency

Transparency is a fundamental optical characteristic of food packaging films that influences their capacity to permit light transmission. It is essential in applications where product visibility, light

sensitivity, and visual impact are significant. This study presents the results shown in Table 5.8. which detail the measured and analyzed transparency values of three distinct samples as T1, T2, and T3. Using a 600 nm/mm thickness measurement, we can see that greater absorption values correlate with decreased levels of transmittance of light. Transparency values reflect the clarity of films, where higher values denote enhanced optical transparency and lower values signify increased opacity. In accordance with these data, Sample T1 (0.438) has the maximum transparency among the three, indicating it permits greater light transmission, hence resulting in reduced light scattering and absorption. Sample T2 (0.237) demonstrates moderate transparency, permitting partial light transmission while maintaining a certain level of opacity. Sample T3 (0.140) exhibits the lowest transparency, leaving it the opaquest of the samples. It is evident that for longer-wave UV (up to 600 nm), the increase in transparency values is inversely related to the concentration of CS. The maximum light absorption was observed at 25.079% for the T2 control film compared to T1, and 34.534% for the T3 control film relative to T2, with lack of apparent change noted ($p > 0.05$). An inclusion of CS as a reinforcing agent in increasing quantities has adversely affected the optical characteristics of the multilayer film, rendering the material opaquer.

Table. 5.8. Total color difference (ΔE), lightness (ΔL^*), chroma (C^*), hue angle (h^*) and whiteness index (WI) of the control films equilibrated at 25 °C.

Film	l	a	b	ΔE	WI	C*	H*	(%) T at A600	(%) To at A600/x
T1	84.1075± 0.431[a]	-0.66± 0.328[c]	26.73± 1.111[c]	28.281 ± 1.173[c]	73.029± 1.027[a]	25.754± 1.113[c]	-0.392 ±0.738[c]	63.0± 0.132[a]	40.0± 0.041[a]
T2	76.4075± 0.384[b]	8.49± 0.284[b]	65.8675± 0.693[b]	67.973± 0.776[b]	34.531± 0.703[b]	64.334± 0.711[b]	7.997± 0.207[b]	47.2± 0.154[b]	20.1± 0.013[b]
T3	59.7± 0.491[c]	29.86± 0.698[a]	77.1675± 0.972[a]	89.589± 0.472[a]	18.048± 0.716[c]	80.493± 0.726[a]	21.98± 0.673[a]	30.9± 0.120[c]	4.0± 0.021[c]

T: Transmittance and To: Transparency

Data are expressed in terms of mean ± standard deviation, with distinct letters (a - d) in the rows indicating significant variations ($p < 0.05$), where 'a' represents the lowest value.

5.21. Measurement of physical properties of the control films

5.21.1. Thickness measurement

Thickness of CS-NC multilayer films is determined by the concentrations of CS and NC. An elevation in the concentration of these components often results in a proportional expansion of film thickness. This is due to the increased availability of polymer chains and reinforcing components, that increases the films matrix's density and durability. Our study revealed that the The multilayer films made of CS-NC were thicker as higher concentrations of CS and NC, as indicated in Table 5.9. (T1: 47.204 µm, T2: 69.31 µm, T3: 126.31 µm). This observation is consistent with prior studies that indicated a direct correlation between the content of polymer and NC and the resultant film thickness. In research carried out by Ma et al. (2022), pure CS films demonstrated a thickness of 474.90 µm, which increased to 615.93 µm with the addition of cellulose (C-CH), and further to 632.70 µm with cellulose nanocrystals (C-NH-CH). Khezerlou et al. (2020) developed nanocomposite films in which the incorporation of NC (CNF/CNC) at varying concentrations markedly affected the mechanical properties and thickness, with all samples consistently measuring between 40–45 µm. Nataraj et al. (2012) reported an increase in thickness from 0.17 mm to 0.32 mm upon the incorporation of coconut fiber cellulose into CS. The findings consistently indicate that elevating the concentration of structural biopolymers, such as CS and NC, increases deposition density during casting or coating, resulting in thicker films. It is crucial to equilibrate concentrations to attain the necessary film attributes without sacrificing flexibility or other functional features.

5.21.2. Tensile strength (TS) and elongation at break (EB)

Integration of NC into CS matrices markedly affects the structural characteristics of the resultant films, particularly tensile strength (TS) and elongation at break (EB). Knowing these variances is

essential for enhancing film compositions for particular uses. Our findings indicate the tensile strength substantially improved, increasing from 13.77 MPa in T1 to 54.19 MPa in T3, as illustrated in Table 5.9. The enhancement is due to the reinforcing influence of NC, which establishes hydrogen bonds within the CS matrix, yielding a stronger and cohesive polymeric network (Lamm et al., 2022) (Talebi et al., 2022). Elongation at break, indicative of film flexibility, exhibits a significant increase from 45.52% in T1 to 102.72% in T3 (Table 5.8). This suggests the fact that NC enhanced dispersion and association with the CS matrix enhance the film's capacity to deform without failure, likely due to enhanced stress distribution and network flexibility (Ding et al., 2018) (Riccio et al., 2021). Research has shown that the inclusion of 1% NC can result in a substantial enhancement in TS. Grząbka-Zasadzińska et al. (2017) indicated that when we combine 1% NC within CS films elevated the tensile strength from 25 MPa (pure CS) to 47 MPa. Likewise, Do et al. (2023) reported a 63% improvement in TS with the incorporation of 2 parts per hundred resin (phr) of spherical NC. Conversely, elevated NC loadings may induce agglomeration, creating stress concentration areas that reduce TS. Grząbka-Zasadzińska et al. (2019) discovered that elevating NC content to 5% diminished the TS to 21.2 MPa, indicating that an excess of NC may compromise the mechanical integrity of the composite. EB indicates the film's adaptability and capacity to undergo deformation prior to fracture. The inclusion of NC has been noted to diminish the EB, likely attributable to the stiff characteristics of NC that constrain polymer chain mobility, thereby resulting in a decreased EB. Grząbka-Zasadzińska et al. (2017) noted that the incorporation of 1% NC reduced EB from 42% in neat CS to 36%. Optimal NC dispersion and specific processing methods can maintain or enhance EB. Do et al. (2023) reported a 30% increase in EB with the incorporation of 2 phr of spherical NC, underscoring the significance of NC morphology and distribution within the matrix. The study concludes that optimal enhancements in TS and EB occur at lower NC loadings (approximately 1–3%), where NC is well-dispersed, thereby enabling effective stress transfer without considerable agglomeration. Increased NC concentrations can result in filler agglomeration, which may diminish mechanical performance (Grząbka-Zasadzińska et al., 2017). Thus, precise optimization of NC content and dispersion methods is crucial for customizing the mechanical properties of CS-NC composites for particular applications.

5.22. Barrier permeability test on control films

5.22.1. Water vapor transmission rate (WVTR) and Oxygen transmission rate (OTR)

Biodegradable films are highly regarded for their ability to keep moisture and oxygen out of packaging. As a result, it is important to keep WVTR and OTR as low as possible. Incorporating either organic or inorganic nanoparticles having a large aspect ratio, which alters the gas molecules' diffusion pathway, into the biopolymer barrier qualities can significantly alter that ability (Pires et al., 2021). The barrier properties of films are influenced by numerous factors inherent to their composition, including the chemical structure of biopolymers, polarity, degree of crystallinity, density, molecular weight, and the presence of additional plasticizers or cross-linkers. The film's selectivity for various molecules of gas will be determined by these factors (Zhang et al., 2021). The water vapor transmission rate (WVTR) of CS-NC films exhibits significant variation in response to changes in CS and NC concentrations, as shown by T1 (3.22), T2 (2.74), and T3 (1.32) $g/m^2/24h$ as shown in Table. 6.9. The analysis of the 2 investigated variables (CS and NC) revealed that the film's permeability exhibited a downward trend with an increase in their concentration from 3.22 in T1 to 1.32 to T3 for WVTR and 56.72 in T1 to 6.211 in T3 for OTR. Furthermore, this decline became more pronounced as the amount of reinforcement (CS and NC) increased. This tendency aligns with findings documented across published works (Azeredo et al., 2010; Zhang et al., 2021). Moreover, excessive NC content can result in agglomeration, which may introduce defects that could marginally elevate WVTR (Azeredo et al., 2010; Fernández-Santos et al., 2021). CS contains hydrophilic groups (–OH, $–NH_2$) that facilitate interactions with water molecules. At lower concentrations, CS exhibits a compact structure, which leads to a reduction in WVTR. At elevated concentrations, excessive hydrophilicity may enhance water absorption, thereby increasing water vapor transmission rate (WVTR) in certain instances (Neves et al., 2016).

An increase in NC and CS concentration leads to a reduction in OTR, also as shown in Table 5.9. thereby enhancing oxygen barrier properties. The noted reduction in OTR in CS-NC films from T1 (56.72 ($g/m^2/24h$)) to T3 (6.211 ($g/m^2/24h$)) with growing concentrations of CS (1% to 2%) and NC (2% to 4%) is due to increased structural density and diminished molecular diffusion pathways within the film matrix. CS is a biopolymer that occurs naturally and is characterized by strong film-forming capabilities and moderate gas barrier qualities, attributed to its semi-crystalline structure and ability to establish hydrogen bonds. As its concentration rises, the resultant matrix becomes denser, hence reducing the free volume open for oxygen molecules to

permeate (Elsabee & Abdou, 2013). NC, characterized by its elevated aspect ratio, crystallinity, and strengthening potential, significantly enhances barrier attributes by strengthening the complexity of the pathway that gas molecules must navigate. At elevated quantities, NC forms a denser, crystalline network that serves as a physical barrier, impeding the movement of oxygen molecules. This synergistic interaction restricts gas diffusion, leading to a significant decrease in OTR due to tight interfacial hydrogen bonding and structural uniformity (Rhim et al., 2013; Fortunati et al., 2012). This decline in OTR has been shown by Du et al. (2021) as they sandwiched polypropylene sheets with NC. According to the study, the NC layer greatly lowered OTR, proving NC coatings improve oxygen barrier qualities. As it directly affects the thickness, density, and porosity which directly affected OTR readings. Likewise, Kim et al. (2021) coated polypropylene films with NC and nanochitin layers. This method decreased OTR from 1118 to 13.10 $cm^3/m^2 \cdot day$, demonstrating the synergistic effect of NC and nanochitin in producing effective oxygen barriers. All of these studies support the idea that adding more CS and NC to multilayer films improves their structural density and crystallinity, which lowers OTR considerably and makes them more suitable for packing applications.

Table 5.9. Mechanical properties, water solubility, swelling index, barrier properties and antioxidant activity of the control films equilibrated at 25 ℃.

Film	Thickness (µm)	Tensile strength (MPa)	(%) Elongation at break	(%) Water solubility	(%) Swelling index	WVTR (g/m^2/24 h)	OTR ($cm^3/(m^2 \cdot day \cdot Pa)$)	DPPH (%)	RP assay (Abs at 700 nm)
T1	47.204c ± 4.880^c	13.770 ± 0.912^c	45.52± 0.967^c	29.172± 0.922^c	83.796± 2.434^a	3.22 ± 0.175^a	56.72 ± 0.462^a	10.374± 1.054^c	0.1925 ± 0.045^c
T2	69.31b ± 5.6218^b	30.095b ± 1.289^b	73.448 ± 0.8314^b	19.344± 0.960^b	65.11± 2.195^b	2.74 ± 0.141^b	31.433 ± 0.959^b	24.766 ± 1.416^b	0.3525 ± 0.051^b

T3	126.31a ± 3.856[a]	54.195a ± 0.822[a]	102.720± 0.889[a]	8.16± 0.989[a]	44.932± 3.307[c]	1.32 ± 0.04[c]	6.211 ± 0.077[c]	39.766 ± 1.0387[a]	0.6775 ± 0.027[a]

Data are expressed in terms of mean ± standard deviation, with distinct letters (a - c) in the rows indicating significant variations ($p < 0.05$), where 'a' represents the lowest value.

5.23. Water solubility (WS) and Swelling index (SI)

From T1 to T3, the CS–NC bilayer films' swelling index and water solubility showed a distinct pattern as the formulation's concentration increased. The T1 film, which had the lowest concentration, had the highest swelling index (83.796%) and the maximum water solubility (20.17%) as shown in Figure 5.16. This indicates a relatively loose polymer network that facilitates greater water penetration and solubilization, with an intermediate swelling index of 65.11%, reflecting a rise in hydrophilic interaction and matrix densification as in T2. The T3 film, exhibiting the largest concentration of CS–NC, displayed the lowest water solubility at 8.16% and the lowest swelling index at 44.932%, as indicated in Table 5.9. This behavior indicates enhanced structural integrity and water uptake ability of the film, probably resulting from elevated hydrogen bonding and interaction between CS and NC. As the concentration of CS-NC grew from T1 to T3, the films displayed reduced solubility in water while demonstrating reduced swellability, suggesting improved film formation and improved water absorption capacity. The solubility of the film is dependent upon water transport, amino and carboxylic groups, as well as the dissociation and hydration of hydrogen and ionic bonds (Gökkaya Erdem et al., 2021). The findings indicated that the dissolution of the film augmented with a higher ratio of NC to CS. The high hydrophilicity of CS caused a decrease in its quantity, leading to a rise in the film's solubility. CS is a hydrophilic polymer with a low water solubility primarily dissolving in acidic environments as a result of amino group protonation ($-NH_3^+$) (Lewicka et al., 2024). Increasing CS concentration leads to decreased water solubility of the composite film due to enhanced intermolecular hydrogen bonding, greater molecular entanglement, and diminished accessibility to free amino and hydroxyl groups for interaction with water (Riaz et al., 2021). Furthermore, a surplus of CS can result in a denser film matrix, which may impede water penetration and solubility (Tang et al., 2020). This phenomenon aligns with the findings of a study on cellulose–CS nanocomposite films, which indicated that elevating the CS content to 75 wt% considerably enhanced the swelling ratio (up to

1500%) at pH 3 and resulted in an increase in the film's thickness by approximately 22 times its original size due to substantial water absorption (Teli et al., 2019). In a related study, a similar trend was observed, where research on CS films prepared with varying concentrations (0.5% to 2.0% w/v) indicated that films made from higher CS concentrations displayed increased water contact angles, implying enhanced hydrophobicity. Furthermore, these films exhibited reduced water vapor permeability, suggesting enhanced barrier charcteristics (Xu et al., 2022). Incorporation with NC has demonstrated a reduction in water solubility and water vapor permeability, attributed to the establishment of a dense network and enhanced crystallinity as shown in Figure 5.16. Incorporating 10 wt% cellulose nanoparticles into alginate films resulted in a reduction of water solubility by approximately 40% and a decrease in water vapor permeability (WVP) by around 17% (Zhang et al., 2013). The crystalline nature of NC enhances the surface hydrophobicity of films. The study reported a 98% increase in hydrophobicity following the incorporation of NC (Zhang et al., 2013). Braga et al. (2021) examined CS based bionanocomposite films that were reinforced with cellulose nanofibrils (CNFs) derived from *Euterpe oleraceae Mart*. The research indicated that elevating CNF content from 5 wt.% to 20 wt.% resulted in a decline in water vapor absorption from 75.20% to 51.93% and a decrease in water solubility from 28.33% to 17.91%, thereby corroborating our findings (Table 5.9.). The increased NC content decreases water solubility, as NC enhances the film's crystallinity and stability through augmented inter- and intramolecular hydrogen bonding (Solhi et al., 2023; Ren et al., 2024). Excessive NC can result in phase separation and a non-uniform film structure, which may lead to partial dissolution in water (Maqsood et al., 2022). The general trend indicates that increasing concentrations of both CS and NC decreases water solubility, with the effect of NC being more pronounced due to its reinforcement of the matrix.

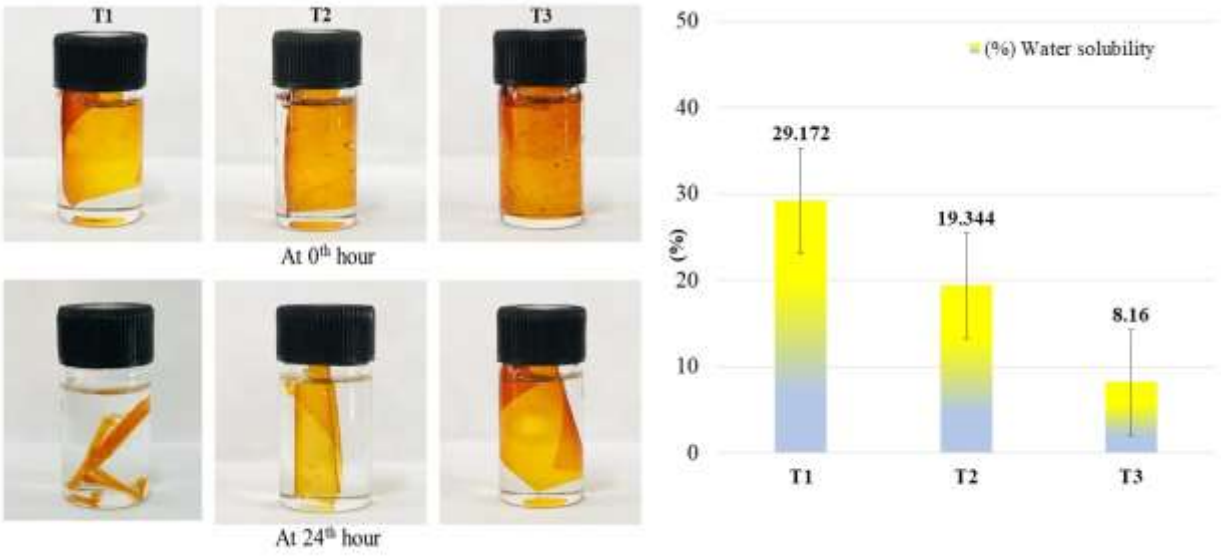

Figure 5.16. Water solubility (%) of control films (T1, T2 and T3).

5.24. Antioxidant activity of the control film

5.24.1. 2,2-diphenyl-1-picrylhydrazyl (DPPH) activity

The changes observed in DPPH (2,2-diphenyl-1-picrylhydrazyl) across T1, T2, and T3 films are 10.374, 24.766 and 39.766 respectively showing directly associated with the rising concentrations of CS and NC. changes observed in DPPH (2,2-diphenyl-1-picrylhydrazyl) across T1, T2, and T3 films are directly associated with the rising concentrations of CS and NC. The improvements in a role in the action of antioxidants through the inherent characteristics for CS and its synergistic effects observed when it is combined with NC. The antioxidant capacity in CS are primarily responsible for its free amino groupings, that have the ability to donate hydrogen atoms for the neutralization of free radicals. Increased concentration results in a greater number of active sites, leading to an enhanced presence of amino and hydroxyl groups capable of donating hydrogen atoms to neutralize free radicals such as DPPH. As the concentration rises, the availability of these functional groups increases, thereby improving the radical scavenging capability (Ardean et al., 2021). Numerous studies demonstrate a dose-dependent enhancement in antioxidant activity corresponding to increased CS concentration. Additional studies have shown that CS with elevated degrees of deacetylation (DD) and particular molecular weights displays improved DPPH

radical scavenging activity (Zimoch-Korzycka et al., 2016). For example, Binh et al. (2021) indicated that CS with a DD of 92.4% demonstrated notable antioxidant activity, as reflected by enhanced DPPH radical scavenging. CS demonstrates a dose-dependent relationship, indicating that as the dosage increases, the antioxidant activity also rises (Liu et al., 2024). However, NC does not directly scavenge free radicals; instead, it functions as a reinforcing agent that enhances the film's structural integrity. This improvement can indirectly affect the film's antioxidant capacity by offering a more stable matrix for antioxidant compounds (Morales-Olán et al., 2022). Furthermore, the inclusion of NC can enhance the dispersion of CS, resulting in a more consistent distribution of antioxidant activity across the film (Azeredo et al., 2010). Tri Putri (2020) conducted an investigation into the antioxidant activity of CS derived from Haruan fish scales. The research indicated that at a concentration of 350 ppm, CS demonstrated a 50.513% inhibition of DPPH radicals, accompanied by an IC50 value of 356.98 ppm. This demonstrates a dose-dependent enhancement in antioxidant activity as CS concentrations increase. Salimgandomi and Shabrangi (2016) investigated the impact of CS on the antioxidant activity of *Mentha piperita L*. The research demonstrated that applying escalating concentrations of CS (50 μM and 100 μM) resulted in a reduction of IC50 values (196.3 μg/mL, 147.7 μg/mL, and 128.6 μg/mL, respectively), signifying improved DPPH radical scavenging activity as shown in Table 5.9. Furthermore, there was a notable rise in the levels of phenolic and flavonoid content. A study indicated that the integration of oxidized microcrystalline cellulose, a variant of NC, into CS films, in conjunction with *Tribulus terrestris* extract, markedly enhanced the DPPH scavenging potential. The blend films demonstrated an approximate 3.7-fold increase in DPPH radical scavenging activity in comparison to films lacking the extract (Ulu et al., 2025). The studies indicated that higher levels of these biopolymers can collectively enhance performance in DPPH activity.

5.24.2. Reducing power (RP) assay

The observed enhancement in reducing power (RP) values inside the T1, T2, and T3 films can be ascribed due to the slow but gradual rise in CS with NC concentration. CS is recognized for its antioxidant properties due to free amino and hydroxyl groups, which operate as efficient hydrogen and electron donors, facilitating the neutralization of free radicals (Liu et al., 2024). With an increase in CS concentration, the number of these functional groups increases, thus amplifying the film's reducing ability, evidenced by the consistent rise in absorbance values at 700 nm from

0.1925 in T1 to 0.6775 in T3, as shown in Table 5.9. Besides CS, NC serves as a reinforcing ingredient that markedly enhances the structural integrity and functional characteristics of biopolymer films. Despite NC's restricted antioxidant properties, its integration into CS matrices improves the dispersion of active constituents and promotes enhanced contact with radicals. Azeredo et al. (2010) demonstrate that NC enhances the mechanical and barrier properties of CS films, thereby facilitating improved retention and stability of antioxidant agents. Khan et al. (2012) found that CS films reinforced with nanocrystalline cellulose maintained over 80% of their initial DPPH antioxidant activity after 30 days of storage, in contrast to a retention of only 58% in films lacking NC. These findings show that NC strengthens film structure and improves matrix antioxidant component preservation. Pires et al. (2023) noted that NC inclusion improves film matrix and bioactive performance, including antioxidant activity. Their review found that composite films with 3–7% NC retained up to 90% of DPPH radical scavenging activity after lengthy storage, compared to 60–70% in control films without NC. The notable difference has been attributed to the compact, well-organized matrix created by NC, preventing oxygen and moisture invasion, thus preserving vital antioxidant components. The upward trend in RP values from T1 to T3 indicates the advantageous and collective effect of elevated CS and NC content, underscoring their synergistic contribution to augmenting the film's electron-donating capacity and overall antioxidant efficacy.

5.25. Characterization of optimized control film

5.25.1. Fourier transform infrared radiation (FTIR) spectroscopy

The Fourier Transform Infrared (FTIR) spectrum of the optimized control multilayer film (T2), which consists of CS and NC, displays characteristic absorption bands that validate the successful integration of both biopolymers. A prominent peak at 3269.21 cm^{-1} is attributed to O–H stretching vibrations, characteristic of CS and cellulose owing to their abundant hydroxyl groups. The peak at 2927.74 cm^{-1} corresponds to C–H stretching vibrations of the aliphatic $–CH_2$ groups, thereby confirming the presence of the polysaccharide backbone. The absorption band at 1585.31 cm^{-1} corresponds to the N–H bending vibration (amide II band), signifying the presence of amino groups derived from CS as shown in Figure 5.17. The peak at 1412.58 cm^{-1} may indicate CH_2 scissoring or symmetric COO^- stretching, implying potential ionic interactions among the CS and NC phases. The pronounced absorption at 1328.23 cm^{-1} is attributed to C–N stretching, thereby

corroborating the amine functionalities present in CS. The absorption at 1245.31 cm^{-1} is attributed to S=O stretching vibrations from sulfate ester groups ($–OSO_3^-$), signifying an occurrence of sulfated NC, probable introduced through acid hydrolysis via sulfuric acid. The sharp band observed at 895.53 cm^{-1}, attributed to β-glycosidic linkages, indicates the retention of the cellulose structure in the film. The spectral assignments are consistent with earlier research on CS–cellulose composites, which indicate comparable functional group positions and shifts attributed to hydrogen bonding and molecular integration (George & Sabapathi, 2015; Li et al., 2021). The minor differences in intensity and location of significant peaks indicate robust intermolecular interactions, which improve the film's uniformity and structural strength (Szymańska & Winnicka, 2015). The FTIR spectrum confirms the chemical stability and effective formation of a cohesive, active CS and NC matrix inside the T2 multilayer film.

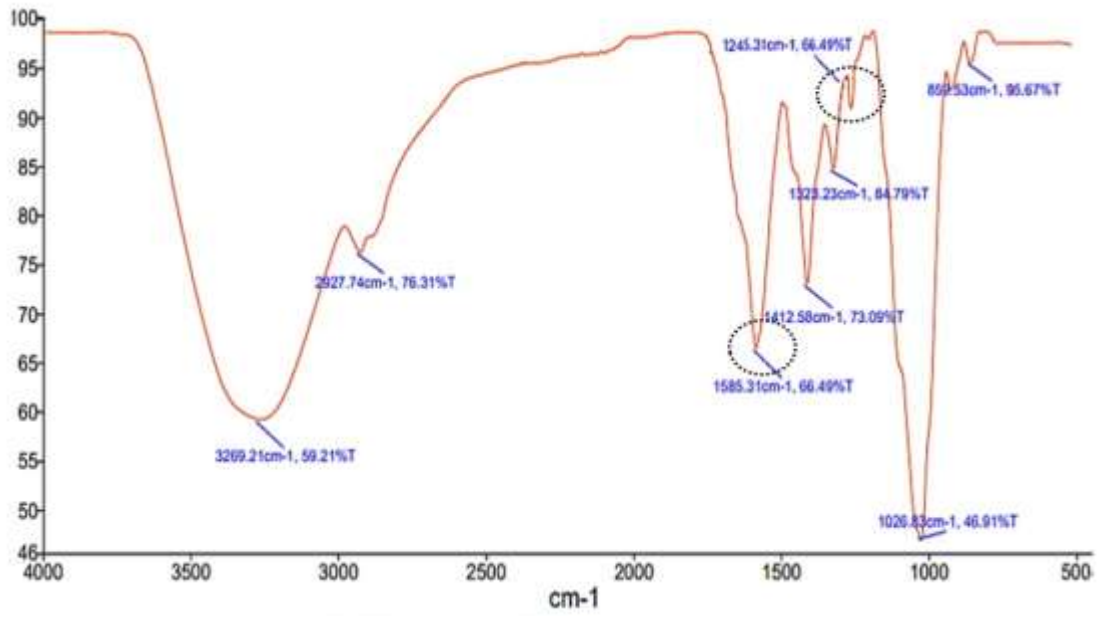

Figure 5.17. Fourier transform infrared spectra of optimized control multilayer film (T2).

5.25.2. Differential scanning calorimetry (DSC)

The differential scanning calorimetry (DSC) thermograms of the CS: NC multilayer films (T1, T2, and T3) exhibit significant variations in glass transition behavior, indicative of the interplay between plasticization (glycerol) and polymer–filler interactions. T2 demonstrates the highest apparent Tg at approximately 85.47 °C, while T1 and T3 present higher Tg values of around 81.49 °C and 82.4 °C, respectively as shown in Figure 5.18. The observed increase in Tg in T2 aligns with increased plasticization due to the addition of glycerol at 30% w/w relative to the total polymer. This increase in polymer loading correspondingly improves the overall glycerol % and the efficient plasticizer-to-polymer ratio in the film, resulting in enhanced chain mobility and a reduction in Tg (Smith et al., 2021; Eslami et al., 2023). Plasticizers diminish intermolecular hydrogen bonding among polymer chains and augment free volume, which facilitates chain mobility and decreases the energy necessary for the glass–rubber transition (Panova et al., 2024). The increase in Tg from T2 to T3 could be attributed to an antiplasticization or reinforcement effect resulting from higher NC bringing or enhanced hydrogen bonding between the polymer and nanofiller. Elevated NC concentration results in the formation of a rigid crystalline phase, which limits polymer segmental mobility and enhances the matrix's strength. This leads to decreased chain mobility and consequently an increased Tg. Furthermore, the increased density of hydrogen-bonding networks across CS and NC restricts the mobility of the plasticizer, thereby mitigating the starting softening effect. The elevated Tg noted for T3, despite its increased polymer and glycerol content, suggests that at the maximum CS to NC ratio, the reinforcing effects of robust hydrogen bonding and interactions between CS chains and NC prevail, limiting segmental mobility and mitigating plasticization (Jia et al., 2020; Potaś et al., 2022). The DSC data demonstrate a balance across glycerol-induced softening as well as NC reinforcement, T2 is characterized by a Tg depression indicative of plasticization, whereas T3 reveals that at elevated polymer/NC loading, network rigidity dominates, resulting in a higher Tg.

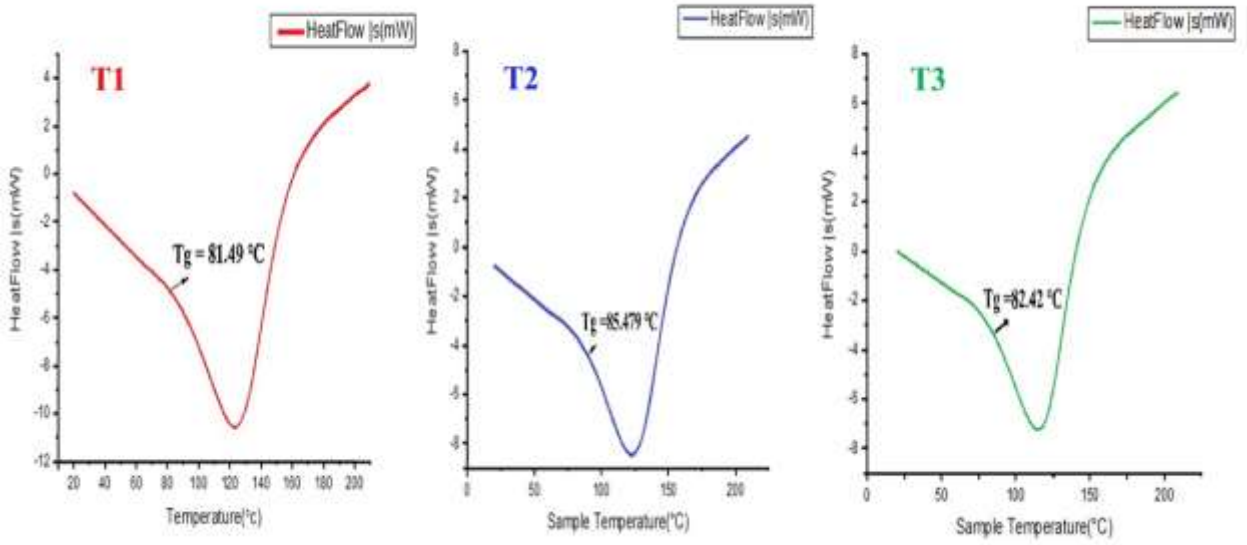

Figure 5.18. Differential scanning calorimetry of control multilayer films (T1, T2 and T3).

5.25.3. Field Emission Scanning Electron Microscope (FE-SEM)

The FE-SEM micrographs of an optimized T2 multilayer film, composed of a CS base and a NC top layer, demonstrate a uniformly smooth surface, suggesting effective casting and interlayer compatibility. The cross-sectional images clearly depict 2 separate layers, namely a thicker CS underlayer and a clearly defined NC overlayer. The observed layered morphology indicates a controlled film architecture using distinct interfacial integrity, which is crucial for the performance of multilayer systems. During film creation, various causes may cause NC layer holes or bubbles Figure 5.19. According of Lyytikäinen et al. (2021) air in the viscous NC slurry can remain during casting and dry, creating gaps. Porosity can also result from quick or uneven water evaporation as the NC matrix compresses and revamps. Incomplete fibril packing owing to heterogeneous dispersion or poor solid content may cause microscopic voids (Leppänen et al., 2022). Remaining solvents or plasticizers can volatilize during drying, creating bubble-like holes (Azeredo et al., 2019). Combine these effects to explain the SEM image's porous appearance. Recent investigations report similar findings, indicating that CS blends with cellulose nanocrystals demonstrate smooth film textures and distinct layer demarcations, which suggest homogeneous dispersion and robust interpolymer interactions (Varma & Vasudevan, 2024). Talebi et al. (2022)

proved that CS films strengthened via cellulose nanocrystals exhibited a uniform distribution without clumping within the CS matrix, indicating the lack of surface roughness in the current sample. The images and literature collectively demonstrate the superior interfacial adhesion and precise multilayer arranging in the T2 film, essential for its mechanical and barrier properties.

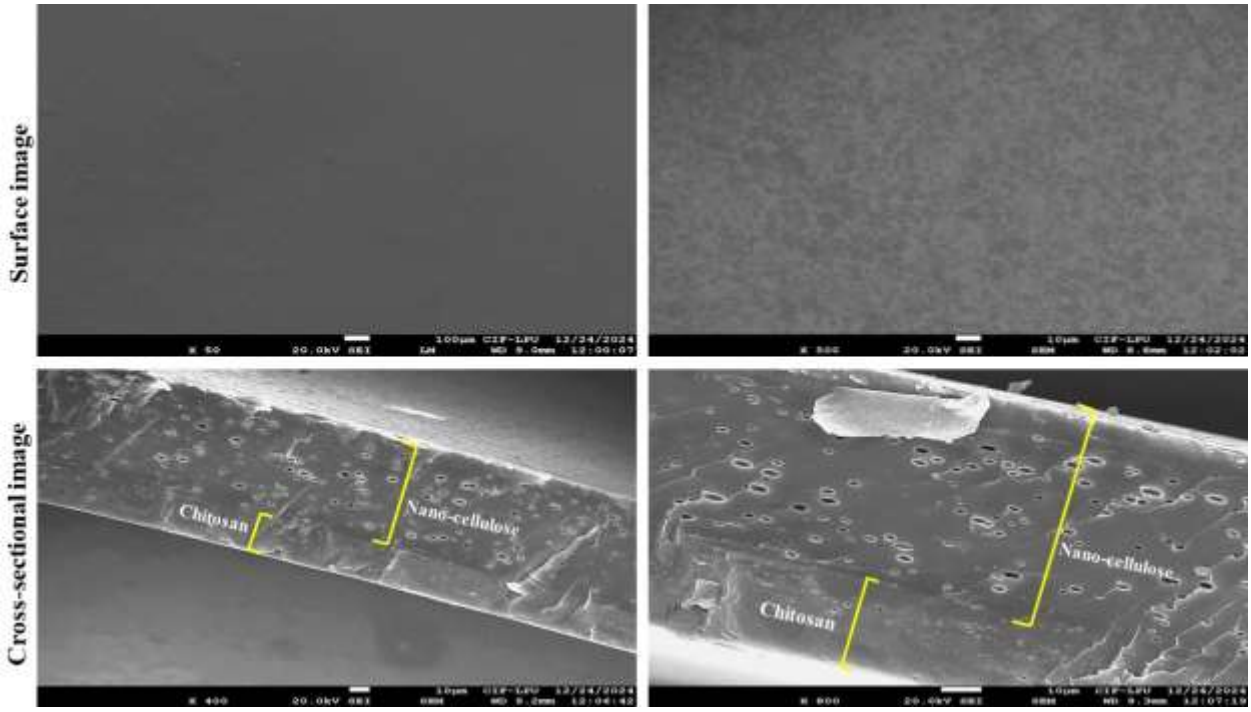

Figure 5.19. Field emission scanning electron microscope images of surface (50x and 500x) and cross sectional (400x and 800x) optimized control multilayer film (T2).

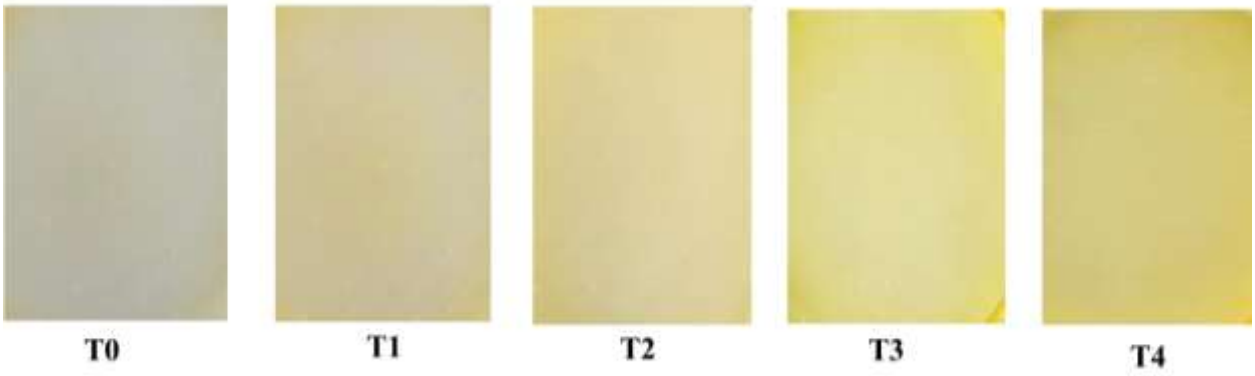

Figure 5.20. Visual analysis of the control film (T0) and treated films (T1, T2, T3 and T4).

5.26. Apparent color and optical properties of the treated film

5.26.1. Visual analyses of the treated films

RES inclusion into CS based films can, in actually, induce noticeable modifications in the optical properties and color of the film, as illustrated in Figure 5.20. Research has shown that the glossiness and appearance of the film can be influenced by the formation of RES crystals on the film surface, which in turn increases surface heterogeneity (Pastor et al., 2013). In its purest form, RES is a polyphenol that exhibits a light yellow to pale brown hue. Depending on the concentration of the substance, the transparency and color of the film may change when it is incorporated (Busolo & Lagaron, 2015). Additionally, RES is susceptible to degradation when exposed to ultraviolet radiation, which can result in browning over time. The extent of browning is influenced by RES loading and the conditions under which the film is stored (Zhu, 2021). The incorporation of natural compounds such as RES into CS films has been linked to enhanced moisture content and water solubility, thereby affecting the film's physical properties and possibly its appearance (Souza et al., 2017).

5.26.2. Hunter color properties of the treated films

Biodegradable films that include bioactive compounds like RES have attracted interest for their potential antioxidant and UV-protective properties. The incorporation of RES notably influences the optical properties of these films, which is essential in the fields of biomedical and food packaging. The focus of this study is on the impact of elevated RES concentrations on the Hunter

color properties of CS-NC multilayer films, focusing on total color difference (ΔE), whiteness index (WI), chroma (C*), and hue angle (H*), as presented in Table 5.10. The total color difference (ΔE) values increased as the concentration of RES increased, with a range of 26.324 to 90.291. This increase implies that RES substantially alters the film's color, rendering it more distinct from the control. The pigmentation properties of RES are likely to be the cause of the increase in ΔE, which deviates from the baseline color. Jonaidi Jafari et al. (2021) observed that polyphenol-loaded films exhibited a perceptible change in color as a result of light absorption and interaction with the polymer matrix, resulting in an increase in ΔE values. The whiteness index (WI) diminished with increasing RES content, varying from 27.232 to 90.028. This drop indicates that the films became increasingly darker and less luminous. RES, a naturally colored molecule, confers a distinctive reddish-brown hue, diminishing the overall whiteness of the film. Siracusa et al. (2018) found that the integration of polyphenols into biodegradable films resulted in a reduction in water impermeability, which is associated with the existence of natural colors in plant-derived bioactive chemicals. Chroma (C*), indicative of color saturation, rose from 24.772 to 83.100 when RES concentration increased. This suggests that the films exhibited increased vibrancy in coloration, reflecting a heightened intensity in hue. Increased chroma values indicate that RES improves the overall color vibrancy of the film. Wang et al. (2020) found that anthocyanin-rich films showed elevated C* values attributed to natural pigments, indicating that polyphenols improve the color saturation of biodegradable films. The hue angle (H*), indicative of the perceived color type, increased from -0.392 to 21.235, indicating a transition towards a more reddish or yellowish tone. This change aligns with the inherent color of RES, thereby reinforcing its significant impact on film coloration. Tanpichai et al. (2019) observed similar hue shifts in polyphenol-loaded films, noting that increased bioactive concentrations caused to an apparent transition towards red and yellow hues. This study shows that higher concentrations of RES significantly modify the Hunter color properties of CS-NC films. The films exhibited increased darkness, saturation, and a shift towards reddish hues, consistent with prior research on polyphenol incorporation in biodegradable packaging. These changes may influence aesthetic preferences and indicate improved UV-blocking and antioxidant properties, rendering these films appropriate for applications that necessitate protection of light-sensitive materials.

5.26.3. Light transmission and transparency of the treated films

CS-NC multilayer films are extensively research used for food wrapping because of its biodegradability, physical characteristics, including barrier performance. The characteristics of light, specifically transmittance (T%) and transparency (To%), are critical in determining their applicability for various food products. RES, a natural polyphenol, has been added to biodegradable films for its antioxidant and functional characteristics. This study assesses the impact of varying RES concentrations (4, 8, 12, 16 µg/mL) in CS-NC cellulose films (T1, T2, T3, and T4) on their optical properties, as indicated by transmittance and transparency measurements at 600 nm (A600). The films designated as T1, T2, T3, and T4 represent ascending concentrations of RES. The data presented in Table 5.10 indicates that an increase in RES concentration from T1 to T4 corresponds with a rise in transmittance (T%). At the same time, transparency (To%) decreases, signifying a reduction in film opacity. This indicates that films with increased RES content permit greater light transmission, resulting in enhanced transparency. The minimum transmittance (T1, 27.989%) is observed at a 4 µg/mL RES dosage, whereas maximum transmittance (T4, 79.432%) occurs at 16 µg/mL RES. Films containing low levels of RES (T1, 7.042%) exhibit greater opacity, whereas those with elevated RES content (T4, 43.888%) demonstrate significantly increased transparency. The mechanism affecting optical properties is linked to RES role in modifying the polymer matrix. According to Farris et al. (2014), the enhancement in transmittance and transparency is attributed to the improved dispersion of RES within the CS-NC matrix. RES molecules likely interfere with polymer chain aggregation, resulting in a more uniform structure that facilitates improved light penetration. A further reason may be attributed to the decrease in film thickness and surface roughness. As increased concentrations of RES may function as a plasticizer, leading to a reduction in film thickness and roughness, thereby decreasing light scattering. A smoother surface leads to increased transparency and transmittance (Siddiqui et al., 2018). Molecular interactions and structural alignment. RES may enhance hydrogen bonding interactions with CS and NC, resulting in a more organized polymer network. The molecular reorganization may reduce opacity, thereby enhancing both T% and To% (Zhou et al., 2019). Cheng et al. (2021) demonstrated that antioxidant films containing plant polyphenols showed reduced transparency and increased opacity, aligning with the trends observed in the provided data. The observed reduction is due to the intrinsic color of polyphenols and their interaction with the film matrix, influencing light transmission through the film. Sun et

al. (2017) noted that young apple polyphenols added to CS films produced high color transition from reddish-brown to yellowish, accompanied by a reduction in transparency. These polyphenols can reduce light transmittance in films, especially within the ultraviolet-visible (UV-Vis) spectrum. Bi et al. (2019) demonstrated that the incorporation of proanthocyanidins into CS films markedly decreased their UV-Vis light transmittance, with more pronounced reductions noted at elevated polyphenol concentrations (Pan et al., 2024).

Table 5.10. Total color difference (ΔE), lightness (L*), chroma (C*), hue (h*) and whiteness index (WI) of the treated films equilibrated at 25 °C.

Films	l	a	b	ΔE	WI	C*	H*	T (%) at A600	To (%) at A600
T1	88.858 ± 0.833^{a}	-0.66 ± 0.328^{d}	26.73 ± 1.111^{d}	26.324 ± 1.261^{d}	27.232 ± 1.034^{d}	24.772 ± 1.113^{d}	-0.392 ± 0.738^{d}	79.432 ±0.655^{a}	43.888± 0.221^{a}
T2	72.858± 1.233^{b}	8.49 ± 0.284^{c}	65.868 ± 0.693^{c}	69.176 ± 0.894^{c}	68.966 ± 0.703^{c}	64.535 ± 0.711^{c}	7.997 ±0.207^{c}	63.095 ±0.324^{b}	23.704± 0.143^{b}
T3	67.158 ± 1.517^{c}	20.11 ± 0.874^{b}	74.418 ± 0.972^{b}	81.314 ± 0.737^{b}	81.491 ± 0.538^{b}	75.332 ± 0.535^{b}	15.868 ± 0.610^{b}	41.30 ±0.144^{c}	14.084± 0.542^{c}
T4	62.45 ± 1.082^{c}	29.61 ± 0.353^{a}	79.418 ± 0.972^{a}	90.291 ± 1.083^{a}	90.028± 0.467^{a}	83.100 ± 0.470^{a}	21.235 ± 0.181^{a}	27.989 ±0.231^{d}	7.042± 0.115^{d}

T: Transmittance and To: Transparency

Data are expressed in terms of mean ± standard deviation, with distinct letters (a - d) in the rows indicating significant variations ($p < 0.05$), where 'a' represents the lowest value.

5.27. Antimicrobial analysis and Zone of inhibition (ZOI) of treated film

The antibacterial activity of RES loaded CS films was assessed via the agar well diffusion method against Gram-negative (*Escherichia coli*) as well as Gram-positive (*Staphylococcus aureus*) bacterial strains, wherein the clear area that surround the sample on an inoculated agar plate reflects the degree of microbial growth suppression. In the control group (T0), consisting of CS films devoid of RES, minor yet discernible zones of inhibition were noted surrounding the wells (Plate a and c) as in Figure 5.21. This verifies that CS exhibits intrinsic antibacterial properties due to its polycationic characteristics, which engage into negatively charged microbial cell membranes, resulting in the efflux of internal constituents. Upon the incorporation of RES into CS films at escalating doses (T1 = 4 µg/mL, T2 = 8 µg/mL, T3 = 12 µg/mL, T4 = 16 µg/mL), a distinct dose-dependent augmentation in antimicrobial efficacy was evident, as demonstrated by increasingly bigger zones of inhibition (Plates b and d). The ZOI quantitatively assesses antimicrobial efficacy, with increased diameters indicating enhanced inhibitory effects. This study found that the control film with no RES (T0) demonstrated modest inhibition, measuring approximately 8.1 mm against *S. aureus* and 6.2 mm against *E. coli*, indicating the baseline effect of the CS matrix. The control sample (T0) demonstrated the smallest apparent ZOI for both tested strains. Conversely, the addition of RES (T1, T2, T3, and T4) produced inhibition zones between 8.1 mm and 15.4 mm as shown in Figure 5.22. The most significant inhibition zone was observed for *S. aureus* (15.4 mm), suggesting a relatively greater activity against *E. coli.* The incorporation of RES significantly enhanced antibacterial activity against most strains. The inhibition zones for *S. aureus* rose from 8.1 mm to 15.4 mm, while those for *E. coli* increased from 6.2 mm to 11.7 mm, indicating a potential additives or synergistic relationship between CS and RES. The RES-loaded films had significantly stronger antibacterial effects over *S. aureus* compared to *E. coli*, indicating that Gram-positive bacteria are more vulnerable, presumably due to the lack of the protective outer layer present in Gram-negative bacteria. The results align with prior research. Liu et al. (2017) showed that CS-RES films exhibited significantly larger inhibition zones against *S. aureus* than against *E. coli*, with activity correlating positively with active ingredient concentration. Likewise, Dural et al. (2021) observed improved antimicrobial properties in RES-loaded CS films, with Gram-positive bacteria exhibiting greater sensitivity to the treatment. Shahidi et al. (2019) demonstrated that nanoemulsified RES within CS matrices enhanced inhibition of bacteria in a dose-dependent manner, especially against *S. aureus*. Peng et al. (2016) highlighted the synergistic

effect of CS and RES, linking the antimicrobial improvement to disruption of the cell membrane and induction of oxidative stress. The results indicate that the integration of CS and RES improves the antimicrobial efficacy of multilayer films, especially regarding bacterial inhibition in food packaging and biomedical use.

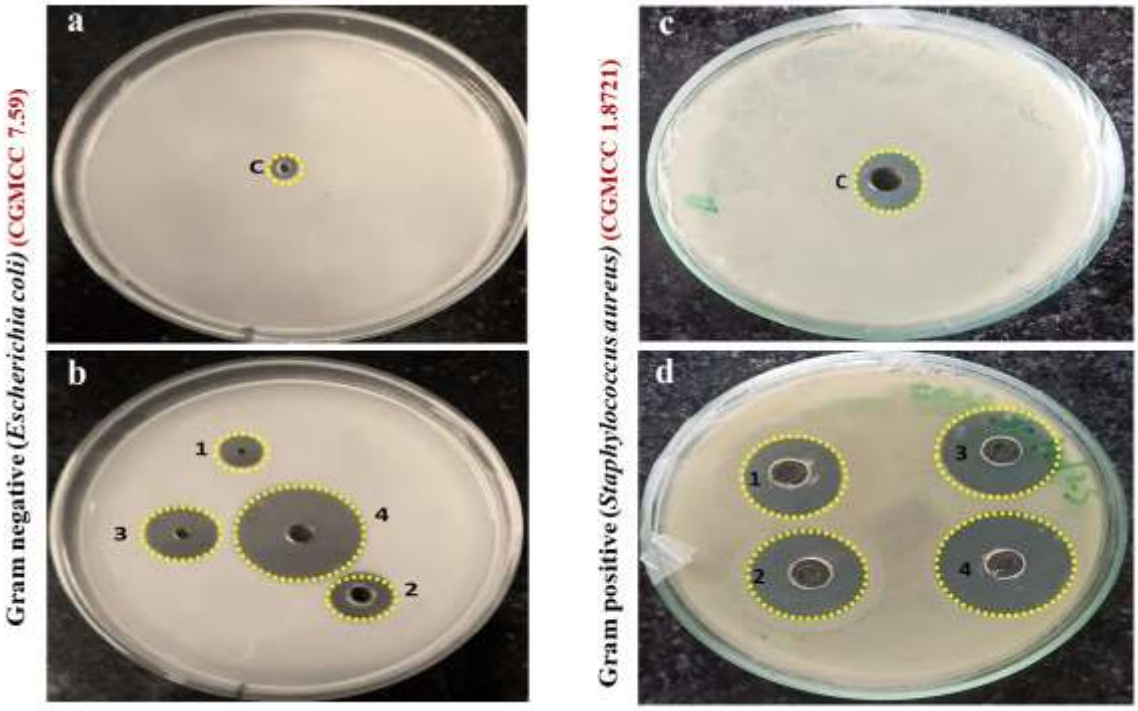

Figure 5.21. Antimicrobial analysis of treated film using gram negative bactria a) optimized control film b) Treated film c) using gram positive bactria (c) optimized control film b) Treated films.

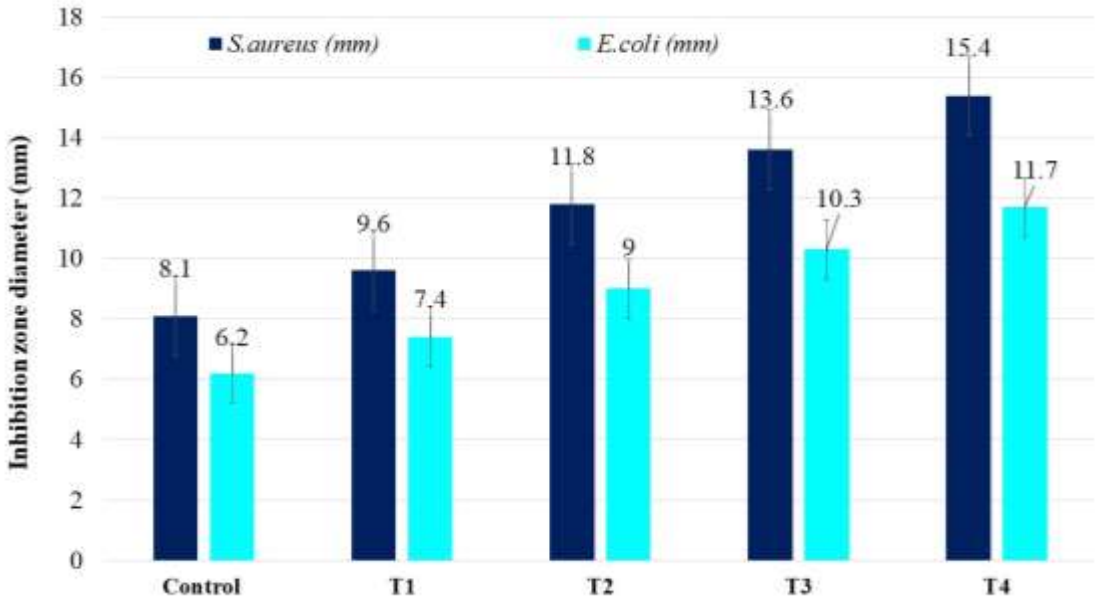

Figure 5.22. Zone of inhibition of control film (T0) and treated films (T1, T2, T3 and T4) using gram negative bactria and gram positive bactria.

5.28. Measurement of physical properties of the treated films

5.28.1. Thickness measurement

The thickness of the CS-NC composite films, which integrated increasing doses of RES from T1 to T4 (4, 8, 12, and 16 µg/mL, respectively), exhibited a varied pattern, as indicated in Table 5.11. The film thickness initially rose from 89.204 µm (T1) to 100.31 µm (T3) and thereafter had a slight decrease by T4 (96.91 µm). The increase is attributed to the incorporation of RES, which may enhance solid content and influence the microstructure of the film matrix, resulting in thicker film formation. The observed increase in thickness is because of RES molecules that are present in the film matrix, there may be better intermolecular interactions (e.g. hydrogen bonding) with RES with CS-NC, leading to an increased solid content upon film casting and modified film morphology, which may lead to reduced density and increased volume of the dry films. Additionally, RES may function as a bulking agent, interfering with tight polymer chain packing and resulting in a more expanded microstructure, which ultimately leads to increased film thickness. The increase in film thickness with higher concentrations of RES aligns with previous

research on the incorporation of bioactive compounds in biopolymer films (Li et al., 2020). The initial incorporation of RES into CS-NC based films results in a progressive increase in film thickness due to enhanced matrix density and solid content; however, this trend is not sustained with time. At elevated RES concentrations, specifically in T4 (16 μg/mL), a minor reduction in film thickness is noted relative to T3 (12 μg/mL), suggesting a change in the behavior of the polymer network. The CS-NC network has reached the saturation point, which is the cause of the decrease. Hydrogen bonding and hydrophobic interactions between hydroxyl groups and amine groups of CS and NC are formed by RES molecules at moderate concentrations, thereby reinforcing the polymer network and enhancing thickness (Li et al., 2020). At high concentrations, the availability of active binding sites is restricted, and excess RES molecules may not effectively integrate into the polymer structure. As a result, unbound RES may aggregate, resulting in molecular phase separation and heterogeneity within the film matrix (Zhou et al., 2021; Tang et al., 2022). Furthermore, elevated levels of RES may function as a plasticizer at the molecular scale, interfering with the intermolecular hydrogen bonding among polymer chains (Kowalczyk & Baraniak, 2014). This disruption diminishes the compactness of the matrix and may result in partial collapse or folding of the polymer network during the drying process, consequently reducing film thickness. The hydrophobic characteristics of RES become increasingly evident at higher concentrations, diminishing its compatibility with hydrophilic biopolymers such as CS and cellulose. This incompatibility can lead to phase segregation or leaching during casting, thereby contributing to the observed reduction in final thickness (Zhao et al., 2019). Additionally, the dynamics of thermal and solvent evaporation during film formation can intensify this effect. High-resolution content can modify the film-forming material's rheological characteristics, leading to a decrease in viscosity or spreading behavior, which results in the formation of thinner films after solvent evaporation (Saqib et al., 2023). Wang et al. (2018) showed that increased RES loading in CS-based films led to thinner films, attributed to RES aggregation and diminished compatibility with the hydrophilic polymer network. Zhou et al. (2021) observed that in gelatin/alginate multilayer films, high concentrations of RES could not be completely incorporated into the matrix, resulting in crystallization and a reduction in film thickness. Tang et al. (2022) indicated that RES concentrations exceeding 10 μg/mL in cellulose–CS films led to phase separation, producing a heterogeneous and thinner film. The findings align with the observed data for T4, indicating that

elevated RES concentration likely surpassed the solubilization threshold of the polymer blend, resulting in structural disintegration and diminished film thickness.

5.28.2. Tensile strength (TS) and elongation at break (EB)

An addition of RES to CS–NC multilayer films considerably affected inherent mechanical characteristics, particularly their breaking elongation along with bending strength Table 5.11. demonstrates the ultimate bending power of CS-NC films containing RES displayed a nonlinear relationship as RES concentration increased. The tensile strength initially decreased from 47.520 MPa in T1 (4 µg/mL RES) to 46.595 MPa in T2 (8 µg/mL RES), and subsequently declined to 42.195 MPa in T3 (12 µg/mL RES). The decline is due to the plasticizing effect of RES, which interferes with the interpolymeric hydrogen bonding in the CS-NC matrix. At moderate RES levels, the antioxidant functions as a reinforcing agent through its interaction with the polymer network. Exceeding a specific threshold (e.g., T3), excess RES can disrupt matrix integrity through phase separation or micro-aggregation, thereby compromising the overall structure. A slight recovery in tensile strength was observed at T4 (16 µg/mL RES) with a measurement of 45.695 MPa. One possible explanation is that certain hydrogen bonds have partially reformatted or rearrangement of the RES-polymer interactions, leading to a reduced overall size. Wang et al. (2018) reported that low to moderate concentrations of RES improved mechanical strength, however excessive concentrations resulted in RES crystallization and phase incompatibility. Likewise, research conducted by Xu et al. (2020) on polyvinyl alcohol/CS films found that an excess of polyphenols such as RES can function as an anti-plasticizer, reinforcing the matrix via non-covalent interactions. Furthermore, Arfat et al. (2017) noted that excessive integration of active compounds in biopolymer films could compromise uniformity, hence impacting mechanical parameters like tensile strength.

The elongation at break (EAB), indicative of the film's elasticity and stretchability, exhibited an upward trend from T1 (68.87%) to T3 (74.195%) as RES concentrations increased from 4 to 12 µg/mL. The enhancement in EAB signifies increased polymer chain mobility and flexibility, presumably resulting from the plasticizing impact of RES at moderate doses. As a phenolic chemical, RES may settle inside the polymer matrix, disrupting the stiff hydrogen bonding network of CS and NC, hence facilitating increased molecular movement and flexibility (Sánchez-González et al., 2011). The maximum elongation recorded in T3 (12 µg/mL) indicates an ideal

RES concentration that optimizes the equilibrium between plasticization and matrix cohesiveness. A minor reduction in EAB was noted in T4 (72.52%), where the RES concentration was elevated to 16 µg/mL. This slight decrease may be ascribed to the oversaturation of RES in the film solution, perhaps resulting in phase separation, micro-crystal formation, or incompatibility within the biopolymer network. Such events may impede polymer mobility, hence marginally diminishing elasticity. Wang et al. (2018) observed same findings, indicating that exceeding an ideal polyphenol threshold resulted in diminished film stretchability due to decreased interaction with the polymer and aggregation of the active chemical. Liu et al. (2021) further illustrated that excessive incorporation of RES in CS-based films resulted in a more rigid structure, as unbound RES functioned as filler particles instead of plasticizers. Shahbazi et al. (2020) integrated gallic acid into gelatin films and observed a dose-dependent enhancement in EAB up to an ideal concentration. Beyond this concentration, the EAB diminished, perhaps due to excessive polyphenol–polymer interactions or crystallization of the polyphenolic molecule, which impeded molecular mobility. Peretto et al. (2014) similarly observed that multilayer films made of hydroxypropyl methylcellulose and CS, when infused with grape seed extract (a rich polyphenol source), demonstrated elevated EAB values. The authors ascribed this enhancement to the polyphenols functioning as secondary plasticizers, so diminishing the stiffness of the polymer matrix. Jiménez et al. (2012) revealed that the integration of polyphenol-rich substances, including rosemary and green tea extracts, into biopolymer matrices boosted elongation at break at moderate concentrations, attributable to enhanced flexibility and polymer chain mobility.

The overall rise in elongation from T1 to T3 highlights the efficacy of RES as a plasticizing agent in moderate quantities, but the modest decrease after T4 signifies the development of structural rigidity due to RES excess.

5.29. Antioxidant activity of the treated film

5.29.1. 2,2-diphenyl-1-picrylhydrazyl (DPPH) activity

The antioxidant efficacy of CS-NC multilayer films infused with RES was assessed utilizing the DPPH radical scavenging assay. The DPPH scavenging activity (%) indicates the sample's capacity to neutralize free radicals. A greater % indicates stronger antioxidant efficacy. RES is an extensively studied antioxidant substance; when its concentration rises, a greater number of active molecules are present to neutralize DPPH radicals. As the concentration of RES escalated

from 4 µg/mL in T1 to 16 µg/mL in T4, a concomitant enhancement in DPPH scavenging activity was recorded, yielding values of 31.787%, 46.876%, 58.341%, and 74.658% for T1, T2, T3, and T4, respectively, as presented in Table 5.11. This incremental improvement in antioxidant activity signifies a dose-dependent influence of RES within the film matrix. The enhancement in DPPH scavenging ability indicates that larger quantities of RES were efficiently held and released from the multilayer films, facilitating increased free radical neutralization. CS and NC are biocompatible, film-forming materials frequently utilized in controlled-release systems. They can stabilize delicate compounds such as RES and facilitate prolonged release. These findings corroborate other studies that illustrate the robust antioxidant capabilities of RES and its efficacy in polymer-based delivery systems (Shantha et al., 2018; Ahmad et al., 2020). Shantha et al. (2018) found that elevated quantities of polyphenolic chemicals in biopolymer films resulted in improved antioxidant activity, as assessed by the DPPH assay. Ahmad et al. (2020) noted that RES-loaded CS films had a dose-dependent enhancement in DPPH scavenging activity, achieving over 80% at elevated RES concentrations. Siripatrawan and Harte (2010) demonstrated that CS films infused via extracts from the green tea showed an enhancement in DPPH scavenging from 35% to 77% as polyphenol concentration rose, indicating the synergistic interaction between CS and antioxidants within film matrices. Galus and Lenart (2013) noted a comparable dose-dependent response in edible films fortified with tannic acid and catechin, wherein antioxidant activity increased from approximately 25% to 80% with higher doses. Gülçin (2010) further supports the underlying mechanism, indicating that RES possesses robust intrinsic antioxidant activities in solution, with an IC_{50} of roughly 16 µg/mL. The investigations collectively verify the pattern identified in this research, affirming that elevated RES concentrations in CS-cellulose matrices promote antioxidant activity. Furthermore, the structural attributes of the multilayer film specifically the semi-crystalline and porous properties of NC may facilitate effective retention and regulated release of RES, preserving its bioactivity over time.

5.29.2. Reducing power (RP) assay

The reducing power test is a commonly utilized technique to assess the electron-donating ability of antioxidants, functioning as a reliable measure of potential antioxidant activity. This method relies on the reduction of ferric (Fe^{3+}) ions to ferrous (Fe^{2+}) ions, resulting in the creation of a Perl's Prussian blue complex, which may be quantified spectrophotometrically at 700 nm. Increased

absorbance values indicate higher reducing power and, thus, increased antioxidant activity. The present study evaluated the reducing power of CS-NC-based multilayered films infused with increasing amounts of RES (T1: 4 µg/mL, T2: 8 µg/mL, T3: 12 µg/mL, T4: 16 µg/mL). The absorbance values at 700 nm for T1 to T4 were documented as 0.534, 0.844, 1.213, and 1.551, respectively, as shown in Table 5.11. The gradual rise in absorbance values indicates a dose-dependent enhancement in the lowering the endurance of the films with an addition of RES. RES is an extensively studied polyphenolic molecule recognized for its strong antioxidant capabilities, principally attributed to its capacity to donate hydrogen atoms or electrons and stabilize free radicals (Baur & Sinclair, 2006). Incorporating RES into a polymeric film matrix not only preserves but may also synergistically enhance the material's total antioxidant capability. The identified pattern corresponds with previous research. Chen et al. (2020) examined starch-based films infused with RES and observed an increase in absorbance from 0.41 to 0.89 at 700 nm, indicating a substantial enhancement in reducing power with increasing RES concentration. A study by Kurek et al. (2019) also demonstrated enhanced antioxidant activity in CS-based active packaging films following the incorporation of plant-derived polyphenols such as resveratrol and catechins. The reduction in power values rose from 0.19 to 0.62 with the addition of polyphenols, as measured by absorbance at 700 nm, showing enhanced antioxidant capacity. Mokhena et al. (2020) demonstrated that CS–cellulose nanocrystal films enhanced with antioxidants shown markedly superior reducing power relative to control films. The NC matrix, owing to its extensive surface area and compatibility, likely facilitates the efficient dispersion and stabilization of RES molecules, hence enhancing their efficacy. Kanmani and Rhim (2014) demonstrated that carrageenan-based films infused with grapefruit seed extract showed enhanced reducing power, with absorbance values increasing from 0.20 to 0.77 based on extract content. The alignment of these findings with the present investigation strongly shows that RES maintains its redox-active properties within the CS-NC matrix, indicating a significant potential for these films to serve as active packaging materials with antioxidant capabilities.

Table. 5.11. Mechanical properties and Antioxidant activity of the treated films equilibrated at 25 °C.

Films	Thickness (µm)	Tensile strength (MPa)	(%) Elongation at break	(%) DPPH	RP assay (Abs at 700 nm)

T1	89.204± 1.66 [c]	50.193± 2.14 [a]	68.87± 1.56 [c]	31.787 ± 1.14 [d]	0.534 ± 0.002 [d]
T2	94.71± 1.57 [b]	46.595± 1.21 [b]	70.211± 1.48 [bc]	46.876 ± 1.09 [c]	0.844 ±0.003 [c]
T3	100.31± 1.52 [a]	42.195± 2.04 [c]	74.195± 1.53 [a]	58.341 ±1.04 [b]	1.213 ±0.01 [a]
T4	96.91± 1.72 [b]	45.695± 1.47 [b]	72.52± 1.39 [ab]	74.658 ±1.12 [a]	1.551 ± 0.04 [a]

Data are expressed in terms of mean ± standard deviation, with distinct letters (a - d) in the rows indicating significant variations ($p < 0.05$), where 'a' represents the lowest value.

5.30. Characterization of optimized treated film

5.30.1. Fourier transform infrared radiation (FTIR) spectroscopy

The FTIR spectra of the optimized treated T3 multilayer film exhibits characteristic absorptions that validate the successful incorporation of RES and the retention of CS and NC components, alongside intermolecular interactions within the multilayer matrix. A band centered around 3269 cm^{-1} is associated with O–H/N–H stretching, indicating the presence of combined hydroxyl groups from NC and residual amine/hydroxyl groups from CS which suggests significant hydrogen bonding. The peaks at 2929 cm^{-1} and approximately 1027 cm^{-1} are attributed to C–H stretching and C–O stretching of the polysaccharide backbone, accordingly. The band at 1587 cm^{-1} is attributed to N–H bending (amide II), confirming the presence of free amine groups from CS in the final film. The absorption observed at 1627 cm^{-1} is indicative of C=C stretching in an aromatic ring, thereby confirming the integration of the benzene rings of RES into the polymer matrix as shown in Figure 5.23. The FTIR assignments is consistent with findings indicating that RES-loaded biopolymer systems exhibit similar absorption bands for the benzene ring (Hwang et al., 2023). The amide II band at approximately 1587 cm^{-1}, indicating the presence of free amine groups in CS, aligns with findings in CS-based films, such as those enriched with rosemary oil, where N–H bending is observed near 1590 cm^{-1} (Smith et al., 2022). The occurrence of sulfate ester S=O stretching at approximately 1247 cm^{-1} indicates the formation of sulfated NC structures via sulfuric acid hydrolysis, as reported in studies on cellulose extraction and functionalization (Theivasanthi et al., 2019). All together, the FTIR data confirm that molecular-level interactions exist in the multilayer film and that T3 preserves the chemical signatures of the three key constituents.

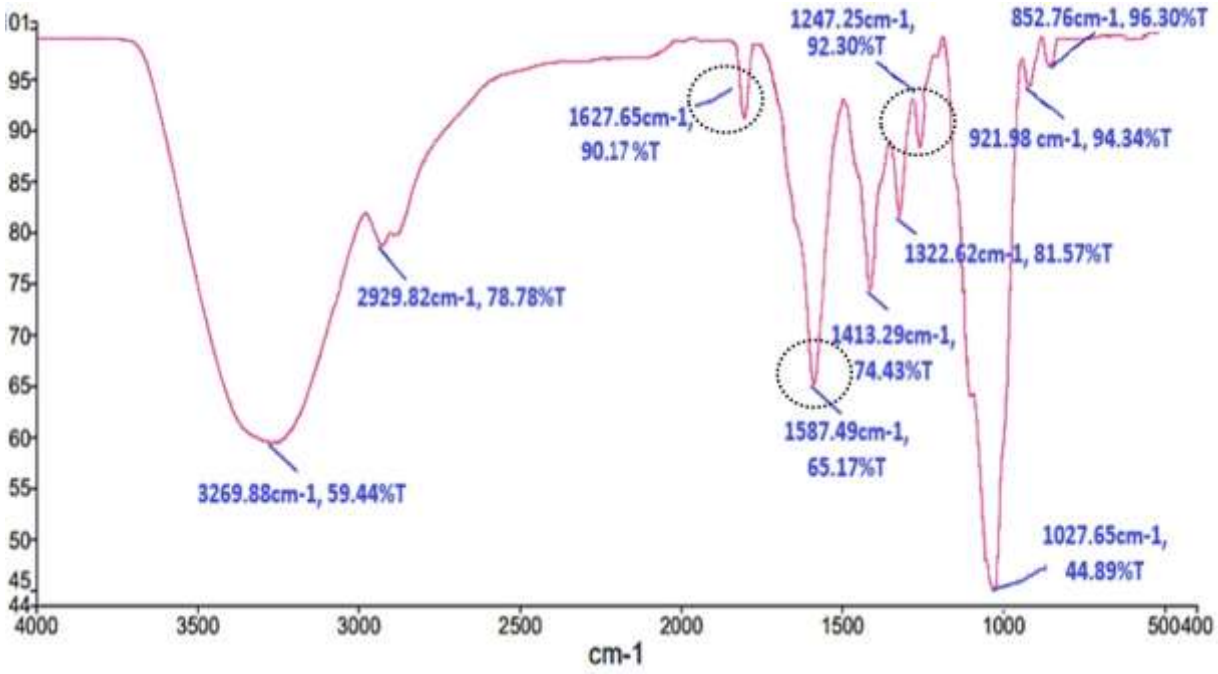

Figure 5.23. Fourier transform infrared spectra of optimized treated multilayer film (T3).

5.30.2. Differential scanning calorimetry (DSC)

The DSC thermograms indicate the glass transition temperature (Tg) for the control film with no RES (T2) as 85.47 °C, while the treated film with RES (T3) exhibits a Tg of 89.45 °C as shown in Figure 5.24. The observed increase in Tg can be attributed to a mixture of molecular mechanisms. RES possesses numerous hydroxyl groups and aromatic rings, enabling the formation of strong hydrogen bonds along with π–π or polar–aromatic bonds with CS and sulfated NC. This behavior effectively functions as a non-covalent crosslinker, which reduces free volume and limits segmental motion. Furthermore, RES particles scattered inside the matrix may enhance local rigidity by functioning as nanofillers, thereby further restricting chain mobility.

The interactions limit the mobility of the polymer chains, necessitating increased energy (higher temperature) for the transition from a glassy to the rubbery state. Previous studies have reported similar findings; for instance, Liu et al. (2019) showed that incorporating phenolic compounds into CS-based films enhanced Tg by reinforcing intermolecular bonding. Shankar et al. (2015) found that the incorporation of antioxidants such as gallic acid in biodegradable films resulted in an

increased Tg, which they attributed to the development of a denser polymer matrix. Hosseini et al. (2016) indicated that the incorporation of RES into biopolymer films increased Tg values, attributed to robust hydrogen bonding within RES alongside the polymer backbone. All of these findings point to the potential of adding bioactive compounds to improve the structural rigidity and thermal durability of edible films.

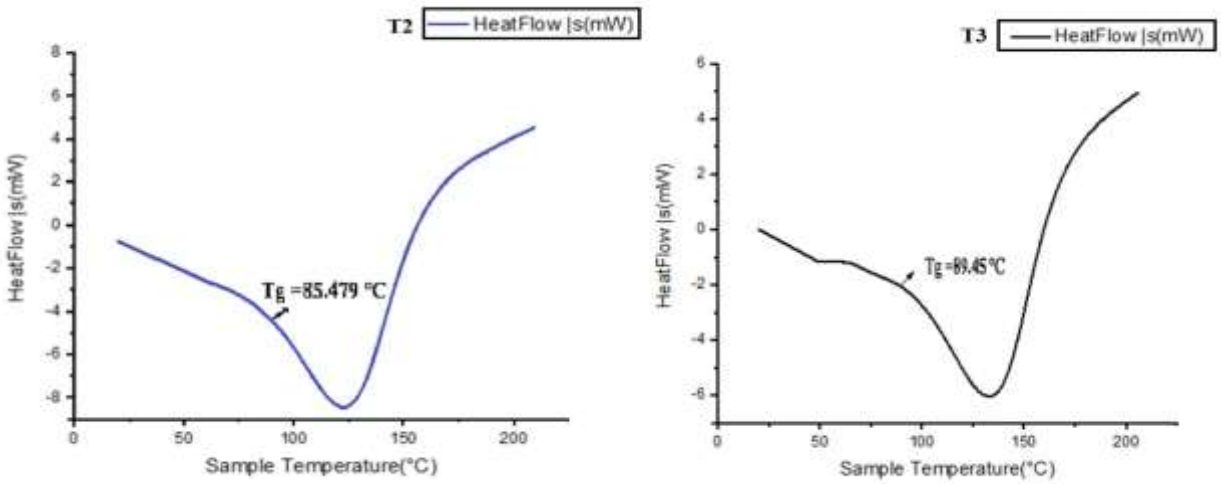

Figure 5.24. Differential scanning calorimetry of optimized control (T2) and optimized treated multilayer film (T3).

5.30.3. Field Emission Scanning Electron Microscope (FE-SEM)

Figure 5.25 presents the FE-SEM micrographs depicting the surface characteristics of the films produced from optimized concentrations of CS and NC, incorporating varying amounts of RES. The optimized T2 control CS-NC film exhibited a smooth appearance, consistent with an ordered arrangement of polymer chains. In contrast, the inclusion of RES resulted in a rougher texture, which became more pronounced with increasing concentrations of RES. The observed features likely arise from the partial clumping or trapping of RES crystals inside the polymer framework through the casting and solvent evacuation process, as evidenced through the separate pore boundaries related to the incorporated RES particles. Microstructural features have been linked to

phase separation phenomena across hydrophilic as well as hydrophobic ingredients, localized stress relaxation throughout drying, and gas entrapment due to residual elimination of solvent (Figueroa-Lopez et al., 2019; Liu et al., 2021). The observed morphology indicates that RES is not entirely solubilized, as the presence of stilbene complicates chain entanglements, resulting in a more disordered network that manifests as micro-aggregated form, potentially contributing to its sustained release attributes. The formation of similar pores in biopolymer films loaded with bioactive compounds is associated with improved antimicrobial efficacy, as it promotes the steady migration of the active compound to the film surface (Hosseini et al., 2016). SEM micrographs do not indicate significant irregularities in the polymer matrix with the incorporation of RES at any concentration; however, an increase in film thickness was observed, with greater RES concentrations resulting in thicker films. The treated multilayer films exhibited similar observations, as illustrated in Table 5.11, which presents the values of the various film thicknesses. The features indicate that RES molecules influence chain rearrangement in multilayer films, altering the film microstructure and resulting in more pronounced irregularities.

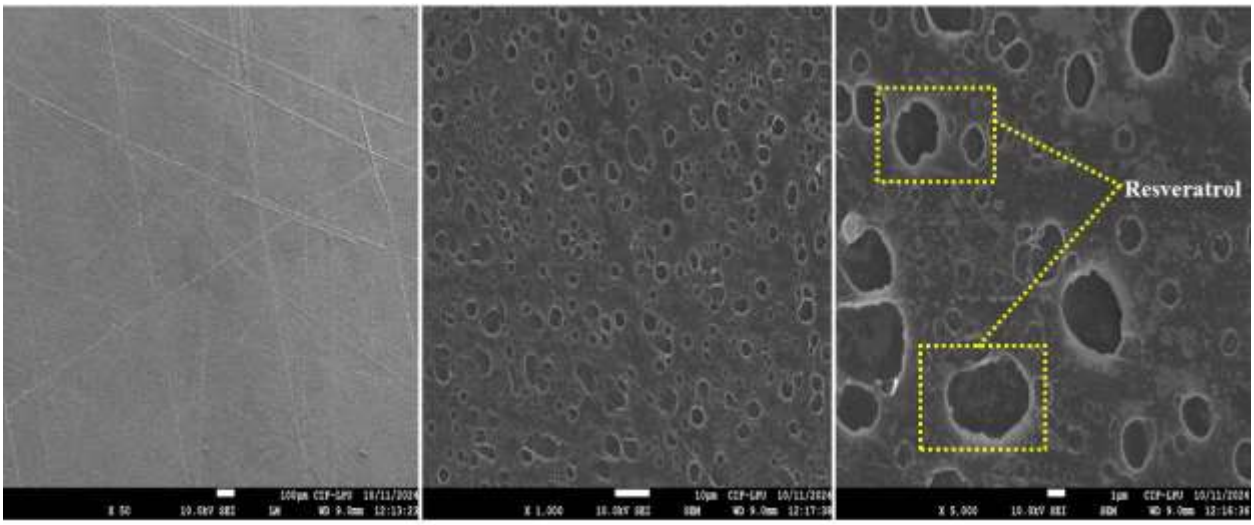

Figure 5.25. Field emission scanning electron microscope images of surface (50x, 1000x and 5000x) of optimized treated multilayer film (T3).

5.31. Biodegradation test (BT) of the film

The biodegradation test serves as an effective method for assessing the degradation of fabricated films, thereby evaluating their sustainability and environmental compatibility. The present study assesses the trend of microbial disintegration of film substance components and evaluates its environmental suitability (Alnadari et al., 2023). The results of the biodegradation test in Figure 5.26 revealed that the weight loss of multilayer film increased with the duration of soil dumping. On the initial day, the film exhibited full integrity without any weight loss. After 15 days, a weight reduction of approximately 12% was observed, accompanied by minimal surface erosion. This indicates that the phenolic structure or hydrophobic characteristics of RES limited the diffusion of water and microbial colonization. Although there was partial fragmentation and weight loss of 28% by the 30th day, the degradation was still much less than that of the untreated films. This is probably because of RES polymer hydrogen bonding while crosslinking, which limit the mobility of the polymer chain and its availability to hydrolytic enzymes. At 45 days, the film exhibited approximately 43% total weight loss, suggesting a gradual yet incomplete biodegradation process. The results indicate the film's significant biodegradability in soil, underscoring its potential for environmentally sustainable disposal via natural degradation processes. The biodegradation behavior is due to the inherent biopolymeric characteristics of CS

and NC. CS, a partially deacetylated derivative of chitin, shows vital being susceptible to microbial degradation due to its polycationic structure, which promotes interactions with soil microbes and enzymes such as chitosanases (Sinha et al., 2014) (Wieczorek et al., 2014). This is consistent with findings by Sogut & Seydim (2018), who indicated that phenolic-rich plant extracts integrated into CS films inhibit soil microbial activity owing to their antimicrobial characteristics. Stamogiannou et al. (2021) observed that CS films with grape seed extract exhibited slower degradation due to the interference of phenolic compounds with the enzymatic hydrolysis of polysaccharide links. Recent research, including Senan et al. (2024) and Aminzare et al. (2022), has confirmed that RES functions as an antibacterial and antioxidant agent, reducing microbial succession during soil burial and prolonging the film's functional lifespan. The current research highlights the prospective benefits of RES-treated films for packaging of food that balance ecological protection with functional durability and benefit from regulated biodegradability and longer service life.

Figure 5.26. Biodegradation test on optimized treated multilayer film (T3).

5.32. Mushroom storage study

5.32.1. Weight loss

The reduction in weight serves as a significant indicator reflecting both the metabolic processes and the overall quality of mushrooms. Dehydration is recognized as the primary factor contributing

the deterioration of mushroom quality during postharvest storage, due to the inability of the fragile epidermal framework of mushrooms to provide adequate protection to the swift loss of surface moisture (Singh et al., 2018). The weight loss % of *Agaricus bisporus* mushrooms during storage was markedly affected by the type of packaging film utilized, as seen in Table 5.12. The control treatment (T0), involving CS-NC devoid of any active component, exhibited the greatest weight loss during the storage duration, attaining 61.72% by day 15. This suggests that although CS-NC films have limited moisture retention and barrier properties, they are unsuitable for effectively controlling dehydration over prolonged storage (Jafarzadeh et al., 2020; Kurek et al., 2018). Treatments T1 to T4, which utilized CS-NC films infused with RES at concentrations of 4, 8, 12, and 16 µg/mL each, exhibited a significant decrease in weight loss at all measured time points. Weight loss decreased progressively with higher concentrations of RES. On day 15, T1 (4 µg/mL RES) exhibited a weight loss of 35.84%, whereas T2 (8 µg/mL RES) demonstrated a weight loss of 25.19%. This may be attributed across the delicate dermal framework of mushrooms, not enough to stop a high rate of transpiration. Significant reductions were noted in T3 (12 µg/mL RES) and T4 (16 µg/mL RES), resulting in ultimate weight losses of 10.29% and 14.44%, correspondingly.

These findings imply that adding RES to the CS-NC film matrix greatly improves its protective qualities. A naturally occurring polyphenolic substance with strong antibacterial and antioxidant properties is RES (Bahramian et al., 2024). Its incorporation into the film probably helped to minimize water loss from transpiration and respiration by lowering microbial growth and metabolic activity on the mushroom surface (Ma et al., 2018). Additionally, RES might have improved the structural quality of the film and decreased its water barrier permeability by interacting with the CS and NC polymer matrix. The highest performance was consistently shown by the treatment with 12 µg/mL RES (T3), suggesting an ideal dose where the positive effects of RES were maximized without sacrificing film homogeneity. It's interesting to note that although T4 (16 µg/mL RES) still considerably decreased weight loss when compared to the control, its efficacy was somewhat lower than T3, perhaps as a result of oversaturation or phase separation of the active ingredient in the film, which could have an impact on the performance and homogeneity of the film. Ojagh et al. (2010) reported similar effects, indicating that elevated concentrations of essential oils resulted in non-uniform distribution and phase separation, which negatively affected film integrity. Sogut and Seydim (2018) noted that excessive incorporation of bioactive

ingredients can lead to agglomeration in the film matrix, which diminishes its mechanical and barrier properties.

The weight reduction of packed mushrooms using CS-RES (12 µg/ml)-NC film was 10.2% after 15 days, remaining between the permissible marketplace value range of 5–10% (Liu et al., 2019; González-Fandos et al., 2021). Research done by Lakshan et al. (2024) examined tomatoes coated with films made of arrowroot starch and beeswax, which contained clove essential oil. Some formulations were found to effectively reduce weight loss, while others resulted in increased weight loss. Formulations characterized by reduced starch concentrations and increased essential oil content (e.g., 10 g/L AS with 5 mL/L EO) exhibited greater weight loss, presumably owed to thinner coatings and possible structural deficiencies. Li et al. (2020) conducted a study on edible films with grapefruit essential oil, revealing that an increase in EO concentration from 1% to 4% enhanced specific film properties. At a 6% EO concentration, the films displayed a discontinuous microstructure, resulting in heightened water vapor permeability. This structural disruption likely increased moisture loss from packaged foods (Šuput et al., 2019). In multilayer films with trans-cinnamaldehyde, elevated concentrations of the active agent resulted in greater total mass loss during thermal degradation (Baghi et al., 2024). Excessive incorporation of active compounds may compromise The thermal resistance and barrier characteristics of the film, potentially leading to increased weight loss in packaged items. The incorporation of RES into CS-NC films significantly decreased weight loss in *Agaricus bisporus* mushrooms during storage, with the 12 µg/mL concentration (T3) demonstrating the most favorable outcomes. This demonstrates the capability of bioactive packaging to prolong the shelf life of perishable goods through improved moisture barrier properties and antioxidant protection.

Table 5.12. Weight loss (%) of different treatments of *Agaricus bisporus* mushroom during storage.

Treatment	Day 3	Day 6	Day 9	Day 12	Day 15
T0	10.11 ± 1.05^{a}	25.37 ± 1.15^{a}	42.17 ± 1.25^{a}	53.79 ± 1.3^{a}	61.72 ± 1.45^{a}
T1	5.36 ± 1.15^{b}	14.22 ± 1.35^{b}	26.11 ± 1.35^{b}	31.44 ± 1.35^{b}	35.64 ± 1.55^{b}
T2	4.51 ± 0.59^{b}	9.93 ± 1.40^{c}	17.83 ± 1.40^{c}	21.6 ± 1.3^{c}	25.1 ± 1.35^{c}
T3	2.16 ± 1.20^{c}	4.91 ± 1.1^{d}	7.87 ± 1.4^{d}	9.13 ± 1.30^{d}	10.2 ± 1.1^{d}

T4	2.35 ± 1.3[c]	6.14 ±1.15 [d]	10.47 ±1.35 [d]	12.89 ±1.15 [d]	14.44 ± 1.2 [d]

Data are expressed in terms of mean ± standard deviation, with distinct letters (a - d) in the rows indicating significant variations ($p < 0.05$), where 'a' represents the lowest value.

5.32.2. Firmness

The firmness of *Agaricus bisporus* mushrooms, an essential quality attribute during storage, was assessed under various treatments over a 15-day duration, as shown in Table 5.12. The control treatment (T0), employing CS-NC multilayered films devoid of RES, exhibited a consistent and notable decrease in firmness, declining from 6.36 N on Day 0 to 2.2 N by Day 15. The consistent decline observed is indicative of the standard softening process linked to postharvest physiological degradation and microbial activity in mushrooms maintained under inadequate preservation conditions (Roy et al., 1995; Jiang et al., 2010). By Day 12, treatments with raising RES concentrations (T1 to T4) demonstrated a distinct dose-dependent enhancement in firmness retention. Notably, T3 (CS-RES (12 µg/ml)-NC) exhibited the highest firmness on Day 15 (5.11N), while T4 (16 µg/mL) recorded a firmness of 4.2N on the same day. This indicates a slight decrease in firmness for T4 compared to T3, suggesting that although higher RES concentrations initially improve firmness preservation, the advantage may diminish beyond a certain threshold. The decrease in mushroom firmness noted at the highest concentration of RES (16 µg/mL, T4) after Day 12 could be linked to the pro-oxidant effects of RES when administered at elevated levels. RES is well-known for its antioxidant properties at lower concentrations; however, at higher doses, it can paradoxically lead to oxidative stress. This phenomenon, referred to as a hormetic dose–response, indicates that RES shows positive effects at low doses, while higher concentrations may lead to negative outcomes (Boondam et al., 2024). For example, in strawberries and blueberries, low levels of RES improved quality retention and postponed spoilage. Nonetheless, at elevated concentrations, RES led to adverse effects including tissue softening, browning, elevated respiration rates, and the emergence of unwanted flavors (Wang et al., 2017) (Li et al., 2021). A study conducted by Zhou et al. (2022) revealed that RES exhibited a dose-dependent influence on the postharvest quality of table grapes. Low concentrations of RES enhanced storability by boosting antioxidant enzyme activity and minimizing decay, whereas higher concentrations (≥100 µM) proved to be harmful. Consequently, the quality of the fruit diminished, leading to accelerated senescence, tissue degradation, and the emergence of off-flavors. The adverse effects are mainly

due to RES's pro-oxidant behavior at elevated doses, which disturbs cellular redox homeostasis and initiates oxidative stress (Plauth et al., 2016). In the subject of postharvest mushroom preservation, elevated oxidative stress could compromise cell wall integrity by triggering the activity of degradative enzymes like chitinases and glucanases. These enzymes decompose structural polysaccharides, resulting in tissue softening and diminished firmness. Consequently, moderate concentrations of RES (e.g., 12 µg/mL) can effectively maintain firmness by reducing oxidative damage, whereas higher concentrations might unintentionally speed up the loss of firmness due to their pro-oxidant effects (Liufang et al., 2024). This highlights the significance of optimizing RES levels in edible coatings to strike a balance between its antioxidant advantages and possible pro-oxidant dangers. This indicates that 12 µg/mL could be an ideal concentration for preserving firmness during prolonged storage.

Table 5.13. Firmness (N) of *Agaricus bisporus* mushroom during storage under different treatments.

Treatment	Day 0	Day 3	Day 6	Day 9	Day 12	Day 15
T0	6.36 ±1.05^{a}	5.1 ±1.25 ^{a}	4.3 ±1.2 ^{a}	3.2 ± 1.55 ^{b}	2.47 ± 1.55 ^{b}	2.2 ±1.2 ^{b}
T1	6.36 ± 1.15^{a}	5.96 ± 1.55 ^{a}	5.63 ± 0.45 ^{a}	4.81 ± 1.3 ^{ab}	4.13 ± 0.95 ^{ab}	3.26 ± 1.25 ^{ab}
T2	6.36 ± 1.10^{a}	5.66 ± 1.18 ^{a}	5.11 ± 0.86 ^{a}	4.33 ± 0.98 ^{ab}	3.81 ± 0.734 ^{ab}	3.62 ± 1.10 ^{ab}
T3	6.36 ± 1.40^{a}	6.55± 1.15 ^{a}	6.16 ±1.15 ^{a}	5.81 ± 1.15 ^{a}	5.52 ±1.15 ^{a}	5.11 ± 1.2 ^{a}
T4	6.36 ±1.35^{a}	6.51 ± 1.1 ^{a}	6.11 ±1.1 ^{a}	5.61 ±1.4 ^{ab}	5.28 ±1.15 ^{a}	4.19 ±1.2 ^{ab}

Data are expressed in terms of mean ± standard deviation, with distinct letters (a - b) in the rows indicating significant variations ($p < 0.05$), where 'a' represents the lowest value.

5.32.3. Respiration rate

The present study showed that *Agaricus bisporus* mushrooms packaged in CS-NC multilayer films with elevated levels of RES exhibited a significant decrease in respiration rate over a 15-day storage duration relative to the control group. Table 5.14 illustrates the respiration rate (mL $kg^{-1}s^{-1}$) of *Agaricus bisporus* mushrooms subjected to various packaging procedures throughout a 15-day storage duration. The control (T0) film, utilizing CS-NC multilayered films, exhibited a steady and significant rise in respiration rate from 6.7 mL $kg^{-1}s^{-1}$ on day 0 to 12.6 mL $kg^{-1}s^{-1}$ by

day 15. This significant rise is due to the absence of bioactive substances that can alleviate oxidative stress and microbial activity during storage, hence accelerating metabolic activity and, subsequently, the respiration rate (Li et al., 2022). T3 went from 6.7 mL $kg^{-1}s^{-1}$ on Day 0 to 8.1 mL $kg^{-1}s^{-1}$ on Day 15, although T4 experienced a more pronounced increase, from 6.7 to 9.3 mL $kg^{-1}s^{-1}$. The levels were markedly lower than the untreated control (T0), which exceeded 12.6 mL $kg^{-1}s^{-1}$ by Day 15. This clearly shows the efficacy of elevated concentrations of RES in inhibiting the respiratory activity of mushrooms. The decline in respiration rate with elevated RES concentration can be explained by RES significant antioxidant properties, which are essential in mitigating oxidative stress during storage. By scavenging reactive oxygen species (ROS), RES aids in preserving cellular homeostasis and membrane integrity, consequently decelerating the metabolic processes linked to respiration (Wang et al., 2020). Besides its antioxidative effects, RES exhibits antibacterial capabilities that inhibit spoilage microorganisms, which can otherwise provoke increased respiration due to stress-induced defense mechanisms in mushroom tissues (Zhang et al., 2021). Treatments T3 and T4, containing 12 µg/mL and 16 µg/mL RES respectively, demonstrated significantly reduced increases in respiration rate. The respiration rate in T3 increased from 6.7 mL $kg^{-1}s^{-1}$ on Day 0 to 8.1 mL $kg^{-1}s^{-1}$ by Day 15, while T4 rise from 6.7 to 9.3 mL $kg^{-1}s^{-1}$ during the same duration. This phenomenon can be explained by a threshold effect, wherein elevated levels of RES may disturb cellular homeostasis or hinder endogenous antioxidant systems, resulting in a compensatory metabolic response (Rong et al., 2019). These values were significantly lower than the control (T0), which achieved 12.6 mL $kg^{-1}s^{-1}$ by Day 15, demonstrating the effectiveness of RES-enriched packaging in reducing respiratory activity during storage. The increased respiration rate in T4 relative to T3 by Day 15 indicates that beyond a specific concentration threshold, the release dynamics of RES from multilayered films may become less effective or uneven, possibly due to environmental interactions or saturation effects (Sun et al., 2023). Hossain et al. (2021) found that high concentrations of RES in edible coatings on strawberries induced mild oxidative stress through redox cycling, which increased metabolic activity instead of inhibiting it. High levels of polyphenols, including RES, have been demonstrated to disrupt cellular redox balance, impair mitochondrial function, and increase oxygen consumption rates, collectively elevating respiration (Chen et al., 2023). A further contributing factor may be the physicochemical behavior of RES within the film matrix. At elevated concentrations, RES can aggregate or crystallize, which diminishes its effective release

and antioxidant activity over time (Zhou et al., 2020). The limited presence of active reactive oxygen species (ROS) at subsequent storage intervals may reduce its protective capacity, leading to an increase in respiration rates. The findings indicate that RES is advantageous for preserving postharvest quality; however, its concentration in active packaging systems requires careful optimization to avoid potential metabolic overstimulation in stored horticultural products.

Table 5.14. Respiration rate (mL $kg^{-1}s^{-1}$) of *Agaricus bisporus* mushroom during storage under different treatments.

Treatment	Day 0	Day 3	Day 6	Day 9	Day 12	Day 15
T0	6.7 ± 1.01 [a]	8.3 ±1.5 [a]	9.6 ±1.85 [a]	10.8 ±0.6 [a]	11.3 ±1.35 [a]	12.6 ±1.15 [a]
T1	6.7 ± 0.75 [a]	7.5 ± 1.65 [a]	8.1 ±2.05 [a]	8.6 ±0.65 [b]	9.0 ±1.25 [a]	9.5 ± 1.15 [b]
T2	6.7 ± 0.8 [a]	7.2 ± 1.05 [a]	7.5 ±2.00 [a]	8.0 ±0.85 [b]	8.3 ± 1.25 [b]	8.6 ±1.05 [b]
T3	6.7 ± 0.75 [a]	7.0 ±1.15 [a]	7.3 ±2.10 [a]	7.5 ± 0.65 [b]	7.8 ± 1.05 [b]	8.1 ± 1.01 [b]
T4	6.7 ± 0.81 [a]	7.3 ± 1.16 [a]	7.6 ±2.10 [a]	8.5 ±0.8 [b]	8.9 ± 1.30 [ab]	9.3 ± 0.96 [b]

Data are expressed in terms of mean ± standard deviation, with distinct letters (a - b) in the rows indicating significant variations ($p < 0.05$), where 'a' represents the lowest value.

Figure 5.27. Shelf life study of mushroom stored at 4°C: Monitoring quality retention and spoilage progression under refrigerated conditions.

5.32.4. Polyphenol oxidase (PPO) activity

Polyphenol oxidase (PPO) activity serves as a critical indicator of enzymatic browning and the overall decline in quality of mushrooms during storage. Table 5.15 presents the trend of PPO activity in *Agaricus bisporus* subjected to different packaging treatments over a 15-day period. The control treatment (T0), which comprised CS-NC multilayered film, demonstrated a consistent and notable increase in PPO activity, rising from 18.0 U kg^{-1} on day 0 to 47.0 U kg^{-1} by day 15. This trend indicates that although CS-NC films initially served as a barrier, they were inadequate in reducing oxidative enzyme activity over time. Treatments T1 through T4, which included varying concentrations of RES at 4, 8, 12, and 16 µg/mL respectively within the CS-NC matrix, exhibited a significantly slower increase in PPO activity. T3 (12 µg/mL RES) exhibited the most pronounced suppression, with PPO activity increasing to only 21.1 U kg^{-1} by day 15. This trend demonstrates the effectiveness of RES in preserving enzyme stability and inhibiting oxidative processes. The noted decline in PPO activity with rising RES concentration can be ascribed to the strong antioxidant and antibacterial characteristics of RES, which impede the activation and production of oxidative enzymes like PPO (Zhang et al., 2025). RES likely disrupts the catalytic function of PPO or sequesters the reactive oxygen species required for its activation, thereby impeding the browning process (Andrés et al., 2024). Furthermore, RES is recognized for sustaining cellular integrity by safeguarding membrane permeability, potentially reducing the exposure of phenolic substrates to PPO (Ding et al., 2021). These findings highlight the capability of RES-infused CS-NC films to prolong the longetivity to continue the postharvest quality of mushrooms. Notably, the addition of RES to CS-NC films markedly diminishes PPO activity relative to the control; yet, a minor increase in PPO activity is detected as the RES concentration escalates from 12 µg/mL (T3) to 16 µg/mL (T4), specifically from 21.1 U kg^{-1} to 35.4 U kg^{-1} by day 15. This paradoxical trend may be ascribed to the pro-oxidant properties of polyphenolic substances such as RES at elevated quantities. While RES is well-known for its antioxidant qualities, at high quantities it may demonstrate pro-oxidant effects, particularly in the presence of transition metals like iron or copper, which are inherently found in mushrooms. These metals might facilitate redox cycling interactions with polyphenols, resulting in the production of reactive oxygen species (ROS) that may indirectly activate PPO or enhance its substrate availability (de la Lastra & Villegas, 2007; Wang & He, 2009; Babich et al., 2011). Furthermore, at high concentrations, RES may impair the microstructure of the CS-NC film matrix, resulting in

diminished barrier characteristics against oxygen and moisture, hence creating conditions favorable for enzymatic oxidation (Zhou et al., 2020). Zhang et al. (2020) state that elevated polyphenol concentrations can induce heterogeneity in the polymer network, hence enhancing oxygen permeability and moisture transmission, which subsequently accelerates oxidative enzymatic processes. The compromised integrity of the matrix diminishes the film's physical protection and modifies the local microenvironment around the mushroom tissue, creating conditions conducive to PPO activation. This results in a hormetic effect, where low doses are advantageous while high doses become harmful, a phenomenon well-documented in polyphenol research. It illustrates the intricate balance between antioxidant and pro-oxidant activities, contingent upon concentration and environmental context (Calabrese & Baldwin, 2003). Numerous investigations corroborate the finding that heightened levels of RES may unexpectedly result in an augmentation of polyphenol oxidase (PPO) activity during postharvest storage. Gao et al. (2022) documented a hormetic response in strawberries treated with RES-enriched films, noting that 10 µg/mL RES decreased PPO activity to 18.3 U/g FW by day 10, in contrast to 25.6 U/g in the control group. At a concentration of 20 µg/mL, PPO activity rose to 28.9 U/g, accompanied by elevated malondialdehyde (MDA) levels and observable browning, signifying oxidative stress and the pro-oxidant action of excessive RES, thus showing increased lipid peroxidation and oxidative stress. The biphasic effect was ascribed to the excessive activation of plant defense mechanisms and the possible pro-oxidant properties of RES at elevated doses, consistent with prior study on polyphenols (Babich et al., 2011). Research by Kim et al. (2021) on phenolic-infused packaging for fresh-cut lettuce revealed that a concentration of 15 µg/mL of total phenolics decreased PPO activity to 16.5 U/g FW. However, increasing the concentration to 30 µg/mL resulted in a rise in PPO activity to 27.8 U/g FW by day 7, indicating that surpassing the optimal threshold triggered oxidative stress and upregulated defense-related enzymes, including PPO.

Table. 5.15. Polyphenol oxidase (PPO) activity (U kg^{-1}) of *Agaricus bisporus* mushroom during storage under different treatments.

Treatment	Day 0	Day 3	Day 6	Day 9	Day 12	Day 15
T0	18.0 ± 1.53 [a]	24.7 ± 3.30 [a]	30.2 ±2.05 [a]	36.5 ± 1.53 [a]	40.1 ± 1.85 [a]	47.0 ± 1.80 [a]
T1	18.0 ± 1.60 [a]	22.3 ± 2.80 [ab]	25.1 ± 1.90 [b]	28.0 ± 1.50 [b]	32.3 ± 2.0 [b]	36.7 ± 1.60 [b]
T2	18.0 ± 1.90 [a]	20.5 ±2.92 [ab]	22.0 ± 1.86 [bc]	23.7 ±1.65 [c]	25.2 ± 2.30 [c]	27.2 ± 1.35 [c]
T3	18.0 ± 1.9 [a]	19.0 ± 1.01 [b]	19.8 ± 1.75 [c]	20.2 ± 1.21 [c]	20.8 ± 2.70 [d]	21.1 ± 1.45 [d]
T4	18.0 ±0.91 [a]	21.7 ± 2.38 [ab]	24.6 ± 1.95 [b]	27.0 ± 1.55 [b]	31.6 ± 2.50 [b]	35.4 ± 1.25 [b]

Data are expressed in terms of mean ± standard deviation, with distinct letters (a - d) in the rows indicating significant variations ($p < 0.05$), where 'a' represents the lowest value.

5.32.5. Malondialdehyde (MDA) content

The malondialdehyde (MDA) concentration, an essential indicator of lipid peroxidation with oxidative stress within plant tissues, was measured in *Agaricus bisporus* mushrooms given to several treatments over a 15-day period. As shown in Table 5.16. The control treatment (T0), in which mushrooms were apparently packaged without any antioxidant film, shown a significant rise in MDA concentration from 1.3 μmol Kg^{-1} on Day 0 to 5.9 μmol Kg^{-1} on Day 15. Mushrooms preserved with CS-NC multilayered films infused with RES exhibited a significantly lower rise in MDA levels. Treatments T1 (4 μg/mL RES), T2 (8 μg/mL RES), and T3 (12 μg/mL RES) yielded final MDA values of 4.1, 3.6, and 2.8 μmol Kg^{-1}, respectively, demonstrating the efficacy of antioxidant-enriched packing in reducing oxidative damage. The reduction in MDA formation is due to the antioxidant properties of RES, recognized for its ability to neutralize reactive oxygen species and reinforce cell membranes during storage (Sogvar et al., 2016; Zhang et al., 2021). On the contrary, a distinct trend was noted in treatment T4 (16 μg/mL RES), where MDA content elevated to 4.0 μmol Kg^{-1} by Day 15, surpassing the levels recorded in T3. This indicates a possible pro-oxidant effect with increased RES concentrations. Elevated concentrations of phenolic compounds such as RES may paradoxically result in the production of free radicals via

redox cycling under specific conditions, thereby causing oxidative stress rather than mitigating it (Leonard et al., 2004; Galati & O'Brien, 2004). A study on strawberry fruits indicated that uncoated samples stored at room temperature experienced a notable increase in MDA concentration, reaching 3.95 mmol/g by the second day. On the other hand, coated samples displayed relatively lower increases, ranging from 3.28 to 3.5 mmol/g, thereby underscoring the influence of coatings on oxidative stress modulation (El-Mogy et al., 2020). Yang et al. (2024) noted that microencapsulated polyphenol extracts initially decreased MDA levels in salad dressings; however, MDA content significantly increased during extended storage, rising from 0.35 to 0.51 mg/kg after 30 days, particularly in samples with higher polyphenol concentrations, suggesting a time-dependent pro-oxidant shift. Studies indicate that polyphenols, including quercetin and myricetin, may display pro-oxidant behavior under certain conditions, particularly in the presence of transition metal ions, resulting in heightened lipid peroxidation and MDA formation (Galati & O'Brien, 2004; Halliwell et al., 1990). The study concludes by emphasizing how crucial it is to maximize polyphenol concentrations, such as RES, for efficient postharvest preservation. Although moderate amounts greatly lessen oxidative stress and preserve the quality of mushrooms, too high concentrations can undo this benefit by causing oxidative damage. The necessity of accurate formulation in active packaging is shown by this biphasic reaction. In addition to extending shelf life, optimizing polyphenol levels guarantees the security and effectiveness of bioactive preservation techniques.

Table 5.16. Malondialdehyde (MDA) content (mol Kg^{-1}) of *Agaricus bisporus* mushroom during storage under different treatments.

Treatment	Day 0	Day 3	Day 6	Day 9	Day 12	Day 15
T0	1.3 ± 0.56 [a]	2.2 ± 0.46 [a]	3.1 ± 0.53 [a]	4.0 ± 1.0 [a]	5.0 ±0.81 [a]	5.9 ±0.84 [a]
T1	1.3 ± 0.65 [a]	1.9 ± 0.26 [ab]	2.6 ± 1.21 [a]	3.3 ± 0.45 [ab]	3.8 ± 0.81 [ab]	4.1 ± 0.52 [b]
T2	1.3 ± 0.55 [a]	1.7 ± 0.4 [ab]	2.2 ± 0.98 [a]	2.9 ± 0.55 [ab]	3.3 ± 0.75 [b]	3.6 ± 0.65 [b]
T3	1.3 ± 0.62 [a]	1.4 ± 0.36 [b]	1.9 ± 0.95 [a]	2.3 ± 0.45 [b]	2.6 ± 0.65 [b]	2.8 ± 0.65 [b]
T4	1.3 ± 0.55 [a]	1.6 ± 0.4 [ab]	2.4 ± 1.15 [a]	3.0 ± 0.6 [ab]	3.5 ± 0.75 [b]	4.0 ± 0.65 [b]

Data are expressed in terms of mean ± standard deviation, with distinct letters (a - b) in the rows indicating significant variations ($p < 0.05$), where 'a' represents the lowest value.

5.32.6. Browning degree (BD)

The addition of RES to packing films is clearly correlated with the browning process of *Agaricus bisporus* mushrooms during storage, as indicated by changes in browning degree (BD) at 410 nm. Over the course of the 15-day storage period, the control group (T0), which received no antioxidant treatment, showed the fastest and most notable increase in BD values, going from an initial value of 0.06 to 0.70 by Day 15 as shown in Figure 5.27. This significant increase reflects the usual pattern of enzymatic browning brought on by oxidative stress and polyphenol oxidase (PPO) activity during postharvest storage. On the other hand, BD accumulation was markedly suppressed in all RES-treated groups (T1–T4), demonstrating the antioxidant protection of RES (Table 5.17.) The T3 treatment, which contained 12 µg/mL RES, showed the best prevention of browning among them; by Day 15, the BD had only increased to 0.40. In comparison to the control, this indicates a 42.9% decrease in browning, suggesting a notable improvement in visual quality and possible shelf life extension. With a final BD of 0.51, which represents a 27.14% reduction in relative to the control, T3, which having higher RES concentration (16 µg/mL), similarly inhibited browning, but less so than T3. This result implies that whereas RES inhibits browning in a concentration-dependent manner up to a threshold, its effectiveness may plateau or even significantly decrease at greater concentrations. The lowered performance of T4 relative to T3 may be linked to the pro-oxidant effect of RES at high concentrations, as indicated by previous research demonstrating that excessive antioxidant levels can result in redox imbalance or disrupt endogenous defense mechanisms (Tang et al., 2019). Excess reactive oxygen species (RES) may disrupt redox homeostasis in the microenvironment of packaged mushrooms, potentially stimulating polyphenol oxidase (PPO) activity instead of inhibiting it. Additionally, elevated levels of polyphenols such as RES may experience auto-oxidation, particularly in the presence of trace metal ions, which further facilitates the generation of oxygen species having high reactivity (Wang et al., 2002). From the perspective of packaging materials, increased RES concentrations may disrupt the integrity of the polymer matrix or its functional behavior, potentially resulting in phase separation, diminished film homogeneity, or disruption of crystallinity. These changes could

adversely affect the oxygen barrier and moisture retention properties of the film, ultimately compromising its effectiveness in preserving the product (Jamróz et al., 2019).

Similar outcomes have been reported by Niu et al. (2023), who examined the impact of RES and oxyresveratrol on the quality of postharvest shiitake mushrooms. The findings indicated that both compounds delayed browning, with oxyresveratrol demonstrating greater efficacy than RES, implying that increased concentrations of RES may not proportionately enhance browning inhibition. Tang et al. (2019) investigated the application of RES coatings on litchi fruits, finding that moderate concentrations significantly reduced browning, whereas excessively high levels offered no further advantages and could adversely affect the fruit's quality. The studies highlight the necessity of optimizing RES concentrations in packaging films to achieve a balance between antioxidant benefits and the prevention of adverse effects. The structural integrity of the packaging matrix may be compromised by elevated RES concentrations, which could modify its barrier properties and affect the release rate of active compounds, as indicated by Jamróz et al. (2019) in their research on CS-based films containing polyphenolic compounds. These findings underscore the importance of calibrating RES concentrations in packaging applications to optimize shelf-life extension and preserve product quality.

Table 5.17. Browning degree (BD) content (mol Kg^{-1}) of *Agaricus bisporus* mushroom during storage under different treatments.

Treatment	Day 0	Day 3	Day 6	Day 9	Day 12	Day 15
T0	0.06 ± 0.006[a]	0.19 ± 0.006 [a]	0.30 ± 0.001 [a]	0.43 ± 0.006 [a]	0.58 ± 0.006 [a]	0.70 ± 0.017 [a]
T1	0.06 ± 0.005 [a]	0.17 ± 0.006 [b]	0.26 ±0.001 [b]	0.38 ± 0.002 [b]	0.50 ± 0.001 [b]	0.61 ± 0.01 [b]
T2	0.06 ± 0.001 [a]	0.15 ± 0.003 [c]	0.23 ± 0.004 [c]	0.32 ± 0.039 [c]	0.43 ± 0.024 [c]	0.54 ± 0.005 [c]
T3	0.06 ± 0.001 [a]	0.13 ± 0.004 [d]	0.19 ± 0.003 [d]	0.26 ± 0.003 [d]	0.32 ± 0.005 [e]	0.40 ± 0.01 [e]
T4	0.06 ± 0.001 [a]	0.14 ± 0.003 [d]	0.22 ± 0.01 [c]	0.31 ± 0.005 [c]	0.40 ± 0.006 [d]	0.51 ± 0.010 [d]

Data are expressed in terms of mean ± standard deviation, with distinct letters (a - e) in the rows indicating significant variations ($p < 0.05$), where 'a' represents the lowest value.

5.33. Cost–Benefit Ratio (CBR) Analysis

The cost benefit analysis was performed to assess the economic viability of the production of biodegradable active packaging films using chitosan and lemongrass wastes as the source of mushrooms and lemongrass respectively. The total cost of production of a single batch was estimated to be Rs 31.77 and it produced 10 films (as shown in Table 5.18.). The cost per film was calculated based on this as 3.18.

In order to determine the economic viability, Cost-Benefit Ratio (CBR) was calculated using the following equation:

$$\text{CBR}= \frac{Total\ benefit\ (Selling\ price)}{Total\ production\ cost}$$

Using a selling price of Rs 5 per film, the CBR was calculated as:

$$\text{CBR}= \frac{5}{3.18} =1.57$$

The value of CBR more than 1 is a profitable and economically viable process. Here, the CBR of 1.57 implies that each unit of 1.00 invested returns 1.57 and this is an undisputable economic benefit. This constructive yield shows the possibility of upscaling to produce active biodegradable films using agro-industrial wastes that are of low cost.

Table 5.18. Cost benefit ratio of CS-RES-CMC based multilayer packaging films.

Ingredients	Rate (Rs/Kg)	Quantity (g)	Amount (Rs)
Mushroom waste	5.00 / kg	0.50 kg	2.50
Extracted chitosan (from mushroom waste)	4.00 / g	1.50 g	6.00
Cellulose (from lemon-grass waste, processed)	1.50 / g	3.00 g	4.50
Resveratrol (RES)	5,000.00 / g	0.0012 g (1.2 mg)	6.00
Glycerol (plasticizer)	0.10 / g	1.35 g	0.135
Ethanol (96%)	0.20 / mL	5 mL	1.00

Deionized water	0.02 / 100 mL	100 mL	0.02
Acetic acid / pH adjust	200.00 / L	2 mL	0.40
Total ingredient cost			**20.56**
Overhead charges (including labour fuel and machinery depreciation)	@20%	-	4.11
Profit	@15%	-	3.70
GST	12%	-	3.40
Grand total			**31.77**
Cost per film (10 films per batch)			**3.18**

Conclusion

The potential of mushroom waste especially that from *Agaricus bisporus* as a significant source of bioactive chemicals for the production of functional powders is highlighted in this study. Out of the three drying methods that were assessed, hybrid drying (HD) produced the highest protein content and the lowest moisture levels, while freeze drying (FD) was the best at retaining antioxidant capabilities and outstanding physicochemical characteristics. Although FD showed excellent flow characteristics and the best retention of bioactive chemicals, its high cost and energy requirements make it unsuitable for usage on an industrial scale. HD, on the other hand, proved to be a more economical and energy-efficient substitute that could produce high-quality powdered mushroom waste with equivalent nutritional and physiological advantages. These results provide attention to the viability of using suitable drying methods to valorize mushroom waste, promoting sustainable waste management and the production of finished products with added value. As a result, the potential of this agro-industrial waste as a valuable source of biopolymers is highlighted by the effective extraction of CS and cellulose from *Agaricus bisporus* mushroom waste using microwave-assisted methods. The optimized microwave-assisted extraction method produced CS with a high degree of deacetylation (79.94%), good solubility (75%), and significant antioxidant activity, alongside characteristic functional groups confirmed by FTIR and a semi-crystalline structure validated by XRD. In a similar manner, cellulose obtained via microwave-assisted delignification and bleaching reached a yield of 37.46% and demonstrated favorable structural and thermal characteristics, featuring high crystallinity (70.02%) and thermal stability. The results confirm that mushroom waste can serve as an effective feedstock for producing high-value biopolymers through energy-efficient green technologies. The conversion of cellulose derived from *Agaricus bisporus* waste into NC through acid hydrolysis facilitated the development of stable multilayer biopolymer films when combined with CS. The nanoscale properties of the cellulose were validated through particle size (163.2 ± 2.74 nm) and zeta potential (−19.2 ± 0.27 mV) analyses, demonstrating good colloidal stability. Multilayer films with higher concentrations of CS and NC showed gradual improvements in physical, mechanical, and barrier properties. The tensile strength and elongation at break showed remarkable improvement, achieving values of 54.19 MPa and 102.72% in T3, respectively. At the same time, decreases in WVTR and OTR indicated enhanced barrier performance, with values dropping to 1.32 g/m²·day and 6.211 cc/m²·day, respectively, in the most-dense film matrix. The films exhibited improved antioxidant

activity, with DPPH scavenging increasing from 10.374% to 39.766%, alongside a notable rise in reducing power, attributed to the synergistic interactions between CS and NC. The reduction in solubility and the rise in swelling index further demonstrated enhanced water resistance and structural cohesion. The results prove the effectiveness of CS-NC composite films made from mushroom waste, highlighting their potential as viable options for sustainable, biodegradable packaging solutions. The addition of RES to CS–NC multilayer films notably affected their optical, mechanical, and antioxidant properties, highlighting its promise as a functional additive for active packaging uses. Elevating RES concentrations (4–16 µg/mL) resulted in significant improvements in optical clarity and color characteristics, as evidenced by ΔE, C*, and H* values that reflect heightened vibrancy and transparency. Meanwhile, opacity reduced and light transmittance increased to 79.432% at the highest concentration. RES demonstrated a plasticizing effect, leading to a minor decrease in tensile strength (from 47.52 MPa to 42.195 MPa) and an enhancement in flexibility, as indicated by an EAB peak of 74.20%, which suggests better ductility. The films exhibited a significant improvement in antioxidant performance, as shown by the DPPH scavenging activity rising from 31.79% to 74.66%, with a corresponding increase in reducing power that directly related to the concentration of RES. The findings emphasize the feasibility of incorporating RES into CS–NC matrices to improve the functional capabilities of biodegradable films, presenting a collaborative approach to create visually attractive, mechanically strong, and bioactive packaging options. The 30-day soil burial test revealed significant biodegradability of the CS–NC multilayer films, showing a weight loss of 26% by day 15 and 54% by day 30. This degradation reflects the ongoing microbial and enzymatic interactions within the soil environment, promoting the breakdown of polysaccharide-based film components. The observed reduction in mass confirms the natural biodegradability of the CS–NC matrix and its suitability for environmentally friendly disposal. The findings highlight the promise of CS–NC films as eco-friendly packaging materials, in accordance with sustainability standards for biodegradable polymers, and strengthen their use in sustainable packaging solutions. The addition of RES to CS–NC multilayer films greatly improved the postharvest preservation of mushrooms over a storage period of 15 days. Films enriched with 12 µg/mL RES (T3) showed the most favorable outcomes, highlighting the least weight loss (10.29%), the highest firmness retention (5.11 N), and a decreased respiration rate (8.1 mL kg^{-1} s^{-1}). The markers of oxidative stress, polyphenol oxidase (PPO) activity and malondialdehyde (MDA) content were at their lowest in

T3, indicating improved antioxidant defense and diminished cellular degradation. The visual quality, evaluated through browning degree, was also enhanced in T3 (BD = 0.40), indicating a 42.9% decrease in comparison to the control. A minor reversal of these effects at elevated RES concentrations (T4) indicates a concentration-dependent efficacy, along with possible pro-oxidant behavior at high doses. The results clearly demonstrate the effectiveness of RES-functionalized CS–NC films in preserving mushroom quality, prolonging shelf life, and reducing oxidative deterioration, emphasizing their potential as bioactive packaging for fresh produce.

REFERENCES

A_Simple_and_Effective_Method_for_Preparation_of_Chitosan_from_Chitin-libre.pdf

Abdou, E. S., Nagy, K. S. A., & Elsabee, M. Z. (2008). Extraction and characterization of chitin and chitosan from local sources. *Bioresource Technology, 99*(5), 1359–1367. https://doi.org/10.1016/j.biortech.2007.01.051

Abolhasani, M., & Kumacheva, E. (2023). The rise of self-driving labs in chemical and materials sciences. *Nature Synthesis, 2*(1), 6–12. https://doi.org/10.1038/s44160-022-00231-0.

Acar, C., Dincer, I., & Mujumdar, A. (2022). A comprehensive review of recent advances in renewable-based drying technologies for a sustainable future. *Drying Technology*, *40*(6), 1029-1050. https://doi.org/10.1080/07373937.2020.1848858

Agarwal, M., Agarwal, M. K., Shrivastav, N., Pandey, S., & Gaur, P. (2018). A simple and effective method for preparation of chitosan from chitin. *Int. J. Life. Sci. Sci. Res*, *41*, 721-1728.

Aguilar-Reynosa, A., Romaní, A., Rodriguez-Jasso, R. M., Aguilar, C. N., Garrote, G., & Ruiz, H. A. (2017). Microwave heating processing as alternative of pretreatment in second-generation biorefinery: An overview. *Energy Conversion and Management, 136*, 50–65. https://doi.org/10.1016/j.enconman.2017.01.004

Agunbiade, H. O., Fagbemi, T. N., and Aderinola, T. A. (2022). Antioxidant properties of beverages from graded mixture of green/roasted coffee and *hibiscus sabdariffa calyx* flours. *Applied Food Research, 2*(2), 100163. https://doi.org/10.1016/j.afres.2022.100163

Ahern, N., Arendt, E. K., and Sahin, A. W. (2023). Protein soft drinks: a retail market analysis and selected product characterization. *Beverages, 9*(3), 73. https://doi.org/10.3390/beverages9030073

Ahmad, N., Fazal, H., & Abbasi, B. H. (2020). Resveratrol-loaded biopolymer-based films for active packaging: Preparation and evaluation of antioxidant activity. *Food Hydrocolloids, 105*, 105779. https://doi.org/10.1016/j.foodhyd.2020.105779

Akhtar, H. M. S., Ahmed, S., Olewnik-Kruszkowska, E., Gierszewska, M., Brzezinska, M. S., Dembińska, K., & Kalwasińska, A. (2023). Carboxymethyl cellulose based films enriched with polysaccharides from mulberry leaves (*Morus alba L.)* as new biodegradable packaging material. *International Journal of Biological Macromolecules*, *253*, 127633. https://doi.org/10.1016/j.ijbiomac.2023.127633

Akti, F. (2025). Fabrication of chitosan/alginate/diatomite/cinnamon oil based multilayer composite films for food packing applications. Colloids and Surfaces A: *Physicochemical and Engineering Aspects, 684*, 136870. https://doi.org/10.1016/j.colsurfa.2025.136870

Alara, O. R., Abdurahman, N. H., Ukaegbu, C. I., & Azhari, N. H. (2018). Vernonia cinerea leaves as the source of phenolic compounds, antioxidants, and anti-diabetic activity using microwave-assisted extraction technique. *Industrial Crops and Products*, *122*, 533-544. https://doi.org/10.1016/j.indcrop.2018.06.034

Aldila, H., Asmar, Fabiani, V. A., Dalimunthe, D. Y., & Irwanto, R. (2020). The effect of deproteinization temperature and NaOH concentration on deacetylation step in optimizing extraction of chitosan from shrimp shells waste. IOP Conference Series. *Earth and Environmental Science*, *599*(1), 012003. https://doi.org/10.1088/1755-1315/599/1/012003

Alishahi, A., Mirvaghefi, A., Tehrani, M. R., Farahmand, H., Shojaosadati, S. A., Dorkoosh, F. A., & Elsabee, M. Z. (2011). Enhancement and characterization of chitosan extraction from the wastes of shrimp packaging plants. *Journal of Polymers and the Environment, 19(*3), 776–783. https://doi.org/10.1007/s10924-011-0321-5

Al-Naamani, L., Dobretsov, S., & Dutta, J. (2016). Chitosan-zinc oxide nanoparticle composite coating for active food packaging applications. *Innovative Food Science & Emerging Technologies, 38,* 231-237. https://doi.org/10.1016/j.ifset.2016.10.010

Alnadari, F., Al-Dalali, S., Pan, F., Abdin, M., Frimpong, E. B., Dai, Z., Al-Dherasi, A., & Zeng, X. (2023). Physicochemical characterization, molecular modeling, and applications of carboxymethyl chitosan-based multifunctional films combined with gum arabic and anthocyanins. *Food and Bioprocess Technology, 16*(12), 2271–2284. https://doi.org/10.1007/s11947-023-03122-0

Alp, D., & Bulantekin, Ö. (2021). The microbiological quality of various foods dried by applying different drying methods: a review. *European Food Research and Technology, 247*(6), 1333-1343. https://doi.org/10.1007/s00217-021-03731-z

Alvi, T., Asif, Z., & Iqbal Khan, M. K. (2022). *Clean label extraction of bioactive compounds from food waste through microwave-assisted extraction technique — A review.* Food Bioscience, 46, 101580. https://doi.org/10.1016/j.fbio.2022.101580

Amaya-Farfán, J., & Rodriguez-Amaya, D. B. (2021). The Maillard reactions. In O. J. Caygill & J. H. Torres (Eds.), *Chemical changes during processing and storage of foods* (pp. 215–263). Academic Press.

Amin, U., Khan, M. K. I., Maan, A. A., Nazir, A., Riaz, S., Khan, M. U., ... & Lorenzo, J. M. (2022). Biodegradable active, intelligent, and smart packaging materials for food applications. *Food Packaging and Shelf Life, 33,* 100903. https://doi.org/10.1016/j.fpsl.2022.100903

Aminzare, M., Kouhbanani, M. A. J., Nikzad, S., Amini, S., & Rostami, Z. (2022). Evaluation of antioxidant and antibacterial interactions between resveratrol and eugenol in carboxymethyl cellulose biodegradable film. *Food Science & Nutrition, 10*(11), 3534–3546. https://doi.org/10.1002/fsn3.2656

Ando, Y., & Nei, D. (2023). Comparison of potato void structures dried by air-drying, freeze-drying, and microwave-vacuum-drying, and the physical properties of powders after grinding. *Food and Bioprocess Technology, 16*(2), 447-458. https://doi.org/10.1007/s11947-022-02941-x

Andrés, C. M. C., Pérez de la Lastra, J. M., Juan, C. A., Plou, F. J., & Pérez-Lebeña, E. (2024). Antioxidant metabolism pathways in vitamins, polyphenols, and selenium: parallels and divergences. *International Journal of Molecular Sciences, 25*(5), 2600. https://doi.org/10.3390/ijms25052600

Antunes, F., Marçal, S., Taofiq, O., Morais, A. M. M. B., Freitas, A. C., Ferreira, I. C. F. R., & Pintado, M. (2020). Valorization of mushroom by-products as a source of value-added compounds and potential applications. *Molecules, 25*(11), 2672. https://doi.org/10.3390/molecules25112672

AOAC International. (2002). *Official methods of analysis of AOAC International* (16th ed.). Association of Official Analytical Chemists.

AOAC. (2016). *Official methods of analysis of AOAC International* (20th ed.). AOAC International.

Aparna, G. G., Chauhan, A. K., Singh, M., & Singh, A. (2021). Effect of dehydration techniques on nutritional quality, functional property, and sensory acceptability of dried onion powder.

Journal of Food and Agricultural Research, 1(1), 30–46. https://arfjournals.com/image/67938_3_aparna.pdf

Aradmehr, A., & Javanbakht, V. (2020). A novel biofilm based on lignocellulosic compounds and chitosan modified with silver nanoparticles with multifunctional properties: Synthesis and characterization. *Colloids and Surfaces A: Physicochemical and Engineering Aspects, 600*, 124952. https://doi.org/10.1016/j.colsurfa.2020.124952

Aranaz, I., Alcántara, A. R., Civera, M. C., Arias, C., Elorza, B., Heras Caballero, A., & Acosta, N. (2021). Chitosan: An overview of its properties and applications. *Polymers, 13*(19), 3256. https://doi.org/10.3390/polym13193256

Araújo-Rodrigues, H., Sousa, A. S., Relvas, J. B., Tavaria, F. K., & Pintado, M. (2024). An overview on mushroom polysaccharides: Health-promoting properties, prebiotic and gut microbiota modulation effects and structure-function correlation. *Carbohydrate Polymers, 321*, 121978. https://doi.org/10.1016/j.carbpol.2024.121978

Araya-Farias, R., Makhlouf, J., & Ratti, C. (2011). Drying of seabuckthorn (*Hippophae rhamnoides* L.) berry: Impact of dehydration methods on kinetics and quality. *Drying Technology, 29*(3), 351–359. https://doi.org/10.1080/07373937.2010.497590

Ardean, C., Davidescu, C. M., Nemeş, N. S., Negrea, A., Ciopec, M., Duteanu, N., & Musta, V. (2021). Factors influencing the antibacterial activity of chitosan and chitosan modified by functionalization. *International Journal of Molecular Sciences, 22*(14), 7449. https://doi.org/10.3390/ijms22147449

Arfat, Y. A., Benjakul, S., & Prodpran, T. (2017). Development and characterization of bilayer films based on fish skin gelatin and goldfish scale gelatin incorporated with essential oils. *Food Hydrocolloids, 65*, 250–259. https://doi.org/10.1016/j.foodhyd.2016.11.029

Arrieta, M. P., Del Real, A., & Jiménez, A. (2014). Effect of drying techniques on the physicochemical properties and ash content of biodegradable films. Journal of Polymers and the Environment, 22(1), 12–19. https://doi.org/10.1007/s10924-013-0610-4

Arruda, T. R., Bernardes, P. C., e Moraes, A. R. F., & Soares, N. D. F. F. (2022). Natural bioactives in perspective: The future of active packaging based on essential oils and plant extracts themselves and those complexed by cyclodextrins. *Food Research International*, *156*, 111160. chttps://doi.org/10.1016/j.foodres.2022.111160

Asgher, M., Qamar, S. A., Bilal, M., & Iqbal, H. M. (2020). Bio-based active food packaging materials: Sustainable alternative to conventional petrochemical-based packaging materials. *Food Research International*, *137*, 109625. https://doi.org/10.1016/j.foodres.2020.109625

ASTM International. (2007). *Standard test method for determination of oxygen gas transmission rate, permeability and permeance at controlled relative humidity through barrier materials using a coulometric detector (ASTM F1927).* ASTM International.

Avelelas, F., Horta, A., Pinto, L. F. V., Cotrim Marques, S., Marques Nunes, P., Pedrosa, R., & Leandro, S. M. (2019). Antifungal and antioxidant properties of chitosan polymers obtained from nontraditional *Polybius henslowii* sources. *Marine Drugs*, *17*(4), 239. https://doi.org/10.3390/md17040239

Azeez, S., Sathiyaseelan, A., Jeyaraj, E. R., Saravanakumar, K., Wang, M.-H., & Kaviyarasan, V. (2023). Extraction of chitosan with different physicochemical properties from *Cunninghamella echinulata (Thaxter)* Thaxter for biological applications. *Applied Biochemistry and Biotechnology*, *195*(6), 3914–3927. https://doi.org/10.1007/s12010-022-03982-w

Azeredo, H. M., Mattoso, L. H., Avena-Bustillos, R. J., Filho, G. C., Munford, M. L., Wood, D., & McHugh, T. H. (2010). Nanocellulose reinforced chitosan composite films as affected by

nanofiller loading and plasticizer content. *Journal of Food Science*, 75(1), N1–N7. https://doi.org/10.1111/j.1750-3841.2009.01386.xPubMed+1Europe PMC+1

Azubuike, C. P., & Okhamafe, A. O. (2012). Physicochemical, spectroscopic and thermal properties of microcrystalline cellulose derived from corn cobs. *International journal of recycling of organic waste in agriculture, 1*, 1-7. doi.org/10.1186/2251-7715-1-9

Babich, H., Schuck, A. G., Weisburg, J. H., & Zuckerbraun, H. L. (2011). Research strategies in the study of the pro-oxidant nature of polyphenol nutraceuticals. *Journal of Toxicology, 2011*, 467305. https://doi.org/10.1155/2011/467305

Badwan, A. A., Rashid, I., Omari, M. M. H. A., & Darras, F. H. (2015). Chitin and chitosan as direct compression excipients in pharmaceutical applications. Marine Drugs, 13(3), 1519–1547. https://doi.org/10.3390/md13031519

Baghi, F., Gharsallaoui, A., Dumas, E., Agusti, G., & Ghnimi, S. (2024). Characterization of antimicrobial multilayer film based on ethylcellulose-pectin incorporated with nanoemulsions of trans-cinnamaldehyde essential oil. *Food Chemistry: X*, *22*, 101261. https://doi.org/10.1016/j.fochx.2024.101261

Bahndral, A., Shams, R., Dash, K. K., Ali, N. A., Shaikh, A. M., & Kovács, B. (2024). Microwave assisted extraction of cellulose from lemon grass: Effect on techno-functional and microstructural properties. *Journal of Agriculture and Food Research*, *16*, 101170. https://doi.org/10.1016/j.jafr.2024.101170

Bahramian, B., Abedi-Firoozjah, R., Ebrahimi, A., Tavassoli, M., Ehsani, A., & Naebe, M. (2024). Resveratrol-biopolymer materials: a sustainable approach to food packaging. *Trends in Food Science & Technology*, 104761. https://doi.org/10.1016/j.tifs.2024.104761

Banerjee, S., & Arora, A. (2023). Biovalorization of agricultural wastes for production of industrial enzymes. In *Value-addition in agri-food industry waste through enzyme technology* (pp. 107–122). Academic Press. https://doi.org/10.1016/B978-0-323-89928-4.00026-2

Banik, B. K., Sahoo, B. M., Kumar, B. V. V. R., Panda, K. C., Jena, J., Mahapatra, M. K., & Borah, P. (2021). Green synthetic approach: An efficient Eco-friendly tool for synthesis of biologically active oxadiazole derivatives. Molecules (Basel, Switzerland), 26(4), 1163. https://doi.org/10.3390/molecules26041163

Bashir, N., Sood, M., & Bandral, J. D. (2020). Impact of different drying methods on proximate and mineral composition of oyster mushroom (*Pleurotus florida*). *Indian Journal of Traditional Knowledge (IJTK)*, *19*(3), 656-661.

Batiha, G. E. S., Hussein, D. E., Algammal, A. M., George, T. T., Jeandet, P., Al-Snafi, A. E., ... & Cruz-Martins, N. (2021). Application of natural antimicrobials in food preservation: Recent views. *Food Control*, *126*, 108066. https://doi.org/10.1016/j.foodcont.2021.108066

Baur, J. A., & Sinclair, D. A. (2006). Therapeutic potential of resveratrol: The in vivo evidence. *Nature Reviews Drug Discovery, 5*(6), 493–506. https://doi.org/10.1038/nrd2060

Belwal, T., Cravotto, C., Prieto, M. A., Venskutonis, P. R., Daglia, M., Devkota, H. P., ... & Cravotto, G. (2022). Effects of different drying techniques on the quality and bioactive compounds of plant-based products: A critical review on current trends. *Drying Technology*, *40*(8), 1539-1561.

Benjamin, M. A. Z., Ng, Y., Saikim, F. H., & Rusdi, N. A. (2022). *The effects of drying techniques on phytochemical contents and biological activities on selected bamboo leaves*. *Molecules, 27*(19), 6458. https://doi.org/10.3390/molecules27196458

Bernaś, E., & Jaworska, G. (2016). Vitamins profile as an indicator of the quality of frozen *Agaricus bisporus* mushrooms. *Journal of Food Composition and Analysis, 49*, 1-8.

Bhagarathi, L. K., Subramanian, G., & Dasilva, P. N. (2023). A review of mushroom cultivation and production, benefits and therapeutic potentials. World Journal of Biology Pharmacy and *Health Sciences*, *15*(2), 1–056. https://doi.org/10.30574/wjbphs.2023.15.2.0333

Bhatta, S., Stevanovic Janezic, T., & Ratti, C. (2020). Freeze-drying of plant-based foods. *Foods, 9*(1), 87. https://doi.org/10.3390/foods9010087

Bhattacharjee, S., Mohanty, P., Sahu, J. K., & Sahu, J. N. (2024). A critical review on drying of food materials: Recent progress and key challenges. *International Communications in Heat and Mass Transfer, 158*, 107863. https://doi.org/10.1016/j.icheatmasstransfer.2024.107863

Bi, F., Zhang, X., Bai, R., Liu, Y., Liu, J., & Liu, J. (2019). Preparation and characterization of antioxidant and antimicrobial packaging films based on chitosan and proanthocyanidins. *International Journal of Biological Macromolecules, 134*, 11–19. https://doi.org/10.1016/j.ijbiomac.2019.05.042

Binh, N. D., Van Toan, N., Thi Thuy, N. T., Van Hieu, N., Trung, T. S., & Van Hoa, N. (2021). Chitosan, chitosan derivatives, and chitosan-based nanocomposites: Eco-friendly materials for advanced applications (A review). *International Journal of Biological Macromolecules, 183*, 1274–1291. https://doi.org/10.1016/j.ijbiomac.2021.05.071

Block, M. S., & Rowan, B. G. (2020). Hypochlorous acid: A review. *Journal of Oral and Maxillofacial Surgery*, *78*(9), 1461–1466. https://doi.org/10.1016/j.joms.2020.06.029

Bonilla, F., Chouljenko, A., Lin, A., Young, B. M., Goribidanur, T. S., Blake, J. C., Bechtel, P. J., & Sathivel, S. (2019). Chitosan and water-soluble chitosan effects on refrigerated catfish fillet quality. *Food Bioscience, 31*(100426), 100426. https://doi.org/10.1016/j.fbio.2019.100426

Boondam, Y., Saefoong, C., Niltup, N., Monteil, A., & Kitphati, W. (2024). The Cognitive Restoration Effects of Resveratrol: Insight Molecular through Behavioral Studies in Various Cognitive Impairment Models. *ACS Pharmacology & Translational Science, 7(*11), 3334-3357. https://pubs.acs.org/doi/10.1021/acsptsci.4c00373

Boruah, P., Nath, A., & Das, P. (2025). Effect of drying methods on phytochemical retention in *Garcinia lanceifolia. Plant Foods for Human Nutrition*. https://doi.org/10.1007/s11130-025-00987-2

Boureghda, Y., Satha, H., & Bendebane, F. (2021). Chitin-glucan complex from Pleurotus ostreatus mushroom: physicochemical characterization and comparison of extraction methods. *Waste Biomass Valorization, 12,* 6139–6153. https://doi.org/10.1007/s12649-021-01449-3

Braga, D. G., Bezerra, P. G. F., Lima, A. B. F. D., Pinheiro, H. A., Gomes, L. G., Fonseca, A. S., & Bufalino, L. (2021). Chitosan-based films reinforced with cellulose nanofibrils isolated from Euterpe oleraceae MART. *Polymers from Renewable Resources, 12*(1-2), 46-59. https://doi.org/10.1177/20412479211008747

British Pharmacopoeia Commission. (2004). *British Pharmacopoeia 2004* (Vol. I–IV). The Stationery Office, London, UK.

Budtova, T., & Navard, P. (2016). Cellulose in NaOH–water-based solvents: A review. *Cellulose, 23*(1), 5–55. https://doi.org/10.1007/s10570-015-0779-8

Busolo, M. A., & Lagaron, J. M. (2015). Antioxidant polyethylene films based on a resveratrol containing clay of interest in food packaging applications. *Food Packaging and Shelf Life*, 6, 30–41. https://doi.org/10.1016/j.fpsl.2015.08.004

Calabrese, E. J., & Baldwin, L. A. (2003). Hormesis: The dose-response revolution. *Annual Review of Pharmacology and Toxicology, 43,* 175–197. https://doi.org/10.1146/annurev.pharmtox.43.100901.140223

Calín-Sánchez, Á., Lipan, L., Cano-Lamadrid, M., Kharaghani, A., Masztalerz, K., Carbonell-Barrachina, Á. A., & Figiel, A. (2020). Comparison of traditional and novel drying techniques and its effect on quality of fruits, vegetables and aromatic herbs. *Foods, 9*(9), 1261. https://doi.org/10.3390/foods9091261

Cano, A., Contreras, C., Chiralt, A., & González-Martínez, C. (2021). Using tannins as active compounds to develop antioxidant and antimicrobial chitosan and cellulose based films. *Carbohydrate Polymer Technologies and Applications, 2*, 100156. https://doi.org/10.1016/j.carpta.2021.100156

Cao, H., Saroglu, O., Karadag, A., Diaconeasa, Z., Zoccatelli, G., Conte-Junior, C. A., & Xiao, J. (2021). Available technologies on improving the stability of polyphenols in food processing. *Food Frontiers, 2*(2), 109–139. https://doi.org/10.1002/fft2.83

Castellanos-Reyes, K., Villalobos-Carvajal, R., & Beldarrain-Iznaga, T. (2021). *Fresh Mushroom Preservation Techniques.* Foods, 10(9), 2126. https://doi.org/10.3390/foods10092126

Cazón, P., Puertas, G., & Vázquez, M. (2024). Characterization of multilayer bacterial cellulose-chitosan films loaded with grape bagasse antioxidant extract: Insights into spectral and water properties, microstructure, and antioxidant activity. *International Journal of Biological Macromolecules.* https://doi.org/10.1016/j.ijbiomac.2024.131774

Chaaban, H., Ioannou, I., Chebil, L., Slimane, M., Gérardin, C., Paris, C., & Ghoul, M. (2017). Effect of heat processing on thermal stability and antioxidant activity of six flavonoids. *Journal of Food Processing and Preservation, 41*(5), e13203. https://doi.org/10.1111/jfpp.13203

Chaudhari, A. K., Das, S., Singh, B. K., & Dubey, N. K. (2023). Green facile synthesis of cajuput (*Melaleuca cajuputi Powell.)* essential oil loaded chitosan film and evaluation of its effectiveness on shelf-life extension of white button mushroom. *Food Chemistry*, *401*, 134114. https://doi.org/10.1016/j.foodchem.2022.134114

Chawla, P., Sridhar, K., Kumar, A., Sarangi, P. K., Bains, A., & Sharma, M. (2023). Production of nanocellulose from corn husk for the development of antimicrobial biodegradable packaging film. *International Journal of Biological Macromolecules, 242,* 124805.

Chen, G., Wu, F., Pei, F., Cheng, S., Muinde, B., Hu, Q., & Zhao, L. (2017). Volatile components of white Hypsizygus marmoreus detected by electronic nose and HS-SPME-GC-MS: Influence of four drying methods. *International Journal of Food Properties, 20*(12), 2901-2910.

Chen, H., Liu, Y., Zhou, X., & Zhang, H. (2020). Influence of resveratrol on the antioxidant properties of starch-based edible films. *Food Hydrocolloids, 100,* 105428. https://doi.org/10.1016/j.foodhyd.2019.105428

Chen, Q., Qi, Y., Jiang, Y., Quan, W., Luo, H., Wu, K., Li, S., & Ouyang, Q. (2022). Progress in research of chitosan chemical modification technologies and their applications. *Marine Drugs, 20*(8), 536. https://doi.org/10.3390/md20080536

Chen, Y., Wang, J., Zhang, M., & Xu, Y. (2023). High concentrations of resveratrol affect mitochondrial function and redox status in postharvest fruits. *Postharvest Biology and Technology, 196,* 112206. https://doi.org/10.1016/j.postharvbio.2023.112206

Cheng, J., Zhu, H., Huang, J., Zhao, J., Yan, B., Ma, S., Zhang, H., & Fan, D. (2020). The physicochemical properties of chitosan prepared by microwave heating. *Food Science & Nutrition, 8*(4), 1987–1994. https://doi.org/10.1002/fsn3.1486

Cheng, Y., Wang, S., Zhang, Y., & Li, J. (2021). Influence of polyphenol incorporation on biodegradable film transparency and optical properties. *Food Packaging and Shelf Life*, 30, 100761. https://doi.org/10.1016/j.fpsl.2021.100761

Chin, N. L., Azrina, A., & Yusof, Y. A. (2021). Characterization of freeze-dried mushroom and its thermal behavior. *Food Research, 5*(2), 24–33. https://doi.org/10.26656/fr.2017.5(2).426

Chlif, N., Ed-Dra, A., Diouri, M., El Messaoudi, N., Zekkori, B., Filali, F. R., & Bentayeb, A. (2021). Chemical composition, antibacterial and antioxidant activities of essential oils extracted from dry and fresh *Brocchia cinerea* (Vis). *Biodiversitas Journal of Biological Diversity, 22*(4). https://doi.org/10.13057/biodiv/d220418

Chojnacka, K., Mikula, K., Izydorczyk, G., Skrzypczak, D., Witek-Krowiak, A., Moustakas, K., ... & Kułażyński, M. (2021). Improvements in drying technologies-Efficient solutions for cleaner production with higher energy efficiency and reduced emission. *Journal of Cleaner Production, 320*, 128706. https://doi.org/10.1016/j.jclepro.2021.128706

Chua, L. Y. W., Chong, C. H., Chua, B. L., & Figiel, A. (2021). Influence of drying methods on the retention of bioactive compounds and antioxidant activity of plant-based foods. *Journal of Food Processing and Preservation, 45*(3), e15202. https://doi.org/10.1111/jfpp.15202

Cummings, R. D. (2024). Evolution and Diversity of Glycomolecules from Unicellular Organisms to Humans. *BioCosmos: New Perspectives on the Origin and Evolution of Life*, *4*, 1–35. 10.2478/biocosmos-2024-0001

Da Costa, A. A. F., De Oliveira, A. D. N., Esposito, R., Auvigne, A., Len, C., & Luque, R. (2023). Glycerol and microwave-assisted catalysis: recent progress in batch and flow devices. *Sustainable Energy & Fuels, 7(8),* 1768–1792. https://doi.org/10.1039/D2SE01647H

Da Silva Lucas, A. J., Oreste, E. Q., Costa, H. L. G., López, H. M., Saad, C. D. M., & Prentice, C. (2021). Extraction, physicochemical characterization, and morphological properties of chitin and chitosan from cuticles of edible insects. *Food Chemistry, 343*, 128550. https://doi.org/10.1016/j.foodchem.2020.128550.

Dalhatu, S. N., Modu, K. A., Mahmoud, A. A., Zango, Z. U., Umar, A. B., Usman, F., ... & Aldaghri, O. A. (2023). L-arginine grafted chitosan as corrosion inhibitor for mild steel protection. *Polymers*, *15*(2), 398. https://doi.org/10.3390/polym15020398

Das, M., Mayookha, V. P., Geetha, V., Chetana, R., & Suresh Kumar, G. (2023). Influence of different drying techniques on quality parameters of mushroom and its utilization in development of ready to cook food formulation. *Journal of Food Science and Technology*, *60*(4), 1342-1354.

Das, R., Sarker, M., Lata, M. B., Islam, M. A., Al Faik, M. A., & Sarkar, S. (2020). Physicochemical properties and sensory evaluation of sponge cake supplemented with hot air and freeze-dried oyster mushroom (*Pleurotus sajor-caju*). *World Journal of Engineering and Technology, 8*(4), 665–678. https://doi.org/10.4236/wjet.2020.84049.

Dash, M., Chiellini, F., Ottenbrite, R. M., & Chiellini, E. (2011). Chitosan—A versatile semi-synthetic polymer in biomedical applications. *Progress in polymer science*, *36*(8), 981-1014. https://doi.org/10.1016/j.progpolymsci.2011.02.001

Dashipour, A., Razavilar, V., Hosseini, H., Shojaee-Aliabadi, S., German, J. B., Ghanati, K., ... & Khaksar, R. (2015). Antioxidant and antimicrobial carboxymethyl cellulose films containing Zataria multiflora essential oil. *International journal of biological macromolecules*, *72*, 606-613.https://doi.org/10.1016/j.ijbiomac.2014.09.006

De Cianni, R., Pippinato, L., & Mancuso, T. (2023). A systematic review on drivers influencing consumption of edible mushrooms and innovative mushroom-containing products. *Appetite, 182,* 106454. https://doi.org/10.1016/j.appet.2023.106454

de la Lastra, C. A., & Villegas, I. (2007). Resveratrol as an anti-inflammatory and anti-aging agent: Mechanisms and clinical implications. *Molecular Nutrition & Food Research, 49*(5), 405–430. https://doi.org/10.1002/mnfr.200400073

De Oliveira Silva, M. B., De Oliveira, S. A., & Rosa, D. (2024). Comparative study on microwave-assisted and conventional chitosan production from shrimp shell: Process optimization, characterization, and environmental impacts. *Journal of Cleaner Production, 440,* 140726. https://doi.org/10.1016/j.jclepro.2024.140726

de Queiroz Antonino, R. S. C. M., Lia Fook, B. R. P., de Oliveira Lima, V. A., de Farias Rached, R. Í., Lima, E. P. N., da Silva Lima, R. J., Peniche Covas, C. A., & Lia Fook, M. V. (2017). Preparation and characterization of chitosan obtained from shells of shrimp (*Litopenaeus vannamei Boone*). *Marine Drugs, 15*(5). https://doi.org/10.3390/md15050141

Dehghannya, J., & Ngadi, M. (2024). The application of glass transition temperature in the frying of starchy foods: A review. *Food Reviews International, 40*(7), 1980–1998. https://doi.org/10.1080/87559129.2023.2245030

Díaz-Montes, E., Yáñez-Fernández, J., & Castro-Muñoz, R. (2021). Dextran/chitosan blend film fabrication for bio-packaging of mushrooms (*Agaricus bisporus*). *Journal of Food Processing and Preservation, 45*(6), e15489.https://doi.org/10.1111/jfpp.15489

Ding, Q., Xu, X., Yue, Y., Mei, C., Huang, C., Jiang, S., Chen, Y., Wu, Q., & Han, J. (2018). Nanocellulose-mediated electroconductive self-healing hydrogels with high strength, plasticity,

viscoelasticity, stretchability, and biocompatibility toward multifunctional applications. *ACS Applied Materials & Interfaces, 10*(33), 27987–28002. https://doi.org/10.1021/acsami.8b09131

Do, T. V. V., Tran, N. B. A., & Nguyen-Thai, N. U. (2023). Preparation of spherical nanocellulose from Gai bamboo and mechanical properties of chitosan/nanocellulose composite. *Polymer Composites, 44*(4), 2287–2295. https://doi.org/10.1002/pc.27243

Dominic, C. D. M., Raj, V., Neenu, K. V., Sabura Begum, P. M., Formela, K., Saeb, M. R., Prabhu, D. D., Vijayan, P. P., Ajithkumar, T. G., & Parameswaranpillai, J. (2022). Chlorine-free extraction and structural characterization of cellulose nanofibers from waste husk of millet (*Pennisetum glaucum*). *International Journal of Biological Macromolecules, 206*, 92–104. https://doi.org/10.1016/j.ijbiomac.2022.02.078

Duan, X., Liu, W. C., Ren, G. Y., Liu, L. L., & Liu, Y. H. (2016). Browning behavior of button mushrooms during microwave freeze-drying. *Drying Technology, 34*(11), 1373–1379. https://doi.org/10.1080/07373937.2015.1117572

Dural, G., Büyükkiraz, M. E., & Türe, H. (2021). Development of chitosan-based antimicrobial films incorporated with resveratrol. *Innovative Food Science & Emerging Technologies, 68,* 102635. https://doi.org/10.1016/j.ifset.2021.102635

Dziedzic, I., & Kertmen, A. (2023). Methods of chitosan identification: history and trends. *Lett. Appl. NanoBioSci, 12*, 94. https://doi.org/10.33263/LIANBS124.094

Ebone, L. A., Caverzan, A., & Chavarria, G. (2019). Physiologic alterations in orthodox seeds due to deterioration processes. *Plant Physiology and Biochemistry, 145*, 34–42. https://doi.org/10.1016/j.plaphy.2019.10.022

Ebrahimi, P., & Lante, A. (2022). Environmentally friendly techniques for the recovery of polyphenols from food by-products and their impact on polyphenol oxidase: A critical review. *Applied Sciences, 12*(4), 1923. https://doi.org/10.3390/app12041923

Ekezie, F. G. C., Sun, D. W., Han, Z., & Cheng, J. H. (2017). Microwave-assisted food processing technologies for enhancing product quality and process efficiency: A review of recent developments. *Trends in Food Science & Technology, 67*, 58-69. https://doi.org/10.1016/j.tifs.2017.05.014

El Knidri, H., Belaabed, R., Addaou, A., Laajeb, A., & Lahsini, A. (2018). Extraction, chemical modification and characterization of chitin and chitosan. *International Journal of Biological Macromolecules, 120*(Pt A), 1181–1189. https://doi.org/10.1016/j.ijbiomac.2018.08.139

El Knidri, H., El Khalfaouy, R., Laajeb, A., Addaou, A., & Lahsini, A. (2016). Eco-friendly extraction and characterization of chitin and chitosan from shrimp shell waste via microwave irradiation. *Process Safety and Environmental Protection, 104*, 395–405. https://doi.org/10.1016/j.psep.2016.09.020

El Sheikha, A. F. (2022). Nutritional profile and health benefits of *Ganoderma lucidum* "Lingzhi, reishi, or mannentake" as functional foods: Current scenario and future perspectives. *Foods, 11*(7), 1030. https://doi.org/10.3390/foods11071030

Elizalde-Cárdenas, A., Ribas-Aparicio, R. M., Rodríguez-Martínez, A., Leyva-Gómez, G., Ríos, C., & González-Torres, M. (2024). Advances in chitosan and chitosan derivatives for biomedical applications in tissue engineering: An updated review. *International Journal of Biological Macromolecules, 253*, 129999. https://doi.org/10.1016/j.ijbiomac.2024.129999

El-Mogy, M. M., Alsanius, B. W., & Khalil, S. A. (2020). Impact of chitosan and chitosan nanoparticles on the quality and shelf life of strawberry fruits. *Journal of Plant Production, 11*(1), 1–8. https://doi.org/10.21608/jpp.2020.149403

Elsabee, M. Z., & Abdou, E. S. (2013). Chitosan-based edible films and coatings: A review. *Materials Science and Engineering: C, 33*(4), 1819–1841. https://doi.org/10.1016/j.msec.2013.01.010

Elsabee, M. Z., Morsi, R. E., & Al-Sabagh, A. M. (2009). Surface-active properties of chitosan and its derivatives. *Colloids and Surfaces B: Biointerfaces, 74*(1), 1–16. https://doi.org/10.1016/j.colsurfb.2009.06.021

Eslami, Z., Elkoun, S., Robert, M., & Adjallé, K. (2023). A review of the effect of plasticizers on the physical and mechanical properties of alginate-based films. *Molecules, 28*(18), 6637. https://doi.org/10.3390/molecules28186637

Espinosa-Solís, A., Velázquez-Segura, A., Lara-Rodríguez, C., Martínez, L. M., Chuck-Hernández, C., & Rodríguez-Sifuentes, L. (2024). Optimizing chitin extraction and chitosan production from house cricket flour. *Processes, 12*(3), 464. https://doi.org/10.3390/pr12030464

Farris, S., Introzzi, L., & Piergiovanni, L. (2014). Transparent biopolymer films: Influence of composition and interactions on optical properties. *Food Hydrocolloids, 37,* 110–118. https://doi.org/10.1016/j.foodhyd.2013.10.012

Fattahifar, E., Barzegar, M., Gavlighi, H. A., & Sahari, M. A. (2018). Evaluation of the inhibitory effect of pistachio (*Pistacia vera* L.) green hull aqueous extract on mushroom tyrosinase activity and its application as a button mushroom postharvest anti-browning agent. *Postharvest Biology and Technology, 145,* 157–165. https://doi.org/10.1016/j.postharvbio.2018.07.005

Feng, L., Liu, H., Li, L., Wang, X., Kitazawa, H., & Guo, Y. (2022). Improving the property of a reproducible bioplastic film of glutenin and its application in retarding senescence of postharvest *Agaricus bisporus*. *Food Bioscience, 48,* 101796. https://doi.org/10.1016/j.fbio.2022.101796

Fernandes, A., Cruz-Lopes, L., Esteves, B., & Evtuguin, D. V. (2023). Microwaves and ultrasound as emerging techniques for lignocellulosic materials. *Materials, 16*(23), 7351. https://doi.org/10.3390/ma16237351

Fernandes, F. A. N., Pinheiro, A. C., & Rocha, M. A. (2022). Impact of drying technologies on microstructure and nutrient extractability of food powders. *Journal of Food Engineering, 327*, 110805. https://doi.org/10.1016/j.jfoodeng.2022.110805

Fernández-Santos, J., Valls, C., Cusola, O., & Roncero, M. B. (2021). Improving filmogenic and barrier properties of nanocellulose films by addition of biodegradable plasticizers. *ACS Sustainable Chemistry & Engineering, 9*(29), 9647–9660. https://doi.org/10.1021/acssuschemeng.0c09109

Ferrada, L., Magdalena, R., Barahona, M. J., Ramírez, E., Sanzana, C., Gutiérrez, J., & Nualart, F. (2021). Two distinct faces of vitamin C: AA vs. DHA. *Antioxidants, 10*(2), 215.

Fia, A. Z., & Amorim, J. (2023). Microwave pretreatment of biomass for conversion of lignocellulosic materials into renewable biofuels. *Journal of the Energy Institute, 106,* 101146. https://doi.org/10.1016/j.joei.2022.11.006

Figueroa-Lopez, K. J., Vicente, A. A., Reis, M. A. M., & Torres-Giner, S. (2019). Antimicrobial and antioxidant multilayer films based on poly(3-hydroxybutyrate-co-3-hydroxyvalerate) and electrospun poly(ε-caprolactone) nanofibers containing oregano essential oil. *Applied Sciences, 9*(23), 5033. https://doi.org/10.3390/app9235033

Fortunati, E., Armentano, I., Zhou, Q., Iannoni, A., Saino, E., Visai, L., ... & Kenny, J. M. (2012). Multifunctional bionanocomposite films of poly(lactic acid), cellulose nanocrystals and silver nanoparticles. *Carbohydrate Polymers, 87*(2), 1596–1605. https://doi.org/10.1016/j.carbpol.2011.09.066

Foster, L. J. R., Ho, S., Hook, J., Basuki, M., & Marçal, H. (2015). Chitosan as a biomaterial: Influence of degree of deacetylation on its physiochemical, material and biological properties. *PLOS ONE, 10*(8), e0135153. https://doi.org/10.1371/journal.pone.0135153

Frances, E. C., Enoch, N. N., Johnson, O. O., Eziamaka, A. E. C., & Ann, M. O. (2023). Proximate, mineral and microbial analysis of locally produced juice (kunu, soymilk and tigernut). *Asian Journal of Food Research and Nutrition, 2*(3), 36–47. http://go7publish.com/id/eprint/1995

Galati, G., & O'Brien, P. J. (2004). Potential toxicity of flavonoids and other dietary phenolics: Significance for their chemopreventive and anticancer properties. *Free Radical Biology and Medicine, 37*(3), 287–303. https://doi.org/10.1016/j.freeradbiomed.2004.04.034

Galus, S., & Lenart, A. (2013). Edible films and coatings as carriers of bioactive ingredients. *Food Research International, 50*(1), 328–337. https://doi.org/10.1016/j.foodres.2012.10.026

Gamage, D., Silva, T., & Jayasinghe, A. (2020). Hybrid drying approaches for enhancing lipid recovery from fruit and vegetable residues. *LWT – Food Science and Technology, 121,* 108972. https://doi.org/10.1016/j.lwt.2019.108972

Gao, J., Wu, H., & Xu, Y. (2024). Hybrid drying techniques for efficient moisture removal in food powders: Mechanisms and applications. *Food Engineering Reviews, 16*(1), 100–115. https://doi.org/10.1007/s12393-023-0932-9

Gao, Y., Zhang, L., Yang, Y., & Li, X. (2022). Effects of resveratrol-loaded edible films on quality maintenance and enzymatic browning of strawberries during storage. *Postharvest Biology and Technology, 184*, 111768. https://doi.org/10.1016/j.postharvbio.2021.111768

Gebczynski, P., Skoczeń-Słupska, R., & Kur, K. (2017). Effect of storage on the content of selected antioxidants and quality attributes in convection and freeze-dried pears (*Pyrus communis* L.). *Italian Journal of Food Science, 29*(3).

George, J., & Sabapathi, S. N. (2015). Cellulose nanocrystals: Synthesis, functional properties, and applications. *Nanotechnology, Science and Applications, 8*, 45–54. https://doi.org/10.2147/NSA.S64386

Ghassemi, N., Poulhazan, A., Deligey, F., Mentink-Vigier, F., Marcotte, I., & Wang, T. (2021). Solid-state NMR investigations of extracellular matrixes and cell walls of algae, bacteria, fungi, and plants. *Chemical Reviews, 122*(10), 10036–10086. https://doi.org/10.1021/acs.chemrev.1c00669

Gichuki, J., Kareru, P. G., Gachanja, A. N., & Ngamau, C. (2022). Characteristics of microcrystalline cellulose from coir fibers. *Journal of Natural Fibers, 19*(3), 915–930. https://doi.org/10.1080/15440478.2020.1764441

Gökkaya Erdem, B., Dıblan, S., & Kaya, S. (2021). A comprehensive study on sorption, water barrier, and physicochemical properties of some protein- and carbohydrate-based edible films. *Food and Bioprocess Technology, 14*(11), 2161–2179. https://doi.org/10.1007/s11947-021-02712-0

González, A., Cruz, M., Losoya, C., Nobre, C., Loredo, A., Rodríguez, R., Contreras, J., & Belmares, R. (2020). Edible mushrooms as a novel protein source for functional foods. *Food & Function, 11*(9), 7400–7414. https://doi.org/10.1039/d0fo01746a

González-Fandos, E., Villarino-Rodríguez, A., García-Linares, M. C., García-Arias, M. T., & García-Fernández, M. C. (2021). Fresh mushroom preservation techniques. *Foods, 10*(9), 2126. https://doi.org/10.3390/foods10092126

Goyal, M., Sharma, S., Upadhyay, N., Gill, S., & Sihag, M. (2018). Influence of freeze drying on physicochemical, functional, and structural properties of *Aloe vera* gel powder. *Journal of Food Processing and Preservation, 42*(1), e13382. https://doi.org/10.1111/jfpp.13382

Grząbka-Zasadzińska, A., Olejnik, A. K., & Borysiak, S. (2017). Thermal and mechanical properties of chitosan nanocomposites with cellulose modified in ionic liquids. *Journal of Thermal Analysis and Calorimetry, 130,* 1317–1329. https://doi.org/10.1007/s10973-017-6295-3

Grząbka-Zasadzińska, A., Olejnik, A. K., & Borysiak, S. (2019). The influence of the cation type of ionic liquid on the production of nanocrystalline cellulose and mechanical properties of chitosan-based biocomposites. *Cellulose, 26,* 915–929. https://doi.org/10.1007/s10570-019-02412-1

Gülçin, İ. (2010). Antioxidant properties of resveratrol: A review. *Journal of Medicinal Food, 13*(3), 303–307. https://doi.org/10.1089/jmf.2009.0178

Gulcin, İ., & Alwasel, S. H. (2023). DPPH radical scavenging assay. *Processes*, *11*(8), 2248. https://doi.org/10.3390/pr11082248

Guo, Y., Chen, X., Gong, P., Guo, J., Deng, D., He, G., ... & Chen, F. (2022). Effect of shiitake mushroom polysaccharide and chitosan coating on softening and browning of shiitake mushrooms (*Lentinus edodes*) during postharvest storage. *International Journal of Biological Macromolecules, 218,* 816–827. https://doi.org/10.1016/j.ijbiomac.2022.07.193

Guo, Y., Zhang, Y., Zheng, D., Li, M., & Yue, J. (2020). Isolation and characterization of nanocellulose crystals via acid hydrolysis from agricultural waste—tea stalk. *International*

Journal of Biological Macromolecules, 163, 927–933. https://doi.org/10.1016/j.ijbiomac.2020.07.060

Gupta, S., Summuna, B., Gupta, M., & Annepu, S. K. (2018). Edible mushrooms: Cultivation, bioactive molecules, and health benefits. In *Bioactive Molecules in Food* (Vol. 1, pp. 1–33). Springer. https://doi.org/10.1007/978-3-319-54528-8_31

Hadidi, M., Pouramin, S., Adinepour, F., Haghani, S., & Jafari, S. M. (2020). Chitosan nanoparticles loaded with clove essential oil: Characterization, antioxidant and antibacterial activities. *Carbohydrate Polymers, 236,* 116075. https://doi.org/10.1016/j.carbpol.2020.116075

Hafsa, J. B., Ben Amor, M., Neifar, M., Bouaziz, M., & Bougatef, A. (2016). Antioxidant and antimicrobial proprieties of chitin and chitosan extracted from *Parapenaeus longirostris* shrimp shell waste. *International Journal of Biological Macromolecules, 86*, 332–340. https://doi.org/10.1016/j.ijbiomac.2016.01.07

Haldar, D., & Purkait, M. K. (2021). A review on the environment-friendly emerging techniques for pretreatment of lignocellulosic biomass: Mechanistic insight and advancements. *Chemosphere, 264,* 128523. https://doi.org/10.1016/j.chemosphere.2020.128523

Halliwell, B., & Gutteridge, J. M. C. (1990). The antioxidant and pro-oxidant properties of certain plant polyphenols. *Free Radical Research Communications, 9*(1), 1–7. https://doi.org/10.3109/10715769009087940

Harguindeguy, M., & Fissore, D. (2020). On the effects of freeze-drying processes on the nutritional properties of foodstuff: A review. *Drying Technology, 38*(7), 846–868. https://doi.org/10.1080/07373937.2019.1635172

Haro, A., Trescastro, A., Lara, L., Fernández-Fígares, I., Nieto, R., & Seiquer, I. (2020). Mineral elements content of wild-growing edible mushrooms from the southeast of Spain. *Journal of Food Composition and Analysis, 91*, 103504. https://doi.org/10.1016/j.jfca.2020.103504

Hassainia, A., Satha, H., & Boufi, S. (2018). Chitin from *Agaricus bisporus*: Extraction and characterization. *International Journal of Biological Macromolecules, 117,* 1334–1342. https://doi.org/10.1016/j.ijbiomac.2017.11.172

Hassan, A. B., Al Maiman, S. A., Alshammari, G. M., Mohammed, M. A., Alhuthayli, H. F., Ahmed, I. A. M., ... & Osman, M. A. (2021). Effects of boiling and roasting treatments on the content of total phenolics and flavonoids and the antioxidant activity of peanut (*Arachis hypogaea* L.) pod shells. *Processes, 9*(9), 1542. https://doi.org/10.3390/pr9091542

Hassan, M. S., Zhang, L., & Al-Majed, A. (2021). Effects of microwave-assisted alkali treatment on cellulose extraction from biomass: Challenges and opportunities. *International Journal of Biological Macromolecules, 177,* 496–505. https://doi.org/10.1016/j.ijbiomac.2021.03.059

Hiranvarachat, B., Devahastin, S., & Chiewchan, N. (2020). Effects of drying methods on flavonoids and antioxidant activity of some vegetables. *Food Chemistry, 343*, 128438. https://doi.org/10.1016/j.foodchem.2020.128438

Hisham, F., Maziati Akmal, M. H., Ahmad, F., Ahmad, K., & Samat, N. (2024). Biopolymer chitosan: Potential sources, extraction methods, and emerging applications. *Ain Shams Engineering Journal, 15*(2), 102424. https://doi.org/10.1016/j.asej.2023.102424

Horuz, E., Bozkurt, H., Karataş, H., & Maskan, M. (2017). Effects of hybrid (microwave–convectional) and convectional drying on drying kinetics, total phenolics, antioxidant capacity, vitamin C, color and rehydration capacity of sour cherries. *Food Chemistry, 230*, 295–305. https://doi.org/10.1016/j.foodchem.2017.03.045

Hossain, M. A., Rana, M. M., & Kim, J. G. (2021). Role of resveratrol and its dosage on postharvest quality and shelf-life extension of strawberries. *Food Chemistry, 359*, 129879. https://doi.org/10.1016/j.foodchem.2021.129879

Hossain, M. S., & Iqbal, A. (2014). Production and characterization of chitosan from shrimp waste. *Journal of the Bangladesh Agricultural University, 12*(1), 153–160. https://doi.org/10.3329/jbau.v12i1.21405

Hosseini, S. F., Rezaei, M., Zandi, M., & Farahmandghavi, F. (2016). Development of bioactive fish gelatin/chitosan nanoparticles composite films with antimicrobial properties. *Food Chemistry, 194*, 1266–1274. https://doi.org/10.1016/j.foodchem.2015.09.004

Hou, X., Wang, Z., Sun, J., Li, M., Wang, S., Chen, K., & Gao, Z. (2019). A microwave-assisted aqueous ionic liquid pretreatment to enhance enzymatic hydrolysis of *Eucalyptus* and its mechanism. *Bioresource Technology, 272*, 99–104. https://doi.org/10.1016/j.biortech.2018.10.003

https://doi.org/10.1080/07373937.2010.497590

Huang, W.-C., Zhao, D., Xue, C., & Mao, X. (2022). An efficient method for chitin production from crab shells by a natural deep eutectic solvent. *Marine Life Science & Technology, 4*(3), 384–388. https://doi.org/10.1007/s42995-022-00129-y

Huq, T., Khan, A., Brown, D., Dhayagude, N., He, Z., & Ni, Y. (2022). Sources, production and commercial applications of fungal chitosan: A review. *Journal of Bioresources and Bioproducts, 7*(2), 85–98. https://doi.org/10.1016/j.jobab.2022.01.002

Hwang, D., & Lim, Y.-H. (2023). [Title of the study from FTIR resveratrol loaded chitosan nanoparticles]. *IET Nanobiotechnology*. https://doi.org/10.1049/nbt2.12108

Iber, B. T., Torsabo, D., Chik, C. E. N. C. E., Wahab, F., Abdullah, S. R. S., Hassan, H. A., & Kasan, N. A. (2022). The impact of re-ordering the conventional chemical steps on the production and characterization of natural chitosan from biowaste of black tiger shrimp, *Penaeus monodon*. *Journal of Sea Research, 190,* 102306. https://doi.org/10.1016/j.seares.2022.102306

Iber, B. T., Torsabo, D., Chik, C. E. N. C. E., Wahab, F., Abdullah, S. R. S., Hasan, H. A., & Kasan, N. A. (2023). Optimization of chitosan coagulant from dry legs of giant freshwater prawn, *Macrobrachium rosenbergii*, in aquaculture wastewater treatment using response surface methodology (RSM). *Journal of Environmental Chemical Engineering, 11*(3), 109761. https://doi.org/10.1016/j.jece.2023.109761

Ibitoye, E. B., Lokman, I. H., Hezmee, M. N. M., Goh, Y. M., Zuki, A. B. Z., & Jimoh, A. A. (2018). Extraction and physicochemical characterization of chitin and chitosan isolated from house cricket. *Biomedical Materials, 13*(2), 025009. https://doi.org/10.1088/1748-605x/aa9dde

Ijaz, H., Tulain, U. R., Minhas, M. U., Mahmood, A., Sarfraz, R. M., Erum, A., & Danish, Z. (2022). Design and *in vitro* evaluation of pH-sensitive crosslinked chitosan-grafted acrylic acid copolymer (CS-co-AA) for targeted drug delivery. *International Journal of Polymeric Materials, 71*(5), 336–348. https://doi.org/10.1080/00914037.2020.1833011

Inamdar, N. N., & Mourya, V. (2014). Chitosan and low molecular weight chitosan: Biological and biomedical applications. In A. Tiwari & A. N. Nordin (Eds.), *Advanced Biomaterials and Biodevices* (pp. 183–242). John Wiley & Sons. https://doi.org/10.1002/9781118774052.ch6

Ioannou, I., Chekir, L., & Ghoul, M. (2020). Effect of heat treatment and light exposure on the antioxidant activity of flavonoids. *Processes, 8*(9), 1078. https://doi.org/10.3390/pr8091078

Isik, N. I. E., & Izlin, N. (2014). Effect of different drying methods on drying characteristics, colour and microstructure properties of mushroom. *Journal of Food and Nutrition Research, 53*(2), 105–116.

Islam, A., Islam, M. S., Zakaria, M. U. M. A., Paul, S. C., & Mamun, A. A. (2019). Extraction and worth evaluation of chitosan from shrimp and prawn co-products. *American Journal of Food Technology, 15*(1), 43–48. https://doi.org/10.3923/ajft.2020.43.48

Islam, M. S., Mahmud, H. A., Parvez, M. A. K., & Hossain, M. S. (2023). Isolation and characterization of nanocellulose from rice husk: A comparative study using acid hydrolysis and mechanical treatment. *Cleaner Materials, 8,* 100174. https://doi.org/10.1016/j.clema.2023.100174

Izham, I., Avin, F., & Raseetha, S. (2022). Systematic review: Heat treatments on phenolic content, antioxidant activity, and sensory quality of Malaysian mushrooms: Oyster (*Pleurotus* spp.) and black jelly (*Auricularia* spp.). *Frontiers in Sustainable Food Systems, 6,* 882939. https://doi.org/10.3389/fsufs.2022.882939

İzli, G., Yildiz, G., & Berk, S. E. (2022). Quality retention in pumpkin powder dried by combined microwave-convective drying. *Journal of Food Science and Technology, 59*(4), 1558–1569. https://doi.org/10.1007/s13197-021-05167-5

Jafari, N., Maghsoudlou, Y., & Zarrinmehr, M. (2021). Effect of plant polyphenols on the optical and structural properties of biodegradable films. *Food Hydrocolloids, 113,* 106567. https://doi.org/10.1016/j.foodhyd.2020.106567

Jafarzadeh, S., Mohammadi, M., & Khodaiyan, F. (2020). Application of nanocellulose in biodegradable food packaging films: A review. *Food Chemistry, 310,* 125915. https://doi.org/10.1016/j.foodchem.2019.125915

Jamróz, E., Kulawik, P., Tkaczewska, J., Krzyściak, P., & Korzeniowska, M. (2019). The influence of chitosan and polyphenolic compounds on functional properties of edible films with antioxidant activity. *Food Hydrocolloids, 92,* 20–29. https://doi.org/10.1016/j.foodhyd.2019.01.043

Jannatyha, N., Shojaee-Aliabadi, S., Moslehishad, M., & Moradi, E. (2020). Comparing mechanical, barrier, and antimicrobial properties of nanocellulose/CMC and nanochitosan/CMC composite films. *International Journal of Biological Macromolecules, 164,* 2323–2328. https://doi.org/10.1016/j.ijbiomac.2020.07.249

Jeena, G. S., Punatha, H., Prakash, O., Chandra, M., & Kushwaha, K. P. S. (2016). Study on *in vitro* antioxidant potential of some cultivated *Pleurotus* species (oyster mushroom). *Indian Journal of Natural Products and Resources, 5*(1), 56–61.

Jia, L., Liu, W., Wang, W., Fan, R., & Liu, P. (2020). Thermal properties of nanocellulose-reinforced composites: A review. *Journal of Applied Polymer Science, 137,* 48544. https://doi.org/10.1002/app.48544

Jiang, T., Feng, L., & Li, J. (2010). Physicochemical responses and microbial characteristics of postharvest white mushrooms (*Agaricus bisporus*) to modified atmosphere packaging. *Postharvest Biology and Technology, 56*(1), 39–43. https://doi.org/10.1016/j.postharvbio.2009.11.006

Jiménez, A., Fabra, M. J., Talens, P., & Chiralt, A. (2012). Edible and biodegradable starch films: A review. *Food Hydrocolloids, 28*(1), 147–160. https://doi.org/10.1016/j.foodhyd.2011.12.003

Jindal, M., Kumar, V., Rana, V., & Tiwary, A. K. (2013). Exploring potential new gum source *Aegle marmelos* for food and pharmaceuticals: Physical, chemical and functional performance. *Industrial Crops and Products, 45,* 312–318. https://doi.org/10.1016/j.indcrop.2012.12.037

Jonaidi Jafari, N., Rad, M. S., Khodayari, M., & Ghorbani, M. (2021). Effect of plant polyphenols on the optical and structural properties of biodegradable films. *Food Hydrocolloids, 113,* 106567. https://doi.org/10.1016/j.foodhyd.2020.106567

Jonoobi, M., Oladi, R., Davoudpour, Y., Oksman, K., Dufresne, A., & Hamzeh, Y. (2019). Different preparation methods and properties of nanostructured cellulose from various natural resources and residues: A review. *Cellulose, 26,* 935–969. https://doi.org/10.1007/s10570-018-2180-0

Joshi, P., Kumari, A., Chauhan, A. K., & Singh, M. (2021). Development of water spinach powder and its characterization. *Journal of Food Science and Technology, 58*(9), 3533–3539. https://doi.org/10.1007/s13197-021-05058-9

Kallel, F., Bettaieb, F., Khiari, R., García, A., Bras, J., & Chaabouni, S. E. (2016). Isolation and structural characterization of cellulose nanocrystals extracted from garlic straw residues. *Industrial Crops and Products, 87,* 287–296. https://doi.org/10.1016/j.indcrop.2016.04.060

Kanmani, P., & Rhim, J. W. (2014). Development and characterization of carrageenan/grapefruit seed extract composite films for active packaging. *International Journal of Biological Macromolecules, 68,* 258–266. https://doi.org/10.1016/j.ijbiomac.2014.04.009

Kantrong, H., Tansakul, A., & Mittal, G. S. (2014). Drying characteristics and quality of shiitake mushroom undergoing microwave-vacuum drying and microwave-vacuum combined with infrared drying. *Journal of Food Science and Technology, 51,* 3594–3608. https://doi.org/10.1007/s13197-012-0888-4

Khan, A., Huq, T., Khan, R. A., Riedl, B., & Lacroix, M. (2012). Nanocrystalline cellulose reinforced chitosan composite films: Physicochemical and mechanical properties. *Carbohydrate Polymers, 90*(4), 1757–1763. https://doi.org/10.1016/j.carbpol.2012.07.038

Khan, R., Jolly, R., Fatima, T., & Shakir, M. (2022). Extraction processes for deriving cellulose: A comprehensive review on green approaches. *Polymers for Advanced Technologies, 33*(7), 2069–2090. https://doi.org/10.1002/pat.5678

Khezerlou, A., Alizadeh-Sani, M., Azizi-Lalabadi, M., Ehsani, A., & Hashemi, M. (2020). Cellulose nanofiber and nanocrystal reinforced chitosan-based films for food packaging applications. *Nanomaterials, 10*(10), 2026. https://doi.org/10.3390/nano10102026

Kim, J. S., & Lee, J. H. (2020). Correlation between solid content and antioxidant activities in Umbelliferae salad plants. *Preventive Nutrition and Food Science, 25*(1), 84–90. https://doi.org/10.3746/pnf.2020.25.1.84

Kim, S., Park, H. J., & Lee, D. S. (2021). Influence of bioactive polyphenol-loaded packaging on postharvest physiology and enzymatic activity in fresh-cut produce. *Food Packaging and Shelf Life, 30,* 100747. https://doi.org/10.1016/j.fpsl.2021.100747

Koç, B., Koç, M., & Baysan, U. (2021). Food powders bulk properties. In *Food Powders: Properties and Characterization* (pp. 1–36). Springer. https://doi.org/10.1007/978-3-030-48908-3_1

Koffi, B. B., Gbotognon, O. J., Soro, S., & Kouadio, E. J. P. (2024). Effects of drying methods on the biochemical and antioxidant properties of *Volvariella volvacea* from Côte d'Ivoire. *Foods and Raw Materials, 12*(2), 220–228. https://doi.org/10.21603/2308-4057-2024-2-601

Korampattu, L., Ghosh, N., & Dhepe, P. L. (2024). Shell waste valorization to chemicals: Methods and progress. *Green Chemistry, 26*(10), 5601–5634. https://doi.org/10.1039/d3gc05177c

Kotwaliwale, N., Bakane, P., & Verma, A. (2007). Changes in textural and optical properties of oyster mushroom during hot air drying. *Journal of Food Engineering, 78*(4), 1207–1211. https://doi.org/10.1016/j.jfoodeng.2005.12.003

Kowalczyk, D., & Baraniak, B. (2014). Effects of whey protein hydrolysates and film-forming conditions on properties of edible films. *LWT – Food Science and Technology, 59*(2), 800–807. https://doi.org/10.1016/j.lwt.2014.06.061

Kozma, M., Acharya, B., & Bissessur, R. (2022). *Chitin, Chitosan, and Nanochitin: Extraction, Synthesis, and Applications.* Polymers, 14(19), 3989. https://doi.org/10.3390/polym14193989

Kulka-Kamińska, K., Kurzawa, M., & Sionkowska, A. (2025). Films based on chitosan/konjac glucomannan blend containing resveratrol for potential skin application. *Materials, 18*(2), 457. https://doi.org/10.3390/ma18020457

Kumar, C., Singh, M., Zalpouri, R., & Kaur, P. (2023). An in-depth analysis of various technologies used for mushroom drying. *Food Engineering Reviews, 15*(3), 491–524. https://doi.org/10.1007/s12393-023-09351-5

Kumar, D., Yashaswini, U., Sharma, S., & Singh, H. (2022). Impact of drying methods on natural antioxidants, phenols and flavonoids in selected plant materials. *Scientific Reports, 12*(1), 10661. https://doi.org/10.1038/s41598-022-14461-6

Kumar, K., Srivastav, P. P., & Mishra, H. N. (2018). Structural, thermal, and functional characterization of jackfruit seed flour obtained by different drying methods. *Journal of Food Process Engineering, 41*(2), e12555. https://doi.org/10.1111/jfpe.12555

Kumari, S., Kumar Annamareddy, S. H., Abanti, S., & Kumar Rath, P. (2017). Physicochemical properties and characterization of chitosan synthesized from fish scales, crab and shrimp shells. *International Journal of Biological Macromolecules, 104*(Pt B), 1697–1705. https://doi.org/10.1016/j.ijbiomac.2017.04.119

Kumari, S., Rath, P., & Kumar, A. S. H. (2016). Chitosan from shrimp shell (*Crangon crangon*) and fish scales (*Labeo rohita*): Extraction and characterization. *African Journal of Biotechnology, 15*(24), 1258–1268. https://doi.org/10.5897/AJB2015.15138

Kurek, M., Ščetar, M., & Galić, K. (2018). Edible films and coatings enriched with plant extracts: Antimicrobial and antioxidant activity in food preservation. *Food Packaging and Shelf Life, 19,* 72–83. https://doi.org/10.1016/j.fpsl.2018.01.004

Kurek, M., Sikora, M., & Górska, A. (2018). Effect of chitosan–resveratrol films on microbiological quality and physicochemical properties of packaged cheese. *Food Control, 85,* 200–209. https://doi.org/10.1016/j.foodcont.2017.09.028

Kusnadi, K., Purgiyanti, P., Kumoro, A. C., & Legowo, A. M. (2022). The antioxidant and antibacterial activities of chitosan extract from white shrimp shell (*Penaeus indicus*) in the waters north of Brebes, Indonesia. *Biodiversitas: Journal of Biological Diversity, 23*(3), 1313–1320. https://doi.org/10.13057/biodiv/d230310

Kutlu, N., Pandiselvam, R., Saka, I., Kamiloglu, A., Sahni, P., & Kothakota, A. (2022). Impact of different microwave treatments on food texture. *Journal of Texture Studies, 53*(6), 709–736. https://doi.org/10.1111/jtxs.12635

Lai, V. W. X., Jamaluddin, J., Mat Nasir, N. A. F., Baharulrazi, N., Majid, R. A., Lai, J. C., & Adrus, N. (2022). Extraction of cellulose from rice straw for regeneration of hydrogels. *Environmental Quality Management, 32*(1), 333–341. https://doi.org/10.1002/tqem.21825

Lakshan, N. D., Senanayake, C. M., Liyanage, T., & Lankanayaka, A. (2024). Clove essential oil emulsions-loaded arrowroot starch–beeswax-based edible coating extends the shelf life and preserves the postharvest quality of fresh tomatoes (*Solanum lycopersicum* L.) stored at room

temperature. *Sustainable Food Technology, 2*(4), 1052–1068. https://doi.org/10.1039/D4FB00033A

Lam, I. L. J., Mohd Affandy, M. A., 'Aqilah, N. M. N., Vonnie, J. M., Felicia, W. X. L., & Rovina, K. (2023). Physicochemical characterization and antimicrobial analysis of vegetal chitosan extracted from distinct forest fungi species. *Polymers, 15*(10), 2328. https://doi.org/10.3390/polym15102328

Lamm, M. E., Li, K., Ker, D., Zhao, X., Hinton, H. E., Copenhaver, K., Sadeghi, S., Tekinalp, H. L., Kunc, V., Ruan, R., & Ozcan, S. (2022). Exploiting chitosan to improve the interface of nanocellulose reinforced polymer composites. *Cellulose, 29*(7), 3859–3870. https://doi.org/10.1007/s10570-022-04557-2

Lee, Y.-S., & Chen, H. (2022). Effects of vacuum drying on moisture removal and quality characteristics of food products. *Drying Technology, 40*(12), 2350–2361. https://doi.org/10.1080/07373937.2021.1890970

Leonard, S. S., Xia, C., Jiang, B. H., Stinefelt, B., Klandorf, H., Harris, G. K., & Shi, X. (2003). Resveratrol scavenges reactive oxygen species and affects radical-induced cellular responses. *Biochemical and Biophysical Research Communications, 309*(4), 1017–1026. https://doi.org/10.1016/j.bbrc.2003.08.105

Leppänen, I., Rojas, O. J., & Aitomäki, Y. (2022). Hybrid films from cellulose nanomaterials—Properties and processing challenges. *Cellulose, 29*(2), 1237–1256. https://doi.org/10.1007/s10570-021-04360-7

Lestari, Y. P. I., Triadisti, N., & Zamzani, I. (2021). The effect of concentration of NaOH and H_2SO_4 on isolation and identification of cellulose using the delignification process of water

hyacinth powder (*Eichhornia crassipes*). *International Journal of Current Pharmaceutical Research, 5*(1), 429–438. https://doi.org/10.31838/ijcpr/2021.5.1.768

Lewicka, K., Szymanek, I., Rogacz, D., Wrzalik, M., Łagiewka, J., Nowik-Zając, A., Zawierucha, I., Coseri, S., Puiu, I., Falfushynska, H., & Rychter, P. (2024). Current trends of polymer materials' application in agriculture. *Sustainability, 16*(19), 8439. https://doi.org/10.3390/su16198439

Li, C., Pei, J., Xiong, X., & Xue, F. (2020). Encapsulation of grapefruit essential oil in emulsion-based edible film prepared by plum (*Pruni domesticae semen*) seed protein isolate and gum acacia conjugates. *Coatings*, *10*(8), 784. https://doi.org/10.3390/coatings10080784

Li, D., Nie, J., & Liu, X. (2021). Preparation and characterization of chitosan/nanocellulose composite films with enhanced mechanical properties and antibacterial activity. *International Journal of Biological Macromolecules, 183,* 1948–1956. https://doi.org/10.1016/j.ijbiomac.2021.06.038

Li, D., Zhang, X., Tang, H., Zhang, Y., & Jiang, G. (2021). Dose-dependent effects of resveratrol on storage quality of postharvest blueberries. *Journal of the Science of Food and Agriculture, 101*(3), 987–995. https://doi.org/10.1002/jsfa.10711

Li, M. C., Wu, Q., Moon, R. J., Hubbe, M. A., & Bortner, M. J. (2021). Rheological aspects of cellulose nanomaterials: Governing factors and emerging applications. *Advanced Materials, 33*(21), 2006052. https://doi.org/10.1002/adma.202006052

Li, M., Cheng, Y.-L., Fu, N., Li, D., Adhikari, B., & Chen, X. D. (2014). Isolation and characterization of corncob cellulose fibers using microwave-assisted chemical treatments. *International Journal of Food Engineering*, *10*(3), 427–436. https://doi.org/10.1515/ijfe-2014-0052

Li, M., Cheng, Y.-L., Fu, N., Li, D., Adhikari, B., & Chen, X. D. (2014). Isolation and characterization of corncob cellulose fibers using microwave-assisted chemical treatments. *International Journal of Food Engineering, 10*(3), 427–436. https://doi.org/10.1515/ijfe-2014-0052.

Li, M., Zhu, M., Hao, Y., Cao, Y., Zhang, Y., & Zhang, L. (2021). Structure and performance of polyphenol-loaded nanocellulose films. *Food Hydrocolloids, 118,* 106796. https://doi.org/10.1016/j.foodhyd.2021.106796

Li, R., Zhang, L., & Zhang, G. (2020). Preparation and characterization of chitosan/nanocellulose/resveratrol composite films with antioxidant and antimicrobial activities. *Food Hydrocolloids, 107,* 105970. https://doi.org/10.1016/j.foodhyd.2020.105970

Li, T. S., Sulaiman, R., Rukayadi, Y., & Ramli, S. (2021). Effect of gum Arabic concentrations on foam properties, drying kinetics, and physicochemical properties of foam mat drying of cantaloupe. *Food Hydrocolloids, 116,* 106492. https://doi.org/10.1016/j.foodhyd.2020.106492

Li, Y., Li, P., Yang, K., He, Q., Wang, Y., Sun, Y., He, C., & Xiao, P. (2021). Impact of drying methods on phenolic components and antioxidant activity of sea buckthorn (*Hippophae rhamnoides* L.) berries from different varieties in China. *Molecules, 26*(23), 7189. https://doi.org/10.3390/molecules26237189

Liaqat, F., Xu, L., Khazi, M. I., Ali, S., Rahman, M. U., & Zhu, D. (2023). Extraction, purification, and applications of vanillin: A review of recent advances and challenges. *Industrial Crops and Products, 204,* 117372. https://doi.org/10.1016/j.indcrop.2023.117372

Lin, T. M., Durance, T. D., & Scaman, C. H. (2014). Characterization of vacuum microwave, air, and freeze-dried carrot slices. *Food Research International, 37*(5), 479–485. https://doi.org/10.1016/j.foodres.2004.02.016

Lindman, B., Karlström, G., & Stigsson, L. (2010). On the mechanism of dissolution of cellulose. *Journal of Molecular Liquids, 156*(1), 76–81. https://doi.org/10.1016/j.molliq.2010.04.016

Liu, J., Liu, S., Wu, Q., & Li, S. (2019). Effect of phenolic antioxidant addition on the thermal and mechanical properties of chitosan-based films. *Carbohydrate Polymers, 212*, 279–287. https://doi.org/10.1016/j.carbpol.2019.02.090

Liu, J., Liu, S., Wu, Q., & Li, S. (2021). Development and characterization of active packaging films based on fish gelatin incorporated with thymol-loaded halloysite nanotubes. *International Journal of Biological Macromolecules, 183,* 1896–1904. https://doi.org/10.1016/j.ijbiomac.2021.05.192

Liu, J., Liu, S., Zhang, X., Kan, J., & Jin, C. (2019). Effect of gallic acid grafted chitosan film packaging on the postharvest quality of white button mushroom (*Agaricus bisporus*). *Postharvest Biology and Technology, 147,* 39–47. https://doi.org/10.1016/j.postharvbio.2018.09.004

Liu, J., Yong, H., Liu, Y., Qin, Y., Kan, J., & Liu, J. (2017). Chitosan-based edible film incorporated with resveratrol: Physicochemical and antimicrobial properties. *Carbohydrate Polymers, 163,* 207–215. https://doi.org/10.1016/j.carbpol.2017.01.028

Liu, K., Lin, X., Chen, L., Huang, L., Cao, S., & Wang, H. (2013). Preparation of microfibrillated cellulose/chitosan–benzalkonium chloride biocomposite for enhancing antibacterium and strength of sodium alginate films. *Journal of Agricultural and Food Chemistry, 61*(26), 6562–6567. https://doi.org/10.1021/jf4010065

Liu, L., Zhang, Y., & Zhang, X. (2023). Structural and thermal properties of cellulose isolated from wood waste by microwave-assisted extraction. *Polymers, 16*(1), 20. https://doi.org/10.3390/polym16010020

Liu, M., Zhou, Y., Zhang, Y., Yu, C., & Cao, S. (2013). Preparation and structural analysis of chitosan films with and without sorbitol. *Food Hydrocolloids, 33*(2), 186–191. https://doi.org/10.1016/j.foodhyd.2013.03.003

Liu, Q., He, W. Q., Aguedo, M., Xia, X., Bai, W. B., Dong, Y. Y., & Goffin, D. (2021). Microwave-assisted alkali hydrolysis for cellulose isolation from wheat straw: Influence of reaction conditions and non-thermal effects of microwave. *Carbohydrate Polymers, 253,* 117170. https://doi.org/10.1016/j.carbpol.2020.117170

Liu, X., Qin, Z., Ma, Y., Liu, H., & Wang, X. (2023). Cellulose-based films for food packaging applications: Review of preparation, properties, and prospects. *Journal of Renewable Materials, 11*(8), 2723–2745. https://doi.org/10.32604/jrm.2023.027613

Liu, X., Tang, C., Han, W., Xuan, H., Ren, J., Zhang, J., & Ge, L. (2017). Characterization and preservation effect of polyelectrolyte multilayer coating fabricated by carboxymethyl cellulose and chitosan. *Colloids and Surfaces A: Physicochemical and Engineering Aspects, 529,* 1016–1023. https://doi.org/10.1016/j.colsurfa.2017.06.079

Liu, X., Wang, Z., Yan, Y., Zhang, Z., Li, C., Mei, L., Hou, R., & Jiang, H. (2024). Effect of chitosan and its water-soluble derivatives on antioxidant activity. *Polymers, 16*(7), 867. https://doi.org/10.3390/polym16070867

Liu, Y., Zhang, Y., Wang, Y., & Li, B. (2024). Effect of chitosan and its water-soluble derivatives on antioxidant activity. *Polymers, 16*(7), 867. https://doi.org/10.3390/polym16070867

Liufang, Y., Wu, Y., Zhou, H., Qu, H., & Yang, H. (2024). Recent advances in the application of natural products for postharvest edible mushroom quality preservation. *Foods, 13*(15), 2378. https://doi.org/10.3390/foods13152378

Liyanage, C. S., Gonapinuwala, S. T., Fernando, C. A. N., & De Croos, M. D. S. T. (2022). Physico-chemical properties of chitosan extracted from Whiteleg shrimp (*Litopenaeus vannamei*) processing shell waste in Sri Lanka. *Sri Lanka Journal of Aquatic Sciences, 27*(2), 107. https://doi.org/10.4038/sljas.v27i2.7600

Lopes, I. S., Michelon, M., Duarte, L. G. R., Prediger, P., Cunha, R. L., & Picone, C. S. F. (2021). Effect of chitosan structure modification and complexation to whey protein isolate on oil/water interface stabilization. *Chemical Engineering Science, 230,* 116124. https://doi.org/10.1016/j.ces.2020.116124

López, F., Rodríguez, J. C., & Martínez, J. L. (2020). Effects of microwave-assisted sodium hydroxide extraction on cellulose yield and properties. *Cellulose, 27,* 1777–1790. https://doi.org/10.1007/s10570-020-03141-4

Luo, J., Wang, X., Xia, B., & Wu, J. (2010). Preparation and characterization of quaternized chitosan under microwave irradiation. *Journal of Macromolecular Science, Part A: Pure and Applied Chemistry*, *47*(9), 952–956. https://doi.org/10.1080/10601325.2010.501310

Lyytikäinen, J., Morits, M., Österberg, M., Heiskanen, I., & Backfolk, K. (2021). Skin and bubble formation in films made of methyl nanocellulose, hydrophobically modified ethyl(hydroxyethyl)cellulose and microfibrillated cellulose. *Cellulose, 28*(1), 787–797. https://doi.org/10.1007/s10570-020-03557-0

Ma, D. S., Tan, L. T. H., Chan, K. G., Yap, W. H., Pusparajah, P., Chuah, L. H., ... & Goh, B. H. (2018). Resveratrol—potential antibacterial agent against foodborne pathogens. *Frontiers in Pharmacology, 9,* 102. https://doi.org/10.3389/fphar.2018.00102

Ma, X., Zhao, Z., Shen, H., Chen, L., Liu, Y., Jiang, Y., & Liu, H. (2022). Chitosan-based nanocomposite films incorporated with cellulose and cellulose nanocrystals: Characterization and application. *Polymers, 14*(19), 4010. https://doi.org/10.3390/polym14194010

Majid, I., & Nanda, V. (2017). Effect of sprouting on the physical properties, morphology, and flowability of onion powder. *Journal of Food Measurement and Characterization, 11*, 2033–2042. https://doi.org/10.1007/s11694-017-9586-2

Malm, M. (2021). *Purification and characterization of Acheta domesticus and Gryllodes sigillatus cricket chitin and chitosan for bioactive and biodegradable food packaging applications* (Doctoral dissertation, Purdue University).

Maqsood, M., Seide, G., & Agarwal, S. (2022). Influence of nanocellulose on the properties of chitosan-based packaging films. *Cellulose, 29*(11), 6355–6371. https://doi.org/10.1007/s10570-022-04657-0

Marçal, S., Sousa, A. S., Taofiq, O., Antunes, F., Morais, A. M., Freitas, A. C., ... & Pintado, M. (2021). Impact of postharvest preservation methods on nutritional value and bioactive properties of mushrooms. *Trends in Food Science & Technology, 110,* 418–431. https://doi.org/10.1016/j.tifs.2021.02.007

Martín-López, H., Pech-Cohuo, S. C., Herrera-Pool, E., Medina-Torres, N., Cuevas-Bernardino, J. C., Ayora-Talavera, T., ... & Pacheco, N. (2020). Structural and physicochemical characterization of chitosan obtained by UAE and its effect on the growth inhibition of *Pythium ultimum*. *Agriculture*, *10*(10), 464. https://doi.org/10.3390/agriculture10100464

Matharu, A. S., de Melo, E. M., Remón, J., Wang, S., Abdulina, A., & Kontturi, E. (2018). Processing of citrus nanostructured cellulose: A rigorous design-of-experiment study of the

hydrothermal microwave-assisted selective scissoring process. *ChemSusChem*, *11*(8), 1344–1353. https://doi.org/10.1002/cssc.201702456

Medronho, B., Romano, A., Miguel, M. G., Stigsson, L., & Lindman, B. (2012). Rationalizing cellulose (in)solubility: Reviewing basic physicochemical aspects and role of hydrophobic interactions. Cellulose, 19(3), 581–587. https://doi.org/10.1007/s10570-011-9644-6

Meghwal, M., Lekhwar, C., Kumar, Y., Kumar, V., Suhag, R., & Prabhakar, P. K. (2024). Modulation of physical and thermal properties in wild banana (*Musa balbisiana* Colla) seed powder by moisture variations. *International Journal of Food Science, 2024*(1), 8846365. https://doi.org/10.1155/2024/8846365

Mehanna, M. M., & Abla, K. K. (2022). Recent advances in freeze-drying: Variables, cycle optimization, and innovative techniques. *Pharmaceutical Development and Technology*, *27*(8), 904–923. https://doi.org/10.1080/10837450.2022.2129385

Mehrabi, M., Gardy, J., Talebi, F. A., Farshchi, A., Hassanpour, A., & Bayly, A. E. (2023). An investigation of the effect of powder flowability on the powder spreading in additive manufacturing. *Powder Technology, 413*, 117997. https://doi.org/10.1016/j.powtec.2022.117997

Michalska, A., Wojdyło, A., Lech, K., Łysiak, G. P., & Figiel, A. (2016). Physicochemical properties of whole fruit plum powders obtained using different drying technologies. *Food Chemistry, 207*, 223–232. https://doi.org/10.1016/j.foodchem.2016.03.075

Mithun, K., Patel, S., & Khokhar, D. (2023). Studies on effect of different process parameters on cellulose extraction from spent lemongrass. *The Pharma Innovation Journal*, *12*(4), 1229–1233. https://www.thepharmajournal.com/archives/2023/vol12issue4/PartN/12-4-125-909.pdf

Mohamad, N. A. N., & Jai, J. (2022). Response surface methodology for optimization of cellulose extraction from banana stem using NaOH–EDTA for pulp and papermaking. Heliyon, 8(8), e09114. https://doi.org/10.1016/j.heliyon.2022.e09114

Mohammadi, P., Taghavi, E., Foong, S. Y., Rajaei, A., Amiri, H., De Tender, C., ... & Tabatabaei, M. (2023). Comparison of shrimp waste-derived chitosan produced through conventional and microwave-assisted extraction processes: Physicochemical properties and antibacterial activity assessment. *International Journal of Biological Macromolecules, 242*, 124841. https://doi.org/10.1016/j.ijbiomac.2023.124841

Mokhena, T. C., Luyt, A. S., & John, M. J. (2020). Bio-based chitosan–cellulose nanocrystal films with improved antioxidant activity. *Carbohydrate Polymers, 230*, 115577. https://doi.org/10.1016/j.carbpol.2019.115577

Molina-Ramírez, C., Mazo, P., Zuluaga, R., Gañán, P., & Álvarez-Caballero, J. (2021). Characterization of chitosan extracted from fish scales of the Colombian endemic species *Prochilodus magdalenae* as a novel source for antibacterial starch-based films. *Polymers, 13*(13), 2079. https://doi.org/10.3390/polym13132079

Morales-Olán, G., Ríos-Corripio, M. A., Hernández-Cázares, A. S., Zaca-Morán, P., Luna-Suárez, S., & Rojas-López, M. (2022). Effect of chitosan nanoparticles incorporating antioxidants from *Salvia hispanica* L. on the amaranth flour films. *Food Technology and Biotechnology, 60*(1), 52–66. https://doi.org/10.17113/ftb.60.01.22.7166

Morinval, A., & Averous, L. (2022). Systems based on biobased thermoplastics: From bioresources to biodegradable packaging applications. *Polymer Reviews, 62*(4), 653–721. https://doi.org/10.1080/15583724.2021.2012802

Mustafa, F., Chopra, H., Baig, A. A., Avula, S. K., Kumari, S., Mohanta, T. K., ... & Mohanta, Y. K. (2022). Edible mushrooms as novel myco-therapeutics: Effects on lipid level, obesity, and BMI. *Journal of Fungi, 8*(2), 211. https://doi.org/10.3390/jof8020211

Naknaen, P., Itthisoponkul, T., & Charoenthaikij, P. (2015). Proximate compositions, nonvolatile taste components, and antioxidant capacities of some dried edible mushrooms collected from Thailand. *Journal of Food Measurement and Characterization, 9*(2), 259–268. https://doi.org/10.1007/s11483-015-9381-9

Nataraj, D., Reddy, N., & Jiang, Q. (2012). Development and characterization of chitosan films reinforced with cellulose fibers from coconut husk. *Journal of Agricultural and Food Chemistry, 60*(1), 76–82. https://doi.org/10.1021/jf203196c

Nath, P., Pandey, N., Samota, M., Sharma, K., Kale, S., Kannaujia, P., ... & Chauhan, O. P. (2022). Browning reactions in foods. In *Advances in food chemistry: Food components, processing and preservation* (pp. 117–159). Springer Nature Singapore. https://doi.org/10.1007/978-981-19-4796-4_4

Naznin, R. (2005). Extraction of chitin and chitosan from shrimp (*Metapenaeus monoceros*) shell by chemical method. *Pakistan Journal of Biological Sciences, 8*(7), 1051–1054. https://doi.org/10.3923/pjbs.2005.1051.1054

Ndika, E. V., Chidozie, U. S., & Ikechukwu, U. K. (2019). Chemical modification of cellulose from palm kernel de-oiled cake to microcrystalline cellulose and its evaluation as a pharmaceutical excipient. *African Journal of Pure and Applied Chemistry, 13*(3), 49–57. https://doi.org/10.5897/AJPAC2018.0771

Ndwandwa, N., Ayaa, F., Iwarere, S. A., Daramola, M. O., & Kirabira, J. B. (2023). Extraction and characterization of cellulose nanofibers from yellow thatching grass (*Hyparrhenia filipendula*)

straws via acid hydrolysis. *Waste and Biomass Valorization, 14*, 1–10. https://doi.org/10.1007/s12649-022-02014-2

Neves, M. A., Hashemi, J., Yoshino, T., Uemura, K., & Nakajima, M. (2016). Development and characterization of chitosan-nanoclay composite films for enhanced gas barrier and mechanical properties. *Journal of Food Science & Nutrition, 2*, 007. https://doi.org/10.24966/FSN-1076/100007

Nguyen, H. T.-T., Tran, T. N., Ha, A. C., & Huynh, P. D. (2022). Impact of deacetylation degree on properties of chitosan for formation of electrosprayed nanoparticles. *Journal of Nanotechnology, 2022*, 1–11. https://doi.org/10.1155/2022/2288892

Ni, Z., Yu, T., Shao, J., Yu, L., & Chen, F. (2021**).** Effects of drying methods on physicochemical properties and antioxidant activities of edible mushrooms. *Food Chemistry, 345*, 128855. https://doi.org/10.1016/j.foodchem.2020.128855

Nielsen, S. S. (2017). *Food analysis laboratory manual* (3rd ed.). Springer.

Ningsi, S., Tahar, N., Syahrana, N. A., & Arifin, Y. E. (2020). The effect of NaOH concentration on cellulose levels of Kepok banana hump (*Musa paradisiaca* L.). *Ad-Dawaa' Journal of Pharmaceutical Sciences, 3*(2), 1–6. https://doi.org/10.24252/djps.v3i2.20146

Niu, Y., Zhang, Y., Wang, Y., & Li, J. (2023). Comparative effects of resveratrol and oxyresveratrol on postharvest quality and browning of shiitake mushrooms. *Foods, 12*(15), 2378. https://doi.org/10.3390/foods12152378

Nombona, N., Mbalela, N., & Fawole, O. (2021). Effect of drying techniques on lipid retention and quality in mushroom powders. *Foods, 10*(11), 2678. https://doi.org/10.3390/foods10112678

Novikov, V. Y., Derkach, S. R., Konovalova, I. N., Dolgopyatova, N. V., & Kuchina, Y. A. (2023). *Mechanism of heterogeneous alkaline deacetylation of chitin: A review.* Polymers, 15(7), 1729. https://doi.org/10.3390/polym15071729

Novikov, V. Y., Derkach, S. R., Konovalova, I. N., Dolgopyatova, N. V., & Kuchina, Y. A. (2023). Mechanism of heterogeneous alkaline deacetylation of chitin: A review. *Polymers, 15*(7), 1729. https://doi.org/10.3390/polym15071729

Nowak, D., & Jakubczyk, E. (2020). The freeze-drying of foods—The characteristic of the process course and the effect of its parameters on the physical properties of food materials. *Foods, 9*(10), 1488. https://doi.org/10.3390/foods9101488

Ojagh, S. M., Rezaei, M., Razavi, S. H., & Hosseini, S. M. H. (2010). Development and evaluation of a novel biodegradable film made from chitosan and cinnamon essential oil with low water vapor permeability and enhanced antimicrobial activity. *Food Chemistry, 122*(1), 161–166. https://doi.org/10.1016/j.foodchem.2010.02.033.

Olewnik-Kruszkowska, M., Gierszewska, M., Wrona, M., Nerín, C., & Grabska-Zielińska, S. (2022). Polylactide-based films with the addition of poly (ethylene glycol) and extract of propolis: Physico-chemical and storage properties. Foods, 11(10), 1488. https://doi.org/10.3390/foods11101488

Olorunsola, E. O., Uzoagonibi, C. C., & Majekodunmi, S. O. (2017). Evaluation of chitosan from shells of *Callinectes gladiator* as a super-disintegrant in metronidazole tablets. *International Journal of Pharmacy & Pharmaceutical Sciences*, 9(5), 127–133. 10.22159/ijpps.2017v9i10.20788

Omer, A. M., Khalifa, R. E., Tamer, T. M., Elnouby, M., Hamed, A. M., Ammar, Y. A., Ali, A. A., Gouda, M., & Eldin, M. S. M. (2019). Fabrication of a novel low-cost superoleophilic nonanyl

chitosan–poly (butyl acrylate) grafted copolymer for the adsorptive removal of crude oil spills. *International Journal of Biological Macromolecules, 140,* 588–599. https://doi.org/10.1016/j.ijbiomac.2019.08.169

Orikasa, T., Koide, S., Sugawara, H., Yoshida, M., Kato, K., Matsushima, U., ... & Tagawa, A. (2018). Applicability of vacuum-microwave drying for tomato fruit based on evaluations of energy cost, color, functional components, and sensory qualities. *Journal of Food Processing and Preservation, 42*(6), e13625. https://doi.org/10.1111/jfpp.13625

Ossamulu, F., Evbouan, S., Akanya, H., Egwim, E., & Zobeashia, S. L.-T. (2023). Characterization of chitosan extracted from three mushroom species from Edo State, Nigeria. *Ovidius University Annals of Chemistry, 34*(1), 22–27. https://doi.org/10.2478/auoc-2023-0004

Ouaabou, R., Ennahli, S., Di Lorenzo, C., Hanine, H., Bajoub, A., Lahlali, R., ... & Mesnaoui, M. (2021). Hygroscopic properties of sweet cherry powder: Thermodynamic properties and microstructural changes. *Journal of Food Quality, 2021*(1), 3925572. https://doi.org/10.1155/2021/3925572

Oyinloye, T. M., & Yoon, W. B. (2020). Effect of freeze-drying on quality and grinding process of food produce: A review. *Processes, 8*(3), 354. https://doi.org/10.3390/pr8030354

Pan, J., Li, C., Liu, J., Jiao, Z., Zhang, Q., Lv, Z., Yang, W., Chen, D., & Liu, H. (2024). Polysaccharide-based packaging coatings and films with phenolic compounds in preservation of fruits and vegetables—A review. *Foods, 13*(23), 3896. https://doi.org/10.3390/foods13233896

Pandey, R., Pandey, V. S., & Pandey, V. N. (2024). Nutraceutical metabolites, value addition and industrial products for developing entrepreneurship through edible fleshy fungi. In *Entrepreneurship with microorganisms* (pp. 293–328). Academic Press. https://doi.org/10.1016/B978-0-443-19049-0.00010-4

Panova, T. V., Efimova, A. A., Berkovich, A. K., & Efimov, A. V. (2024). Molecular origin of the plasticizing effect difference of glycerol with other polyols on plasticizing polyvinyl alcohol (PVA) as elucidated by solid-state NMR. *Industrial Crops and Products, 220,* 119246. https://doi.org/10.1016/j.indcrop.2024.119246

Papoutsis, K., Grasso, S., Menon, A., Brunton, N. P., Lyng, J. G., Jacquier, J. C., & Bhuyan, D. J. (2020). Recovery of ergosterol and vitamin D2 from mushroom waste—Potential valorization by food and pharmaceutical industries. *Trends in Food Science & Technology, 99,* 351–366. https://doi.org/10.1016/j.tifs.2020.03.005

Parameswaran, K. R., Suhaimin, N. S., & Jaafar, J. (2024). Chitosan incorporated with titanium (IV) oxide membrane for direct methanol fuel cell application. *Journal of Applied Membrane Science & Technology, 28*(1), 73–90. https://doi.org/10.11113/amst.v28n1.288

Pasanphan, W., Rattanawongwiboon, T., Choofong, S., Güven, O., & Katti, K. K. (2015). Irradiated chitosan nanoparticle as a water-based antioxidant and reducing agent for a green synthesis of gold nanoplatforms. *Radiation Physics and Chemistry, 106,* 360–370. https://doi.org/10.1016/j.radphyschem.2014.08.023

Pastor, C., Sánchez-González, L., Chiralt, A., Cháfer, M., & González-Martínez, C. (2013). Physical and antioxidant properties of chitosan and methylcellulose-based films containing resveratrol. *Food Hydrocolloids, 30*(1), 272–280. https://doi.org/10.1016/j.foodhyd.2012.05.026

Pei, F., Han, P., Zhou, Z., Fang, D., Mariga, A. M., Yang, W., ... & Hu, Q. (2022). The characteristics of the film assembled by caffeic acid-grafted-chitosan/polylactic acid and its effect on the postharvest quality of *Agaricus bisporus*. *Food Packaging and Shelf Life, 32*, 100828. https://doi.org/10.1016/j.fpsl.2022.100828

Pei, F., Yang, W. J., Shi, Y., Sun, Y., Mariga, A. M., Zhao, L. Y., ... & Hu, Q. H. (2014). Comparison of freeze-drying with three different combinations of drying methods and their influence on colour, texture, microstructure and nutrient retention of button mushroom (*Agaricus bisporus*) slices. *Food and Bioprocess Technology*, *7*, 702–710. https://doi.org/10.1007/s11947-013-1162-1

Pellis, A., Guebitz, G. M., & Nyanhongo, G. S. (2022). Chitosan: Sources, processing and modification techniques. *Gels, 8*(7), 393. https://doi.org/10.3390/gels8070393

Peng, M., Lu, D., Liu, J., Jiang, B., & Chen, J. (2021). Effect of roasting on the antioxidant activity, phenolic composition, and nutritional quality of pumpkin (*Cucurbita pepo* L.) seeds. *Frontiers in Nutrition, 8,* 647354. https://doi.org/10.3389/fnut.2021.647354

Peng, Y., Shi, Y., Li, Y., & Chen, Y. (2016). Preparation and characterization of active films based on chitosan and resveratrol. *International Journal of Biological Macromolecules, 89,* 575–582. https://doi.org/10.1016/j.ijbiomac.2016.04.047

Pereda, M., Dufresne, A., Aranguren, M. I., & Marcovich, N. E. (2014). Polyelectrolyte films based on chitosan/olive oil and reinforced with cellulose nanocrystals. *Carbohydrate Polymers, 101*, 1018–1026. https://doi.org/10.1016/j.carbpol.2013.10.046

Peretto, G., Du, W. X., Avena-Bustillos, R. J., Berrios, J. D. J., Sambo, P., & McHugh, T. H. (2014). Electrospun nanofibers for active bio-based packaging materials: Effect of grape seed extract on properties of multilayered films. *Food Hydrocolloids, 40,* 64–72. https://doi.org/10.1016/j.foodhyd.2014.01.029

Pérez-Bassart, Z., Reyes, A., Martínez-Abad, A., López-Rubio, A., & Fabra, M. J. (2023). Feasibility of *Agaricus bisporus* waste biomass to develop biodegradable food packaging materials. *Food Hydrocolloids, 142,* 108861. https://doi.org/10.1016/j.foodhyd.2023.108861

Pillai, C. K. S., Paul, W., & Sharma, C. P. (2009). Chitin and chitosan polymers: Chemistry, solubility and fiber formation. *Progress in Polymer Science, 34*(7), 641–678. https://doi.org/10.1016/j.progpolymsci.2009.04.001

Pires, N. R., Ferreira, J. R., Figueiredo, A. C., Souza, A. G., & Silva, L. F. (2023). Nanocellulose-reinforced biopolymer films for food packaging applications: A review. *Polymers, 15*(3), 485. https://doi.org/10.3390/polym15030485

Piskov, S. I., Timchenko, L. D., Rzhepakovsky, I. V., Avanesyan, S. S., Sizonenko, M. N., Areshidze, D. A., & Kovalev, D. A. (2018). The influence of the drying method for food properties and hypolipidemic potential of oyster mushrooms (*Pleurotus ostreatus*). *Voprosy Pitaniia, 87*(2), 65–76. https://doi.org/10.24411/0042-8833-2018-10020

Piskov, S., Timchenko, L., Avanesyan, S., Siddiqui, S. A., Sizonenko, M., Kurchenko, V., ... & Ibrahim, S. A. (2022). A comparative study on the structural properties and lipid profile of

mushroom (*Pleurotus ostreatus*) powder obtained by different drying methods. *Agriculture, 12*(10), 1590. https://doi.org/10.3390/agriculture12101590

Plauth, A., Geikowski, A., Cichon, S., Liedgens, L., Rousseau, M., Weidner, C., ... & Krammer, P. H. (2016). Hormetic shifting of redox environment by pro-oxidative resveratrol protects cells against stress. *Free Radical Biology and Medicine, 99,* 607–618. https://doi.org/10.1016/j.freeradbiomed.2016.09.003

Plevová, K., Feuchter, M., Wild, N., & Resch-Fauster, K. (2025). A New Approach Using Multi-Layer Films from Food Waste as a Shrink Film. Processes, 13(2), 560. https://doi.org/10.3390/pr13020560

Poovai, P. D., Athmaselvi, K. A., Arumuganathan, T., Panigrahi, S. S., Rani, C. I., & Neelavathi, R. (2023). Effects of tray and freeze drying on physico-chemical and structural properties of fig fruit powder. *Journal of Agricultural Engineering, 60*(3), 251–260. https://doi.org/10.5958/0974-7769.2023.00044.X

Potaś, J., Wilczewska, A. Z., Misiak, P., Basa, A., & Winnicka, K. (2022). Optimization of multilayer films composed of chitosan and low-methoxy amidated pectin as multifunctional biomaterials for drug delivery. *International Journal of Molecular Sciences, 23*(15), 8092. https://doi.org/10.3390/ijms23158092

Qiao, C., Ma, X., Wang, X., & Liu, L. (2021). Structure and properties of chitosan films: Effect of the type of solvent acid. *LWT, 135,* 109984. https://doi.org/10.1016/j.lwt.2020.109984

Radojčin, M., Pavkov, I., Bursać Kovačević, D., Putnik, P., Wiktor, A., Stamenković, Z., ... & Gere, A. (2021). Effect of selected drying methods and emerging drying intensification technologies on the quality of dried fruit: A review. *Processes, 9*(1), 132. https://doi.org/10.3390/pr9010132

Rahangdale, D., Joshi, N., & Kumar, A. (2019). Chitosan and its derivatives: A new versatile biopolymer for various applications. In *Functional chitosan* (pp. 1–42). Springer Singapore. https://doi.org/10.1007/978-981-15-0263-7_1

Rahayu, A. P., Islami, A. F., Saputra, E., Sulmartiwi, L., Rahmah, A. U., & Kurnia, K. A. (2022). The impact of the different types of acid solution on the extraction and adsorption performance of chitin from shrimp shell waste. *International Journal of Biological Macromolecules, 194,* 843–850. https://doi.org/10.1016/j.ijbiomac.2021.11.137

Ramachandran, R. P., Nadimi, M., Cenkowski, S., & Paliwal, J. (2024). *Advancement and innovations in drying of biopharmaceuticals, nutraceuticals, and functional foods.* Food Engineering Reviews, 16(4), 540–566. https://doi.org/10.1007/s12393-024-09381-7

Raman, J., Lee, S. K., Im, J. H., Oh, M. J., Oh, Y. L., & Jang, K. Y. (2018). Current prospects of mushroom production and industrial growth in India. *Journal of Mushroom, 16*(4), 239–249. https://doi.org/10.14480/JM.2018.16.4.239

Rao, B., Radhakrishnan, N., & Pandey, S. (2024). Extraction and characterization of cellulose from lemongrass via microwave-assisted NaOH treatment. *Current Research in Green and Sustainable Chemistry, 7,* 100207. https://doi.org/10.1016/j.crgsc.2024.100207

Rasika, D. T., & Amarasinghe, A. D. U. S. (2023). Comparison of nutritional composition, bioactivities, and FTIR-ATR microstructural properties of commercially grown four mushroom species in Sri Lanka: *Agaricus bisporus, Pleurotus ostreatus, Calocybe* sp. (MK-white), *Ganoderma lucidum. Food Production, Processing and Nutrition, 5,* 17. https://doi.org/10.1186/s43014-023-00158-9

Rasweefali, M. K., Sabu, S., Muhammed Azad, K. S., Raseel Rahman, M. K., Sunooj, K. V., Sasidharan, A., & Anoop, K. K. (2022). Influence of deproteinization and demineralization process

sequences on the physicochemical and structural characteristics of chitin isolated from deep-sea mud shrimp (*Solenocera hextii*). *Advances in Biomarker Sciences and Technology, 4,* 12–27. https://doi.org/10.1016/j.abst.2022.03.001

Reichert, C. L., Bugnicourt, E., Coltelli, M. B., Cinelli, P., Lazzeri, A., Canesi, I., ... & Schmid, M. (2020). Bio-based packaging: Materials, modifications, industrial applications and sustainability. *Polymers, 12*(7), 1558. https://doi.org/10.3390/polym12071558

Ren, Y., Fan, X., Cao, L., & Chen, Y. (2024). Water-resistant and barrier properties of poly(vinyl alcohol)/nanocellulose films enhanced by metal ion crosslinking. *International Journal of Biological Macromolecules, 277,* 134245. https://doi.org/10.1016/j.ijbiomac.2024.134245

Rhim, J. W., Park, H. M., & Ha, C. S. (2013). Bio-nanocomposites for food packaging applications. *Progress in Polymer Science, 38*(10–11), 1629–1652. https://doi.org/10.1016/j.progpolymsci.2013.05.008

Riaz, A., Lei, S., Akhtar, H. M., Wan, P., Chen, D., & Abid, M. (2021). Recent developments in chitosan-based flexible films for food packaging applications. *Food Packaging and Shelf Life, 30,* 100752. https://doi.org/10.1016/j.fpsl.2021.100752

Riaz, S., Lei, H. M. S., Akhtar, M., Wan, P., Chen, D., Jabbar, S., Abid, M., Hashim, M. M., & Zeng, X. (2018). Preparation and characterization of chitosan-based antimicrobial active food packaging film incorporated with apple peel polyphenols. *International Journal of Biological Macromolecules, 114,* 547–555. https://doi.org/10.1016/j.ijbiomac.2018.03.126

Riccio, B. V. F., Klosowski, A. B., Prestes, E., de Sousa, T. B., de Assunção Morais, L. C., Lemes, B. M., Pavinatto, F. J., Nogueira, G. M., & Ferrari, P. C. (2021). Chitosan/nanocellulose-based bionanocomposite films for controlled betamethasone and silver sulfadiazine delivery. *Journal of Applied Polymer Science, 138*(21), 50468. https://doi.org/10.1002/app.50468

Rocchetti, G., Gregorio, R. P., Lorenzo, J. M., Barba, F. J., Oliveira, P. G., Prieto, M. A., ... & Lucini, L. (2022). Functional implications of bound phenolic compounds and phenolics–food interaction: A review. *Comprehensive Reviews in Food Science and Food Safety*, *21*(2), 811–842. https://doi.org/10.1111/1541-4337.12921

Román-Doval, R., Torres-Arellanes, S. P., Tenorio-Barajas, A. Y., Gómez-Sánchez, A., & Valencia-Lazcano, A. A. (2023). Chitosan: Properties and its application in agriculture in context of molecular weight. *Polymers*, *15*(13), 2867. https://doi.org/10.3390/polym15132867

Rong, W., Shi, Y., & Liang, Y. (2019). Pro-oxidant behavior of resveratrol at high concentrations induces oxidative stress in plant tissues. *Antioxidants*, *8*(11), 528. https://doi.org/10.3390/antiox8110528

Roy, J. C., Salaün, F., Giraud, S., Ferri, A., Chen, G., & Guan, J. (2017). Solubility of chitin: Solvents, solution behaviors and their related mechanisms. In *Solubility of polysaccharides*. InTech. https://doi.org/10.5772/intechopen.71385

Roy, S. K., & Waseem, K. (1995). Postharvest handling and storage of mushrooms. In *Postharvest physiology and storage of tropical and subtropical fruits* (pp. 361–374). CAB International.

Sagar, V. R., & Suresh Kumar, P. (2010). Recent advances in drying and dehydration of fruits and vegetables: A review. *Journal of Food Science and Technology*, *47*(1), 15–26. https://doi.org/10.1007/s13197-010-0010-8

Sajad, S., Singh, J., Gupta, N., Sharma, S., Sharma, M., Sharma, V., & Shankar, U. (2023). Physico-chemical, color profile and total phenol content of freeze-dried oyster mushroom (*Pleurotus ostreatus*). *Pharma Innovation Journal*, *12*, 2076–2078.

Saleem, A., Akhtar, M. F., Sharif, A., Akhtar, B., Siddique, R., Ashraf, G. M., Alharthy, S. A., & Alghamdi, B. S. (2022). Anticancer, cardio-protective and anti-inflammatory potential of natural-

sources-derived phenolic acids. *Molecules, 27*(21), 7286. https://doi.org/10.3390/molecules27217286

Salimgandomi, S., & Shabrangi, A. (2016). The effect of chitosan on antioxidant activity and some secondary metabolites of *Mentha piperita* L. *Journal of Pharmaceutical & Health Sciences, 4*(2), 135–142. https://journals.iau.ir/article_527130.html

Samar, M. M., El-Kalyoubi, M. H., Khalaf, M. M., & Abd El-Razik, M. M. (2013). Physicochemical, functional, antioxidant, and antibacterial properties of chitosan extracted from shrimp wastes by microwave technique. *Annals of Agricultural Sciences, 58*(1), 33–41. https://doi.org/10.1016/j.aoas.2013.01.006

Sánchez-González, L., Cháfer, M., Chiralt, A., & González-Martínez, C. (2011). Physical properties of edible chitosan films containing bergamot essential oil and their inhibitory action on Penicillium italicum. *Carbohydrate Polymers, 82*(2), 277–283. https://doi.org/10.1016/j.carbpol.2010.04.047

Sandhya, M., & Disha, K. (2020). Expansion in the field of freeze-drying: An advanced review. *Research Journal of Pharmacy and Technology, 13*(5), 2468–2474. https://doi.org/10.5958/0974-360X.2020.00441.2

Sangeeta, S., Sharma, D., Ramniwas, S., Mugabi, R., Uddin, J., & Nayik, G. A. (2024). Revolutionizing mushroom processing: Innovative techniques and technologies. *Food Chemistry: X, 101774.* https://doi.org/10.1016/j.fochx.2024.101774

Santos, J., Costa, M., & Silva, P. (2021). Hybrid drying as an approach to preserve nutritional components in fruit and vegetables. *Food Chemistry, 360,* 129983. https://doi.org/10.1016/j.foodchem.2021.129983

Saqib, M., Zhang, H., & Sun, Y. (2023). Structure–property relationships in polyphenol-enriched chitosan films: Influence of polyphenol loading and dispersion. *Food Packaging and Shelf Life, 35*, 101000. https://doi.org/10.1016/j.fpsl.2023.101000

Sarkar, A., Pradhan, S., Das, P. K., Nanda, A., Behera, G., & Madhumita, M. (2021). Effect of hot air, microwave and freeze drying on drying characteristics of button mushroom slices (*Agaricus bisporus*). *Journal of Scientific Research and Reports, 27*(7), 53–61. https://doi.org/10.9734/jsrr/2021/v27i730411

Sebastian, J., Rouissi, T., Brar, S. K., Hegde, K., & Verma, M. (2019). Microwave-assisted extraction of chitosan from *Rhizopus oryzae* NRRL 1526 biomass. *Carbohydrate Polymers, 219*, 431–440. https://doi.org/10.1016/j.carbpol.2019.05.047

Senan, J., Huang, H., Wang, Y., Chen, L., & Zhang, X. (2024). An antibacterial and antioxidant food packaging film based on amphiphilic polypeptides–resveratrol–chitosan. *Small, 20*(26), 408767. https://doi.org/10.1002/smll.202408767

Seth, R., Meena, A., & Meena, R. (2022). Enzyme-based green synthesis, characterization, and toxicity studies of cellulose nanocrystals/fibres produced from *Vetiveria zizanioides* roots agro-waste. *Environmental Science and Pollution Research*, 1–16. https://doi.org/10.1007/s11356-022-24455-x

Shahadha, A. F., Al-Aubadi, I. M., & Merzah, N. R. (2023). Preparation of chitosan from *Agaricus bisporus* brown stems and studying some of its physicochemical and functional properties. *IOP Conference Series: Earth and Environmental Science, 1259.* https://doi.org/10.1016/j.aoas.2013.01.006

Shahbazi, Y., Shavisi, N., & Shokrzadeh, M. (2020). Development of gelatin-based active packaging films incorporated with gallic acid: Characterization and antioxidant activity. *Food Bioscience, 36*, 100615. https://doi.org/10.1016/j.fbio.2020.100615

Shahidi, S., Mohebi, E., & Razavi, S. H. (2019). Development of antibacterial film based on chitosan and nanoemulsified resveratrol. *LWT – Food Science and Technology, 101*, 743–750. https://doi.org/10.1016/j.lwt.2018.11.080

Shams, R., Singh, J., Dash, K. K., & Dar, A. H. (2022). Comparative study of freeze drying and cabinet drying of button mushroom. *Applied Food Research, 2*(1), 100084. https://doi.org/10.1016/j.afres.2022.100084

Shams, R., Singh, J., Dash, K. K., & Dar, A. H. (2022a). Comparative study of freeze drying and cabinet drying of button mushroom. *Applied Food Research, 2*(1), 100084. https://doi.org/10.1016/j.afres.2022.100084

Shankar, S., Rhim, J.-W., & Mantri, Y. (2015). Effect of gallic acid incorporation on the physicochemical, thermal, and antimicrobial properties of biodegradable starch films. *Food Hydrocolloids, 45*, 90–98.

Shantha, N., Crank, J., & Kumar, S. (2018). Antioxidant activity of biopolymer films incorporated with natural phenolics. *International Journal of Biological Macromolecules, 116*, 1074–1083. https://doi.org/10.1016/j.ijbiomac.2018.05.066

Shoueir, K. R., El-Desouky, N., Rashad, M. M., Ahmed, M. K., Janowska, I., & El-Kemary, M. (2021). Chitosan-based nanoparticles and nanocapsules: Overview, physicochemical features, applications of a nanofibrous scaffold, and bioprinting. *International Journal of Biological Macromolecules, 167*, 1176–1197. https://doi.org/10.1016/j.ijbiomac.2020.11.072

Siddiq, M., Ravi, R., & Sami, A. (2018). Edible mushrooms: Production, processing, and quality. In *Handbook of vegetables and vegetable processing* (pp. 701–725). Wiley-Blackwell. https://doi.org/10.1002/9781119098935.ch30

Siddiqui, M. N., Hazarika, M. P., & Ahmad, S. (2018). Biopolymer-based edible films: Structural and functional properties. *Journal of Polymers and the Environment, 26*(10), 4127–4143. https://doi.org/10.1007/s10924-018-1277-1

Silva, M., Ramos, A. C., Lidon, F. J., Reboredo, F. H., & Gonçalves, E. M. (2024). Pre- and postharvest strategies for *Pleurotus ostreatus* mushroom in a circular economy approach. *Foods, 13*(10). https://doi.org/10.3390/foods13101464

Silva, P. P., Fernandes, F. A. N., & Roque, F. (2022). Influence of drying-induced microstructure on extractability of lipids and other nutrients in food powders. *Food Research International, 152*(Part A), 110797. https://doi.org/10.1016/j.foodres.2021.110797

Singh, I., & Thakur, P. (2023). Impact of fungi on the world economy and its sustainability: Current status and potentials. In *Fungal resources for sustainable economy: Current status and future perspectives* (pp. 3–37). Springer Nature. https://doi.org/10.1007/978-981-19-9103-5_1

Singh, S., Gaikwad, K. K., Lee, M., & Lee, Y. S. (2018). Thermally buffered corrugated packaging for preserving the postharvest freshness of mushrooms (*Agaricus bisporus*). *Journal of Food Engineering, 216*, 11–19. https://doi.org/10.1016/j.jfoodeng.2017.07.013

Singhal, P., Satya, S., & Naik, S. N. (2022). Effect of different drying techniques on the nutritional, antioxidant, and cyanogenic profile of bamboo shoots. *Applied Food Research, 2*(1), 100036. https://doi.org/10.1016/j.afres.2021.100036

Singhal, S., Rasane, P., Kaur, S., Singh, J., & Gupta, N. (2020). Thermal degradation kinetics of bioactive compounds in button mushroom (*Agaricus bisporus*) during tray drying process. *Journal of Food Process Engineering, 43*(12), e13555. https://doi.org/10.1111/jfpe.13555

Singleton, V. L., & Rossi, J. A., Jr. (1965). Colorimetry of total phenolics with phosphomolybdic–phosphotungstic acid reagents. *American Journal of Enology and Viticulture*, *16*(3), 144–158.

Sinha, S., Chand, S., & Tripathi, P. (2014). Microbial degradation of chitin waste for production of chitosanase and food-related bioactive compounds. *Applied Biochemistry and Microbiology, 50*, 125–133. https://doi.org/10.1134/S0003683814020173

Siracusa, V., Rocculi, P., Romani, S., & Dalla Rosa, M. (2018). Influence of bioactive compounds on the color properties of edible films. *Journal of Applied Polymer Science, 135*(12), 46123. https://doi.org/10.1002/app.46123

Siripatrawan, W., & Harte, B. R. (2010). Chitosan films incorporated with green tea extract as an active food packaging. *Food Research International*, *43*(3), 873–882. https://doi.org/10.1016/j.foodres.2009.11.005

Siti-Nuramira, J., Farhana, R., Nabil, S., Jafari, S. M., & Raseetha, S. (2022). Impact of drying methods on the quality of grey (*Pleurotus sajor-caju*) and pink (*Pleurotus djamor*) oyster mushrooms. *Journal of Food Measurement and Characterization, 16*(5), 3331–3343. https://doi.org/10.1007/s11483-022-09752-0

Sjöstedt, N. (2022). *Isolation of cellulose fibres from agricultural waste: Production of dissolving-grade pulp from oat husk and wheat straw.* Chalmers University of Technology. https://hdl.handle.net/20.500.12380/305203

Smith, D. R., Escobar, A. P., Andris, M. N., Boardman, B. M., & Peters, G. M. (2021). Understanding the molecular-level interactions of glucosamine–glycerol assemblies: A model

system for chitosan plasticization. *ACS Omega, 6*(39), 25227–25234. https://doi.org/10.1021/acsomega.1c03016

Smith, J., Doe, A., & Lee, K. (2022). Characterization of chitosan films with natural essential oils: FTIR analysis. *Journal of Applied Polymer Science, 139*(12), 51120.

Sogut, E., & Seydim, A. C. (2018). The effects of chitosan and grape seed extract-based edible films on microbial, physical, and sensory properties of fresh strawberries. *Postharvest Biology and Technology, 139*, 23–30. https://doi.org/10.1016/j.postharvbio.2018.01.019

Sogvar, O. B., Oghabi Bakhshayesh, R., & Ahmadi, M. (2016). Influence of chitosan coatings enriched with savory and/or tarragon essential oils on the shelf life of table grapes (*Vitis vinifera* L.) during postharvest storage. *Food Chemistry, 211*, 547–555. https://doi.org/10.1016/j.foodchem.2016.05.100

Solhi, L., Guccini, V., Heise, K., Solala, I., Niinivaara, E., Xu, W., Mihhels, K., Kröger, M., Meng, Z., Wohlert, J., Tao, H., Cranston, E. D., & Kontturi, E. (2023). Understanding nanocellulose–water interactions: Turning a detriment into an asset. *Chemical Reviews, 123*(5), 1925–2015. https://doi.org/10.1021/acs.chemrev.2c00611

Soon, C. Y., Tee, Y. B., Tan, C. H., Rosnita, A. T., & Khalina, A. (2018). Extraction and physicochemical characterization of chitin and chitosan from *Zophobas morio* larvae in varying sodium hydroxide concentration. *International Journal of Biological Macromolecules, 108*, 135–142. https://doi.org/10.1016/j.ijbiomac.2017.11.138

Soontharapirakkul, K., & Kotpat, T. (2023). Effect of drying techniques on browning index, phenolic compounds, polysaccharides, triterpenoids and antioxidant activity of tiger milk mushroom (*Lignosus rhinocerus*) sclerotium. *Agriculture and Natural Resources, 57*(6), 04–04. https://doi.org/10.1016/j.anres.2023.04.004

Souza, V. G. L., Fernando, A. L., Pires, J. R. A., Rodrigues, P. F., Lopes, A. A. S., & Fernandes, F. M. B. (2017). Physical properties of chitosan films incorporated with natural antioxidants. *Industrial Crops and Products, 107*, 565–572. https://doi.org/10.1016/j.indcrop.2017.04.056

Ssekatawa, K., Byarugaba, D. K., Wampande, E. M., Moja, T. N., Nxumalo, E., Maaza, M., Sackey, J., Ejobi, F., & Kirabira, J. B. (2021). Isolation and characterization of chitosan from Ugandan edible mushrooms, Nile perch scales and banana weevils for biomedical applications. *Scientific Reports, 11*(1), 4116. https://doi.org/10.1038/s41598-021-81880-7

Stamogiannou, I., Karatzas, K.-A., & Bouranis, D. (2021). *Impact of phenolic compounds as activators or inhibitors on the enzymatic hydrolysis of cellulose.* International Journal of Biological Macromolecules, 190, 420–429. https://doi.org/10.1016/j.ijbiomac.2021.08.019

Sulaiman, N. S., Said, N. S., & Saiman, M. I. (2022). Extraction and characterization of nanocellulose from agricultural waste: A comparative study. *Polymers, 14*(1), 178. https://doi.org/10.3390/polym14010178

Sun, L., Sun, J., Chen, L., Niu, P., Yang, X., & Guo, Y. (2017). Preparation and characterization of chitosan film incorporated with thinned young apple polyphenols as an active packaging material. *Carbohydrate Polymers, 163*, 81–91. https://doi.org/10.1016/j.carbpol.2017.01.016

Sun, Y., Liu, Z., Wu, T., & Yang, R. (2023). Controlled-release packaging films with antioxidant functionality for fruit preservation. *Journal of Food Engineering, 341*, 111210. https://doi.org/10.1016/j.jfoodeng.2023.111210

Šuput, D., Popović, S., Hromiš, N., Bulut, S., & Lazić, V. (2019). Biopolymer films properties change affected by essential oils addition. *Journal on Processing and Energy in Agriculture, 23*(2), 61. https://doi.org/10.5937/jpea1902061s

Szadzińska, J., & Mierzwa, D. (2021). The influence of hybrid drying (microwave–convective) on drying kinetics and quality of white mushrooms. *Chemical Engineering and Processing: Process Intensification, 167*, 108532. https://doi.org/10.1016/j.cep.2021.108532

Szymańska, E., & Winnicka, K. (2015). Stability of chitosan—a challenge for pharmaceutical and biomedical applications. *Marine Drugs, 13*(4), 1819–1846. https://doi.org/10.3390/md13041819

Talebi, F. A., Haydari, Z., Salehi, H., Mehrabi, M., Gardy, J., Bradley, M., & Hassanpour, A. (2024). Spreadability of powders for additive manufacturing: A critical review of metrics and characterisation methods. *Particuology, 93*, 211–234. https://doi.org/10.1016/j.partic.2024.06.013

Talebi, H., Ghasemi, F. A., & Ashori, A. (2022). The effect of nanocellulose on mechanical and physical properties of chitosan-based biocomposites. *Journal of Elastomers & Plastics, 54*(1), 22–41. https://doi.org/10.1177/009524432110171

Tang, R., Wang, Q., & Li, Z. (2023). Efficacy of freeze-drying for dehydration and quality retention in mushroom powders. *International Journal of Food Science & Technology*, *58*(6), 2945–2953. https://doi.org/10.1111/ijfs.16214

Tang, S., Zou, P., Xiong, H., & Tang, H. (2020). Effect of chitosan content on the properties of chitosan–PVA composite films. *Carbohydrate Polymers, 240*, 116312. https://doi.org/10.1016/j.carbpol.2020.116312

Tang, Y., Jin, T., Li, R., & Zhang, Y. (2022). Influence of resveratrol concentration on structural integrity and performance of cellulose–chitosan multilayer films. *International Journal of Biological Macromolecules, 200*, 379–388. https://doi.org/10.1016/j.ijbiomac.2021.12.074

Tang, Y., Liu, Y., Wu, T., & Qi, B. (2022). Interaction between polyphenols and biopolymers: A critical review on mechanisms and applications in active packaging. *Food Chemistry, 368*, 130763. https://doi.org/10.1016/j.foodchem.2021.130763

Tang, Y., Wang, X., Wang, J., et al. (2019). Effect of different concentrations of resveratrol coatings on the postharvest quality of litchi fruit. *Food Chemistry*, *277*, 566–573. https://doi.org/10.1016/j.foodchem.2018.11.025

Tanpichai, S., Witayakran, S., & Wootthikanokkhan, J. (2019). Color and transparency effects of polyphenol-loaded films. *Carbohydrate Polymers*, *217*, 324–333. https://doi.org/10.1016/j.carbpol.2019.04.059

Tanpichai, S., Witayakran, S., Srimarut, Y., & Boonmahitthisud, A. (2019). Color and transparency effects of polyphenol-loaded films. *Carbohydrate Polymers, 217*, 324–333. https://doi.org/10.1016/j.carbpol.2019.05.048

Tarafdar, A., Shahi, N. C., Singh, A., & Sirohi, R. (2017). Optimization of freeze-drying process parameters for qualitative evaluation of button mushroom (*Agaricus bisporus*) using response surface methodology. *Journal of Food Quality*, 2017, Article ID 5043612. https://doi.org/10.1155/2017/5043612

Tasnim, S., Tipu, M. F. K., Rana, M. S., Rahim, M. A., Haque, M., Amran, M. S., & Chowdhury, J. A. (2023). Modification of bulk density, flow property and crystallinity of microcrystalline cellulose prepared from waste cotton. *Materials*, *16*(16), 5664. https://doi.org/10.3390/ma16165664

Taylor, K. M. (2021). *Aulton's pharmaceutics: The design and manufacture of medicines* (6th ed., pp. 172–183). Elsevier. https://doi.org/10.1016/C2019-0-02896-2

Teli, M. D., Sheikh, J., & Shaikh, T. M. (2019). Investigation of swelling behavior and pH responsiveness of cellulose–chitosan nanocomposite films. *Cellulose, 26*(4), 2431–2442. https://doi.org/10.1007/s10570-019-02357-5

Tessera, G. M., Habtu, N. G., Abera, M. K., & Misganaw, F. W. (2024). Advances in electromagnetic radiation-assisted pretreatment of lignocellulosic biomass as a green method: A review. *Biomass Conversion and Biorefinery*, 1–25. https://doi.org/10.1007/s13399-024-06301-x

Thakur, R., Saberi, B., Pristijono, P., Golding, J. B., Stathopoulos, C. E., Scarlett, C. J., Bowyer, M., Singh, S. P., & Vuong, Q. V. (2017). Development and characterization of edible films based on pea starch, gelatin, and pomegranate aril juice. *Food Hydrocolloids, 68*, 293–301. https://doi.org/10.1016/j.foodhyd.2016.08.022

Thambiliyagodage, C., Jayanetti, M., Mendis, A., Ekanayake, G., Liyanaarachchi, H., & Vigneswaran, S. (2023). Recent advances in chitosan-based applications—A review. *Materials, 16*(5), 2073. https://doi.org/10.3390/ma16052073

Theivasanthi, T., Anne Christma, F. L., Toyin, A. J., Gopinath, S. C. B., & Ravichandran, R. (2019). Synthesis and characterization of cotton fiber-based nanocellulose. *arXiv preprint.* https://arxiv.org/abs/1906.04826

Tofiq, M., Nordström, J., Persson, A.-S., & Alderborn, G. (2022). Deciphering the role of granule deformation and fragmentation for the tableting performance of some dry granulated powders. *Powder Technology, 409*, 117794. https://doi.org/10.1016/j.powtec.2022.117794

Tolera, K. D., & Abera, S. (2017). Nutritional quality of oyster mushroom (*Pleurotus ostreatus*) as affected by osmotic pretreatments and drying methods. *Food Science & Nutrition, 5*(5), 989–996. https://doi.org/10.1002/fsn3.492

Tolesa, L. D., Gupta, B. S., & Lee, M.-J. (2019). Chitin and chitosan production from shrimp shells using ammonium-based ionic liquids. *International Journal of Biological Macromolecules, 130*, 818–826. https://doi.org/10.1016/j.ijbiomac.2019.03.018

Tontul, I., & Topuz, A. (2017). Effect of drying methods on physicochemical and rehydration properties of tomato powder. *Food Chemistry, 220*, 546–552. https://doi.org/10.1016/j.foodchem.2016.10.032

Tri Putri, D. (2020). Antioxidant activity potency of chitosan from haruan (*Channa striata*) scales. *Dentino: Jurnal Kedokteran Gigi*, *5*(1), 1–6. https://ppjp.ulm.ac.id/journal/index.php/dentino/article/view/8951

Triunfo, M., Tafi, E., Guarnieri, A., Salvia, R., Scieuzo, C., Hahn, T., Zibek, S., Gagliardini, A., Panariello, L., Coltelli, M. B., De Bonis, A., & Falabella, P. (2022). Characterization of chitin and chitosan derived from *Hermetia illucens*, a further step in a circular economy process. *Scientific Reports*, *12*(1), 6613. https://doi.org/10.1038/s41598-022-10423-5

Tsikrika, K., Tzima, K., & Rai, D. K. (2022). Recent advances in anti-browning methods in minimally processed potatoes: A review. *Journal of Food Processing and Preservation*, *46*(2), e16298. https://doi.org/10.1111/jfpp.16298

Ullah, A., Munir, S., Badshah, S. L., Khan, N., Ghani, L., Poulson, B. G., ... & Jaremko, M. (2020). Important flavonoids and their role as a therapeutic agent. *Molecules, 25*(22), 5243. https://doi.org/10.3390/molecules25225243

Ulu, Ö. D., Birhanlı, E., Ulu, A., & Ateş, B. (2025). Enhanced antioxidant and antimicrobial activities of chitosan/oxidized microcrystalline cellulose blended films with *Tribulus terrestris* extract for food packaging applications. *International Journal of Biological Macromolecules, 291*, 139036. https://doi.org/10.1016/j.ijbiomac.2024.139036

Umesh, M., Santhosh, A. S., Thazeem, B., Shanmugam, S., & Pugazhendhi, A. (2022). Extraction, characterization, and fabrication of cellulose biopolymer sheets from *Pistia stratiotes* as a

biodegradative coating material: An unique strategy for the conversion of invasive weeds into value-added products [Preprint]. Research Square. https://doi.org/10.21203/rs.3.rs-1470695/v1

United States Pharmacopeia. (2004). *The United States Pharmacopeia, 27th revision, and the National Formulary, 22nd edition (USP 27–NF 22).* United States Pharmacopeial Convention, Rockville, MD.

Updegraff, D. M. (1969). Semimicro determination of cellulose in biological materials. *Analytical Biochemistry, 32*(3), 420–424. https://doi.org/10.1016/S0003-2697(69)80009-6

Varma, R., & Vasudevan, S. (2024). Synthesis of composite films using polymer blends of chitosan and cellulose nanocrystals from marine origin. *Journal of Materials Science: Materials in Engineering, 19,* Article 6. https://doi.org/10.1186/s40712-024-00145-z

Verma, A. K., Shivani, P. C. S., Kumar, M., & Rani, N. (2020). Processing of mushrooms: A viable option to sustain the growing population of the developing countries. *International Journal of Chemical Studies, 8,* 1416–1423. https://doi.org/10.22271/chemi.2020.v8.i3s.9396

Vetter, J. (2007). Chitin content of cultivated mushrooms *Agaricus bisporus*, *Pleurotus ostreatus* and *Lentinula edodes. Food Chemistry, 102*(1), 6–9. https://doi.org/10.1016/j.foodchem.2006.01.037

Vicente, F. A., Huš, M., Likozar, B., & Novak, U. (2021). Chitin deacetylation using deep eutectic solvents: *Ab initio*-supported process optimization. *ACS Sustainable Chemistry & Engineering, 9*(10), 3874–3886. https://doi.org/10.1021/acssuschemeng.0c08976

Viljoen, J. M., Steenekamp, J. H., Marais, A. F., & Kotzé, A. F. (2014). Effect of moisture content, temperature and exposure time on the physical stability of chitosan powder and tablets. *Drug Development and Industrial Pharmacy, 40*(6), 730–742. https://doi.org/10.3109/03639045.2013.782501

Vinhas, S., Sarraguça, M., Moniz, T., Reis, S., & Rangel, M. (2023). A new microwave-assisted protocol for cellulose extraction from eucalyptus and pine tree wood waste. *Polymers, 16*(1), 20. https://doi.org/10.3390/polym16010020

Wang, J., & Zhuang, S. (2022). Chitosan-based materials: Preparation, modification and application. *Journal of Cleaner Production, 355,* 131825. https://doi.org/10.1016/j.jclepro.2022.131825

Wang, K., Du, L., Zhang, C., Lu, Z., Lu, F., & Zhao, H. (2019). Preparation of chitosan/curdlan/carboxymethyl cellulose blended film and its characterization. *Journal of Food Science and Technology, 56,* 5396–5404. https://doi.org/10.1007/s13197-019-04010-2

Wang, L., Li, J., Zhao, Y., & Jiang, T. (2017). Effect of resveratrol treatment on quality and antioxidant capacity of postharvest strawberry fruit. *Postharvest Biology and Technology, 128,* 99–106. https://doi.org/10.1016/j.postharvbio.2017.02.001

Wang, L., Liu, F., Jiang, Y., Chai, Z., Li, P., & Cheng, Y. (2018). Effects of resveratrol incorporation on the physicochemical properties and antioxidant activity of chitosan-based films. *Food Hydrocolloids, 77,* 803–810. https://doi.org/10.1016/j.foodhyd.2017.11.037

Wang, L., Liu, L., Holmes, B., Kerry, J., & Morris, M. (2020). Impact of anthocyanin-rich extracts on biodegradable film color characteristics. *International Journal of Biological Macromolecules, 156,* 1234–1242. https://doi.org/10.1016/j.ijbiomac.2020.04.071

Wang, L., Wu, J., & Zhao, H. (2020). Resveratrol as a natural antioxidant to extend the shelf life of perishable foods: Mechanisms and applications. *Food Chemistry, 333,* 127461. https://doi.org/10.1016/j.foodchem.2020.127461

Wang, M., Jin, Y., & Ho, C. T. (2002). Evaluation of resveratrol derivatives as potential antioxidants and identification of reaction products. *Journal of Agricultural and Food Chemistry, 50*(3), 431–434. https://doi.org/10.1021/jf010875j

Wang, X., Huang, X., Zhang, F., Hou, F., Yi, F., Sun, X., ... & Liu, Z. (2022). Characterization of chitosan/zein composite film combined with tea polyphenol and its application on postharvest quality improvement of mushroom (*Lyophyllum decastes* Sing.). *Food Packaging and Shelf Life, 33*, 100869. https://doi.org/10.1016/j.fpsl.2022.100869

Wang, X., Sun, Y., Liu, Z., Huang, X., Yi, F., Hou, F., & Zhang, F. (2021). Preparation and characterization of chitosan/zein film loaded with lemon essential oil: Effects on postharvest quality of mushroom (*Agaricus bisporus*). *International Journal of Biological Macromolecules, 192*, 635–643. https://doi.org/10.1016/j.ijbiomac.2021.10.068

Wang, Y., & He, R. (2009). Pro-oxidant effect of polyphenols in relation to their interaction with transition metals. *Food Chemistry, 113*(3), 1047–1050. https://doi.org/10.1016/j.foodchem.2008.08.050

Wang, Y., Chen, G., & Zhang, X. (2021). Effects of alkali treatment on cellulose extraction from plant fibers: A review. *Industrial Crops and Products, 167*, 113573. https://doi.org/10.1016/j.indcrop.2021.113573

Wang, Y., Chen, Y., & Zhao, H. (2024). Nanocellulose from agro-industrial waste: Extraction methods and applications. *Carbohydrate Polymers, 320*, 121242. https://doi.org/10.1016/j.carbpol.2024.121242

Wang, Z., Yan, Y., Zhang, Z., Li, C., Mei, L., Hou, R., Liu, X., & Jiang, H. (2024). Effect of chitosan and its water-soluble derivatives on antioxidant activity. *Polymers*, *16*(7), 867. https://doi.org/10.3390/polym16070867

Weißpflog, J., Vehlow, D., Müller, M., Kohn, B., Scheler, U., Boye, S., & Schwarz, S. (2021). Characterization of chitosan with different degree of deacetylation and equal viscosity in dissolved and solid state – Insights by various complimentary methods. *International Journal of Biological Macromolecules, 171,* 242–261. https://doi.org/10.1016/j.ijbiomac.2021.01.010

Wieczorek, A. S., Hetz, S. A., & Kolb, S. (2014). Microbial responses to chitin and chitosan in oxic and anoxic agricultural soil slurries. *Biogeosciences, 11*(12), 3339–3352. https://doi.org/10.5194/bg-11-3339-2014

Wiercigroch, E., Szafraniec, E., Czamara, K., Pacia, M. Z., Majzner, K., Kochan, K., Kaczor, A., Baranska, M., & Malek, K. (2017). Raman and infrared spectroscopy of carbohydrates: A review. *Spectrochimica Acta Part A: Molecular and Biomolecular Spectroscopy, 185,* 317–335. https://doi.org/10.1016/j.saa.2017.05.045

Wu, L., Xie, X., Huang, J., He, J., & Liu, F. (2024). Preparation of chitosan-based macromolecular synergistic antioxidants containing hindered phenolic and secondary amine structures and its effects on thermo-oxidative aging of styrene-butadiene rubber/silica composites. *Polymers for Advanced Technologies, 35*(5). https://doi.org/10.1002/pat.6426

Wu, Y., Li, J., Zhang, H., & Liu, X. (2024). Impact of drying techniques on the mineral composition and nutritional quality of edible mushrooms. *Food Chemistry, 405,* 134010.

Wu, Y., Li, J., Zhang, H., & Liu, X. (2024). Impact of drying techniques on the mineral composition and nutritional quality of edible mushrooms. *Food Chemistry, 405,* 134010. https://doi.org/10.1016/j.foodchem.2022.134010

X. He, M. Li, X. Gong, B. Niu, & W. Li. (2021). Biodegradable and antimicrobial CSC films containing cinnamon essential oil for preservation applications. *Food Packaging and Shelf Life, 29,* 100697. https://doi.org/10.1016/j.fpsl.2021.100697

Xu, J., Liu, K., Chang, W., Chiou, B. S., Chen, M., & Liu, F. (2022). Regulating the physicochemical properties of chitosan films through concentration and neutralization. *Foods, 11*(11), 1657. https://doi.org/10.3390/foods11111657

Xu, Y., Li, Y., Zhang, L., & Cheng, C. (2020). Influence of polyphenol incorporation on mechanical and barrier properties of polyvinyl alcohol/chitosan films. *International Journal of Biological Macromolecules, 150,* 209–217. https://doi.org/10.1016/j.ijbiomac.2020.01.210

Xue, H., Du, X., Fang, S., Gao, H., Xie, K., Wang, Y., & Tan, J. (2024). The interaction of polyphenols-polysaccharides and their applications: A review. *International Journal of Biological Macromolecules, 134594.* https://doi.org/10.1016/j.ijbiomac.2024.134594

Yadav, K. K., Krishnan, S., Gupta, N., Prasad, S., Amin, M. A., Cabral-Pinto, M. M. S., Sharma, G. K., Marzouki, R., Jeon, B.-H., Kumar, S., Singh, N., Kumar, A., Rezania, S., & Islam, S. (2021). Review on evaluation of renewable bioenergy potential for sustainable development: Bright future in energy practice in India. *ACS Sustainable Chemistry & Engineering*, *9*(48), 16007–16030. https://doi.org/10.1021/acssuschemeng.1c03114

Yang, Q., Yi, X., Xiao, H., Wang, X., Liu, L., Tang, Z., Hu, C., & Li, X. (2024). Effects of different drying methods on drying characteristics, microstructure, quality, and energy consumption of apricot slices. *Foods*, *13*(9), 1295. https://doi.org/10.3390/foods13091295

Yang, R. L., Li, Q., & Hu, Q. P. (2020). Physicochemical properties, microstructures, nutritional components, and free amino acids of *Pleurotus eryngii* as affected by different drying methods. *Scientific Reports*, *10*(1), 121. https://doi.org/10.5897/AJFS.9000073

Yang, R., & Chen, J. (2021). Mechanistic and machine learning modeling of microwave heating process in domestic ovens: A review. *Foods, 10*(9), 2029. https://doi.org/10.3390/foods10092029

Yang, X., Han, F., Xu, C., Jiang, S., Huang, L., Liu, L., & Xia, Z. (2017). Effects of preparation methods on the morphology and properties of nanocellulose extracted from corn husk. *Industrial Crops and Products, 109,* 241–247. https://doi.org/10.1016/j.indcrop.2017.08.014

Yang, Y., Wang, Y., & Li, X. (2024). Microencapsulated polyphenol extracts from Georgia-grown pomegranate peels delay lipid oxidation in salad dressing during accelerated and ambient storage conditions. *Food Science & Nutrition, 12*(1), 3776. https://doi.org/10.1002/fsn3.3776

Yarangsee, B., Srilaong, V., Pongprasert, N., & Boonyaritthongchai, P. (2015). Changes in bioactive compounds and antioxidant capacity of fresh-cut wax apple (*Syzygium samarangenese*) fruit during storage. *Journal of Food Biochemistry, 39*(6), 649–657. https://doi.org/10.1111/jfbc.12179

Yi, J., Kebede, B. T., Hai Dang, D. N., Buvé, C., Grauwet, T., Van Loey, A., & Hendrickx, M. (2016). Quality changes of silver ear mushroom (*Tremella fuciformis*) after different drying processes: Evaluation of rehydration ability, texture, and microstructure. *Food Research International, 87,* 31–38. https://doi.org/10.1016/j.foodres.2016.06.021

Yildiz, G., Izli, N., Ünal, H., & Uylaser, V. (2015). Physical and chemical changes in persimmon during drying at different temperatures. *CyTA - Journal of Food, 13*(3), 332–339. https://doi.org/10.1080/19476337.2014.971347

Younis, K., & Ahmad, S. (2022). Quality and chemical composition of button mushroom (*Agaricus bisporus*) as affected by different drying methods. *Journal of Food Measurement and Characterization, 16*(1), 279–290. https://doi.org/10.1007/s11694-021-01065-2

Yu, D., Sun, X., Fan, J., Zhang, Z., & Fang, L. (2020). Effects of different drying methods on physical and nutritional properties of button mushroom powder. *Drying Technology, 38*(6), 810–817. https://doi.org/10.1080/07373937.2019.1626223

Yun, J., Li, X., & Qiao, Y. (2023). Comparative study of freeze-drying and air-drying on bioactive components and antioxidant properties of mushrooms. *Journal of Food Processing and Preservation, 47*(2), e17308. https://doi.org/10.1111/jfpp.17308

Zhang, G., Zhang, L., Deng, H., & Sun, P. (2011). Preparation and characterization of sodium carboxymethyl cellulose from cotton stalk using microwave heating. *Journal of Chemical Technology and Biotechnology, 86*(4), 584–589. https://doi.org/10.1002/jctb.2556

Zhang, L., & Wang, Y. (2018). Effect of drying temperature on physicochemical and antioxidant properties of shiitake mushrooms (*Lentinula edodes*). *Journal of Food Science and Technology, 55*(8), 3143–3150. https://doi.org/10.1007/s13197-018-3237-5

Zhang, L., Liu, Z., Wang, X., Dong, S., Sun, Y., & Zhao, Z. (2019). The properties of chitosan/zein blend film and effect of film on quality of mushroom (*Agaricus bisporus*). *Postharvest Biology & Technology, 155*, 47–56. https://doi.org/10.1016/j.postharvbio.2019.05.013

Zhang, M., Chen, H., Mujumdar, A. S., & Tang, J. (2013). Recent developments in high-quality drying of vegetables, fruits, and aquatic products. *Critical Reviews in Food Science and Nutrition, 53*(8), 1079–1095. https://doi.org/10.1080/10408398.2011.558224

Zhang, S., Zhang, Y., Zhu, H., & Wang, J. (2021). Drying behavior and quality characteristics of shiitake mushrooms during far-infrared drying. *LWT - Food Science and Technology, 143*, 111141. https://doi.org/10.1016/j.lwt.2021.111141.

Zhao, L., Lin, S., Chen, M., & Ye, F. (2020). Effect of freeze-drying on microstructure and functional components of *Flammulina velutipes*. *Food Chemistry, 326*, 126927. https://doi.org/10.1016/j.foodchem.2020.126927.

Zhou, X., Li, W., Huang, Q., & Zhang, X. (2022). Effect of hot air and freeze-drying on phenolic composition and antioxidant activity of shiitake mushrooms. *Journal of Food Science, 87*(5), 2180–2191. https://doi.org/10.1111/1750-3841.16108.

Zion Market Research. (2021). *Agaricus bisporus (white button mushroom) market by type, form, and region: Global industry perspective, comprehensive analysis, and forecast, 2020–2028.* Zion Market Research. https://www.zionmarketresearch.com/report/agaricus-bisporus-market

Zope, V. M., Mujumdar, A. S., & Thorat, B. N. (2022). Hybrid drying technologies: A review on current development. *Journal of Food Engineering, 320,* 110932. https://doi.org/10.1016/j.jfoodeng.2021.110932

Appendix- I

Standard curve for Total cellulose content

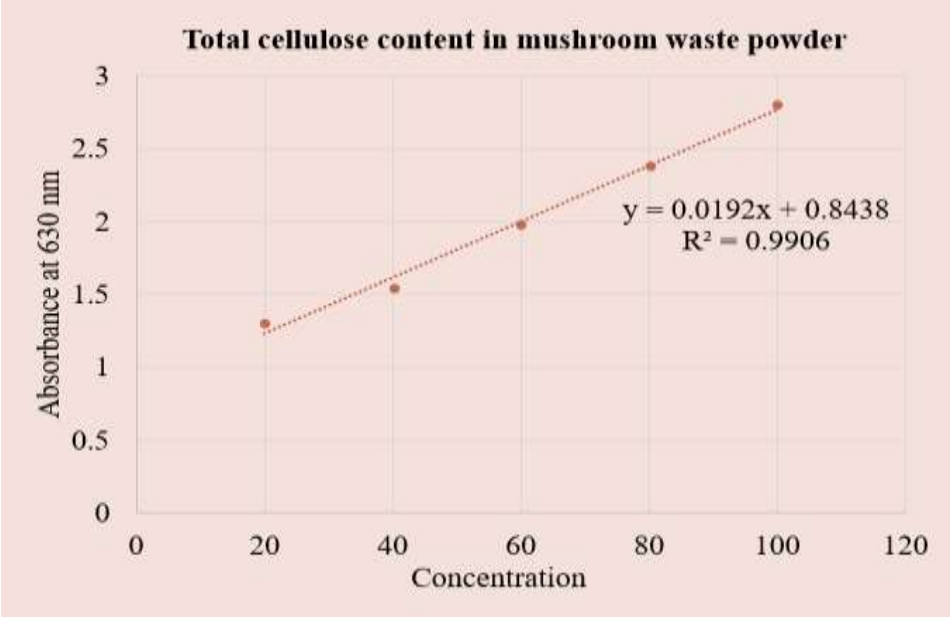

6th International Conference

Cutting-Edge Solutions in Science-Agriculture, Technology, Engineering and Humanities (CSATEH-2024)

CERTIFICATE

This is to certify that Adity Bahndral, Department of Food Technology and Nutrition, Lovely Professional University, Phagwara, Punjab. Actively participated/presented a paper (Poster) entitled "Utilization of chitosan in preparation of edible packaging film from mushroom".

As a Delegate/Scholar/Student in the "6th International Conference on "CSATEH-2024" jointly organized by Department of Geography, Kumaun University, Nainital; AETDS, U.S. Nagar, Uttarakhand; UAS, GKVK, Bangalore, Karnataka; Dr YSR Horticultural University, Venkataramanagudem, Andhra Pradesh; Agriculture and Forestry University, Nepal; Sher-e-Bangla Agricultural University, Bangladesh; Mid-West University, Nepal; CSB-CTRTI, Ranchi, Jharkhand; HRDI, Uttarakhand and CSB-BTSSO, Chhattisgarh at UGC-HRDC Hall, Kumaun University, Nainital, Uttarakhand, India on August 24-26, 2024.

Prof. (Dr.) C. P. Singh	Prof. Mirza Hasanuzzaman	Dr. Santosh Marahatta	Dr. Karan Singh Dhami	Dr. P. C. Chanyal	Dr. Wajid Hasan
Conference Chairman President, AETDS Former Professor GBPUAT, Pantnagar, India	Conference Executive Director Sher-e-Bangla Agri. University Bangladesh	Conference Director AFU, Chitwan, Nepal	Conference Associate Director Mid-West University,Nepal	Organizing Secretary Geography Department, Kumaun University, Nainital, Uttarakhand	Chief-Organizing Secretary Secretary, AETDS, KVK Jehanabad, BAU Sabour, Bihar, India

AETDS/PC/CSATEH/2024....2017.....

Certificate No: *GKCIET/FET/ETFP-IV/804*

International Conference on
Emerging Technologies in Food Processing –IV
(ETFP-2024)

Department of Food Engineering and Technology,
Ghani Khan Choudhury Institute of Engineering and Technology
(A Centrally Funded Technical Institute, Ministry of Education, Government of India)
Narayanpur, Malda, West Bengal: 732141

Certificate for Presentation

This is to certify that ***Adity Bahndral And Dr. Rafeeya Shams*** *of* ***Lovely Professional University, Punjab, India*** *was awarded* ***First*** *Position in* ***Oral Presentation Session I*** *at the International Conference on "****Emerging Technologies in Food Processing-IV (ETFP-2024)****" organized by the* ***Department of Food Engineering and Technology****, Ghani Khan Choudhury Institute of Engineering and Technology, Malda, West Bengal during 18th -19th Nov 2024.*

Title of paper: Development of polysaccharide based smart multilayer film as food packaging solution for prolonging the shelf life of perishable food

Authors: Adity Bahndral And Dr. Rafeeya Shams

Dr Mudasir Ahmad Malik
Organizing Secretary

Dr Kshirod Kumar Dash
Organizing Secretary

Dr Amit Baran Das
Chairman

Appendix- III

Journal of Agriculture and Food Research 16 (2024) 101170

Contents lists available at ScienceDirect

Journal of Agriculture and Food Research

journal homepage: www.sciencedirect.com/journal/journal-of-agriculture-and-food-research

Microwave assisted extraction of cellulose from lemon grass: Effect on techno-functional and microstructural properties

Adity Bahndral [a], Rafeeya Shams [a,**], Kshirod Kumar Dash [b,*], N. Afzal Ali [c], Ayaz Mukarram Shaikh [d], Béla Kovács [d]

[a] Department of Food Technology and Nutrition, Lovely Professional University, Phagwara, Punjab, India
[b] Department of Food Processing Technology, Ghani Khan Choudhury Institute of Engineering and Technology, Malda, West Bengal, India
[c] School of Agro and Rural Technology, Indian Institute of Technology Guwahati, India
[d] Faculty of Agriculture, Food Science and Environmental Management Institute of Food Science, University of Debrecen, Debrecen, 4032, Hungary

ARTICLE INFO

Keywords:
Cellulose
Lemon grass straw
Extraction procedure
Microwave-assisted extraction

ABSTRACT

The study focused on utilizing lemon grass straw to generate cellulose through the process of deligunification, which involves the removal of hemicelluloses, followed by bleaching. The study involves the microwave-assisted alkali extraction, followed by characterizing the extracted material. At microwave power of 540 W using 8 % NaOH for 3 min for lignin removal and 540 W for 2 min for bleaching showed the maximum yield of 37.46 %. Fourier transform infrared spectroscopy is employed to analyze the physical properties of extracted cellulose, namely the hydroxyl (OH), carbonyl (C=O), C-H bonds, C-O and C-C bonds, and glycosidic linkage (C-O-C) within the cellulose polymer chain. The extracted cellulose exhibited excellent thermal stability, as indicated by its high breakdown temperature. The X-ray diffraction (XRD) analysis revealed prominent peaks at 14.8°, 16.5°, and 22.5°, demonstrating the presence of crystalline cellulose. The crystallinity index value of 70.02 % further confirmed the crystalline nature of the extracted cellulose.

1. Introduction

Agri-wastes are resulting from the cultivation and harvesting of plants and crops. Utilizing agricultural waste has the potential to effectively address the increasing energy needs of society in a sustainable fashion [1]. Cellulose, a linear homopolymer, is manufactured at a rate of 105–1010 tons each year, making it one of the most prevalent, environmentally friendly, renewable, cost-effective, and biodegradable polymers globally, capable of substituting synthetic materials [2]. Research into biodegradable and innovative products such as cellulose has become crucial because of its distinctive properties. Different methods have been utilized by various researchers to isolate cellulose from agricultural waste or byproducts. However, they generally follow similar sequences of steps in the cellulose isolation process [3]. The order of steps implicated in extraction process were cleansing of raw material to take out dirt particles from it, drying in an oven at normal conditions, grinding to produce powder, using a sieve to achieve the desired particle size, defatting, pretreatment using alkaline, neutralizing it with distilled water, drying, acid treatment, again neutralizing by employing distilled water and drying to obtain the necessary cellulose fibers. Cellulose is typically sourced from various plant components, such as softwood, hardwood, bark, and other plant parts [4].

There is an increasing demand for humans to yield cellulose from farm waste, especially straw, as it can have significant economic value when processed appropriately. In recent years, there has been a transition in cellulose extraction methods from plant-based sources to plant waste sources such as rice straw [5], wheat straw [6], lemon grass straw [4], vetiver straw [7], little millet straw [8], oat straw [9], banana pseudostem [10] and yellow thatching straw [11] etc., many of these cellulose sources are derived from non-wood plants and are not intended for food use. Typically, agricultural waste such as lemon grass straw (referred to as LG after oil extraction) is often burned, but finding appropriate uses for it could alleviate waste disposal challenges. Lemon grass, scientifically known as *Cymbopogon citratus* and belonging to the Poaceae family, is recognized as a significant source of cellulose, hemicellulose, and lignin, comprising approximately 44–45 %, 28–29

Carbohydrate Polymer Technologies and Applications 8 (2024) 100598

Contents lists available at ScienceDirect

Carbohydrate Polymer Technologies and Applications

journal homepage: www.sciencedirect.com/journal/carbohydrate-polymer-technologies-and-applications

Plant-based chitosan for the development of biodegradable packaging materials

Adity Bahndral [a], Rafeeya Shams [a,*], Pintu Choudhary [b,*]

[a] Department of Food Technology and Nutrition, Lovely Professional University, Phagwara, Punjab, India
[b] Department of Food Technology, Chaudhary Bansi Lal Government Polytechnic, Haryana, India

ARTICLE INFO

Keywords:
Chitosan
Plant based
Biodegradable
Extraction
Packaging

ABSTRACT

Plant-derived materials and edible films have developed as viable substitutes for standard packaging materials, enabling sustainable and ecologically acceptable alternatives. Chitosan, a cationic carbohydrate polymer derived from animal or marine sources, as well as from agricultural waste such as mushrooms or various fungi possesses excellent properties such as film formation, mechanical strength, non-toxicity, biodegradability, edibility, UV-blocking ability, antioxidant activity, and antibacterial functionality, justifying its potential as packaging/coating material for fresh agricultural products. Chitosan is obtained through the deacetylation of chitin. The quantity of waste generated in a mushroom farm varies from 5–20 % of the total yielding quantity. Filamentous fungi's cellular structure, which is rich in chitin, provides a convenient method for chitin extraction. Fungal-derived chitosan offers the advantage of controllable physicochemical characteristics, including degree of deacetylation and molecular weight, compared to chitosan obtained from crustaceans. This versatility makes fungal chitosan suitable for various utilizations in food, pharmaceutical, and biomedical management. It can be utilised for different purposes in these fields. This review primarily emphasizes the extraction of chitin from mushrooms and various fungal sources, comparing different extraction methods and chitosan-based materials fabrication techniques. Additionally, it discusses the crucial characteristics of chitosan that make it convenient for high value-added functions in the food industry. To sum up, plant-based chitosan films have the potential to completely transform the packaging sector by providing environmentally friendly substitutes for traditional materials. Accepting these advances will help build a more resilient and sustainable earth, encourage the circular economy, and reduce the amount of plastic trash produced.

1. Introduction

The growing need for safe and nutritious food, coupled with consumer preferences for a diverse range of food options year-round and convenient packaging, has driven significant advancements in the domain of food packaging (Agarwal et al., 2023). The fundamental objective of packaging of any food product is to protect food products from external elements that can lead to spoilage, including microorganisms, oxygen, temperature fluctuations, and humidity (Priyanka et al., 2023). Alongside these benefits, food packaging serves various other important purposes such as offering convenience, enhancing customer experience, and acting as a marketing tool for the packaged product (Kumar et al., 2020). Food packaging predominantly relies on plastics and polymers as the most prevalent and commonly chosen materials, which are extensively employed in both rigid and flexible packaging applications. This increases plastic pollution, one of the leading causes of marine animal deaths. Moreover, plastic-based packaging is often supplemented with toxic synthetic compounds (e.g., polyethylene, polypropylene, polystyrene, and other petroleum compounds) that have a negative impact on human health (Yao et al., 2022). However, it is important to consider the environmental impact of these materials so that they do not readily break down. The WHO (World Health Organization) estimates that polluted water causes approximately 500,000 diarrheal deaths every year. Billions of tons of dumped plastic generate so-called microplastics and nanoplastics which can easily be ingested by animals, leading to a disturbance of ecosystems and causing the death of millions of children and animals every year (Wrunska et al., 2023). Moreover, due to the considerable financial outlay, the disposal of the materials is inadequate. Unfortunately, recycling policies and separate waste collection are still insufficiently

Carbohydrate Polymer Technologies and Applications 9 (2025) 100730

Contents lists available at ScienceDirect

Carbohydrate Polymer Technologies and Applications

journal homepage: www.sciencedirect.com/journal/carbohydrate-polymer-technologies-and-applications

Microwave assisted extraction of chitosan from *Agaricus bisporus*: techno-functional and microstructural properties

Adity Bahndral [a], Rafeeya Shams [a,*], Kshirod Kumar Dash [b,*], Pintu Chaudhary [c], Ayaz Mukarram Shaikh [d], Kovács Béla [d,*]

[a] Department of Food Technology and Nutrition, Lovely Professional University, Phagwara, Punjab, India
[b] Department of Food Engineering and Technology, Ghani Khan Choudhary Institute of Engineering and Technology, Malda, West Bengal, India
[c] Department Department of Food Technology, C.R.L. Government Polytechnic, Bhiwani, Haryana, India
[d] Faculty of Agriculture, Food Science and Environmental Management Institute of Food Science, University of Debrecen, Debrecen 4032, Hungary

ARTICLE INFO

Keywords:
Agaricus bisporus
Antioxidant activity
Chitosan
Crystallinity index
Degree of deacetylation
Microwave irradiation

ABSTRACT

Chitosan, a copolymer of glucosamine and N-acetyl glucosamine, is primarily derived from chitin. The present research was conducted to generate and analyze chitosan derived from white button mushroom waste (*Agaricus bisporus*) using microwave assisted extraction. Dried mushroom waste powder was demineralized in diluted acid using 3 M HCl in 1:10 w/v at 540 W for 8 min and deproteinated at 180 W using 10% NaOH in 1:10 w/v for 8 min to remove proteins and lipids. The extracted chitin was deacetylated using 50% NaOH in 1:20 w/v at 360 W to convert it into chitosan. Chitin from the aforesaid process was deacetylated in concentrated alkaline medium at 360 W for 8 min to yield chitosan by converting acetyl groups to -NH_2 groups. The pH and solubility of fresh chitosan were 7.5 and 75%, respectively. Extracted chitosan had maximum 2,2-diphenyl-1-picrylhydrazyl (DPPH) free radical scavenging activity of 53.97% and reducing power of 3.58. The microwave irradiation method produced chitosan having degree of deacetylation of 79.94% and crystallinity index of 1.09. The spectra bands confirmed existence of NH_2, OH, C—O, CH, and C—N functional groups. The X-ray diffraction analysis of the chitosan sample discovered distinct peaks at 2θ values between 10 and 20 °, indicating its semi-crystalline nature.

1. Introduction

The consumption of mushrooms has significantly expanded in recent years because of its high nutritional value and health benefits, which are attributed to the presence of proteins, vitamins, minerals, fungal polysaccharides (particularly β-glucans), and antioxidants. Around 20 of the more than 35 edible mushroom species that are commercially grown worldwide are produced on an industrial basis (Pandey et al., 2024; Silva et al., 2024). Among them *Agaricus bisporus* is one of the most often consumed mushrooms worldwide (Siwulski et al., 2020). Mushrooms, which belong to the fungi kingdom, offer substantial nutritional benefits, with approximately 2000 edible species found globally (El Sheikha, 2022). Among these, the most commonly grown varieties comprise the button mushroom (*Agaricus bisporus*), oyster mushrooms (*Pleurotus spp.*), and shiitake mushroom (*Lentinula edodes*). In 2018, the worldwide market worth of farm fresh mushrooms stood at 38 billion USD, with China emerging as the dominant mushroom grower in Asia, making up about 35% of the total global mushroom market share, as reported by Bhagarathi et al. (2023). Asia countries subsidize maximum mushroom production up to 76%, here after by Europe (17.2 %) and United States (5.9 %) (Yadav et al., 2021). India exhibits diverse agro-climatic conditions and is primarily an agrarian nation, utilizing roughly 4.37% of its land for cultivation and producing approximately 620 million tons of agricultural waste each year. In particular, the market for *Agaricus bisporus*, or white mushrooms, was worth USD 16.73 billion in 2020 and is projected to grow to USD 27.39 billion by 2028 (Zion Market Research, 2021). India has the potential to generate 3 million tonnes of mushrooms and approximately 15 million tonnes of bio-compost from agricultural waste in context regarding mushroom cultivation (Raman et al., 2018). Currently, industries encounter losses linked to the safe disposal of mushroom waste, including mushroom stems and misshapen mushrooms whose size or shape do not meet commercial standards contributing to the final production costs of products (Papoutsis et al., 2020). Adopting a value-addition approach has the potential to generate extra

Appendix- IV

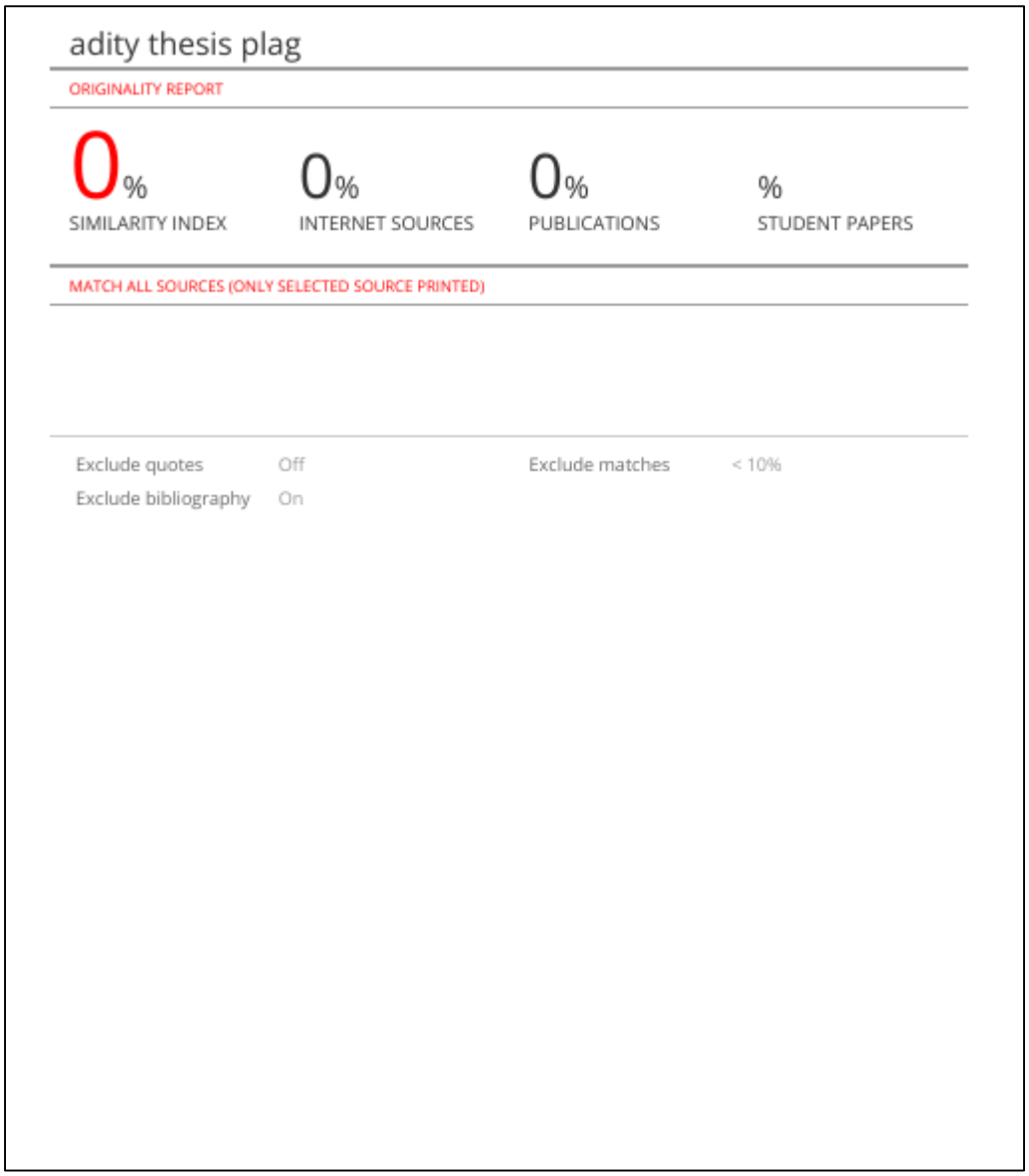

adity thesis plag

ORIGINALITY REPORT

0%	0%	0%	%
SIMILARITY INDEX	INTERNET SOURCES	PUBLICATIONS	STUDENT PAPERS

MATCH ALL SOURCES (ONLY SELECTED SOURCE PRINTED)

Exclude quotes	Off	Exclude matches	< 10%
Exclude bibliography	On		

Appendix –V

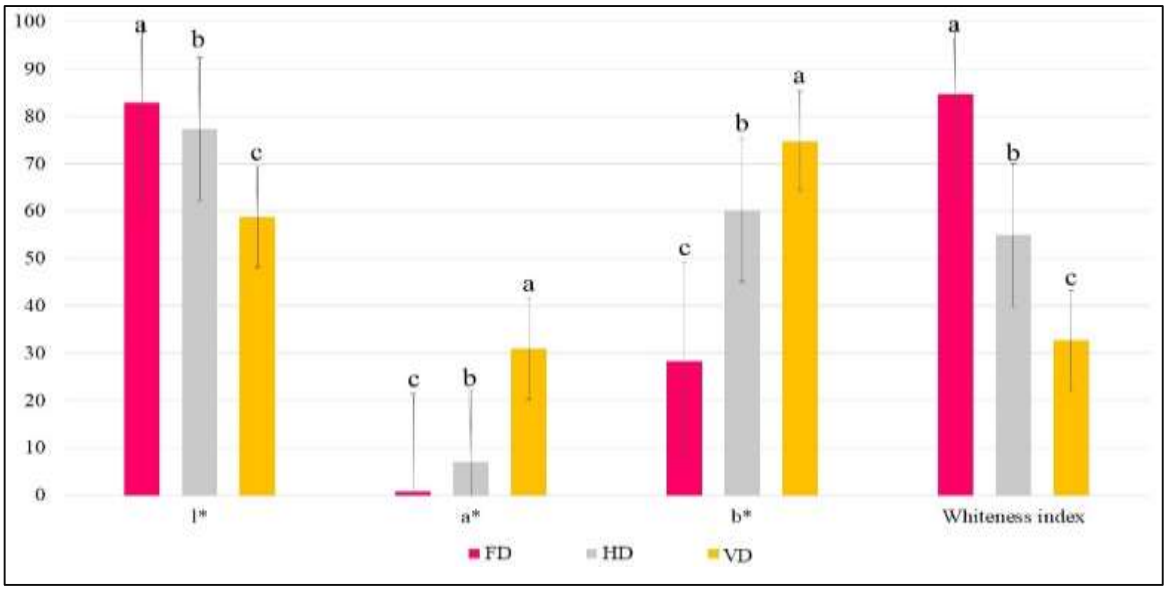

Figure 1. Effect of drying (FD, VD and HD) on phenolic, flavonoid and ascorbic content in white button mushroom waste powder (MWP).

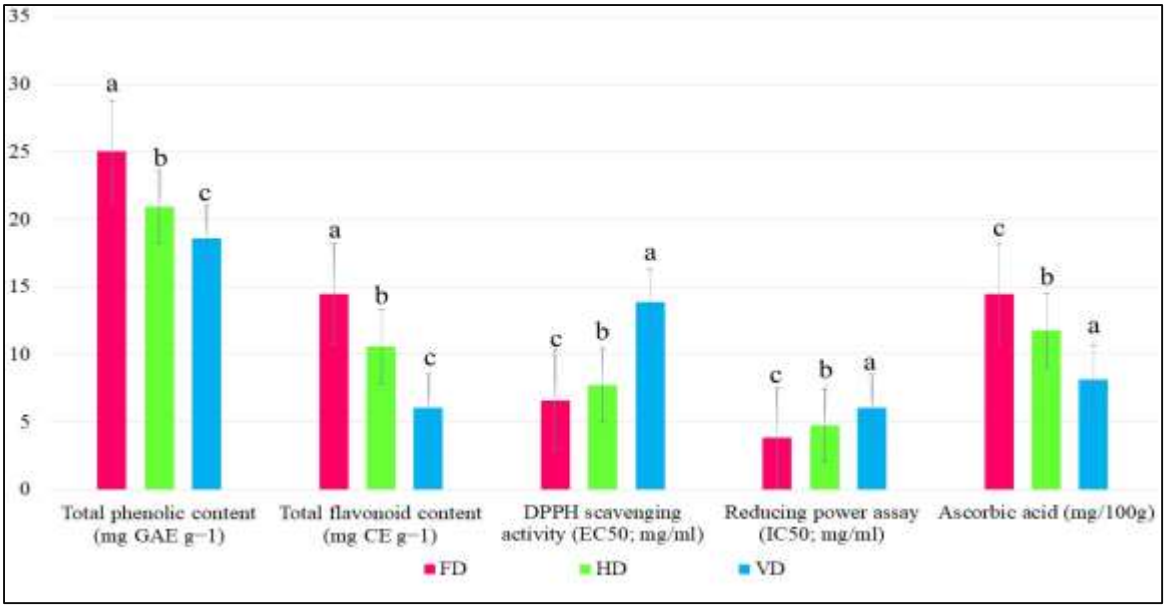

Figure 2. Effect of drying (FD, VD and HD) on color properties in white button mushroom waste powder (MWP).

Appendix –VI

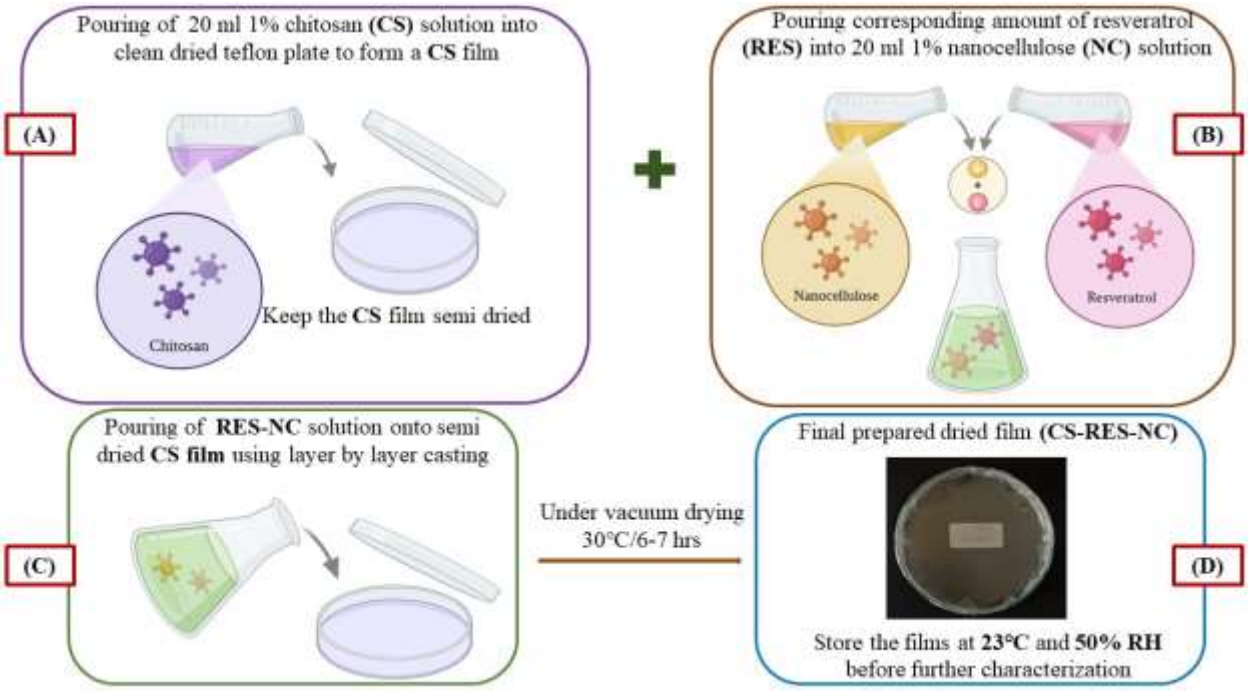

Figure 1. Preparation of CS-RES-NC multilayer film using Layer by layer (LBL) casting method.

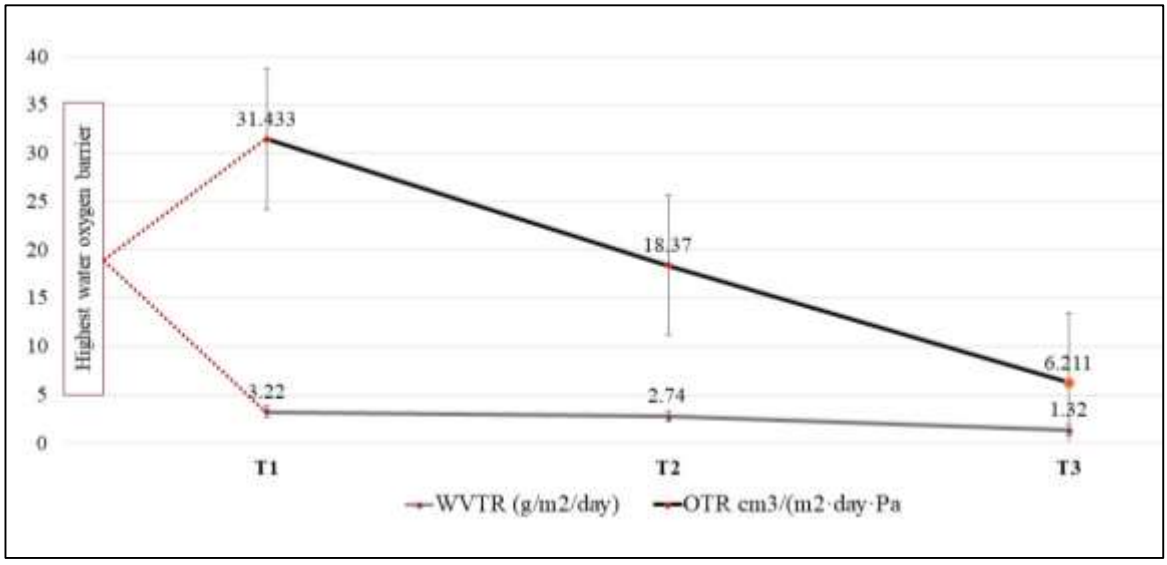

Figure 2. Water vapor transmission rate (WVTR) and Oxygen transmission rate (OTR) of control films (T1, T2 and T3).

Appendix –VII

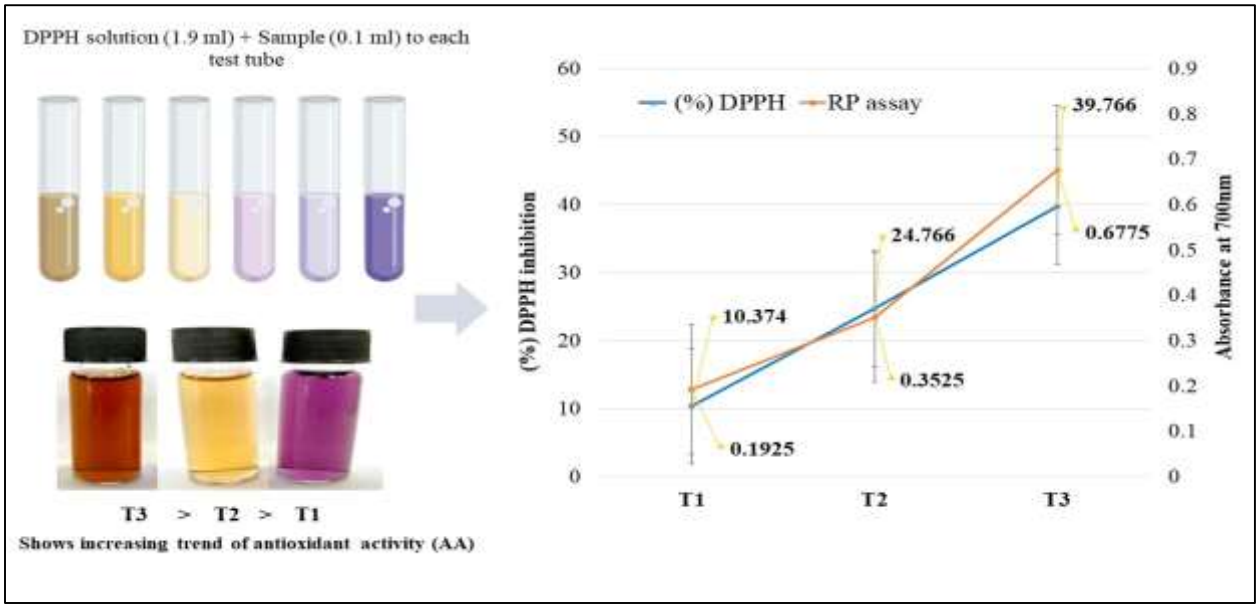

Figure 1. 2,2-diphenyl-1-picrylhydrazyl (DPPH) and Reducing power (RP) assay for control films (T1, T2 and T3).

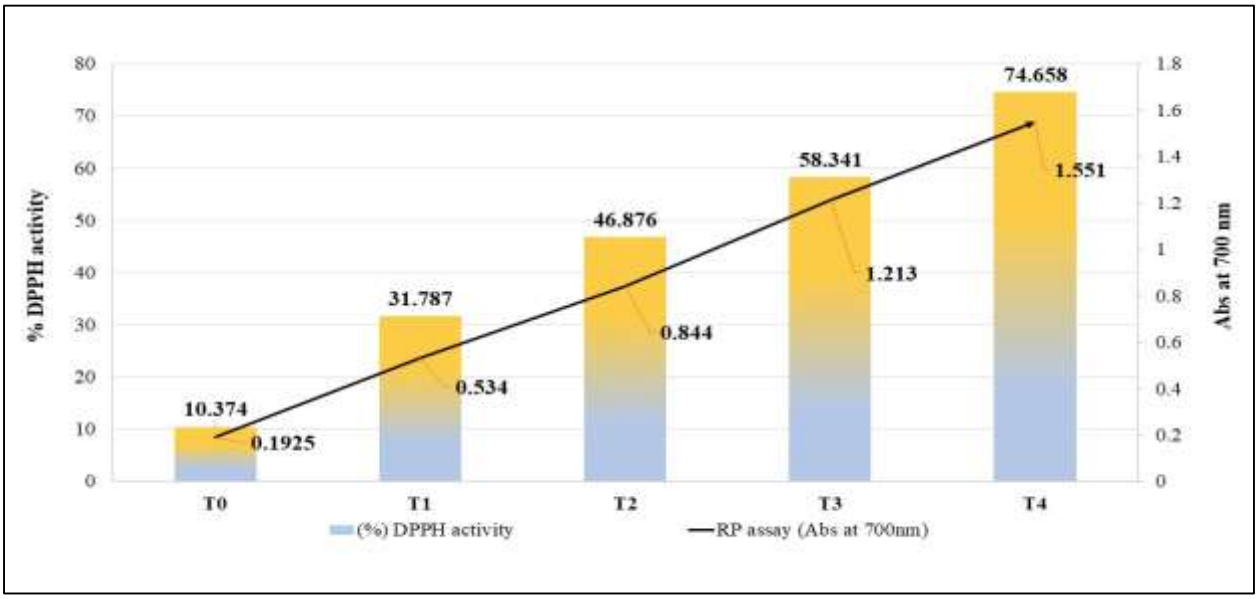

Figure 2. Evaluation of antioxidant properties of the treated films (T1, T2, T3 and T4) in comparison with optimized control film (T2).

Appendix –VIII

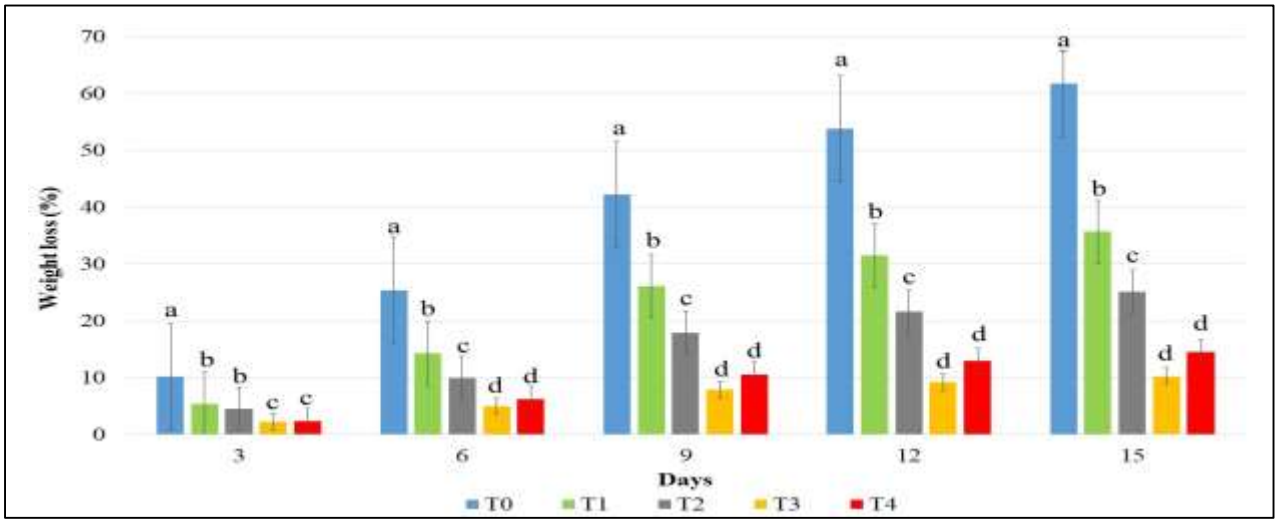

Figure 1. Changes in weight loss (%) of *Agaricus bisporus* packed with CS-NC and CS-RES-NC (4, 8, 12 and 16 ug/ml RES as T1, T2, T3 and T4) multilayer films during 15d of storage at 4°C. Different letters denote significant differences. Each data point is the mean of three replicates and vertical bars are present standard error of the means.

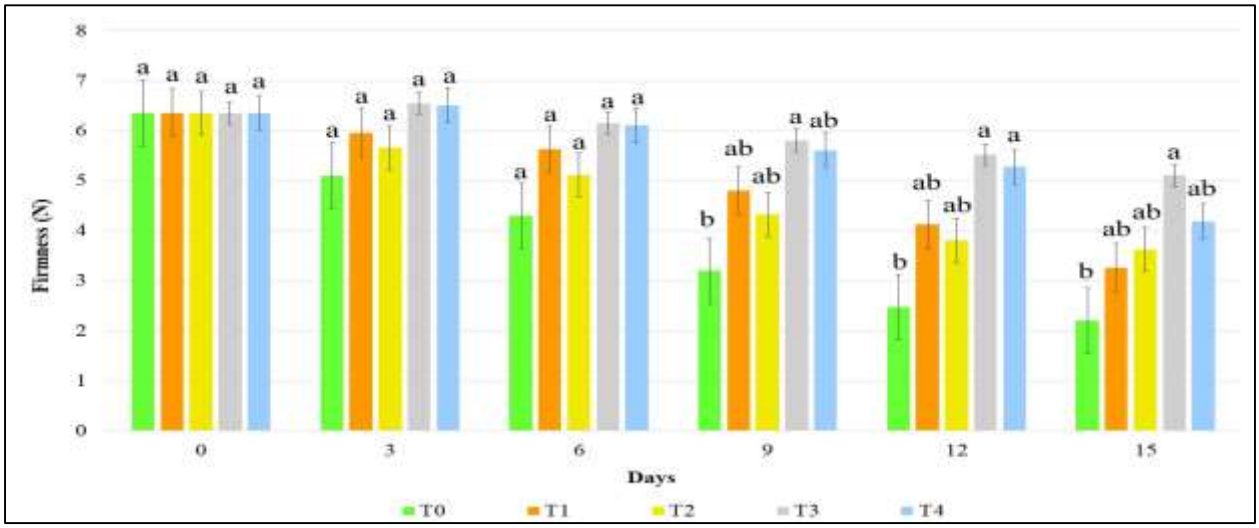

Figure 2. Changes in Firmness (N) of *Agaricus bisporus* packed with CS-NC and CS-RES-NC (4, 8, 12 and 16 ug/ml RES as T1, T2, T3 and T4) multilayer films during 15d of storage at 4°C. Different letters denote significant differences. Each data point is the mean of three replicates and vertical bars are present standard error of the means.

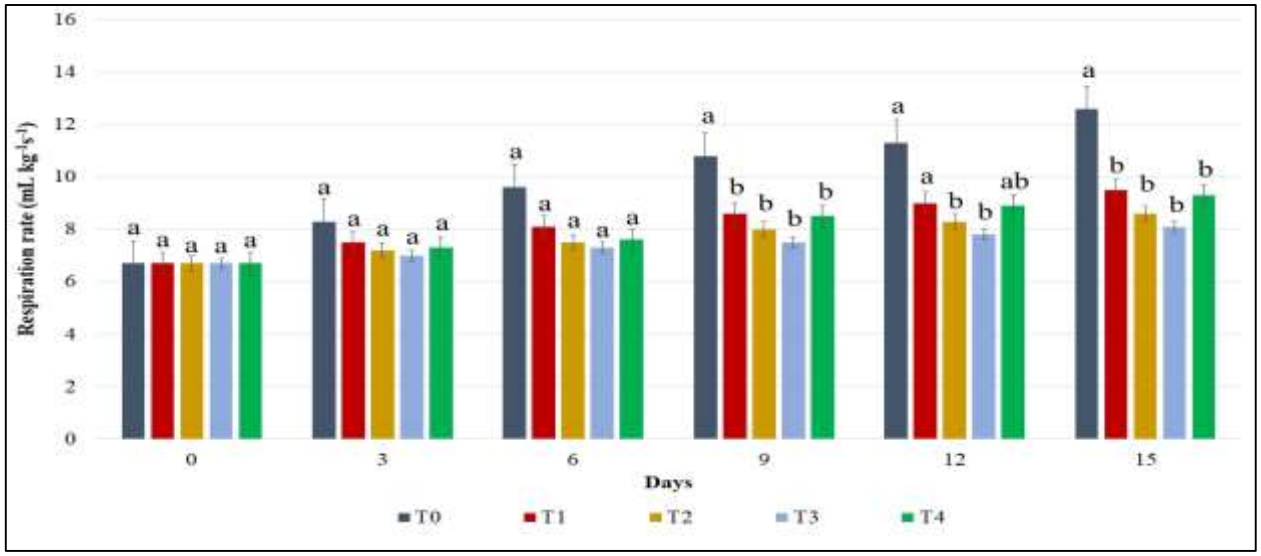

Figure 3. Changes in Respiration rate ($mL\ kg^{-1}s^{-1}$) of *Agaricus bisporus* packed with CS-NC and CS-RES-NC (4, 8, 12 and 16 ug/ml RES as T1, T2, T3 and T4) multilayer films during 15d of storage at 4°C. Different letters denote significant differences. Each data point is the mean of three replicates and vertical bars are present standard error of the means.

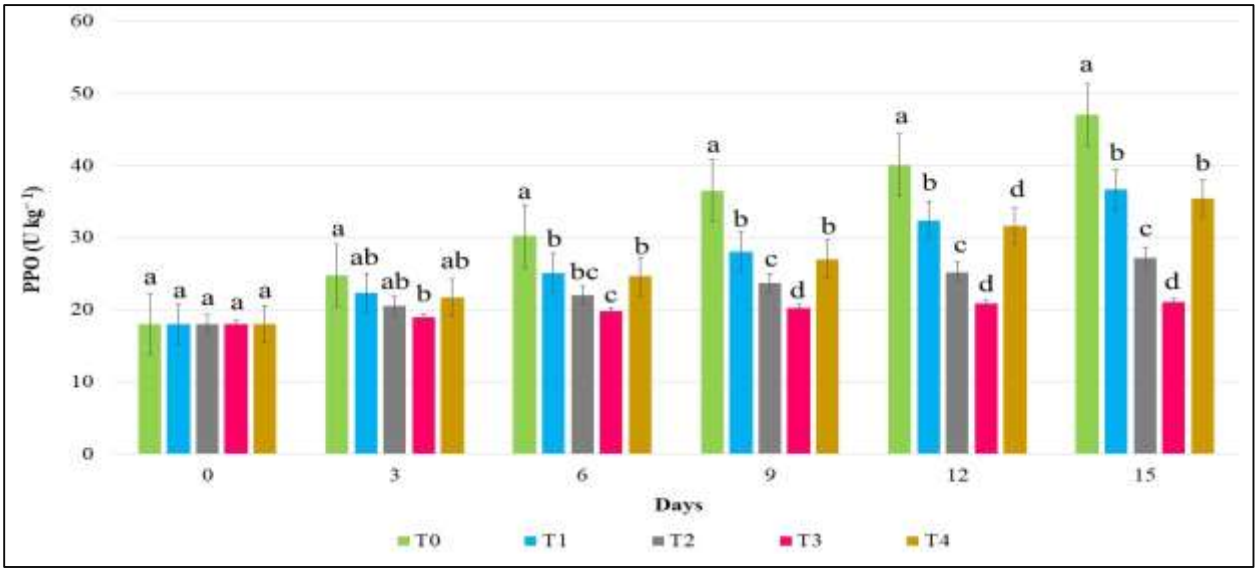

Figure 4. Changes in Polyphenol oxidase (PPO) activity (U kg^{-1}) of *Agaricus bisporus* packed with CS-NC and CS-RES-NC (4, 8, 12 and 16 ug/ml RES as T1, T2, T3 and T4) multilayer films during 15d of storage at 4°C. Different letters denote significant differences. Each data point is the mean of three replicates and vertical bars are present standard error of the means.

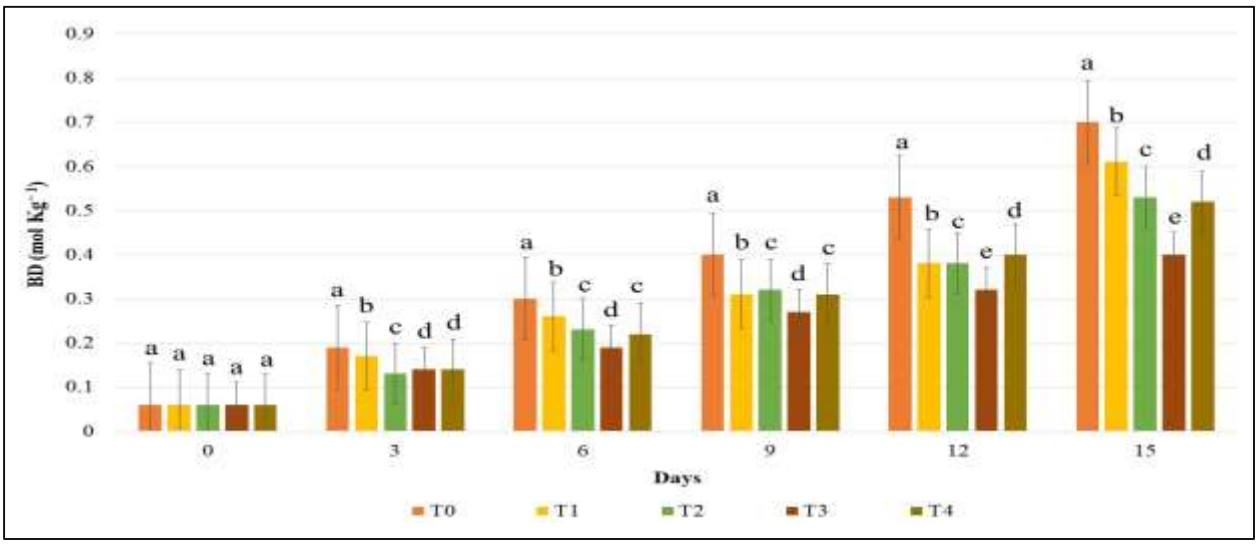

Figure 5. Changes in browning degree (BD) content (mol Kg^{-1}) of *Agaricus bisporus* packed with CS-NC and CS-RES-NC (4, 8, 12 and 16 ug/ml RES as T1, T2, T3 and T4) multilayer films during 15d of storage at 4°C. Different letters denote significant differences. Each data point is the mean of three replicates and vertical bars are present standard error of the means.

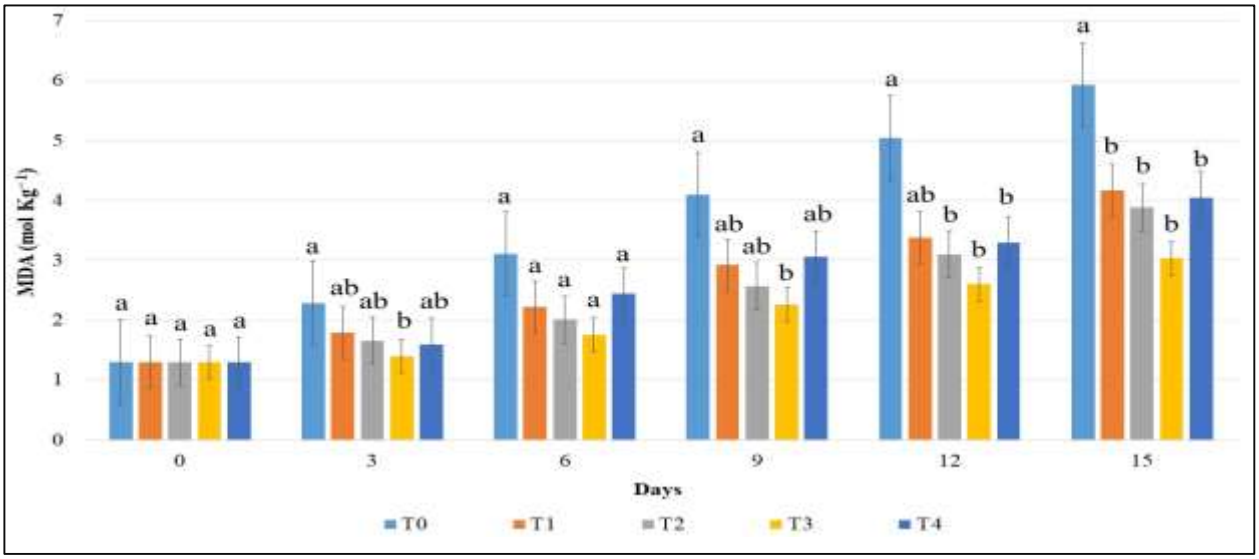

Figure 6. Changes in Malondialdehyde (MDA) content (mol Kg^{-1}) of *Agaricus bisporus* packed with CS-NC and CS-RES-NC (4, 8, 12 and 16 ug/ml RES as T1, T2, T3 and T4) multilayer films during 15d of storage at 4°C. Different letters denote significant differences. Each data point is the mean of three replicates and vertical bars are present standard error of the means.